ISSN 1606-9277
Frequency: Annually
Vol. 17, No. 01 (2025)

TECHNICAL JOURNAL

River Research Institute

RIVER RESEARCH INSTITUTE
MINISTRY OF WATER RESOURCES
GOVT. OF THE PEOPLE'S REPUBLIC OF BANGLADESH

ISSN 1606-9277

TECHNICAL JOURNAL

Vol. 17 No. 01 JUNE 2025

RIVER RESEARCH INSTITUTE
MINISTRY OF WATER RESOURCES
GOVT. OF THE PEOPLE'S REPUBLIC OF BANGLADESH

EDITORIAL BOARD

Chief Editor

S M Abu Horayra
Director General
River Research Institute

Executive Editor

Dr. Fatima Rukshana
Principal Scientific Officer
Geotechnical Research Directorate, River Research Institute

Member

Dr. Moniruzzaman Khan Eusufzai
Principal Scientific Officer
Dhaka Office, River Research Institute

Engr. Md. Johurul Islam
Principal Scientific Officer
Hydraulic Research Directorate, River Research Institute

Engr. Md. Zubayerul Islam
Senior Scientific Officer
Geotechnical Research Directorate, River Research Institute

Physicist Nayan Chandra Ghosh
Senior Scientific Officer
Dhaka Office, River Research Institute

Md. Moniruzzaman
Senior Scientific Officer
Geotechnical Research Directorate, River Research Institute

Engr. Omar Al Maimun
Senior Scientific Officer
Hydraulic Research Directorate, River Research Institute

Engr. Bikash Roy
Senior Scientific Officer
Hydraulic Research Directorate, River Research Institute

Mst. Shamima Akter
Librarian
Administration and Finance Directorate, River Research Institute

Engr. Md. Masuduzzaman
Assistant Programmer
Administration and Finance Directorate, River Research Institute

Reviewers Panel of Technical Journal - River Research Institute

Dr. Md. Munsur Rahman
Professor
Institute of Water and Flood Management
Bangladesh University of Engineering and Technology, Dhaka

Dr. Mehedi Ahmed Ansary
Professor
Department of Civil Engineering
Bangladesh University of Engineering and Technology, Dhaka

Dr. Md. Shahidul Islam
Professor and Chairman
Department of Geography & Environment
University of Dhaka, Dhaka

Dr. Nasreen Jahan
Professor and Head
Department of Water Resources Engineering
Bangladesh University of Engineering and Technology, Dhaka

Dr. Sajal Kumar Adhikary
Professor
Department of Civil Engineering
Khulna University of Engineering & Technology, Khulna

Dr. Aysha Akter
Professor and Head
Department of Civil Engineering
Chittagong University of Engineering & Technology, Chittagong

Dr. Mohammed Mizanur Rahman
Professor
Department of Irrigation and Water Management
Bangladesh Agricultural University, Mymensingh

Dr. Md. Rokonuzzaman
Professor
Department of Civil Engineering
Khulna University of Engineering & Technology, Khulna

Dr. G. M. Sadiqul Islam
Professor
Department of Civil Engineering
Chittagong University of Engineering & Technology, Chittagong

Dr. Mohammad Amir Hossain Bhuiyan
Professor
Department of Environmental Sciences
Jahangirnagar University, Dhaka

TECHNICAL JOURNAL
River Research Institute
Vol. 17, No. 01, June 2025

Table of Contents

Note: The last article is a replacement of authorship, published in *Tech.J.RiverRes.Inst.: 13(1): 11-25, October 2016,* without any changes to the original content (* and **).

Technical Journal
River Research Institute ISSN: 1606-9277

Estimating Suspended Sediment Concentration using Acoustic Doppler Current Profiler (ADCP)

S. Ferdhous[1]*, B. Roy[2] and M. Moniruzzaman[1]

Abstract

Suspended sediment concentration (SSC) is an important parameter in the studies of sediment transport and highly important in river management. However, the measurement of SSC still uses conventional techniques. These techniques have limitations, especially in temporal resolution. With advanced technology, the measurement of sediment concentration can be done using hydroacoustic technology such as the Acoustic Doppler Current Profiler (ADCP). The signal-to-noise ratio (SNR) data of ADCP can be used to indicate sediment concentration in the river water. This study evaluated SNR data from ADCP to estimate SSC in the branch channel to the river Padma. The frequencies of ADCP used in this study were 1 MHz and 3 MHz. Calibration and validation of SCC_{ADCP} have been achieved using a linear regression model, considering SSC_{meas} as an independent variable. The linear regression model for the validation of SSC_{ADCP} showed a good relationship with $R^2 = 0.97$ for cross-section 01 and $R^2 = 0.94$ for cross-section 02, respectively. This technique can be highly useful for practical applications, particularly in scenarios where collecting sediment samples is challenging. By utilizing ADCP-based hydroacoustic technology, real-time and continuous monitoring of suspended sediment concentration becomes feasible, overcoming the limitations of conventional sampling methods.

Keywords: *ADCP, Suspended sediment concentration, Signal to Noise Ratio (SNR), Hydroacoustic sediment monitoring, Sediment transport measurement.*

Introduction

Fluvial river systems are used for numerous purposes like water supply, hydroelectric power generation, transportation etc. all over the world. The production of the sediment is one of the effects caused by the use of these systems in the basin (Wosiacki et al., 2018). Sediment is an integral part of river system and plays very important role in the context of sustainability of riverine environments (Bečvář, 2006). Suspended sediment concentration (SSC) is an important parameter in the studies of sediment transport and highly valuable in overall river management and planning (Dwinovantyo et al., 2017; Woochul et al., 2022). The monitoring of fluvial suspended sediment transport is much needed for the assessment of hydro-morphological processes, river environments and many social activities associated with river management (Flóra and Baranya, 2020).

The measurement of SSC in the water column can be conducted in several ways, such as conventional, optical, and acoustic methods (Dwinovantyo et al., 2017). The conventional gravimetric method for the assessment of SSC in laboratory is relatively difficult to achieve because it requires collection of numerous water samples in each point of interest with simultaneous lack of continuous temporal and spatial data (Zhang et al., 2013). Slow and relatively higher measurement cost is another disadvantage of conventional gravimetric method (Holdaway et al., 1999). The measurement of flow velocities in order to determine river discharge is the main application field of Acoustic Doppler current profilers (ADCPs) (Baranya and Józsa, 2013). Over the past two decades, the development of hydroacoustic instrument such as the Acoustic Doppler Current Profilers (ADCP) for measuring water velocity by detecting acoustic energy backscattered from suspended matter in the water column has permitted the detection of suspended sediment with very high temporal and spatial resolution. It is also a substantial advantage for sediment flux estimation that these instruments can return data of both velocity and sediment concentration (Venditti et al., 2016). Recent studies demonstrated good correlation between acoustic backscatter from ADCP and measured concentration by direct measurement (Guerrero et al., 2016). Many researchers also used numerical analysis to compare the measured SSC from ADCP and sediment transport model/ numerical model (Bayram et al., 2012). This paper describes the results of a field experiment where SSC were estimated at multiple layers of depth from the ADCP. The aim of this study was to compare laboratory measured SSC data to SSC data derived from SNR data of ADCP.

Methods

Theoretical Background

The method of conversion of Signal to Noise Ratio (SNR) data into SSC can be done based on the principle of sonar equation (Wall et al., 2006). The direct measurement of SSC can be correlated with SSC data derived from SNR data of ADCP using simple regression linear model. After that, SNR value from the ADCP can be converted into SSC in mg L-1. The relationship between SSC and the relative SNR can be expressed as (Gartner and Ganju, 2007)

[1]Geotechnical Research Directorate, River Research Institute (RRI), Faridpur-7800, Bangladesh.
*Corresponding Author: (E-mail: sumiya_eee@yahoo.com)
[2]Hydraulic Research Directorate, River Research Institute (RRI), Faridpur-7800, Bangladesh.

$SSC=10^{(A+B.SNR)}$ Eq. (1)

where A and B in Eq. (1) are empirical parameters that can be derived from known SSC and SNR data pairs using e.g., least squares fitting.

The corrected signal is the measurement of SNR corrected for transmission losses in units of dB. The corrected signal is computed using the following equation.

Corrected Signal = SNR_{mean} + $10\psi log_{10}$ (R) + $R_{\alpha w}$ + $R\alpha s$ Eq. (2)

where SNR_{mean} is the mean of SNR of the 4 beams of the ADCP along of each vertical, $10log_{10}(\psi R)$ is the spread attenuation, $R_{\alpha w}$ is the water absorption $R_{\alpha s}$ is the sediment attenuation term. Also, R is the slant range from transducer head to measured beam (m). When calculating the effect of spherical spreading close to the transducer, a near-field correction factor ψ has to be introduced, according to Downing et al. (1995). This correction can be calculated based on the critical range $R_{critical}$, where $R_{critical} = \pi a_t^2/\lambda$. Here a is the transducer radius in cm, and λ is the acoustic wavelength. The correction factor for near-field spreading loss is

$$\psi = \frac{1+1.35Z+(2.5Z)^{3/2}}{1.35Z+(2.5Z)^{3/2}}$$ Eq. (3)

where Z equals to $R/R_{critical}$.

In this study, the above presented correction factor was used for near-field calculations of spreading losses.

The speed of sound had been computed by the following equation

$$c = 1404.3 + 4.7T - 0.04T^2$$ Eq. (4)

where T is the water temperature, in °C.

For the estimation of energy dissipation by absorption in the water, we used the formula of Schulkin and Marsh (1962) as follows:

$$\alpha_w = 8.687 \frac{3.3810^{-6}f^2}{21.9\times10^{6-\left[\frac{1520}{273+T}\right]}}$$ Eq. (5)

where f is the acoustic frequency, in kilocycles per second, T is the water temperature, in °C.

Attenuation from suspended sediment (α_s) is caused by both scattering and absorbing the energy. It is shown that energy dissipation depends mainly on particle size and sound frequency (DRL Software Ltd, 2003), and under certain conditions one or both of them can be neglected. We did not consider attenuation due to absorption by the sediment here.

Study Site

The study site is located at North-East of Faridpur Town. A branch channel of the Padma River is flowing there. The study site is situated in the 45Q UTM zone. It lies between 2615000 mN to 2625500 mN and 788700 mE to 794900 mE (**Fig. 1**).

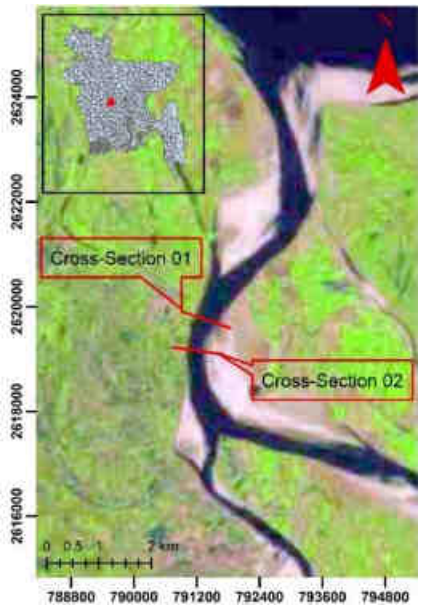

Fig. 1. Location map of Study Site

Materials and equipment

Equipment used in this study was Sontek M9 ADCP. The survey, which involved moving boats operating in two cross-sections with an average distance of 600 meters between them, was conducted in January 2023. All water samples were preserved in pre-cleaned

polyethylene bottles. Water samples were collected in 1-liter bottles from 10 different depths, starting from 2 meters until 10 meters for each 2-meter interval. The amount of water sample was 1 liter. To avoid loss of water volume due to evaporation, the bottles were stored in a cooler box with ice cube (< 4 °C) before analyzing in the laboratory.

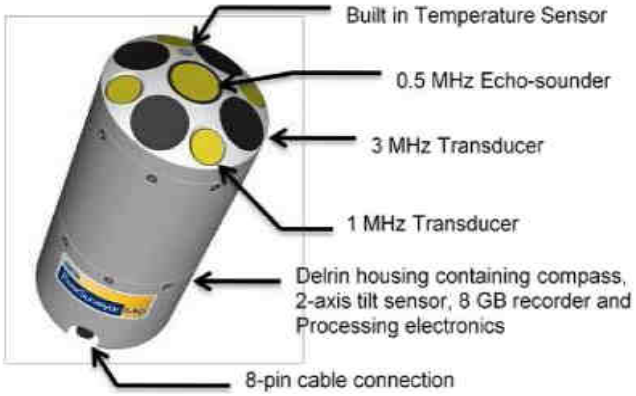

Fig. 2. Different features of Sontek M9 ADCP

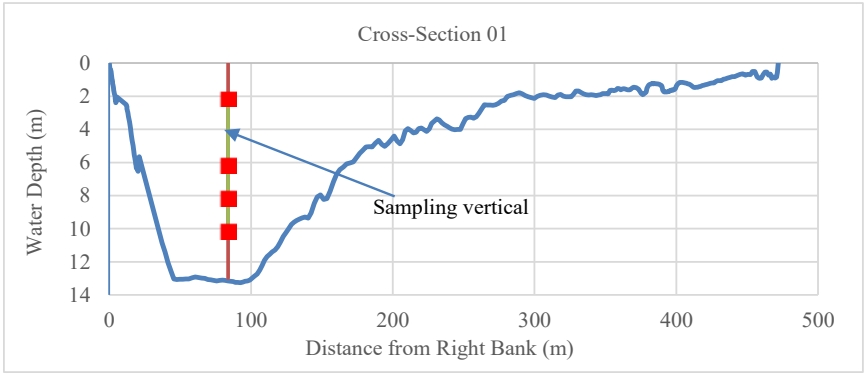

Fig. 3. Cross sectional profile (Section-1)

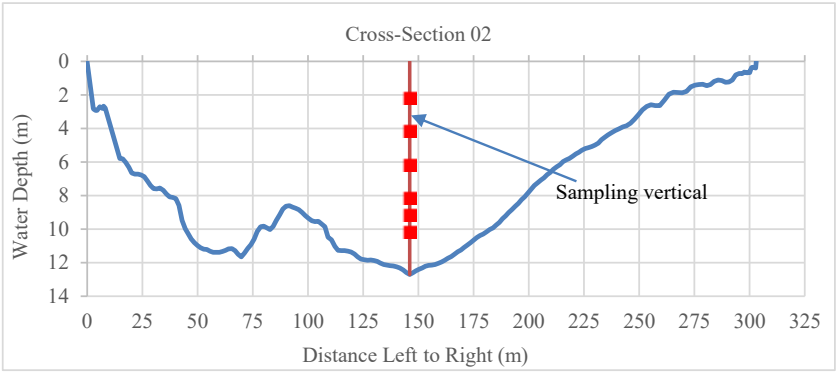

Fig. 4. Cross sectional profile (section-2)

Laboratory Analysis

Suspended sediment concentration of ten (10) river water samples were analyzed in the Sediment Laboratory at River Research Institute, Faridpur. Suspended sediment portion of each sample was separated from the liquid portion by using filter paper (Whatman, 42 ASHLESS). Filter papers with the retained materials were oven dried. The 1 liter of water was then filtered using filter paper (Whatman, 42 ASHLESS). Before the filtration process, the filter paper was dried at a temperature of 105 °C for 1 hour and then the filter paper was cooled in a desiccator and weighed. After water filtration process, filter paper plus residue was dried again for two hours at 105 ˚C (Flóra Pomázi, 2020).

Estimation of suspended sediments concentration

For ADCP-based SSC estimate, direct measurement of SSC with known concentration values requires

calibration. The following formula used to calculate the direct SSC measurement (mg L^{-1})

$$SSC = \frac{(A-B)\times 1000}{\text{Sample Volume, mL}} \quad \text{Eq. (6)}$$

where, A = final weight of filter + dried residue in mg, B = weight of filter in mg.

For final conversion of SSC from $SNR_{corrected}$ value the following relationship $SSC = 10^{(A+B.SNR_{corrected})}$ was used. The values of empirical parameters A and B were determined using least squares fitting between data pairs of SSC_{meas} and $SNR_{corrected}$. And for our case $SNR_{corrected}$ was computed using the following equation-

$$SNR_{corrected} = SNR_{mean} + 10\psi log_{10}(R) + R\alpha_w + R\alpha_s \quad \text{Eq. (7)}$$

Results and Discussion

Calibration curve was built to relate $SNR_{corrected}$ values to SSC_{meas}. The direct measurement of suspended sediment concentration were matched with $SNR_{corrected}$ values from the corresponding depth layer or bin to establish the calibration relationship (Dwinovantyo, 2017). For creating calibration curve, SSC_{meas} was plotted as ordinate and $SNR_{corrected}$ was plotted as abscissa (Venditti et al., 2016).

Table 1. Sample collecting depth with corresponding SNR, SSC_{meas}, SSC_{ADCP} values for Cross-Section 1

Depth (m)	$SNR_{corrected}$ (dB)	SSC_{meas} (mg L^{-1})	$\log_{10}$ (SSC_{meas})	SSC_{ADCP} (mg L^{-1})
2.14	45.90	3.51	0.55	3.85
6.14	38.14	15.81	1.20	12.60
8.14	34.56	20.41	1.31	21.77
10.14	31.76	30.95	1.49	33.38

Fig. 5 (a) displays the results least squares fitting between data pairs of $SNR_{corrected}$ and measured suspended sediment concentration (SSC_{meas}) $\log_{10}$ (SSC_{meas}). It can be seen that empirical parameter values A = 3.629 and B = – 0.0663 with an acceptable fit of coefficient of determination R^2 = 0.974 for cross-section 1. According to **Fig. 5 (b)** the relation between SSC_{ADCP} and SSC_{meas} has strong correlation which R-squared value is 0.97. In such a case Dwinovantyo, et al., (2017) found R-squared value = 0.7196 between SSC_{ADCP} and SSC_{meas} at Lembeh Strait, North Sulawesi, Indonesia.

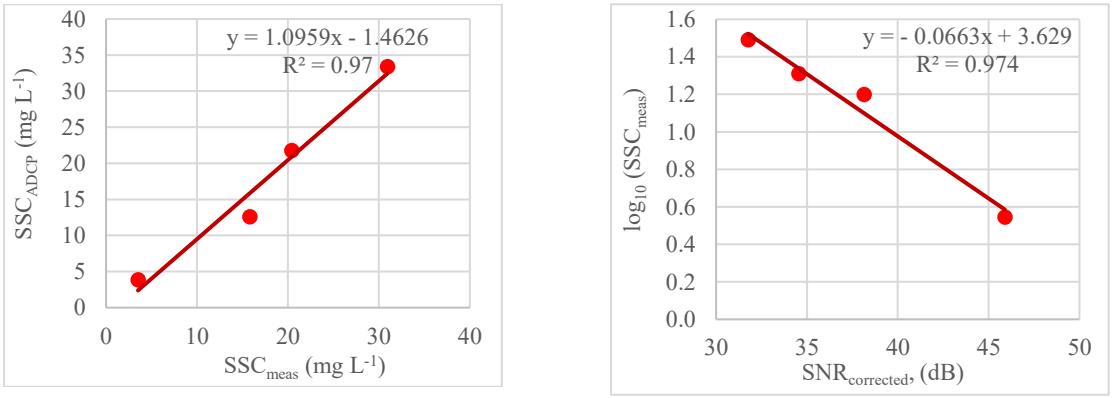

(a) (b)

Fig. 5. (a) Calibration and (b) Validation of SNR using direct sample measurement for the samples collected from cross-section 1

Table 2. Sample collecting depth with corresponding SNR, SSC_{meas}, SSC_{ADCP} values for Cross-Section 2

Depth (m)	$SNR_{corrected}$	SSC_{meas} (mg L^{-1})	$\log_{10}$ (SSC_{meas})	SSC_{ADCP} (mg L^{-1})
2.14	55.80	4.1	0.61	3.84
4.14	41.22	12.6	1.10	15.75
6.14	40.21	18.2	1.26	17.35
8.14	37.26	21.0	1.32	23.10
9.14	35.98	28.2	1.45	26.13
10.14	35.08	32.8	1.52	28.51

Similarly for cross-section 2 least squares fitting had been performed between data pairs of $SNR_{corrected}$ and measured suspended sediment concentration (SSC_{meas}) (**Fig. 6**). This analysis yields the empirical parameter values A = 2.9284 and B = – 0.042 with an acceptable fit of coefficient of determination $R^2 = 0.968$ for cross-section 2. Results of the acoustic method compared to direct measurement shows good agreement showed at **Fig. 6** by $R^2 = 0.9439$ for cross-section 2.

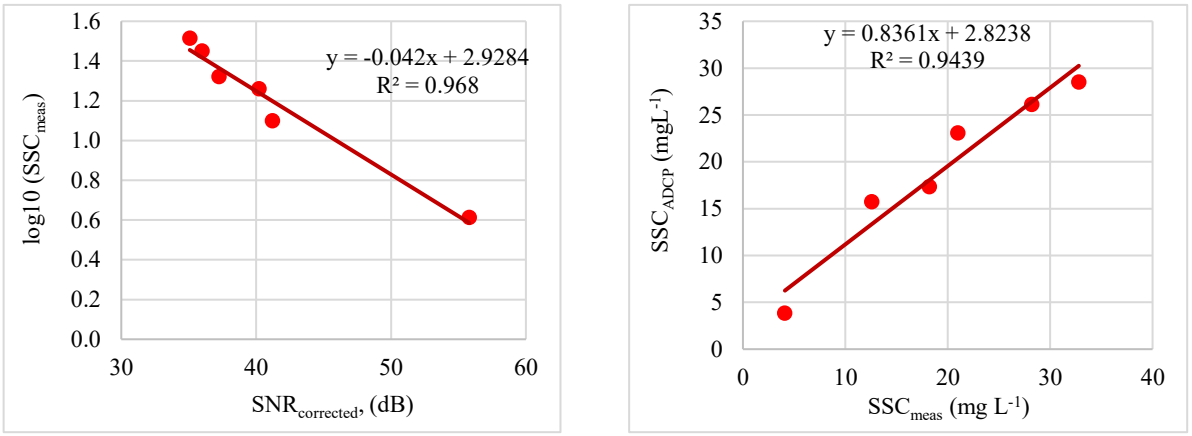

Fig. 6. (a) Calibration and (b) Validation of SNR using direct sample measurement for the samples collected from cross-section 2

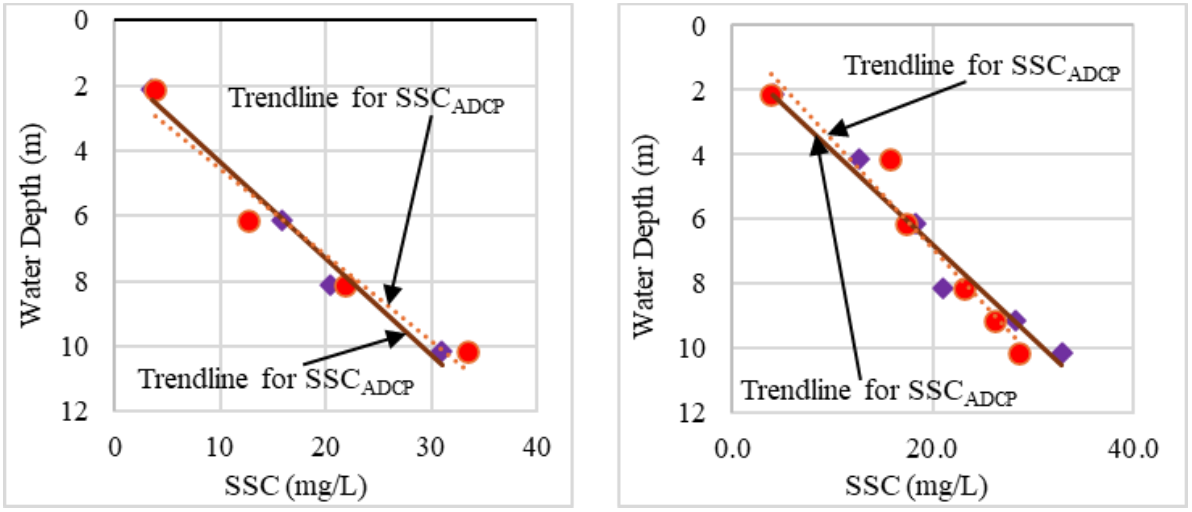

Fig. 7. Depth vs SSC relationship

Another key observation is the depth-dependent variation in SSC. As shown in **Tables 1** and **2** and illustrated in **Fig. 7**, SSC generally increases with depth. This pattern is consistent with natural fluvial dynamics, where coarser or denser particles tend to settle at deeper layers due to gravity and reduced turbulence. The ADCP-based estimates captured these vertical trends effectively, affirming the device's capability to resolve depth-stratified sediment profiles with high resolution.

The implications of these results extend beyond mere accuracy. Utilizing ADCP for sediment concentration monitoring offers a scalable and efficient alternative to conventional sampling, which is labor-intensive and often spatially limited. The ability to derive SSC from SNR in near real-time could be invaluable for sediment budgeting, flood prediction, infrastructure design, and habitat assessment in dynamic river systems like the Padma.

Moreover, despite the study's modest scale—limited by vessel type and sample size—the high correlation values suggest that the method is robust and adaptable to varying field conditions. This strengthens the case for broader adoption of ADCP technology in sediment monitoring, especially in regions with limited access to advanced sampling infrastructure.

Overall, the results demonstrate that SNR data from ADCP not only correlate strongly with direct SSC measurements but also reflect physically meaningful sediment transport processes. These findings support

the feasibility of integrating ADCP-based SSC estimation into routine river monitoring protocols, enhancing both efficiency and data richness.

Limitations

The limitation of the current study is that the sample size is not large. In this study, the usual motorized boat was used as a survey vessel, not a specialized one suitable for survey purposes. It is very difficult to maintain a particular transect (cross-section line) for the ADCP survey and sample collection using the usual motorized boat.

Conclusion

Suspended sediment concentrations could be estimated using the Signal-to-Noise Ratio (SNR) data. The SNR results confirmed a comparable estimation performance with respect to those given by direct measurement of SSC. The error of estimation between ADCP and direct measurement was not more than 5 mgL^{-1}. The monitoring of SSC with ADCP could be considered a good method to observe time series data of SSC, where it is usually not possible with conventional measurement. Although ADCP shows potential for estimating SSC quickly, several issues remain to be explored, such as the Rayleigh parameter for different grain sizes of suspended sediment, a better understanding of instrument error, and the need for a water sample analysis to calibrate the sonar equation. However, we are sanguine that this study will usher in new prospects for the estimation of sediment concentration using SNR data from ADCP.

Conflict of Interest

The authors declare no conflict of interest.

References

Baranya, S. and Józsa, J. (2013). Estimation of suspended sediment concentrations with ADCP in Danube River. *J. Hydrol. Hydromech. 61*(3): 232-240.

Bayram, A., Kankal, M. and Önsoy, H. (2012). Estimation of suspended sediment concentration from turbidity measurements using artificial neural networks. *Environ. Monit. Assess. 184*: 4355-4365.

Bečvář, M. (2006). Sediment load and suspended sediment concentration prediction. *Soil & Water Res. 1*(1): 23-31.

Dwinovantyo, A., Manik, H. M., Prartono, T. and Susilohadi, S. (2017). Quantification and analysis of suspended sediments concentration using mobile and static acoustic Doppler current profiler instruments. *Advances in Acoustics and Vibration.* 2017 (4890421): 1-14.

Gartner, J. W. and Ganju, N. K., (2007). Correcting acoustic Doppler current profiler discharge measurement bias from moving-bed conditions without global positioning during the 2004 Glen Canyon Dam controlled flood on the Colorado River, Limnol. Oceanogr.: *Methods 5*(6): 156-162.

Guerrero, M., Rüther, N., Szupiany, R., Haun, S., Baranya, S. and Latosinski, F. (2016). The acoustic properties of suspended sediment in large rivers: consequences on ADCP methods applicability. *Water. 8*(1): 13.

Holdaway, G. P., Thorne, P. D., Flatt, D., Jones, S. E. and Prandle, D. (1999). Comparison between ADCP and transmissometer measurements of suspended sediment concentration. *Continental Shelf Research. 19*(3): 421-441.

Kang, W., Lee, K. and Kim, J. (2022). Prediction of suspended sediment concentration based on the turbidity-concentration relationship determined via underwater image analysis. *Appl. Sci. 12*(12): 6125.

Pomázi F. and Baranya S. (2020). Comparative Assessment of Fluvial Suspended Sediment Concentration Analysis Methods. *Water*. 2020, 12, 873; doi:10.3390/w12030873.

Pomázi, F. and Baranya, S. (2020). Comparative assessment of fluvial suspended sediment concentration analysis methods. *Water. 12*(3): 873.

Venditti, J. G., Church, M., Attard, M. E. and Haught, D. (2016). Use of ADCPs for suspended sediment transport monitoring: An empirical approach. *Water Resources. Res. 52*(4): 2715–2736.

Wall, G. R., Nystrom, E. A. and Simon, L. (2006). Use of an ADCP to compute suspended-sediment discharge in the tidal Hudson River, New York. U.S. *Geological Survey Scientific Investigations Report* 2006-5055, 16 p.

Wosiacki, L. F. K., Suekame, H. K., Carvalho, G. A., Campos, M., Gonçalves, F. V. and Bleninger, T. (2018). Suspended sediment estimative through an ADCP analysis-Study Case: Taquari River, Pantanal, Brazil. *The XIII Brazilian Meeting of Sediment Engineering. Hotel Comfort Suítes Vitória, Vitória -*

Espírito Santo, Brazil, 24 – 28 September. ISSN: 2359-2141.

Zhang, T., Stansbury, J. and Branigan, J. (2013). Development of a field test method for Total Suspended Solids analysis. *Final Reports & Technical Briefs from Mid-America Transportation Center 52*.

Technical Journal
River Research Institute ISSN: 1606-9277

Irrigation Challenges and Opportunities in the Selected Polders of Coastal Bangladesh

M. M. Rahman[1]*

Abstract

The agricultural sector in Bangladesh, crucial for economic stability and food security, faces significant climate change-induced challenges, especially in coastal polders. This study examines irrigation challenges and opportunities in these regions, focusing on rising food demand and climate change impacts. The construction of 139 polders in the 1960s initially boosted productivity but later caused river siltation, waterlogging, and reduced freshwater availability. Using system dynamics modeling, this research evaluates irrigation demands and solutions under various scenarios, including salinity-tolerant crops and policy interventions like canal re-excavation and groundwater management. Findings reveal disparities in water availability across six selected polders. Monsoon rainfall supports irrigation, but dry-season Boro cultivation is constrained by high surface water salinity. Groundwater is largely unsuitable, except in Polder 29 and Polder 17/1, where salinity remains within limits. Future projections indicate increased irrigation demands, particularly for Polder 29 and Polder 17/1, which can be met through sustainable groundwater use and canal rehabilitation. In contrast, polders like 35/1 and 46 require canal re-excavation to enhance water storage. Rising sea levels and soil salinity are expected to reduce cultivable land, though salt-tolerant crops may partially offset losses. Policy interventions prioritizing surface water management, including canal excavation, are essential to mitigating water scarcity. This research highlights the need for integrated water resource management and climate adaptation strategies, offering insights to guide sustainable irrigation practices in Bangladesh's vulnerable coastal regions.

Keywords: *Cause and loop diagram, Climate change, Coastal zone, Groundwater, Irrigation, Surface water, Stock flow diagram, System dynamics (SD) model.*

Introduction

Agriculture is one of the most paramount sectors of the economy of Bangladesh together with ready-made garments (RMG), remittances, and others (Islam and Haque, 2018; Rahman, 2017). Traditionally, Bangladesh is an agricultural country characterized by fertile land and a favorable climate for crop production, with approximately 83% of the rural population relying on agriculture for their livelihoods. Of the cultivable land, 28% is dedicated to single cropping, 49% to double cropping, and 22% to triple cropping, while 5% remains fallow (BBS, 2018). However, the sector faces significant challenges, including rising food demand from a growing population and the decline of agricultural land due to urbanization and hydro-climatic hazards such as salinity and waterlogging (IWWI, 2015; Mainuddin and Kirby, 2015). Bangladesh is particularly vulnerable to climate change, experiencing severe impacts like sea-level rise, salinity and storm surge which threaten agricultural productivity, especially in the low-lying coastal areas where 28% of the population resides (Brammer, 2014; Hossain and Majumder, 2018; Xiaoying and Sikder, 2014). Recent studies have highlighted that soil and water salinity levels in coastal areas such as Assasuni, Dacope, and Morrelganj have continued to rise, particularly affecting irrigation availability in the dry season (Shapna et. al., 2024). These issues result in lower crop intensity in the southwest coastal zone compared to the national average (Rashid et al., 2018). Additionally, rising temperatures due to climate change onward to higher evapotranspiration rates, increasing the water requirements for agriculture (Dang et. al., 2024). While agricultural activities in the wet season primarily rely on rainwater, dry season crops depend heavily on irrigation. However, elevated salinity levels render surface water unsuitable for irrigation during this period.

Challenges in Polder Irrigation Water Management

To make the land productive, the government of Bangladesh constructed 139 large-scale polders with the help of donors, occupying 1.2 million hectares and involving 5,107 km of embankments, water control structures, drainage canals, and storage channels in the 1960s and 1970s. Polders were constructed in the coastal zone to protect communities from tidal flooding, and salinity intrusion, and make agricultural land more productive (Islam and Rahman, 2015; Rahman and Rahman, 2015). The polders had an immediate and significant impact on agricultural output, which increased in the first 10-15 years (Nowreen et al., 2014). This infrastructure enabled greater access to markets for trading goods, resulting in a boost in income and standard of living for people.

However, after a few decades, negative consequences of the polders have risen (Deb, 1998; Paul et al., 2013; Rahman et al., 2010). Polder construction has significantly altered the sediment balance in the delta, inducing subsidence and waterlogging in some of the polders (Ahmed, 2011; Islam et al., 2002). The intrusion of storm surge saline water causes long-term problems for crops and drinking water sources. After a storm surge, a long time is needed to drain out saline water due to the low elevation difference between the river and the inside polder. Moreover, the lack of proper functioning of water control structures (sluice

[1]Institute of Water and Flood Management (IWFM), Bangladesh University of Engineering and Technology, Dhaka 1000, Bangladesh.
*Corresponding Author: (E-mail: mostafizsust@gmail.com)

gates, inlets, outlets) allows saline water to intrude during the dry season, polluting stored freshwater in canals intended for irrigation and domestic use. Over time, canals have become silted up due to poor maintenance and topsoil erosion from nearby land (Ahsan et. al., 2022, Shawkhatuzamman et. al., 2023).

The present research highlights the growing threats of salinization and waterlogging in Dutch polders, which are driven by climate change, sea-level rise, and intensified agricultural activity. Van Der Burg et. al., (2024) outline five key adaptation strategies to maintain agricultural productivity under saline conditions: development of salt-tolerant crop varieties, cultivation of halophytes, application of soil management techniques, use of bio stimulants, and implementation of advanced irrigation systems. These strategies are assessed for sustainability across environmental, social, and economic dimensions. Complementary to these findings, Ritzema and Stuyt (2014) discuss land drainage strategies to cope with climate change in the Netherlands, emphasizing the importance of controlled drainage systems to manage water levels and mitigate salinization in polders.

Rainfall is generally sufficient to meet the irrigation water demand for the Kharif I and Kharif II seasons, with only a small amount of irrigation needed during the transplanting stage of Kharif II. This demand is typically satisfied using surface water, as salinity levels are acceptable for irrigation during the Kharif II or monsoon season. However, dry season crops primarily depend on irrigation, and raised salinity levels during this period reduce surface water unsuitable for agricultural use. Consequently, the lack of irrigation water restricts crop cultivation in the dry season within the coastal zones of Bangladesh. Groundwater in most polders in the southwest coastal region is also unsuitable for irrigation and domestic purposes due to high salinity, and failing to meet drinking water standards (Bahar and Reza, 2010). As a result, irrigation in these polders relies heavily on surface water during the dry season. Unfortunately, since the construction of the Farakka Barrage, surface water salinity has increased due to reduced upstream flow during dry periods (Mahtab and Zahid, 2018). Furthermore, high salinity in irrigation water significantly reduces yields for Boro and Aman paddy (Khanom and Salehin, 2012). However, research indicates that improving canal systems for storing fresh water, such as rainwater, could enhance crop production and increase cultivated land (Ahmed and Islam, 2013; Begum et al., 2024; Sharifullah et al., 2008). Another significant challenge for agriculture in the polder areas is the increasing salinity caused by rising sea levels, which reduces the amount of cultivable land.

In light of these challenges, the present study aims to assess future irrigation water demand under various plausible scenarios and explore potential irrigation options for dry season Boro crops in selected polders of the southwest coastal zones of Bangladesh using a system dynamics approach.

Methodology

Study area selection

For this study, Polder 17/1, Polder 29, Polder 32, Polder 35/1, Polder 43/2F, and Polder 46 from the southwest and south-central regions of coastal Bangladesh were selected to investigate irrigation water availability for Boro and rabi crops during the dry season (**Fig. 1**). Additionally, plausible options and interventions for improving irrigation water availability were analyzed in light of climate change scenarios.

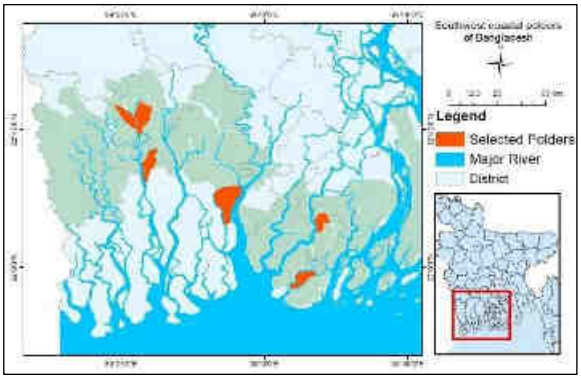

Fig. 1. Selected study polders

Data collection

Secondary data on rainfall, groundwater, water control structures, polder canals, water quality, agriculture, and irrigation were collected from sources like BMD, BWDB, BBS, and various reports. These included rainfall records, groundwater depth, canal specifications, water quality metrics, and agricultural statistics. Additionally, primary data were gathered through Key informant interviews (KIIs), focus group discussions (FGDs) and group discussions (GDs), and interviews to understand local perceptions of irrigation water scarcity, assess cultivated land, and explore potential solutions. Union Parishad members and Upazila agriculture officers provided insights on Boro cultivation areas, irrigation sources, and related challenges.

Model Development

The System Dynamics (SD) model integrates both qualitative/conceptual and quantitative/numerical modeling methods. Qualitative modeling, such as using a causal loop diagram (CLD), enhances our conceptual understanding of the system. Quantitative modeling, such as employing a stock-and-flow diagram (SFD), allows us to investigate and visualize the effects of

different intervention strategies through simulation. The model incorporates biophysical and socio-economic elements, including surface water (SW), groundwater (GW), rainfall, water control structures, crop water requirements, population, and more. These elements are interconnected through 'cause and effect' relationships. Detailed descriptions of each modeling step are provided in the following sections. The model was developed using the Vensim DSS tool by Ventana Systems Inc., Harvard, Massachusetts, USA (Ventana Systems, 2019).

Causal Loop Diagram for qualitative model development

In a causal loop diagram (CLD), system elements are interconnected by arrows that link cause-and-effect variables to form causal chains. **Fig. 2** illustrates the causal loop diagram, featuring positive (+) and negative (-) signs to indicate the nature of these relationships. A positive sign denotes a direct relationship between variables: when the causative variable increases, the effect variable also increases, and conversely, a decrease in the causative variable results in a decrease in the affected variable. For example, an increase in population leads to higher food requirements, which in turn drives an increase in cultivated land within a tolerable threshold, assuming other variables remain constant. In contrast, a negative sign indicates an inverse relationship between the variables; for instance, increased groundwater consumption results in a decrease in groundwater levels. Feedback loops are a crucial component of the system dynamics model, and they can be categorized into two types: balancing loops (B) and reinforcing loops (R).

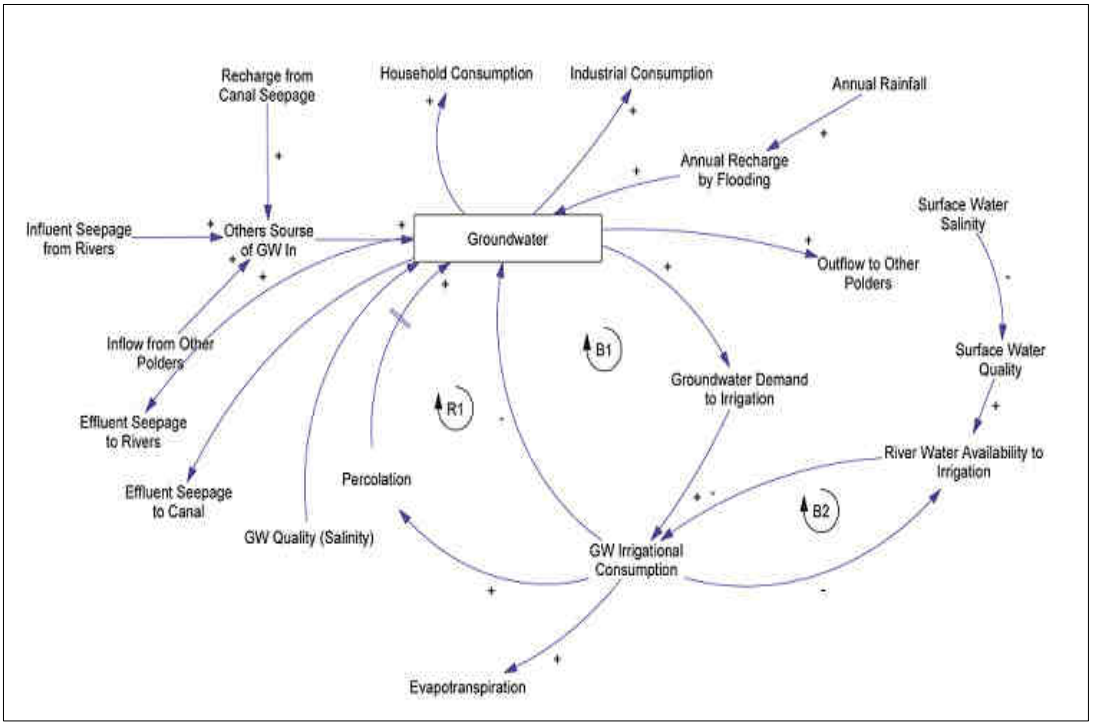

Fig. 2(a). Groundwater component with irrigation water demand.

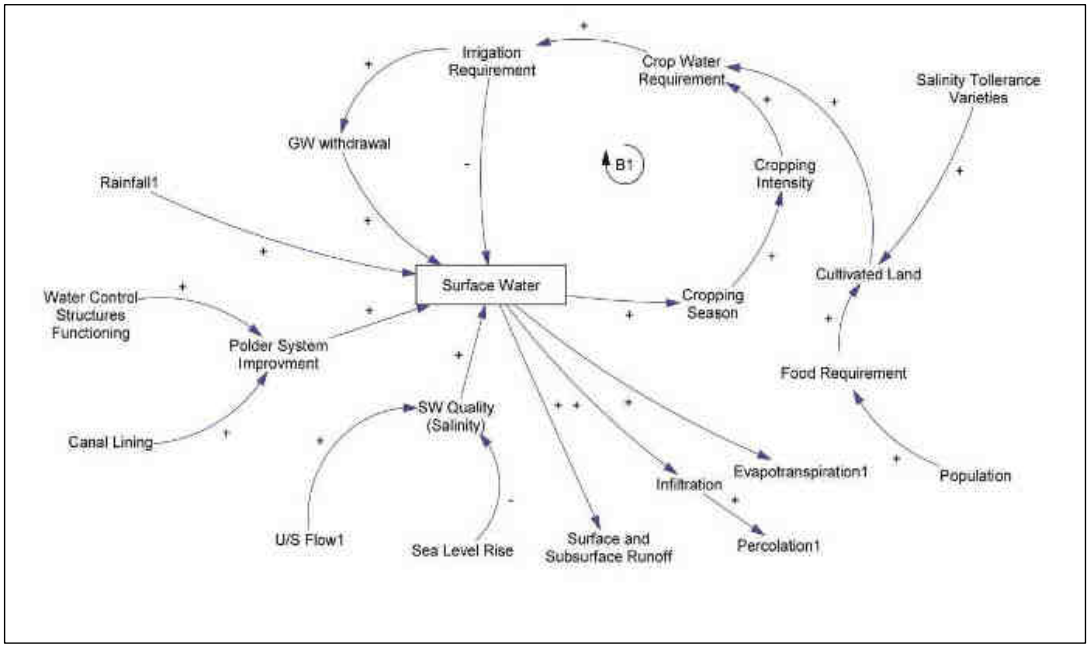

Fig. 2(b). Surface water component with irrigation water demand.

Fig. 2. CLD of the study model. Arcs describe the directions of influence. A positive arc reads as "an increase in variable A leads to an increase in variable B". A negative arc reads as "an increase in variable A leads to a decrease in variable B".

Stock Flow Diagram for Quantitative Model Development

A causal loop diagram was used to visually represent the system, while a stock-flow diagram was used for quantitative analysis. This included deterministic, stochastic, and empirical equations. The stock-flow diagram, shown in **Fig. 3** illustrates how rainfall, water volume, pluvial flooding, and crop losses are connected. The detailed mathematical equations are explained in the following sections.

Surface and groundwater

Groundwater volume at any time can be computed by Eq.

$$Stock\ (t) = \int_0^{t_n} [GW(t) + GR(t) - I(t)]dt + GWL\ (t_0) \qquad \text{Eq. (1)}$$

Where, GW(t) = Groundwater level, GR(t) = Groundwater recharge, I(t) = Irrigation water withdrawal from groundwater, GWL (t_0) = Groundwater level t_0

Groundwater, surface water at any time can be computed by Eq. (2):

$$Stock\ (t) = \int_0^{t_n} [SW(t) + SWI(t) - SWO(t)]dt + SWL\ (t_0) \qquad \text{Eq. (2)}$$

Where, SW(t) = Surface water volume, SWI(t) = Surface water inflow, SWO(t) = Surface water outflow

SWL (t_0) = Surface water volume t_0

Population

Projection of population of polders logistic growth method has been implied. If P_0, P_1 and P_2 are the populations of an area at time t_0, t_1 and t_2, the saturation population equivalent to the carrying capacity of the area can be calculated using the following equation.

$$Saturation\ population, Ps = \frac{2P_0P_1P_2 - [P_1 \times P_1(P_0 + P_2)]}{(P_0P_2 - P_1P_1)} \qquad \text{Eq. (3)}$$

Sea Level Rise

This study assumes a linear increase in the sea level over time, based on IPCC projection. The SL, at a given time, is calculated by:

$$SL_t = \int dRdt + SL_0 \qquad Eq. (4)$$

Where SL_t is the linear sea level at time t, dR is the rate of rising at each time step dt, and SL_0 is the initial sea level at the beginning of the simulation. According to the IPCC 5th assessment report, in the GBM delta, sea level may rise 0.63 to 0.88 m by 2090 (Kay et al., 2015).

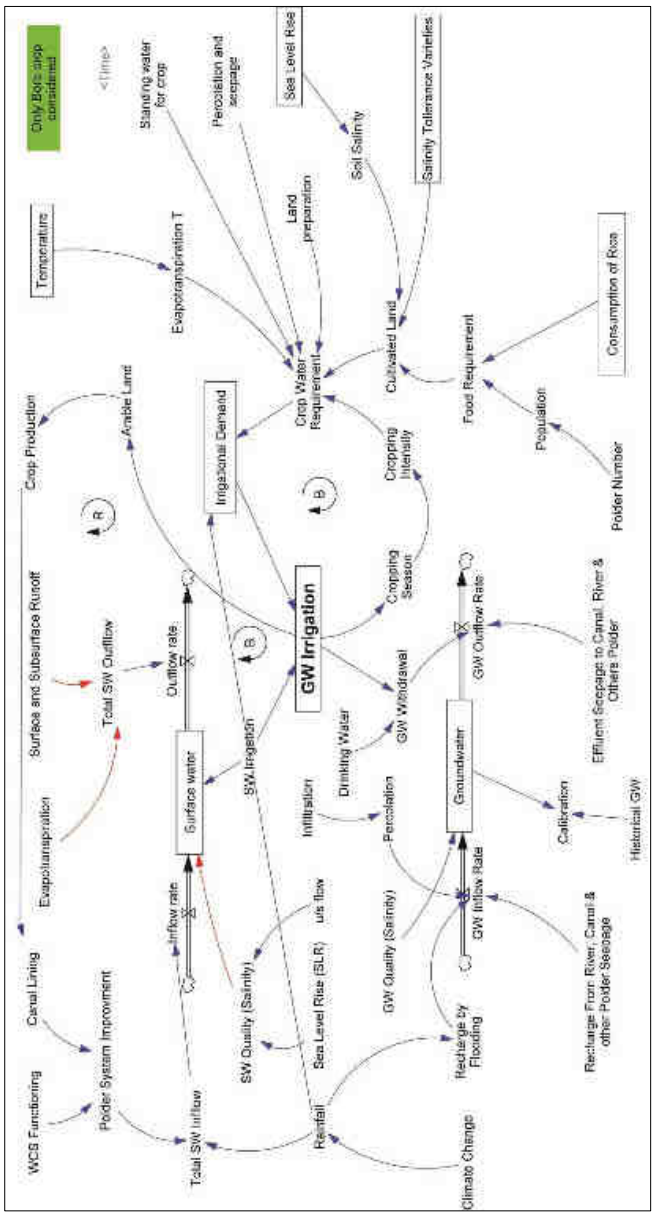

Fig. 3. SFD of the study model. Boxed variables represent stocks, double arrows represent flows that increase or decrease stock levels.

Groundwater quality

Detailed groundwater scenarios of selected polders are shown in **Table 1.**

Table 1. Different aquifers' salinity level (dry season), March 2012 (Data Source: IWM, CEIP, Blue Gold).

Polder No	1st (upper shallow) aquifer (up to 30m) EC (µS-cm^{-1})	1st (lower shallow) aquifer (up to 100m) EC µS-cm^{-1})	2nd Aquifer (above 100m) EC (µS-cm^{-1})	Remarks
Polder 17	1000-3000	<2000	<1000	usable
Polder 29	1000-3000	<2000	<1000	usable
Polder 32	8000-9000	6000-7000	4000-5000	Not usable
Polder 35	13000-14000	8000-9000	7000-8000	Not usable
Polder 43/2F	14000	13600	941	Not usable
Polder 46	27400	30000	21000	Not usable

Surface water salinity

Table 2 shows the salinity level of different polders of different coastal areas.

Table 2. Different polders surface water salinity level (Data Source: CEIP, Blue Gold, BWDB).

Polder Name	River	District	Upazila	Date of sampling	EC (µS-cm^{-1})
Polder 29	Bhadra, Haparkhali	Khulna	Dumuria, Batiaghata	11.11.2012	323
				08/12/2012	1710
				20/01/2013	3060
Polder 17/1	Teliganga-Gengrail	Khulna	Dumuria	11.11.2012	475
Polder 32	Shibsa, Bhadra,	Khulna	Dacope	08/11/2012	1790
	Chunkuri,			15/12/2012	2510
	Sutarkhali			20/01/2013	4850
Polder 35/1	Baleswer, Bhola,	Bagerhat	Sarankhola	29.11.2012	1415
	Sannasir Khal			22.12.2012	1680
				27.10.2013	2080
Polder 43/2F	Gulishakhali,	Barguna	Amtali	06.10.2012	203
	Payra, Kukua			10.12.2012	315
				21.02.2012	580
Polder 46	Tiakhali, Nilakhi	Patuakhali	Kalapara	05.10.2012	441

Canal storage

The present canal capacity of selected polders, design capacity and dry season capacity are shown in **Table 3**.

Table 3. The length and the capacity of canals of selected polders (Data sources: Blue Gold, CEIP, BWDB).

Polder No	Length (km)	Design Capacity (Mm^3)	Present capacity (60% of design capacity) (Mm^3)	Present capacity during monsoon (60% of present capacity) (Mm^3)	Design Capacity during Monsoon (60% of design capacity) (Mm^3)
Polder 29	157.00	6.62	3.97	2.38	3.97
Polder 43/2F	93.50	2.63	1.58	0.95	1.58
Polder 32	70.00	4.30	2.58	1.55	2.58
Polder 35/1	251.26	7.08	4.25	2.55	4.25
Polder 17/1	58.00	3.14	1.88	1.13	2.35
Polder 46	71.84	1.43	0.86	0.51	0.86

Irrigation water requirements

The FAO model was used to determine the irrigation water requirement of the Boro crop. According to this model, total irrigation water requirement can be calculated as,

$$W_{irr} = ET_{crop} + W_{lp} + W_{ps} + W_l - P_e \quad Eq.\ (5)$$

Where, W_{irr} – Irrigation water requirements
ET_{crop} - Crop evapotranspiration
W_{lp} – Water required for land preparation
W_{ps} – Percolation and seepage losses of water from the field
W_l – Water to establish a standing water layer
P_e – Effective precipitation

Crop evapotranspiration is calculated as,

$$ET_{crop} = K_c * ET_{ref} \qquad Eq.\ (6)$$

Where K_c is the crop coefficient, and ET_{ref} is the reference evapotranspiration. The Penman-Monteith method was used to calculate reference evapotranspiration from climate data.

Results and Discussion

Model verification

The model verification results showed a strong alignment between simulated and historical Boro cultivated land percentages. In Polder 29, the model estimated 22.0% cultivation in 2008, while historical data ranged from 13.0% to 21.0%. For 2015, the model predicted 23.8%, closely matching the historical 23.3%. Similarly, in Polder 17/1, the model estimated 21.7% in 2008, with historical data ranging from 12.0% to 22.0%, and for 2015, the model projected 23.0% compared to the observed 23.4%. These results confirm the model's accuracy in simulating Boro cultivation trends.

Scenario development

Three scenarios and two policies were considered in the study. The first scenario, "Business as Usual," assumes that Boro-cultivated land will expand with increasing food demand while other factors remain unchanged. The second scenario incorporates climate change impacts, including rising temperatures (Increased 4°C by 2100; Fahad et al., 2018), sea-level rise (0.63 to 0.88 m by 2090; Kay et al., 2015), and rainfall increased -8.22 % in dry by 2080 for southwest (SW); Fahad et al., 2018. The third scenario explores the use of salinity-tolerant crop varieties to adapt to changing conditions. In terms of policy interventions, two options were evaluated: surface water management through re-excavation and excavation of polder internal canals, and groundwater management by installing tube wells to enhance irrigation capacity.

The present condition of irrigation

Rainfall typically provides enough water to meet irrigation needs during the Kharif I and Kharif II seasons. However, a small amount of additional irrigation is required during the transplanting stage of Kharif II. This irrigation is generally supplied using surface water, as its salinity levels remain suitable for irrigation throughout the Kharif II or monsoon season. However, dry season crops, particularly Boro rice, primarily rely on irrigation, and higher salinity levels during this period reduce surface water unsuitable for agricultural use. Groundwater in most polders is also not viable for irrigation, leading to significant fallow land during the dry season. Farmers in some areas of the selected polders cultivate sesame, vegetables, and Boro rice during this time. **Table 4** presents the present cultivated land, irrigation water demand, and sources of irrigation. The table indicates that irrigation water is not required for sesame and vegetables. Polder 29 and Polder 17/1 have higher cultivated land areas compared to other polders, and their irrigation demand is also greater. Surface water is the primary source of irrigation for all polders, except for Polder 29 and Polder 17/1, which predominantly depend on groundwater for irrigation, with only 20% of their irrigation sourced from surface water. Polder 43/2F does not require irrigation water as there is no Boro cultivation due to socio-economic factors. Although this polder has access to both groundwater and surface water sources, farmers do not cultivate Boro rice, as it is considered less profitable than other crops. Farmers primarily use shallow tube wells for groundwater irrigation and low-lift pumps (LLPs) for surface water irrigation.

Table 4. Present condition of dry season irrigation (estimated).

Polder No	Boro cultivated land (ha)	Sesame and Vegetables cultivated (ha)	Water requirement (mm)	Water Used (Mm^3)	Type of irrigation	GW used (Mm^3)	SW used (Mm^3)
P29	1273		1220	15.53	Groundwater irrigation is provided in 80% of areas, the remaining portion is provided by LLPs	12.20	3.33
		219	300	0.66	No irrigation is required	-	-
P17/1	935		1220	11.41	Groundwater irrigation is provided in 80% of areas, the remaining portion is provided by LLPs	9.13	2.28
		177	300	0.53	No irrigation is required	-	-
P43/2F			1220	0.00	Surface water irrigation	-	-
		623	300	1.87	No irrigation is required	-	-
P32	300		1220	3.66	Surface water irrigation	-	3.66
		270	300	0.81	No irrigation is required	-	-
P35/1	225		1220	2.75	Surface water irrigation	-	2.75
		4910	300	14.73	No irrigation is required	-	-
P46	28.88		1220	0.35	Surface water irrigation	-	0.35
		1917	300	5.75	No irrigation is required	-	-

Future Boro cropland under different scenarios

The scarcity of quality irrigation water during the dry season limits the cultivation of Boro rice and other crops. Despite these challenges, some farmers manage to grow Boro rice, sesame, and vegetables, while many others leave their land fallow. This study simulates future Boro rice cultivation under a business-as-usual (BAU) scenario, which considers the increasing food demand from the growing population without accounting for factors such as climate change, sea-level rise, soil salinity, or the introduction of salt-tolerant varieties (STVs). In the BAU scenario, it is assumed that the area dedicated to Boro crops will increase in response to rising food demand, while the impacts of climate change and salt-tolerant varieties are not factored in. Conversely, the climate change (CC) scenario anticipates a decrease in Boro cropland due to the exacerbation of soil salinity caused by climate change and rising sea levels. Additionally, the introduction of salt-tolerant varieties is considered in a separate scenario, which represents two competing situations: an increase in Boro cropland due to the availability of improved crop varieties, and a decrease in Boro cropland resulting from climate change-induced soil salinity. **Fig. 4** shows future simulated Boro cropland under different scenarios for six selected polders. The figure shows that Boro rice land will increase in the BAU scenario for all polders, but the land will decrease in the climate change scenario. Instead of a negative impact, salt tolerant variety will positively impact Boro rice cropland.

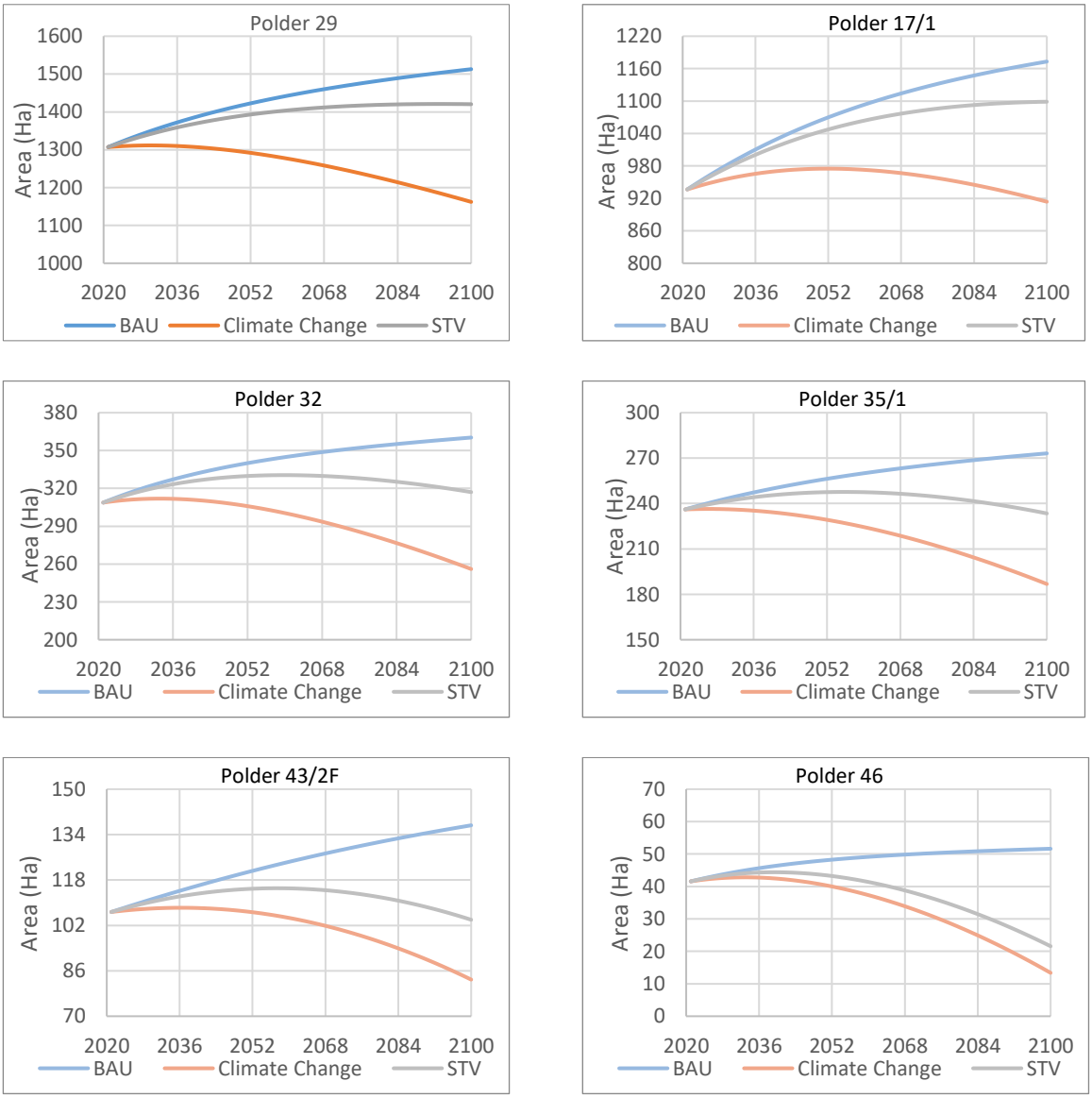

Fig. 4. Boro cropland areas under business as usual (BAU), climate change, salt tolerant crop variety (STV) scenarios.

Fig. 5 illustrates the future simulated water demand for Boro crops under three scenarios: business-as-usual (BAU), climate change, and salt-tolerant crop variety (STV). In the BAU scenario, water demand is projected to increase as Boro cultivation expands to meet the growing population's food demand. However, in the climate change scenario, Boro water demand is expected to decrease due to increasing soil salinity, which will ultimately reduce the land available for Boro cultivation. The introduction of salt-tolerant crop varieties is expected to increase Boro water demand, as more land will come under cultivation. Changes in evapotranspiration due to rising temperatures will also impact water demand, although the effect is not significant. Boro crop water demand is higher in Polder 29 and Polder 17/1 because more land will be cultivated due to lower soil salinity levels. In Polder 43/2F, the change in Boro water requirement is not significant because people are not interested in Boro cultivation due to socioeconomic factors. In the other polders, Boro crop water demand is not as high because more land will not come under cultivation due to higher soil salinity levels.

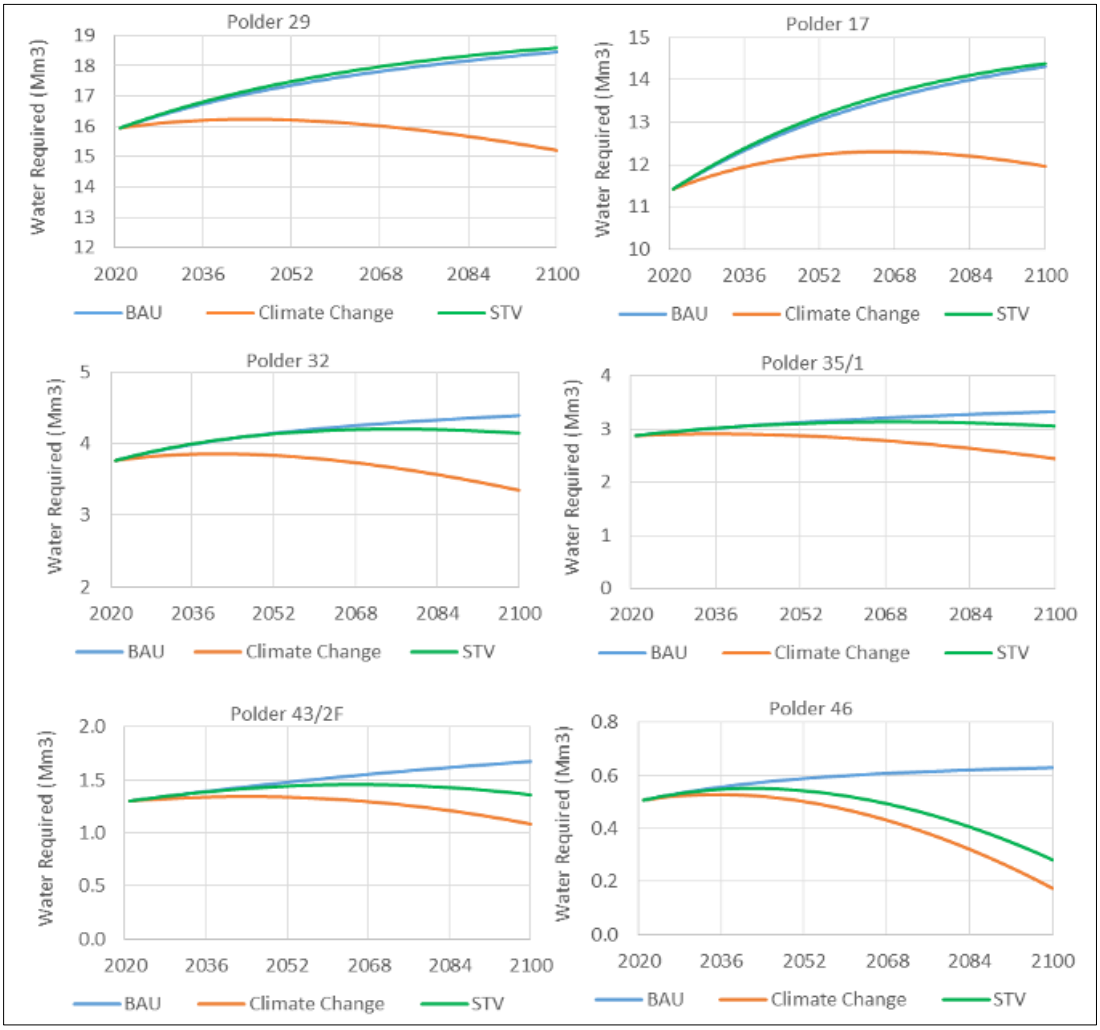

Fig. 5. Boro water requirement under business as usual (BAU), climate change, salt tolerant crop variety (STV) scenarios.

Crop water versus irrigation water

Fig. 6 illustrates the total crop water requirement and irrigation water demand. While rainfall during the dry season is limited, it still contributes to meeting crop water needs alongside irrigation. Boro rice, however, relies primarily on irrigation water to satisfy its water requirements.

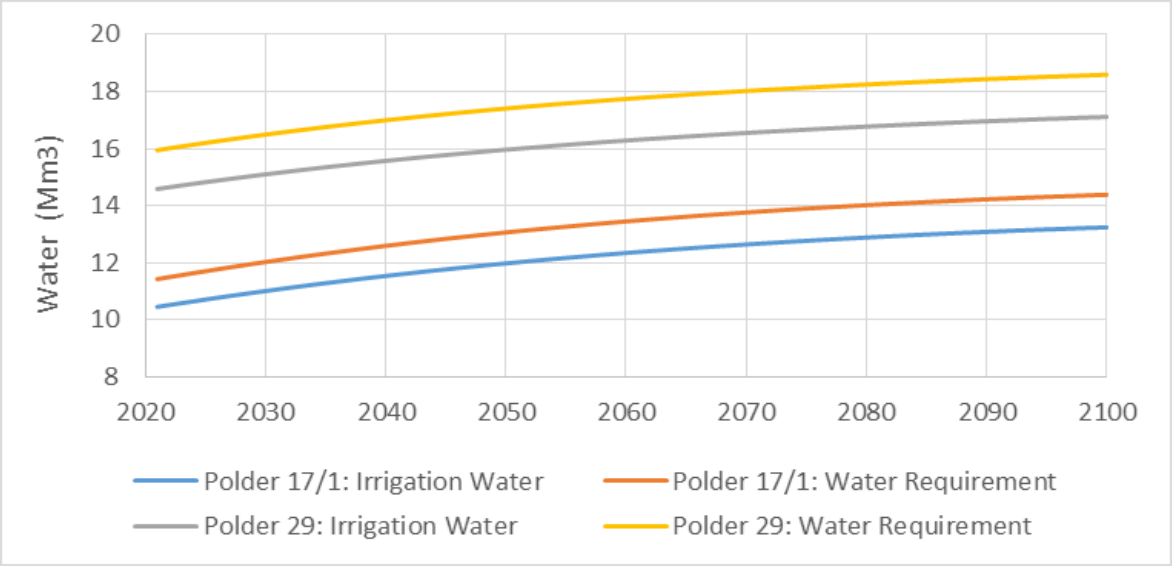

Fig. 6. Crop water requirement versus irrigation water requirement

Surface and groundwater availability for irrigation

Table 5 presents the current and future irrigation water demand and sources for six selected polders. It indicates that Polder 29 and Polder 17/1 possess sufficient groundwater potential to expand Boro cultivation. Although Polder 43/2F has access to both groundwater and surface water for irrigation, the future irrigation water demands of Polder 35/1, Polder 46, and Polder 43/2F can only be met through the re-excavation of existing canals. In contrast, Polder 32 will require the excavation of new canals to satisfy its future irrigation water needs. Overall, re-excavation of canals across all polders is essential to enhance their storage capacity.

Table 5. Future irrigation water, its sources and probable interventions for selected polders.

Polder No.	Year	Irrigation water demand (Mm^3)	Sources of water		Interventions & remarks
			SW (Mm^3) (Present and after re-excavation)	GW (Mm^3)	
P 29	2021	14.59	2.92	11.67	Have groundwater potential
	2050	15.96	4.63	11.33	
	2100	17.11	4.63	12.48	
P 17/1	2021	10.45	2.09	8.36	Have groundwater potential
	2050	11.98	2.20	9.89	
	2100	13.24	2.20	11.15	
P 35/1	2021	2.63	3.54	No need & not usable	Need re-excavation of canal
	2050	2.84	4.96	No need & not usable	
	2100	2.81	4.96	No need & not usable	
P 32	2021	3.44	2.58	Need but not usable	Construction of more canals and reservoirs
	2050	3.78	3.23	Need but not usable	
	2100	3.82	3.23	Need but not usable	
P 43/2F	2021	1.19	1.32	No need but usable	Have the potential to extend Boro rice
	2050	1.32	1.84	No need but usable	
	2100	1.25	1.84	No need but usable	
P 46	2021	0.46	0.71	No need & not usable	Need re-excavation of canal
	2050	0.50	1.01	No need & not usable	
	2100	0.46	1.01	No need & not usable	

Groundwater sustainability

There are two primary concerns regarding groundwater use in the coastal zone of Bangladesh. Excessive pumping leads to a decline in groundwater levels, which may threaten groundwater sustainability. Additionally, increased water withdrawal can cause saline water intrusion into the groundwater supply. Polder 29, Polder 17/1, and Polder 43/2F have the potential to utilize groundwater effectively, as salinity levels are within acceptable limits for irrigation. **Fig. 7** displays the observed groundwater table at the Dumuria station in Polder 29. The graph indicates a significant recovery of groundwater levels during the monsoon season, following recharge from monsoon rainfall. Furthermore, there has been no significant trend in the groundwater table over the past twenty-two years.

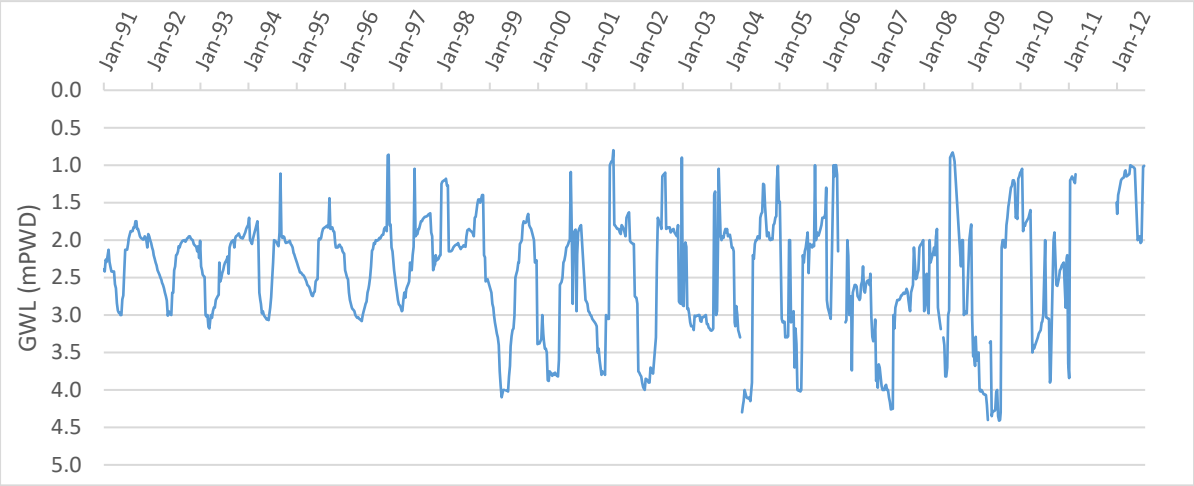

Fig. 7. Temporal variation of groundwater level for Polder 29 (Data source: BWDB).

Conclusion

Climate change-induced salinity is projected to impact Boro rice cultivation and irrigation water demand in coastal Bangladesh. While salinity may reduce Boro cropland, the introduction of salinity-tolerant varieties could increase water demand. Currently, the irrigation water demands for Polder 29, Polder 17/1, Polder 32, Polder 35/1, Polder 43/2F, and Polder 46 are 14.59, 10.45, 2.63, 3.44, 1.19, and 0.46 million cubic meters (Mm^3), respectively. By 2050, the demands are projected to rise to 15.96, 11.98, 2.84, 3.78, 1.32, and 0.50 Mm^3, respectively. The increase in water demand is substantial only for Polder 29 and Polder 17/1. In terms of water availability, surface and groundwater sources are insufficient to meet the Boro rice cultivation needs. Groundwater in all polders, except Polder 29 and Polder 17/1, is unusable due to high salinity. Although the second aquifer groundwater in Polder 43/2F is usable, national policy restricts its use for irrigation. To address increased water demand, re-excavation of existing canals is needed for Polder 35/1 and Polder 46. Polder 32 requires both new canal excavation and re-excavation of existing canals, as surface water is the only available irrigation source. Polders 29, 17/1, and 43/2F can meet their irrigation water needs through groundwater and canal re-excavation, with no significant groundwater sustainability issues.

Conflict of Interest

The authors declare no conflict of interest.

References

Ahmed, A. (2011). Some of the major environmental problems relating to land use changes in the coastal areas of Bangladesh: A review. *Journal of Geography & Reg. Planning*, *4*(January), 1–8.

Ahsan, K., Rashid, M. B., & Talukder, S. (2022). Tidal River siltation and its impact in the coastal parts of Bangladesh. *Int J Econ Environ Geol, 13*(2), 35-41.

Ahmed, S. N., and Islam, A. (2013). Agriculture Adaptation in Coastal Zone of Bangladesh. *Disaster Risk Reduction*, *January 2013*, 143–163.

Bahar, M. M., and Reza, M. S. (2010). Hydrochemical characteristics and quality assessment of shallow groundwater in a coastal area of southwest Bangladesh. *Environmental Earth Sciences*, *61*(5), 1065–1073.

BBS. (2018). *Yearbook of Agricultural Statistics-2018.* Ministry of Planning, Government of the People's Republic of Bangladesh.

Begum, S., Huq, H., Salahuddin, A., Nelson, K., & Amin, M. R. (2024). *Water management challenges in coastal polders of Bangladesh: Rethinking institutional and policy issues*. Dhaka, Bangladesh: Institute of Development Studies and Sustainability, United International University, and International Rice Research Institute. CGIAR Initiative on Asian Mega-Deltas. https://hdl.handle.net/10568/172759

Brammer, H. (2014). Bangladesh's dynamic coastal regions and sea-level rise. *Climate Risk Management*,

1, 51–62.

Dang, C., Zhang, H., Yao, C., Mu, D., Lyu, F., Zhang, Y., & Zhang, S. (2024). IWRAM: A hybrid model for irrigation water demand forecasting to quantify the impacts of climate change. *Agricultural Water Management*, 291, 108643.

Deb, A. K. (1998). Fake blue revolution: Environmental and socio-economic impacts of shrimp culture in the coastal areas of Bangladesh. *Ocean and Coastal Management*, *41*(1), 63–88.

Fahad, M. G. R., Saiful Islam, A. K. M., Nazari, R., Alfi Hasan, M., Tarekul Islam, G. M., and Bala, S. K. (2018). Regional changes of precipitation and temperature over Bangladesh using bias-corrected multi-model ensemble projections considering high-emission pathways. *International Journal of Climatology, 38*(4), 1634–1648.

Haque, S. A. (2006). Salinity problems and crop production in coastal regions of Bangladesh. *Pakistan Journal of Botany*, *38*(5 SPEC. ISS.), 1359–1365.

Hossain, M., and Majumder, A. (2018). Impact of climate change on agricultural production and food security: a review on coastal regions of Bangladesh. *International Journal of Agricultural Research, Innovation and Technology*, *8*(1), 62–69.

Islam, M. R., and Gregorio, G. B. (2013). Progress of salinity tolerant rice variety development in Bangladesh. *Sabrao Journal of Breeding and Genetics*, *45*(1), 21–30.

Islam, Mohammad Rafiqul, and Haque, M. (2018). The Trends of Export and Its Consequences to the GDP of Bangladesh. *Journal of Social Sciences and Humanities*, *1*(1), 63–67.

Islam, S. A., and Rahman, M. M. (2015). Coastal afforestation in Bangladesh to combat climate change induced hazards. *Journal of Science, Technology and Environment Informatics*, *02*(01), 13–25.

Islam, S. M., Wahab, M. A., and Miah, A. A. (2002). Socioeconomic and Environmental Impacts of Alternate Shrimp-Crop Farming in Bangladesh. *Bangladesh Journal of Agricultural Economics*, *1*, 63

Khan, S., Yufeng, L., and Ahmad, A. (2009). Analysing complex behaviour of hydrological systems through a system dynamics approach. *Environmental Modelling and Software*, *24*(12), 1363–1372.

Kay, S., Caesar, J., Wolf, J., Bricheno, L., Nicholls, R. J., Saiful Islam, A. K. M., Haque, A., Pardaens, A., and Lowe, J. A. (2015). Modelling the increased frequency of extreme sea levels in the Ganges-Brahmaputra-Meghna delta due to sea level rise and other effects of climate change. *Environmental Sciences: Processes and Impacts*, *17*(7), 1311–1322.

Khanom, S., and Salehin, M. (2012). Salinity constraints to different water uses in coastal area of Bangladesh: A case study. *Bangladesh Journal of Scientific Research*, *25*(1), 33–41.

Mahtab, M. H., and Zahid, A. (2018). Coastal surface water suitability analysis for irrigation in Bangladesh. *Applied Water Science*, *8*(1), 1–12.

Mainuddin, M., and Kirby, M. (2015). National food security in Bangladesh to 2050. *Food Security*, *7*(3), 633–646.

Nowreen, S., Jalal, M. R., and Khan, M. S. A. (2014). Historical analysis of rationalizing South West coastal polders of Bangladesh. *Water Policy*, *16*(2), 264–279.

Paul, A., Nath, B., and Abbas, R. (2013). *Tidal River Management (TRM) and its implication in disaster management: A geospatial study on Hari-Teka river basin, Jessore*. *4*(1), 125–135.

Rahman, M. T. (2017). Role of Agriculture in Bangladesh Economy: Uncovering the Problems and Challenges. *International Journal of Business and Management Invention ISSN*, *6*(7), 36–46.

Ritzema, H. P., and Stuyt, L. C. P. M. (2015). Land drainage strategies to cope with climate change in the Netherlands. *Acta Agriculturae Scandinavica, Section B—Soil & Plant Science*, *65*(sup1), 80-92.

Shapna, K. J., Li, J., Hossain, M. L., et al. (2024). Strengthening adaptation in coastal Bangladesh: Community-based approaches for sustainable agriculture and water management. *Disaster Prevention and Resilience*, *4*(2). https://doi.org/10.20517/dpr.2023.41.

Sharifullah, A. K., Tuong, T. P., Mondal, M. K., & Franco, D. T. (2008). *Assessing water supply and demand for dry season rice in coastal polders of Bangladesh. Increasing. Proceedings of the Workshop on Increasing the Productivity and Sustainability of Rainfed Cropping Systems of Poor, Smallholder Farmers, Tamale, Ghana*, 22-25.

Shawkhatuzamman, M., Roy, S. R., Alam, M. Z., Majumder, P., Anka, N. J., and Hasan, A. K. (2023). Soil salinity management practices in coastal area of Bangladesh: a review. *Research in Agriculture Livestock and fisheries*, *10*(1), 1-7.

Van den Burg, S., Deolu-Ajayi, A. O., Nauta, R., Cervi, W. R., van der Werf, A., Poelman, M., ... & van der Meer, I. M. (2024). Knowledge gaps on how to adapt crop production under changing saline circumstances in the Netherlands. *Science of The Total Environment*, *915*, 170118.

Ventana Systems. (2019). *Vensim DSS 7.2, Ventana Systems Inc, Harvard, MA*.

Technical Journal
River Research Institute ISSN: 1606-9277

Modeling Fish Habitat Suitability in the Karnafuli River, Bangladesh

A. Akter[1*] and A. Dayem[2]

Abstract

The Physical Habitat Simulation (PHABSIM) system is a numerical modeling tool that assesses the suitability of hydraulic habitats for different fish species. In this study, the PHABSIM system is used to evaluate the functioning area for three life stages of Rohu fish (Labeo Rohita) at a specific discharge level. Multiple options for habitat simulation are utilized, allowing for a wide range of habitat and hydraulic conditions to be considered. By obtaining precise and comprehensive data regarding hydrological and fish habitat-related parameters, researchers can enhance the reliability and effectiveness of the PHABSIM system in predicting habitat suitability for fish species in the Karnafuli River.

Keywords: *PHABSIM; Rohu fish; Karnafuli River.*

Introduction

River flow assessment for data-scarce rivers depends on examining various scenarios, and to overcome these issues, predictive models are often used. Physical Habitat Simulation (PHABSIM), initially developed by the U.S. Fish and Wildlife Service in the 1970s, has been extensively used across the USA and is now applied worldwide. PHABSIM has been applied in water resources and fisheries in the U.K. (Spence and Hickley, 2000), environmental flow assessment of rivers Europe (Ceola et al., 2018), ASEAN (Stucchi and Bocchiola, 2023), and identified its importance while dealing with environmental flow requirements using other hydrological models (Akter and Tanim, 2018; Sayed and Akter, 2022). The PHABSIM model could reasonably assess the physical habitats in waterbodies considering the combination of factors of discharge, velocity, and specific depth (Kim et al., 2020; Kim and Choi, 2018; Meng et al., 2023; Nagaya et al., 2008). Until now, no single study has focused on habitat simulation. This research employs the PHABSIM model to assess the physical habitat area for Labeo rohita (Rohu fish) upstream of the Karnafuli River. Furthermore, it provides an overview of the various components of the PHABSIM model.

Methodology

The Karnafuli River (22°12'60.00" N, 91°47'59.99" E) originates from the Lushai Hills in Mizoram, India. As the largest and most significant river for Chittagong and the Chittagong Hill Tracts, it spans 180 km. The river follows a steep course, passing through Rangamati in a confined loop before continuing in a meandering pattern with pronounced zigzags, forming two additional main loops at Dhuliachhari and Kaptai. From the Kaptai loop, it flows through the Sitapahar Hill Range, crosses the Chittagong plain via the Chandraghona Hills, and eventually empties into the Bay of Bengal. The Karnafuli River is rich in fish biodiversity and is a vital hydropower resource. A field survey was carried out in its upstream section, covering approximately 50 km from the Halda estuaries to the Kaptai Dam. Eleven cross-sectional measurements were recorded using an eco-sounder, including river width, depth, and velocity (**Fig. 1**). Depth measurements were collected using an eco-sounder, while velocity was recorded with a velocity meter. The river's width varied from 600 m upstream to 900 m at the downstream end. The maximum depth was observed at the farthest upstream cross-section to range from 20 to 43 m, with velocity measurements across the sections ranging from 0.10 to 3.16 ms^{-1}.

Water Surface Modeling

This study applied a stage-discharge regression method using the Stage-Discharge Approach (STGQ) program within the PHABSIM module to model water surface elevations. The STGQ model employs a stage-discharge relationship (i.e., a rating curve) to determine water surface elevations at each cross-section. Each cross-section is analyzed independently in this approach, without accounting for interactions with other sections. The computational process involves performing a log-log regression between observed stage and discharge pairs at each cross-section. The resulting regression equation is then used to estimate water surface elevations across various flow conditions, effectively simulating the stage-discharge relationship.

The relationship between stage (i.e., water surface elevation) and discharge can often be represented at a cross section in a channel by the following equation:

$$(WSL - SZF) = a\,Q^{b} \qquad \text{Eq. (1)}$$

Where:

Q = Discharge

W.S.L. = Water surface elevation

[1]Dept of Civil Engineering, Chittagong University of Engineering & Technology, Chittagong-4349, Bangladesh.
[*]Corresponding Author: (E-mail: aysha_akter@cuet.ac.bd)
[2]Assistant Town Planner, Chattogram Metropolitan Master Plan Project (2020-2041), Chattogram Development Authority.

SZF =Stage-Zero Flow, i.e., WSL of zero flow

a = Constant calculated based on recorded discharge and stage measurements.

b = The coefficient is calculated based on recorded discharge and stage measurements.

Incorporating SZF in Eq.1 is essential, as the stage-discharge relationship at a given channel cross-section depends on the SZF at that location. By applying a base-10 logarithm to Eq.1, the equation can be transformed into a linear relationship between stage and discharge, yielding the following expression:

$$log_{10}(WSL - SZF) = log_{10}(a) + b * log_{10}(Q) \quad \text{Eq. (2)}$$

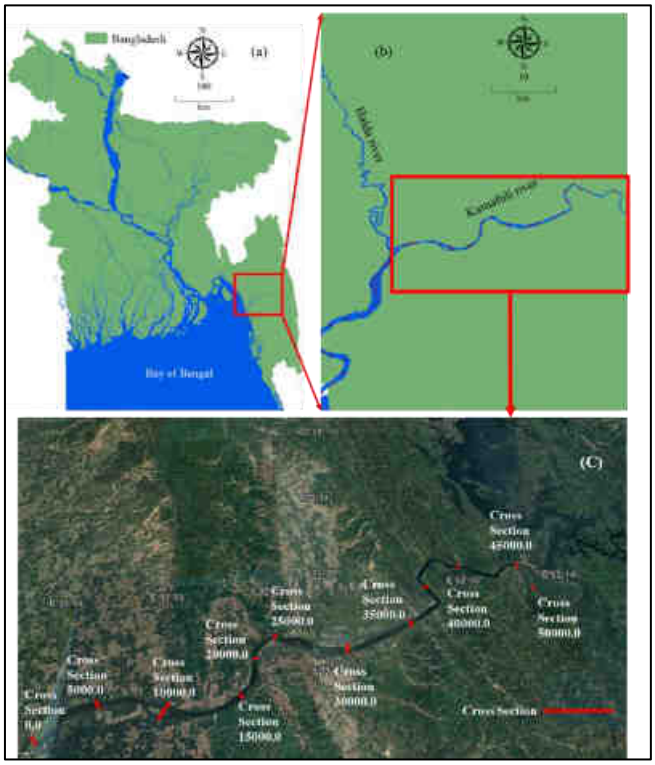

Fig. 1. a) Bangladesh Map b) Karnafuli river c) Selected site for PHABSIM.

Three sets of stage-discharge data were provided for a specific cross-section to determine the constant and coefficient in Eq.2. Using these data, a regression equation was developed to predict stage levels within a specified discharge range. The accuracy of this modeling approach in simulating water surface elevations depends not only on the observed data but also on factors such as channel geometry and the relative slope variations between regression lines of adjacent cross-sections. During regression-based modeling, several parameters were selected, including appropriate calibration discharges (reasonable discharge estimates for each cross-section), the determination of an accurate SZF, and the selection of calibration water surface elevations. In this study, regressions were based on reasonable discharge estimates and average water surface elevations. This study's regressions were based on reasonable discharge estimates and average water surface elevations. The SZF was determined using the thalweg bed elevations at each cross-section, where the thalweg represents the lowest points along the streambed. **Fig. 2** presents the water surface elevations (excluding SZF) plotted against the reasonable discharge estimates for all eleven cross-sections of the Karnafuli River. For this study, the required flow estimate was determined by analyzing measured discharges at each cross-section.

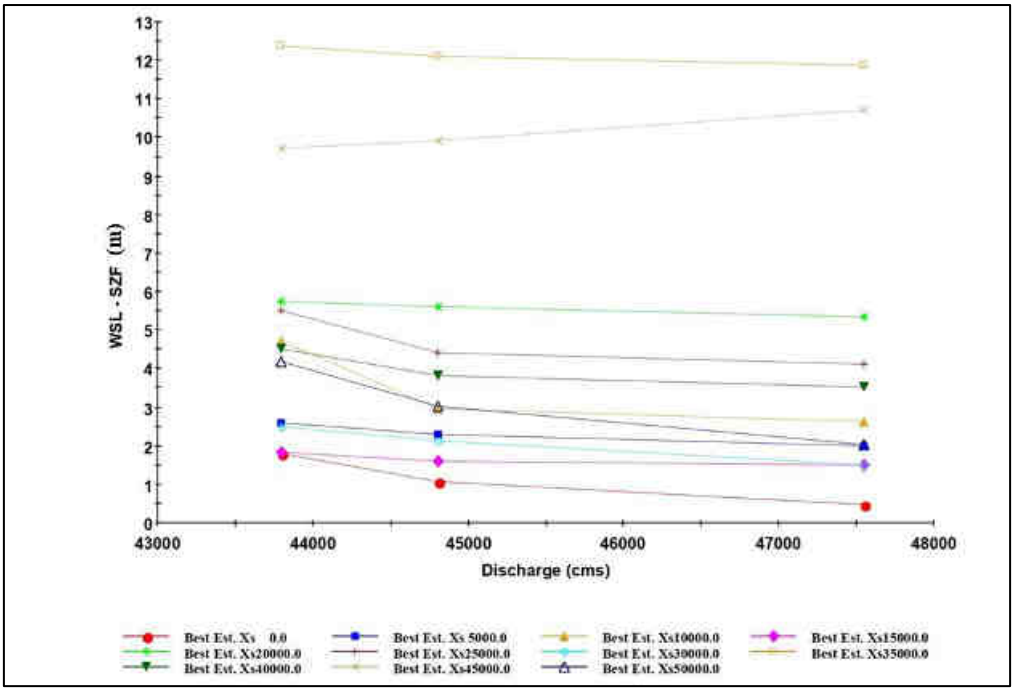

Fig. 2. Stage-discharge relationship for eleven cross sections in the PHABSIM model

Water surface level data were used to simulate the available depths and velocity distribution at each cross-section. For most downstream cross-sections, WSL were modeled using a simple rating curve approach based on water level data obtained from the field study. In contrast, a one-dimensional STGQ model was applied to simulate water surface elevations upstream, providing insights into the upstream cross-section of the Karnafuli River. This method is considered the most physically based approach within the suite of PHABSIM modeling tools following Bovee (1998). It allows for the incorporation of spatial variations in roughness and changes in roughness that occur with increasing discharge, enhancing the accuracy of water surface modeling.

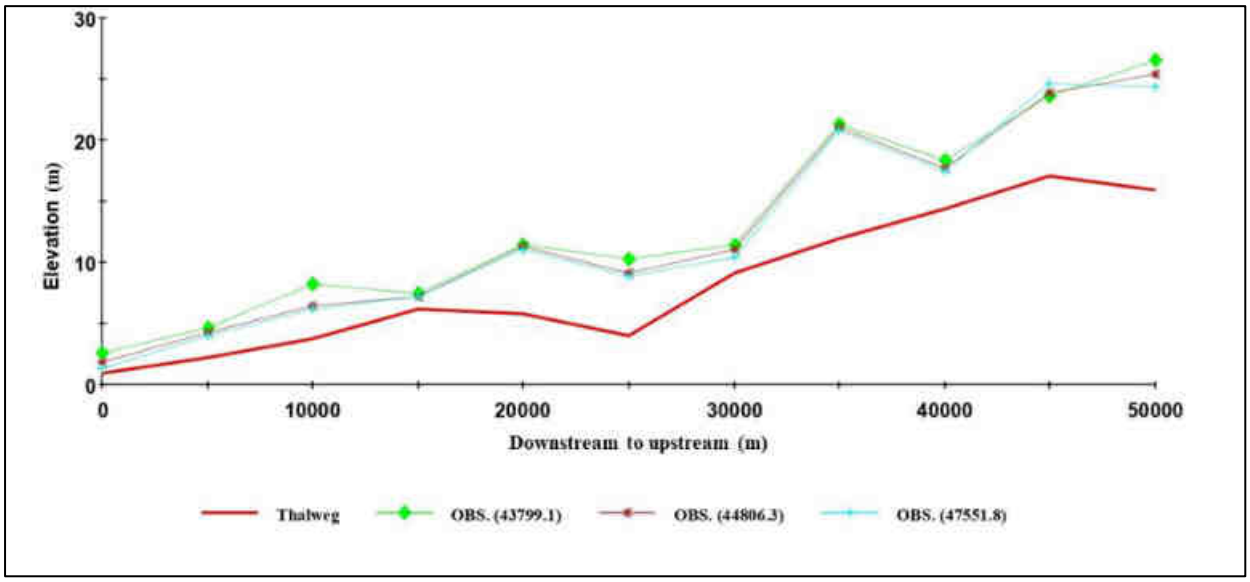

Fig. 3. Observed water surface and thalweg profiles.

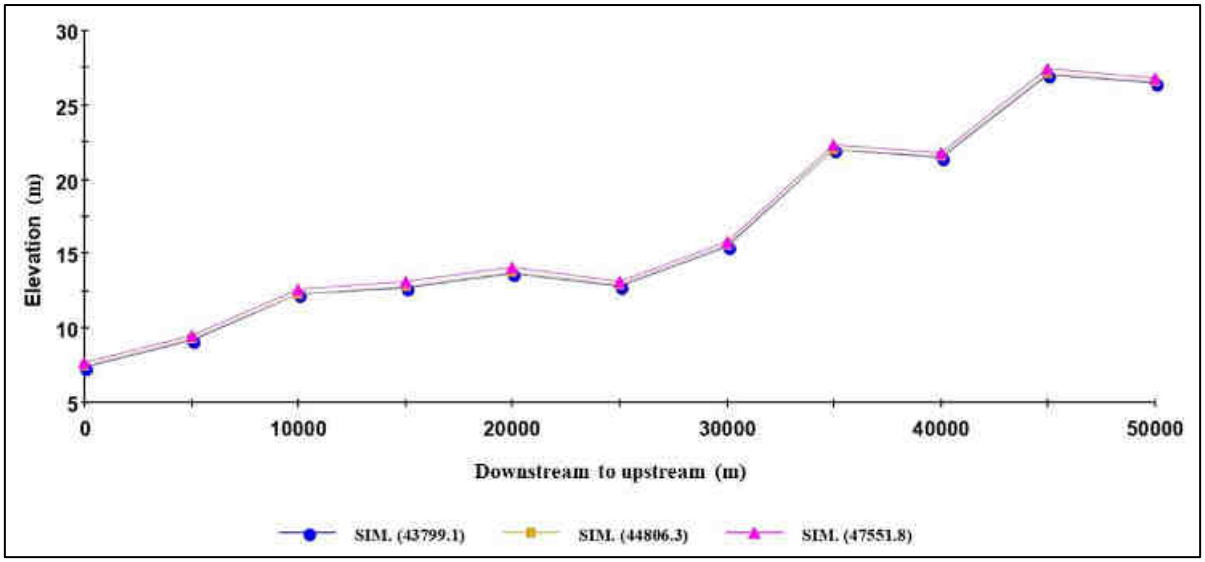

Fig. 4. Water surface profiles simulated with STGQ

Fig. 3 presents the observed longitudinal water surface elevations and thalweg versus discharge data for the eleven cross-sections, while **Fig. 4** illustrates the simulated water surface profiles derived from the stage-discharge relationships for these sections. In **Fig. 3**, the top line, labeled SIM (47551.8), represents the predicted water surface elevation at a discharge of 47,551.8 cms, while the bottom line corresponds to the expected water surface elevation at a discharge of 43,799.1 cms. The indicated water surface elevations for each cross-section are obtained using the regression equation specific to that section, based on three calibration data sets. The modeling results confirm the reliability of the stage-discharge approach, as the simulated WSL closely aligns with the observed WSL data.

Results and discussion

Velocity Modeling

This study employs various empirical approaches to simulate velocity distributions. The Velocity Simulation (VELSIM) module utilizes specific velocity calibration sets for different discharge ranges. When calibration velocities are unavailable, a conveyance area-based velocity distribution can be developed. The selection of the most suitable approach depends on the available data, model performance, and study objectives. This study also explores multiple combinations of velocity sets and simulation control options within VELSIM. Furthermore, it examines the impact of selecting a particular water surface elevation model and its subsequent effects on velocity simulation in VELSIM. The primary goal of velocity calibration and simulation is to determine the optimal combination of calibration velocities and simulation options that accurately represent velocity profiles at each cross-section across the simulated flow range. Before initiating the modeling process, it is crucial to analyze the observed velocity profiles at each cross-section using the three provided calibration discharge datasets, as illustrated in **Fig. 5, 6, 7**, and **8**. As expected, velocity profiles vary significantly depending on cross-section geometry.

Habitat Suitability Criteria (HSC) in PHABSIM

PHABSIM integrates biological data into its habitat modeling by using HSC (suitability-of-use criteria) within various habitat models. The development of HSC is addressed within PHABSIM, outlining the methods for inputting and manipulating HSC data. In PHABSIM, HSC data is created, edited, and stored, consisting of coordinate data for different species and life stages, with consideration of factors such as depth, velocity, and temperature. HSCs for a specific species and life stage are typically organized into four datasets, representing the relationships between depth, velocity, temperature, channel index, and their corresponding suitability values (**Fig. 9-11**).

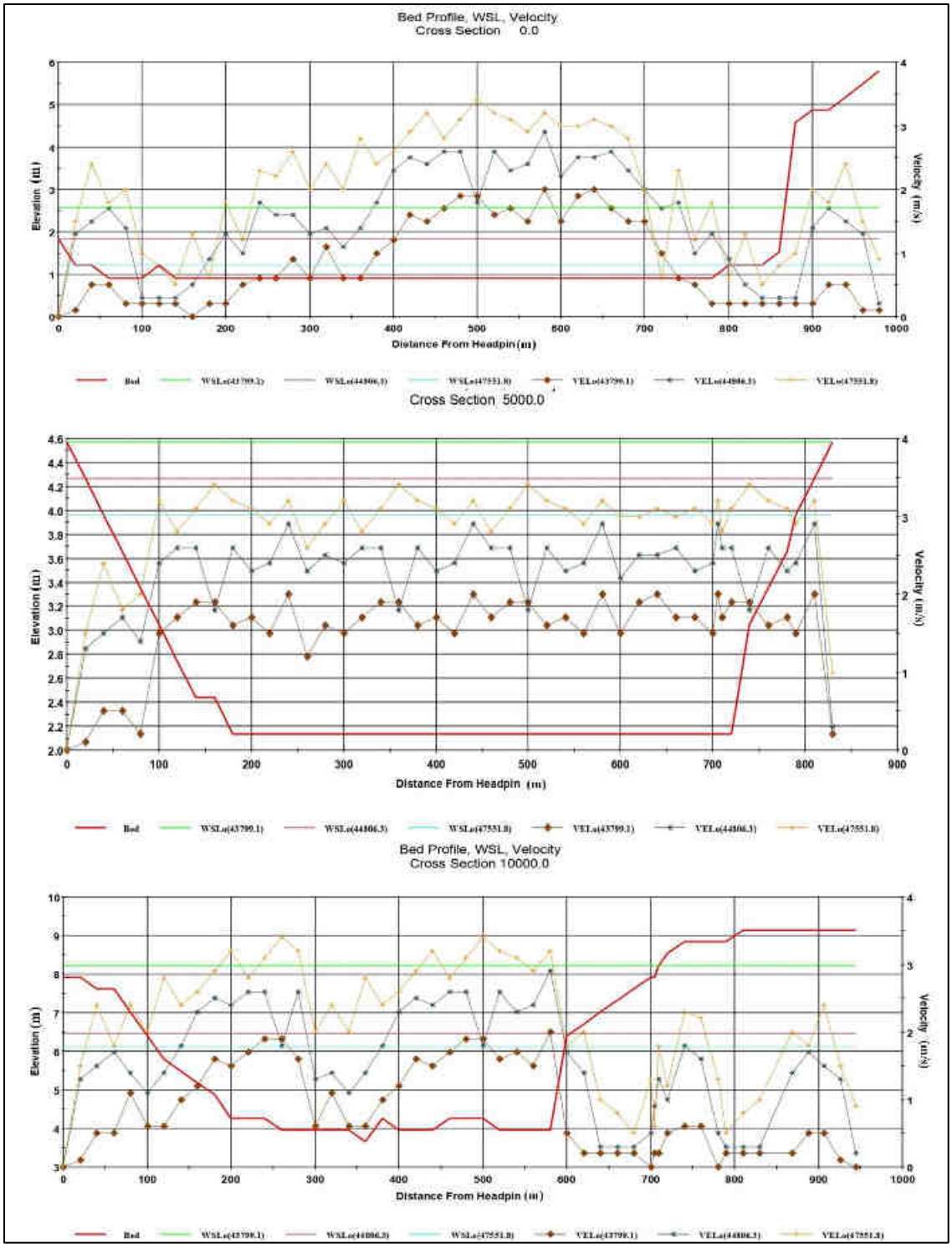

Fig. 5. Velocity profile cross section 0.00, cross section 5000.00, and cross section 10000.00

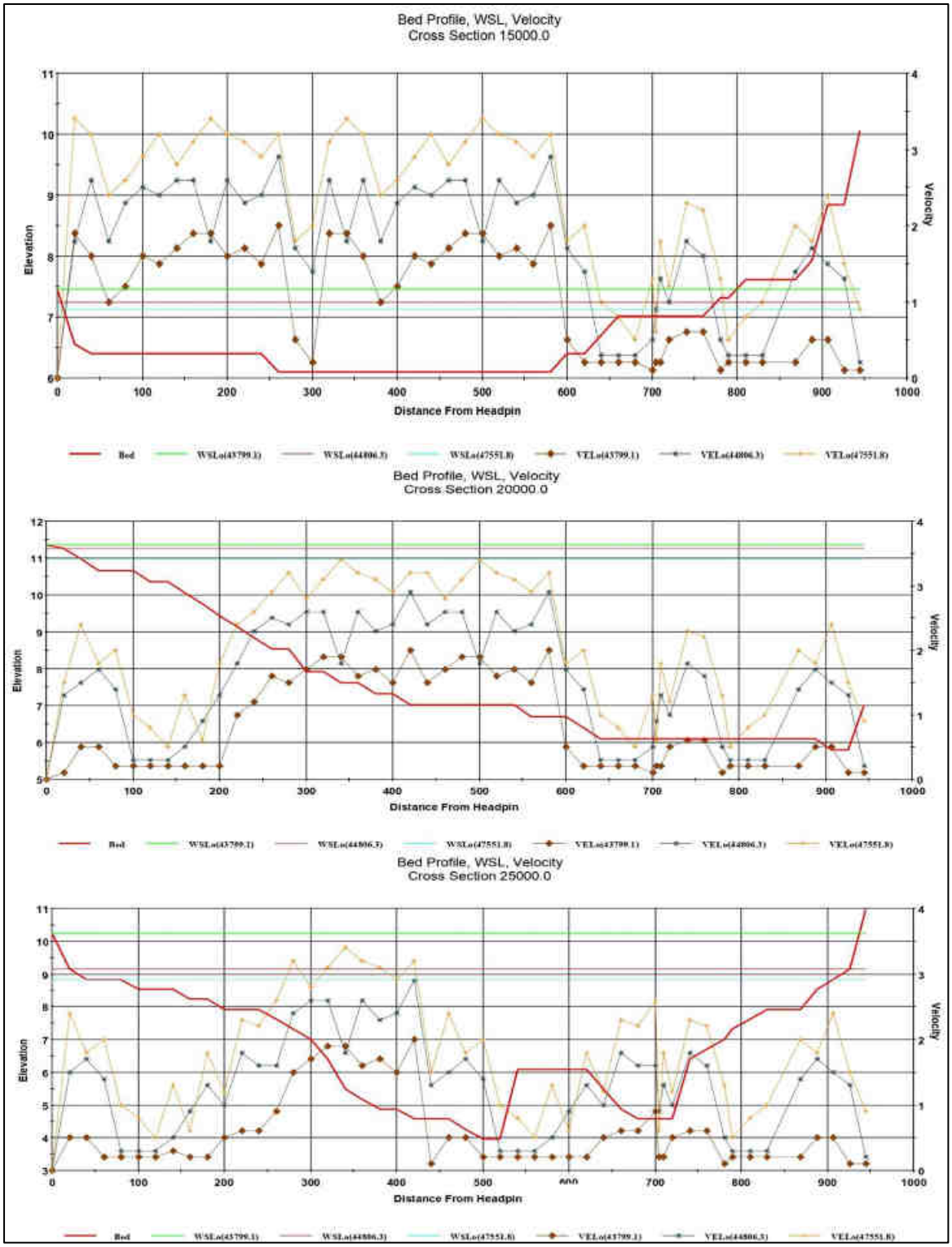

Fig. 6. Velocity profile from cross section 15000.00, cross section 20000.00, cross section 25000.00

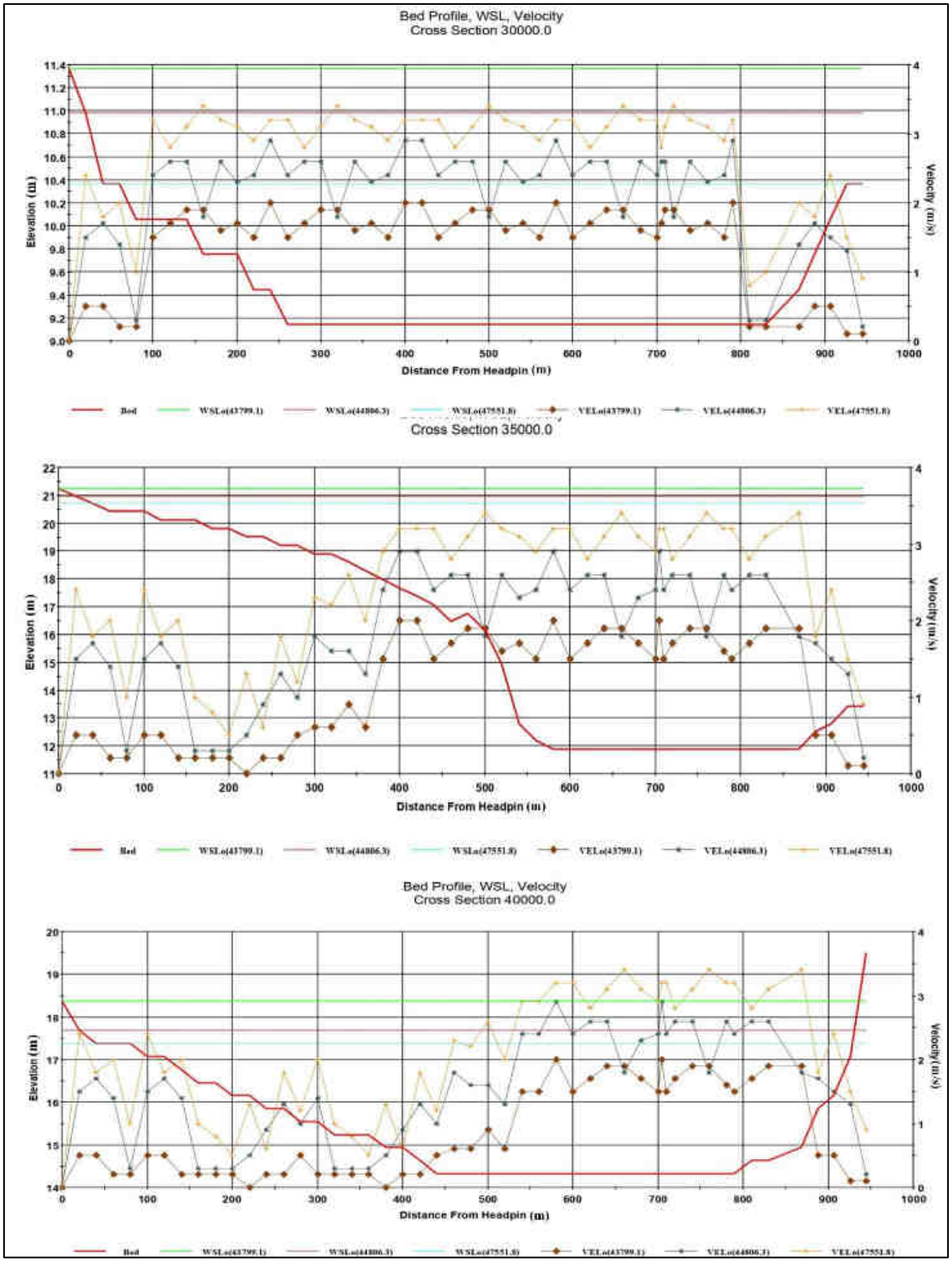

Fig. 7. Velocity profile from cross section 30000.00, cross section 35000.00 and cross section 40000.00

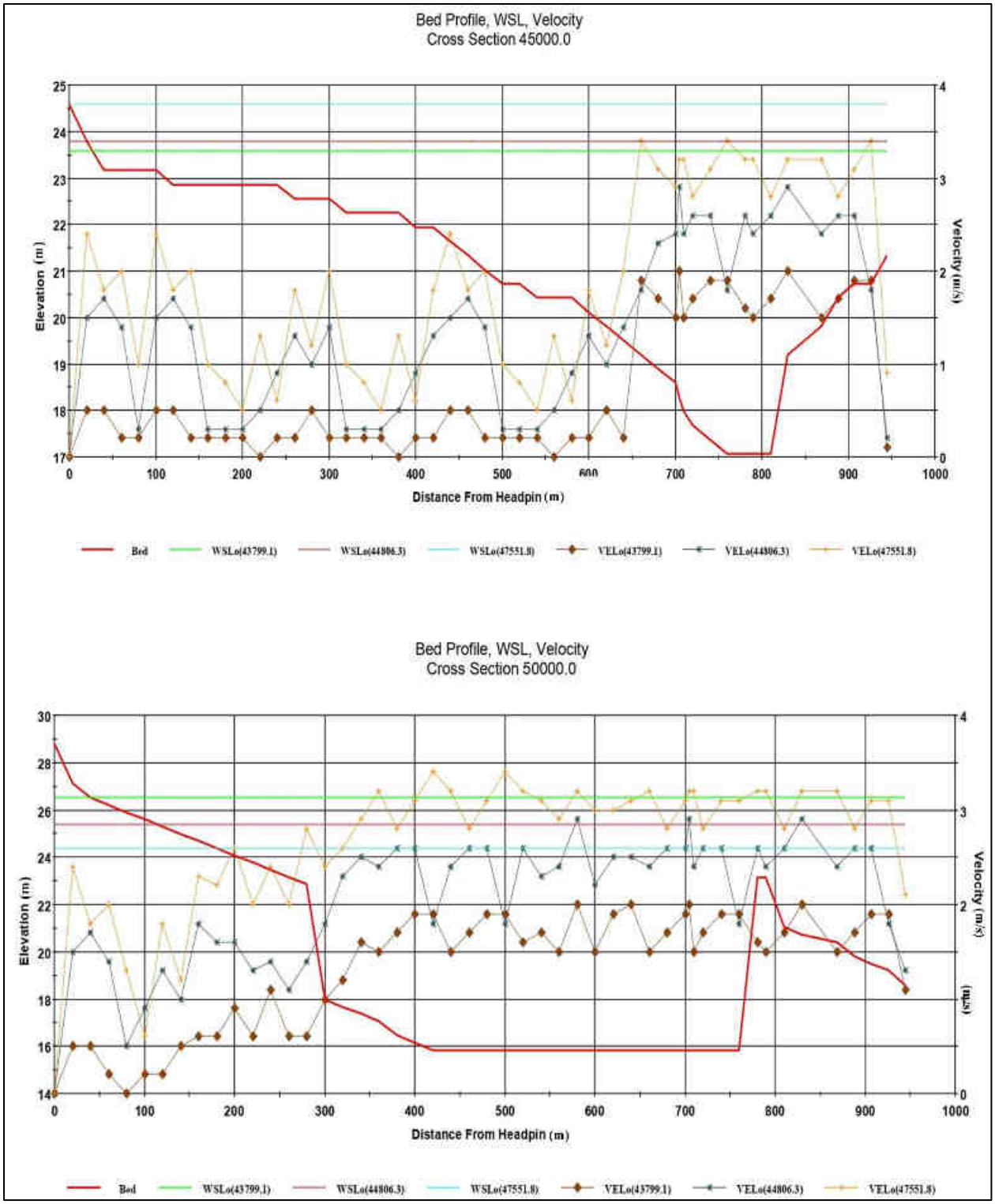

Fig. 8. Velocity profile in cross section 45000.00 and cross section 50000.00

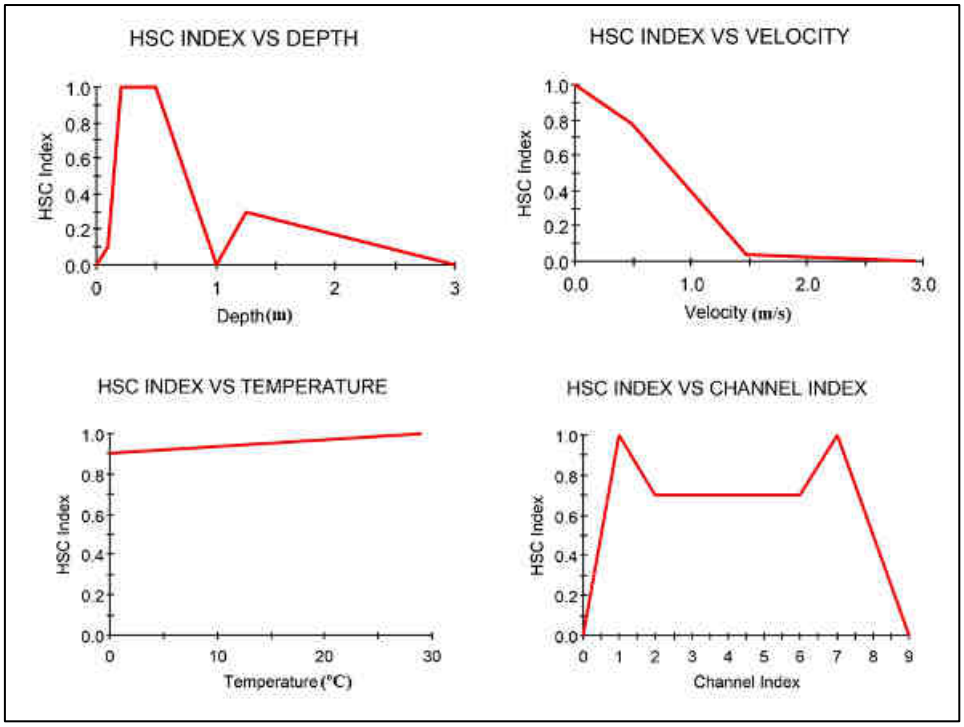

Fig. 9. Habitat suitability indices for different fry stages of Labeo rohita (Rohu fish)

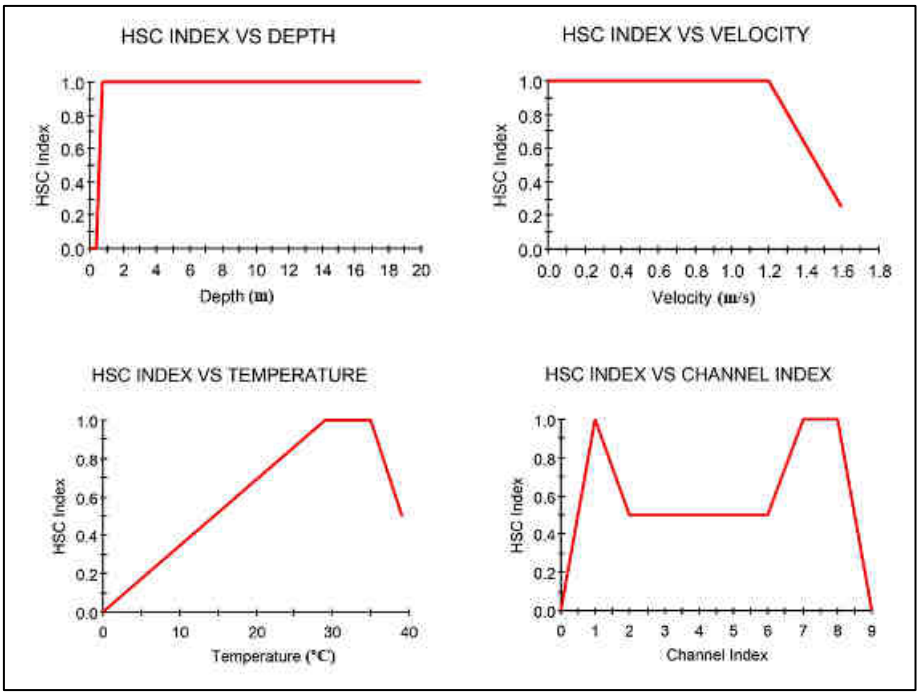

Fig. 10. Habitat suitability indices for different Juvenile stages of Labeo rohita (Rohu fish)

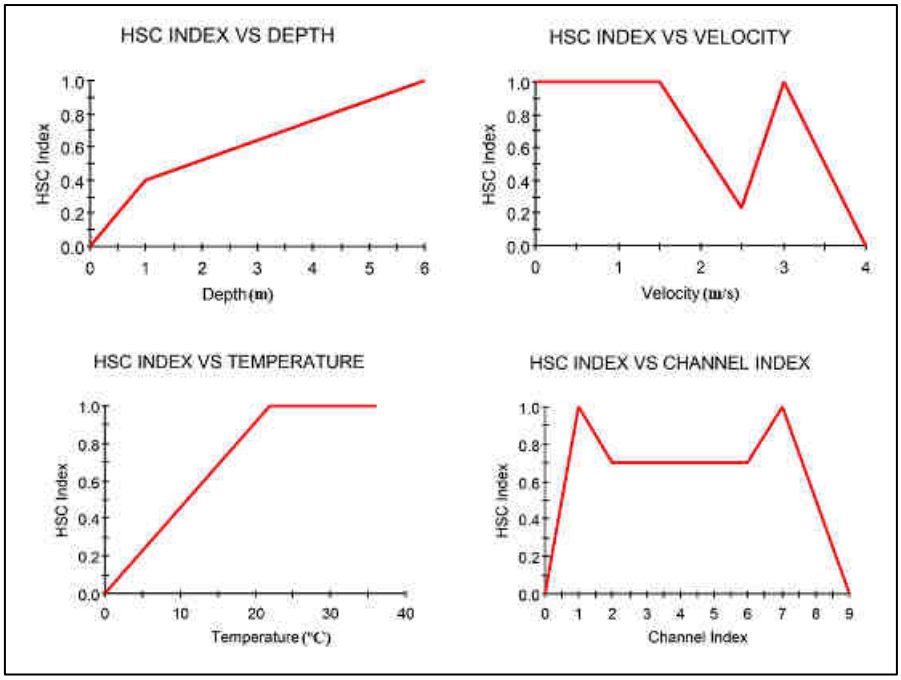

Fig. 11. Habitat suitability indices for different adult stages of Labeo rohita (Rohu fish)

Habitat modeling

The primary goal of this study is to introduce the concepts of habitat modeling by using PHABSIM. During the habitat modeling process, this information is integrated with habitat suitability criteria (HSC) to assess the extent of available physical habitat in relation to discharge. The fundamental theory behind the habitat modeling programs in PHABSIM is based on the assumption that aquatic species respond to changes in the hydraulic environment. These changes are simulated for each cell within a defined stream reach. Simulating the stream reach involves a multi-dimensional matrix that calculates the surface areas of the stream for various combinations of hydraulic parameters, such as depth, velocity, and channel index. For each cell, the depth and velocity values are derived from the average of simulated values obtained during the hydraulic simulation phase of PHABSIM. As discharge changes, the depth and velocity attributes also vary, resulting in alterations to both the quantity and quality of available habitat. The outcome of the habitat modeling process is a description of the habitat area as a function of discharge. This habitat-discharge relationship serves as the foundation for further analysis, supporting decision-making in fishery and recreation management.

Conclusions

The available data on population responses to changes in habitat area over time are limited. Additional data on fish swimming speeds can be used to understand the impact of model predictions on fish populations. Further research is necessary to evaluate the effects of temporal variations in habitat areas on fish populations. It should be noted that water quality can significantly influence the suitability of a physical habitat site for fish. In some cases, fish may not be observed even in areas with suitable physical habitats due to poor water quality. Exploring the connection between water quality, physical habitat requirements, and the physiological state of fish is a promising avenue for future research. More comprehensive data and studies are needed to better understand fish populations' response to habitat area changes. Additionally, considering the influence of water quality on fish habitat and physiology can provide valuable insights for future research endeavors.

Acknowledgments

This research was supported by a research project titled 'Application of Eco-hydraulic Model cascades on the selected Rivers (AEMR) CUET/DRE/2018-19/CE/028.' The Department of Civil Engineering, Chittagong University of Engineering and Technology (CUET), Bangladesh, provided logistic support. The authors thank BWDB and BMD for providing the required information during the study.

Conflict of Interest

The authors declare no conflict of interest.

References

Acreman, Elliott, (1996). Evaluation of the river Wey restoration project using the Physical HABitat SIMuation (PHABSIM) model, in: *Proceedings of the 31st MAFF Conference of River and Coastal Engineers*. Keele Universit, uk.

Akter, A., Tanim, A.H., (2018). A modeling approach to establish environmental flow threshold in ungauged semidiurnal tidal river. *J Hydrol (Amst) 558*. https://doi.org/10.1016/j.jhydrol.2018.01.061

Bovee KD, (1998). Development and Application of Habitat Suitability Criteria for Use in The Instream Flow Incremental Methodology. *US Fish and Wildlife Service 2, 1535*. https://doi.org/10.1136/bmj.2.5423.1535

Ceola, S., Pugliese, A., Ventura, M., Galeati, G., Montanari, A., Castellarin, A., (2018). Hydro-power production and fish habitat suitability: Assessing impact and effectiveness of ecological flows at regional scale. Adv *Water Resour 116*, 29–39. https://doi.org/https://doi.org/10.1016/j.advwatres.2018.04.002

Chen, D., Yang, Z., Zeng, Q., Wang, W., Yan, L., Zhang, P., Li, X., Hu, P., Wang, H., (2023). Analysis of the suitable ecological flow of benthic animals in the lower reaches of Xiangjiaba Reservoir in the upper reaches of the Yangtze River based on the physical habitat model. *J Hydrol (Amst) 625*, 130132. https://doi.org/https://doi.org/10.1016/j.jhydrol.2023.130132

Crisp, D.T., Carling, P.A., (1989). Observations on siting, dimensions and structure of salmonid redds. *J Fish Biol 34*, 119–134. https://doi.org/10.1111/j.1095-8649.1989.tb02962.x

Freeman, M.C., Bowen, Z.H., Bovee, K.E.N.D., Irwin, E.R., (2001). Flow and Habitat Effects on Juvenile Fish Abundance in Natural and Altered Flow Regimes. *Ecological Applications 11*, 179–190.

Gibbins, C.N., Acornley, R.M., (2000). Salmonid habitat modelling studies and their contribution to the development of an ecologically acceptable release policy for Kielder Reservoir, North-east England. Regulated Rivers: *Research & Management 16*, 203–224. https://doi.org/10.1002/(sici)1099-1646(200005/06)16:3<203::aid-rrr579>3.3.co;2-#

Gibbins, C.N., Soulsby, C., Jeffries, M.J., Acornley, R., (2001). Developing ecologically acceptable river flow a regimes: A case study of Kielder water transfer system. *Fish Manag Ecol 8*, 463–485. https://doi.org/10.1046/j.1365-2400.2001.00274.x

Hatfield, T., Bruce, J., (2000). Predicting Salmonid Habitat–Flow Relationships for Streams from Western North America. *N Am J Fish Manag 20*, 1029–1032. https://doi.org/10.1577/1548-8675(2000)020

Hearne, J., Johnson, I., Armitage, P., (2002). Determination of ecologically acceptable flows in rivers with seasonal changes in the density of macrophyte. Regulated Rivers: *Research & Management 9*, 177–184. https://doi.org/10.1002/rrr.3450090304

Hung, H.-J., Lo, W.-C., Chen, C.-N., Tsai, C.-H., (2022). Fish' habitat area and habitat transition in a river under ordinary and flood flow. *Ecol Eng 179*, 106606. https://doi.org/https://doi.org/10.1016/j.ecoleng.2022.106606

Johnson, A.I., (1963). *A field-method for measurement of infiltration. U.S. Gov. Print*. Off., Washington, D.C.

Johnson, I.W., Elliott, C.R.N., Gustard, A., (1995). Modelling the effect of groundwater abstraction on salmonid habitat availability in the river Allen, Dorset, England. Regulated Rivers: *Research & Management 10*, 229–238. https://doi.org/10.1002/rrr.3450100217

Jung, S.H., Choi, S.-U., (2015). Prediction of composite suitability index for physical habitat simulations using the ANFIS method. *Appl Soft Comput 34*, 502–512. https://doi.org/https://doi.org/10.1016/j.asoc.2015.05.028

Kim, H.J., Kim, J.H., Ji, U., Jung, S.H., (2020). Effect of Probability Distribution-Based Physical Habitat Suitability Index on Environmental-Flow Estimation. *KSCE Journal of Civil Engineering 24*, 2393–2402. https://doi.org/https://doi.org/10.1007/s12205-020-1923-z

Kim, S.K., Choi, S.-U., (2018). Prediction of suitable feeding habitat for fishes in a stream using physical habitat simulations. *Ecol Modell 385*, 65–77. https://doi.org/https://doi.org/10.1016/j.ecolmodel.2018.07.014

Knack, I.M., Huang, F., Shen, H.T., (2020). Modeling fish habitat condition in ice affected rivers. *Cold Reg Sci Technol 176*, 103086. https://doi.org/https://doi.org/10.1016/j.coldregions.2020.103086

Maddock, I.P., Bickerton, M.A., Spence, R., Pickering, T., (2001). Reallocation of compensation releases to restore river flows and improve instream habitat availability in the upper derwent catchment,

derbyshire, UK. *River Res Appl 17*, 417–441. https://doi.org/10.1002/rrr.663

Meng, Y., Xu, W., Guan, X., Guo, M., Wang, X., Yan, D., (2023). Ecology-habitat-flow modular simulation model for the recommendation of river ecological flow combination. *Environmental Modelling & Software 169*, 105823. https://doi.org/https://doi.org/10.1016/j.envsoft.2023.105823

Moir, H.J., Gibbins, C.N., Soulsby, C., Webb, J., (2004a). Linking channel geomorphic characteristics to spatial patterns of spawning activity and discharge use by Atlantic salmon (Salmo salar L.). *Geomorphology 60*, 21–35. https://doi.org/10.1016/j.geomorph.2003.07.014

Moir, H.J., Gibbins, C.N., Soulsby, C., Webb, J., (2004b). Linking channel geomorphic characteristics to spatial patterns of spawning activity and discharge use by Atlantic salmon (Salmo salar L.). *Geomorphology 60*, 21–35. https://doi.org/10.1016/j.geomorph.2003.07.014

Nagaya, T., Shiraishi, Y., Onitsuka, K., Higashino, M., Takami, T., Otsuka, N., Akiyama, J., Ozeki, H., (2008). Evaluation of suitable hydraulic conditions for spawning of ayu with horizontal 2D numerical simulation and PHABSIM. *Ecol Modell 215*, 133–143. https://doi.org/https://doi.org/10.1016/j.ecolmodel.2008.02.043

Nale, J.P., Pakhale, G.K., (2024). Implications of digital elevation models on habitat analysis of Golden Mahseer in the Upper Ganga Basin, India. *Water Biology and Security 3*, 100278. https://doi.org/https://doi.org/10.1016/j.watbs.2024.100278

Sayed, A., Akter, A., (2022). *The Low Flow Assessment of Padma River in Bangladesh 8*, 1–10. https://doi.org/10.22146/jcef.

Spence, R., Hickley, P., (2000). The use of PHABSIM in the management of water resources and fisheries in England and Wales. *Ecol Eng 16*, 153–158. https://doi.org/https://doi.org/10.1016/S0925-8574(00)00099-9

Strevens, A.P., (1999). Impacts of groundwater abstraction on the trout fishery of the River Piddle, Dorset; and an approach to their alleviation. *Hydrol Process 13*, 487–496. https://doi.org/10.1002/(SICI)1099-1085(19990228)13:3<487::AID-HYP752>3.0.CO;2-W

Stucchi, L., Bocchiola, D., (2023). Environmental Flow Assessment using multiple criteria: A case study in the Kumbih river, West Sumatra (Indonesia). *Science of The Total Environment 901*, 166516. https://doi.org/https://doi.org/10.1016/j.scitotenv.2023.166516

Stucchi, L., Fugazza, D., Sharifi, A., Traversa, G., Diolaiuti, G., Bocchiola, D., (2024). An algorithm to generate 2D bathymetry of an Alpine river for habitat suitability assessment. *Science of The Total Environment 918*, 170703. https://doi.org/https://doi.org/10.1016/j.scitotenv.2024.170703

Webb, J.H., Gibbins, C.N., Moir, H., Soulsby, C., (2001). Flow requirements of spawning atlantic salmon in an upland stream: Implications for water-resource management. *Water and Environment Journal 15*, 1–8. https://doi.org/10.1111/j.1747-6593.2001.tb00296.x

Wen, X., Liu, Z., Lei, X., Lin, R., Fang, G., Tan, Q., Wang, C., Tian, Y., Quan, J., (2018). Future changes in Yuan River ecohydrology: Individual and cumulative impacts of climates change and cascade hydropower development on runoff and aquatic habitat quality. *Science of The Total Environment 633*, 1403–1417. https://doi.org/https://doi.org/10.1016/j.scitotenv.2018.03.309

Yi, Y., Cheng, X., Yang, Z., Wieprecht, S., Zhang, S., Wu, Y., (2017). Evaluating the ecological influence of hydraulic projects: A review of aquatic habitat suitability models. *Renewable and Sustainable Energy Reviews 68*, 748–762. https://doi.org/https://doi.org/10.1016/j.rser.2016.09.138

Technical Journal
River Research Institute ISSN: 1606-9277

Environmental Flow Estimation for the Jamuna River

S. A. Jawad[1*], M. Wardi[2] and A. F. M. Saleh[3]

Abstract

A river's natural prominence is verified by the environmental flow criterion. This study project aims to evaluate the Jamuna River's e-flow. The goal is to evaluate the e-flow for fisheries, maintaining the river ecology and morphological balance. Analyzing, daily discharge data, according to the Tennant method, the Jamuna River must flow at least 6287 m^3s^{-1} from December to March and 42580 m^3s^{-1} from July to September to be sustainably managed. The FDC Method indicates that the 90th percentile flow is 6480 m^3s^{-1} in the dry season and 17008 m^3s^{-1} in the rainy season. The Wetted Perimeter method estimates that 6531 m^3s^{-1} e-flow should be present in the river all year round to ensure aquatic accommodation for marine species. The Habitat Simulation analysis shows flow requirements for key species. The BBM estimates e-flow of 5363 m^3s^{-1} in the dry season. The minimum flow requirement for morphology dominates in November to April, and the flushing flood requirement dominates from July to September. Compared to low flow threshold, historically, enough flow is not present in most times of the dry seasons to meet e-flow demands, meaning no scope of consumptive use of river water. But recent trends in hydrological variations, particularly precipitation events during the latter times of the year suggests meeting e-flow demands for Jamuna in the upcoming years but regular use of excess water for consumptive purposes is less likely according to this study.

Keywords: *Building blocks, Environmental flow, Habitat, Holistic, Hydrological, Hydraulic, Jamuna River, Low flows.*

Introduction

Environmental flows are referred as the river flow features required to safeguard the integrity of riverine ecosystems. It is as the minimum flow that remains in rivers during dry seasons to maintain ecological health. Over time, this definition has evolved to include not only the minimum flow but also the water consumption needs of various species, reflecting a more holistic approach to water management (Morrison & Bray, 2019). Integrated Water Resources Management (IWRM) emphasizes the importance of balancing economic efficiency, equity, and ecological sustainability in the governance of water resources, ensuring that both ecosystem and human needs are met. One of the primary reasons environmental flows is important is that it supports biodiversity. Healthy river systems rely on adequate water flow to provide habitat for various species, including fish, birds, and other wildlife. Without sufficient flow, these species may struggle to survive, leading to declines in biodiversity (Naiman et al., 2002).

The Brahmaputra-Jamuna, which flows through China, Tibet, India and Bangladesh, is the second-largest river in Bangladesh and one of the biggest rivers in the world. The Jamuna is the downstream channel of Brahmaputra, which was altered followed by the devastating flood and earthquake that took place between 1782 and 1787. The Jamuna River runs between Bahadurabad and Aricha, while the Brahmaputra currently continues south-east from Bahadurabad (Dewanganj upazila of Jamalpur district). Brahmaputra-Jamuna is 276 km long, of which Jamuna is 205 km. The river's width ranges from 3 km to 20 km, averaging roughly 10 km. The river has multiple channels that are braided together. It forms a single water channel and is surrounded with bars (chars) for most of its course within Bangladesh, most of which are submerged during the wet season. This river thus qualifies as one of the largest in the world just based on its width (Chowdhury, 2021). For this study, the section of the Jamuna River from the Jamalpur district to its confluence point has been chosen. along this segment of the Jamalpur river, the districts of Sirajganj, Pabna, and Manikganj are situated adjacent to the riverbank, each offering distinct ecological and socio-economic characteristics that affect the river's well-being and utilization.

Despite environmental flows being traditionally more important for relatively smaller channels, it can also be of interest for larger channels like the Jamuna River in terms of safeguarding the ecological balance as well as water security and socio-economic stability by protecting river ecosystems, sustaining fisheries & livelihoods, protecting riverbank erosion & sedimentation, supporting agriculture & irrigation, adapting to climate change and strengthen negotiation in transboundary water sharing agreements.

In Bangladesh, several e-flow studies have been conducted in some important rivers. Holistic approach has been used to assess the e-flow in the Ganges River (J. Akter, 2010). Hydrological methods have been used for a series of rivers from Gorai to Balaswar river (Islam, 2019). The BBM has been studied regarding four blocks of the flow required for Halda. E-flow has been estimated using Log-Pearson Type – (iii) Distribution for Halda (A. Akter & Ali, 2012) and Padma (Sayed & Akter, 2021). Gorai River has been

[1]Department of Water Resources Engineering, Bangladesh University of Engineering and Technology, Dhaka -1000, Bangladesh.
[*]Corresponding author: (E-mail: azmaeen990@gmail.com)
[2]Institute of Water and Flood Management. Bangladesh University of Engineering and Technology, Dhaka -1000, Bangladesh.
[3]Department of EWCE, Military Institute of Science and Technology, Mirpur, Dhaka -1216, Dhaka, Bangladesh.

analyzed using the PHABSIM approach to predict the instream flow demand as well as the salinity intrusion level (Saha, 2007). A study has been carried out dealing with the calculation of the Instream Flow Requirement (IFR) of the Dudhkumar River utilizing the Tennant, FDC and Constant Yield methods of the hydrological approach (Hossain, 2010).

The key objectives are to estimate the e-flow requirements through available methodologies and to assess available flow of Jamuna through e-flow.

Methodology

Study Area

Stations from both upstream and downstream reaches of the Jamuna River have been considered for the analysis (25.133ºN, 89.741ºE to 23.951ºN, 89.762ºE). All necessary hydrologic and channel geometry dataset were collected from Bangladesh Water Development Board (BWDB) which included historical discharge, water levels, and channel morphology of different cross sections. Historical non-tidal discharge data of upstream were collected from 1956 to 2012. WL for Bahadurabad (SW 46.9L), Kazipur (SW 49A), Sirajganj (SW 49), and Mathura (SW 50.3) were used for calculations. Morphological data of RMJ 2, RMJ 4, RMJ 9, and RMJ 13 (downstream to upstream) were used for hydraulic analysis for the year 2021.

For the habitat analysis, The Carp, Golda, and Hilsha were used as fish indicators and Gangetic dolphin and Ghorial were used as habitat indicators in this study. In the past, these aquatic species have been used for the Ganges River study (Akter, 2010).The Golda has been used in the Gorai-Madhumati-Kaliganga-Balaswar river system (Islam, 2019).

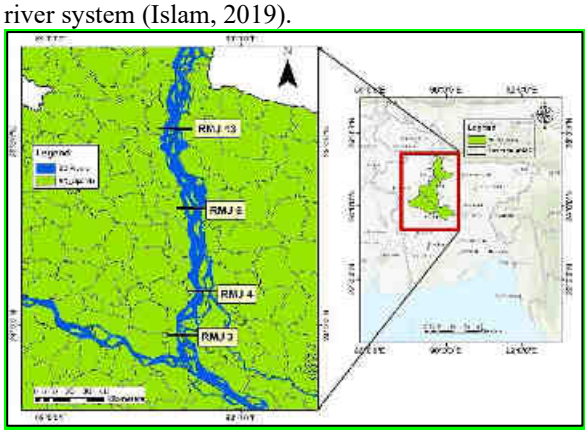

Fig. 1. Study area including gauge stations.

E-flows have been calculated using more than 200 different methods in numerous nations all over the world. These methods can be broadly classified into four significant methodologies that are frequently employed for e-flow assessment. Which are: (i) Hydrological Approach (ii) Hydraulic Approach (iii) Habitat Rating Approach (iv) Holistic Approach.

Hydrological Approach

Hydrological approaches are the most basic way to measure e-flow, as they rely on past hydrological data to make flow recommendations. Most of the time, historical, daily, or monthly discharge records have this information. The most common hydrological methods are: Tennant Method, Flow Duration Curve (FDC) Method, Aquatic Base Flow Method (ABFM) and Range of Variability Approach (RVA).

Table 1. Hydrological and hydraulic datasets used for the analysis.

Data Type	Station ID	Station Name	Latitude	Longitude	Period
Discharge	SW 46.9L	Bahadurabad	25.13	89.73	1956 to 2012 & 2021
Water Level	SW 46.9L	Bahadurabad	25.13	89.734	2021
	SW 49A	Kazipur	24.67	89.649	
	SW 49	Sirajganj	24.466	89.72	
	SW 50.3	Mathura	23.948	89.652	
Morphology	RMJ 13	N/A	25.133	89.741	2021
	RMJ 9		24.644	89.815	
	RMJ 4		24.139	89.794	
	RMJ 2		23.951	89.762	

Tennant Method consists of eight flow categorization classes by analyzing a series of field measurements and observations to associate habitat quality with varied percentages of mean annual flow (Tennant, 1976); (Arthington, 2012) ;(Reiser et al., 1989); (Jowett, 1997); (Bari & Machand, 2006). Minimum 10% of Average annual flow (AAF) during low flow season and 30% of MAF during high flow seasons is the threshold for the river to sustain.

The FDC Method illustrates the link between river flow volume and duration to generate a flow duration curve (FDC). The monthly flow duration curve's 50^{th} percentile flow (for high flow seasons) and 90^{th} percentile flow (for low flow seasons) is chosen as the environmental flow requirements (EFR) (Smakhtin, 2001). The flow exceedance probability curve can be constructed to accommodate daily, weekly, or monthly data and is produced using existing hydrologic flow data from a chosen time of interest. To develop the probability of flow exceedance, Weibull formula is broadly used:

$$P = \frac{M}{n+1} * 100\% \quad \text{Eq. (1)}$$

Where, P is the percentage probability that the given flow will be equaled or exceeded, M is the assigned rank number of the flow values in descending order and n is the total number of days that minimum flow value is observed.

The Aquatic Base Flow Method (ABFM) is based on hydrologic indices on the presumption that the lowest monthly median discharge is sufficient to fisheries for the entire year, unless supplementary flow is required for spawning, incubation and hatching. This method is only applicable for perennial rivers and unregulated streams (Armstrong et al., 2003).

The Range of Variability (RVA) technique seeks to deliver a thorough statistical analysis of a flow regime's ecologically significant properties. According to the features of the regime, which include amplitude, timing, length, frequency, and deviation rate of discharge are distributed into five categories (Richter et al., 1997). For this approach, the tool known as Indicators of Hydrologic Alteration (IHA) is used.

Hydraulic Approach

These methods establish a quantitative relationship between discharge and the caliber of an instream resource, such as a habitat for fishery (Lina et al., 2010). Wetted-Perimeter (WP) Method is the most recognized hydraulic approach.

In the WP Method, wetted perimeter vs discharge curve is generated at a specific cross-section of the given stream. The steepest slope or the point of inflection indicates a drastic change of wetted perimeter for a slight change of discharge. The endmost breakpoint of the plot is considered as e-flow in case of multiple inflection points for any river section.

Habitat Rating Approach

Preferable habitat criteria are considered to find out the demand of discharge for that species. Physical Habitat Simulation Method is one of the most practiced habitat rating approaches. The objective of the Physical Habitat Simulation Method (PHABSIM) is to conserve particular and pre-selected target species for which the habitat requirements in the research region may be accurately predicted or are believed to be known from earlier studies elsewhere. The strategy aims to pinpoint this idea by simulating the discharge conditions and selecting a target flow (typical recommendations include a static minimum flow level) so that the amount of physical habitat for the selected group of target species does not fall below an arbitrary conservation threshold (Bullock et al., 1991). The accommodation condition for the species for a given flow condition is determined by:

$$Q = A*V \quad \text{Eq. (2)}$$

Where, Q is the flow rate, A is the cross-sectional wetted area and V is the flow velocity.

Holistic Approach

The e-flow measured by the other three approaches is not enough to meet the need for the flow in rivers. Hence, the river scientists developed Building Block Method in workshops during the 1990s (King & Tharme, 1994).The Building Block Method (BBM) requires parameters not only from river discharge but also the discharge required for the life and growth of species living in the river.

Channel maintenance, also known as flushing flows, is vital for the preservation of numerous geomorphological and sedimentological properties of river channels. The required flushing flows are calculated from the 200% of AAF by the Tennant method (Tennant, 1976).

The flow requirement for morphological equilibrium has been considered the 80% dependable flow for each month. The Gumbel distribution equation is calculated as 80% dependable flow (Akter, 2010).

$$Q(T) = q + K * \sigma_{n-1} \quad \text{Eq. (3)}$$

Here, Q(T) is the dependable flow and q is average discharge of each month;

$$\sigma_{n-1} = \sum \left(Q_i - Q_{mean}\right)^2 / (n-1) \quad \text{Eq. (4)}$$

σ_{n-1} is the standard deviation of discharge of each month.

$$K = - \ln \{ \ln (\frac{T}{T-1}) \} + \frac{Y_n}{S_n} \quad \text{Eq. (5)}$$

K = the frequency factor.

Y_n= Reduced mean in Gumbel's extreme value distribution = 0.5362

S_n = Reduced standard deviation in Gumbel's extreme value distribution = 1.1124

T = 2.33 years return period (considering only the dry periods or an average of 5 years which is the probability of 0.2)

Results and Discussions

Hydrologic Approach

The average annual flow (AAF) is found to be 21290 m^3s^{-1} after analyzing 30 years of discharge data. According to Tennant, during dry seasons there must be at least 10% of the AAF for the river to be in fair condition. But since Jamuna is such a big river with broad cross sections, 30% has been the criteria considered to be in fair condition in this analysis. So, more than 30% of the AAF should be present from December to March. The 200% flow of the AAF is also a crucial component during the flood seasons (**Table 2**).

Table 1. Flow criteria for different conditions.

% AAF	Flow Requirements (m^3s^{-1})
200% (Flushing flow)	42580
60-100% (Optimum range)	12774-21290
60% (Outstanding)	12774
50% (Excellent)	10645
40% (Good)	8516
30% (Fair or Degrading)	6387
10% (Poor)	2129
<10% (Severe Degradation)	<2129

The flows in January, February, and March are lesser than the river system's fair condition (30% of AAF). The flows of April, May, October, and November keep the river system in outstanding condition. The flow of June preserves the river's optimum condition, while the flow of July, August, and September serve as the river's flood peaks. As a result, the e-flow needed for December to March is 6387 m^3s^{-1}, and for July to September, it is 42580 m^3s^{-1} (**Table 3**).

Table 2. E-flow according to Tennant Method.

Months	Environmental Flow (m^3s^{-1})	
December	30% of AAF (Fair condition for dry season)	6387
January		6387
February		6387
March		6387
July	200% of AAF (Flushing floods for wet season)	42580
August		42580
September		42580

In ABFM, firstly, monthly median flows were calculated for each year, from 1981 to 2010. Then median flow for each specific month throughout the time span of 30 years have been calculated (**Table 4**). It has been found that the lowest median flow is in February. So, 4570 m^3s^{-1} is the estimated e-flow according to ABFM.

Table 3. E-flow according to ABFM.

Months	Median monthly flows (m^3s^{-1})
January	5158
February	4570
March	5026
April	9012
May	15150
June	31753
July	49943
August	41084
September	38800
October	25400
November	12265
December	7629

In the FDC method, 50th and 90th percentile flow values from 2001 to 2010 were determined, then the mean values of Q50 and Q90 have been used as EFR for dry and wet seasons (**Table 5**).

Table 4. E-flow according to FDC Method.

Environmental Flow Requirement from the Flow Duration Curve Method												
Months	April	May	June	July	Aug	Sep	Oct	Nov	Dec	Jan	Feb	Mar
Flow Season	Low Flow Season (Q90)		High Flow Season (Q50)						Low Flow Season (Q90)			
Suggested EFR (m^3s^{-1})	6479		17008						6479			

IHA software was used for the RVA throughout a 50-year period, 1961 to 2010. Environmental flow components such as extreme low flows, high flows, small floods, large floods etc. have been quantified. The four horizontal lines (purple, blue, green & red) indicate minimum large flood peak flow, minimum small flood peak flow, high flow threshold and extreme low flow threshold which are 76000 m^3s^{-1}, 65500 m^3s^{-1}, 32000 m^3s^{-1} and 4100 m^3s^{-1} respectively (**Fig. 2**).

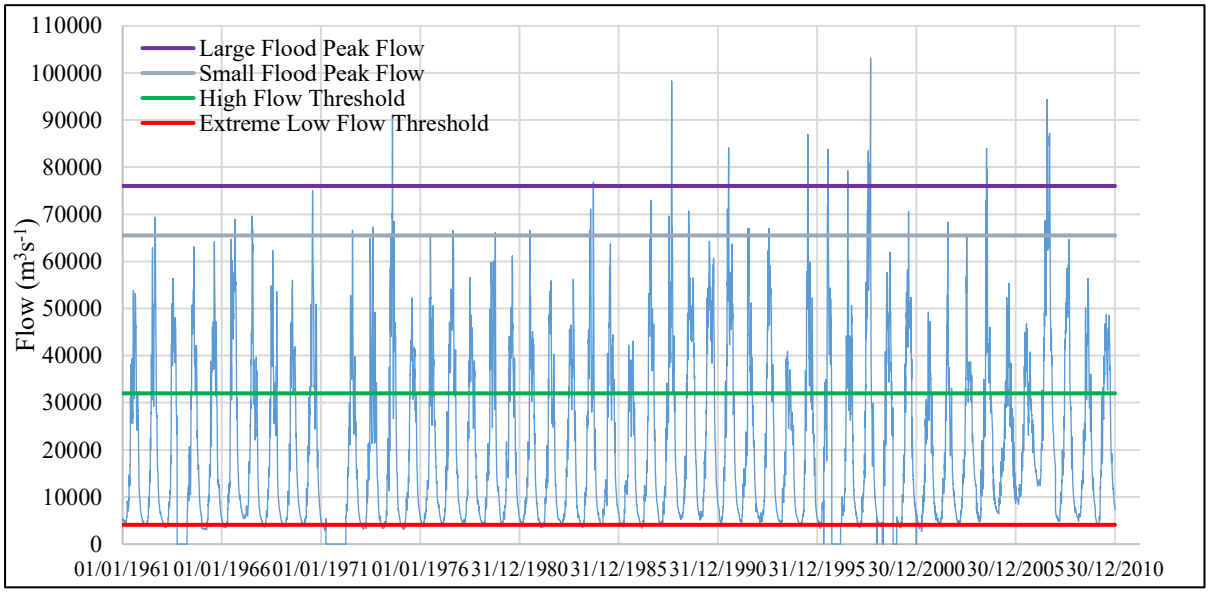

Fig. 2. E-flow components in RVA.

Hydraulic Approach

Wetted perimeters (WP) for the cross-sections were obtained using steady flow simulation in HEC-RAS software. Manning's 'n' was assumed to be 0.025 for the model. Corresponding perimeters were found for different water levels for Mathura station (RMJ 2), discharge from the last breakpoint has been found 6531 m^3s^{-1} for 2021. Same process was repeated for all stations.

Water level corresponding to 6531 m^3s^{-1} is shown in the cross-section (**Fig. 3**). If discharge decreases from this point, more braid bars also known as "chars" would emerge, resulting in lesser aquatic space to accommodate marine species. In the same way the critical flow values of other stations were determined (**Table 6**).

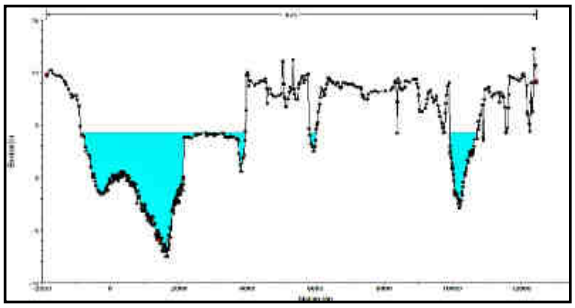

Fig. 3. Cross-sectional profile with required e-flow for Mathura station in 2021.

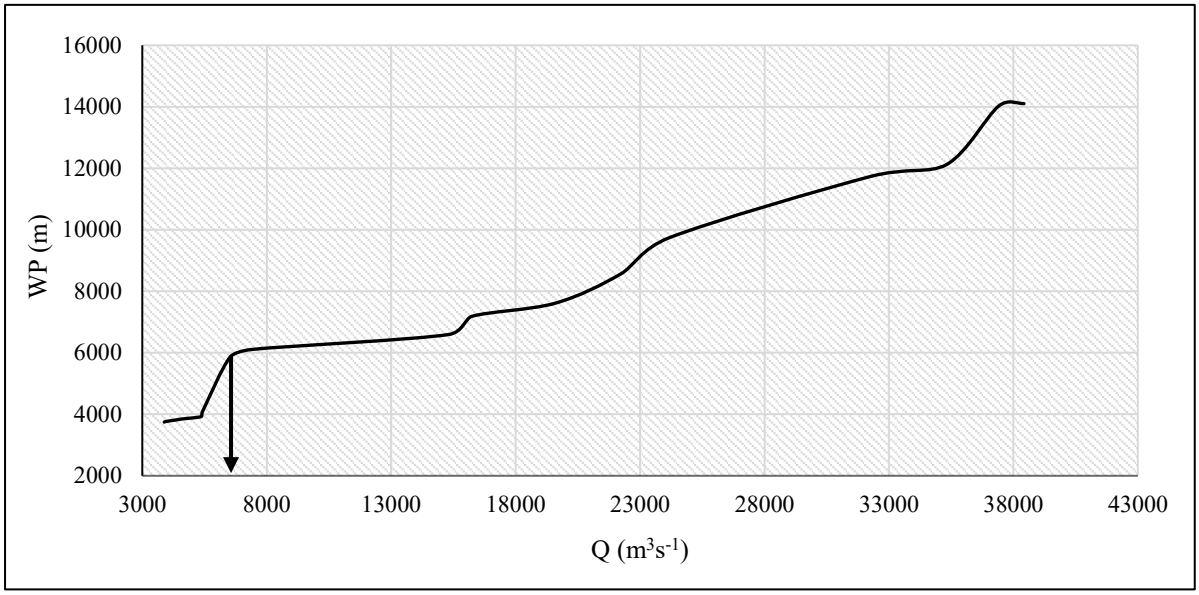

Fig. 4. WP vs Q for Mathura station in 2021.

Table 5. E-flow according to WP Method.

Stations	WP (m)	Q (m^3s^{-1})
Bahadurabad	4851	7419
Kazipur	4484	7419
Sirajganj	7737	16238
Mathura	5865	6531
E-flow (m^3s^{-1})	6531	

Habitat Approach

EFR was estimated using the physical habitat simulation approach from the 4 stations. The flow demands for the species Ghorial, Golda, Hilsha, Carp, and Dolphin were calculated. The lowest flow demand out of the 4 stations has been selected after determining the species' necessary discharge criteria. Next, the governing values have been chosen as the e-flow based on those species' required flow values. The least demanded flow has been chosen as e-flow, which is 5179 m^3s^{-1} in March.

Table 6. E-flow requirements according to PHABSIM Method.

Month	Required e-flow (m^3s^{-1})
January	6388
February	5312
March	5179
April	6291
May	14514
June	28612
July	34087
August	38406
September	40997
October	25031
November	9833
December	6605

Holistic Approach

This method calculates the flow demand of each indicator for Bahadurabad, Mathura, Sirajganj and Kazipur stations. The indicators are fisheries (Carp, Golda, Hilsha), habitat (Ghorial, Gangetic Dolphin), flushing floods, and morphology.

The histograms (Fig. 5) show the e-flow demand of fisheries and habitat at Bahadurabad station. The first histogram shows that the Golda (the e-flow of 22,213 m^3s^{-1} in November) dominates during the dry season (November-April) and the Hilsha (the e-flow of 61,714 m^3s^{-1} in August) dominates during the wet season (May-October) in the river. The Carp (the e-flow demand of 11,107 m^3s^{-1} in November, and 41,143 m^3s^{-1} in August) shows the lowest demand of e-flow in all year than the other two fishes.

Similarly, by evaluating the demands of fish habitats for other stations (Mathura, Sirajganj, and Kazipur), it is established that the demand for Golda dominates

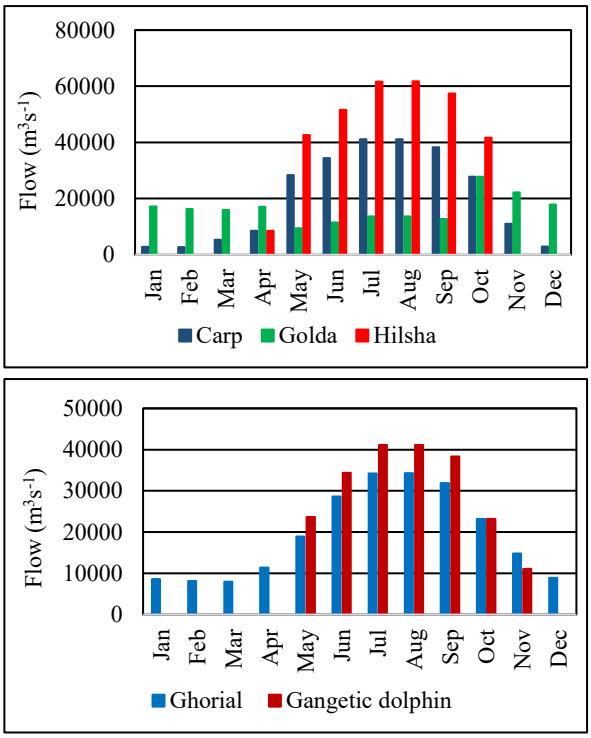

Fig. 5. E-flow for fisheries and habitat at Bahadurabad

from October to April and the demand for Hilsha dominates from May to October.

In the dry season, the highest flow requirement for Ghorial is 14,809 m^3s^{-1} in November, while the highest flow requirement in the wet season is 34,286 m^3s^{-1} in August. The maximum flow needed for Gangetic Dolphin in the wet season is 41,143 m^3s^{-1} (**Fig. 5**). The Gangetic Dolphin is seen in the river when the water level rises from May to October.

The results of Gangetic Dolphin and Ghorial habitats suggest that Ghorial has the highest discharge requirements during the dry season and Gangetic dolphin has the highest discharge needs during the wet season (May to October). This conclusion applies to other stations as well.

The flushing flow is a hydrological indicator that can be determined. According to the BB Method, it mostly signifies a river's high flow value. The 200% of AAF is 42580 m^3s^{-1} which is required for flushing flow. The flushing flow dominates in July, August and September.

To estimate e-flow demand, the monthly flow requirements for key indicators have been summarized for Bahadurabad (**Table 8**). Golda has the highest flow demand from November to April, Hilsha has the highest flow demand in May to October. Same procedure is followed for the other 3 stations. Then the required monthly e-flows of all the stations have been compared with each other to obtain the river's monthly e-flow requirements (**Table 9**). Among the 12 months the minimum e-flow is in March at Kazipur station.

Hence, it is the e-flow for the Jamuna River. Therefore, according to BBM, the lowest flow requirement among the four stations is 5363 m^3s^{-1}.

Considering relevant parameters, the building blocks have been developed (**Fig. 6**) showing the monthly flow demands for the river to sustain. 30% of the average monthly flows are considered as low flows, flows needed for morphological balance are calculated from Gumbel's distribution and the flushing floods are 200% of the historical AAF

Table 7. Monthly e-flow requirements according to BBM at Bahadurabad station.

Month	Carp	Golda	Hilsha	Gharial	Gangetic Dolphin	Flushing flow	Morphology	Required e-flow (m^3s^{-1})
January	2865	17189	0	8594	0	0	5327	17189
February	2707	16245	0	8122	0	0	4697	16245
March	5311	15933	0	7967	0	0	5043	15933
April	8551	17101	8551	11401	0	0	7210	17101
May	28378	9459	42567	18919	23649	0	11624	42567
June	34395.5	11465	51593	28663	34396	0	21263	51593
July	41109	13703	61664	34258	41109	42580	38697	61664
August	41143	13714	61714	34286	41143	42580	37007	61714
September	38314	12771	57471	31928	38314	42580	31592	57471
October	27797	27797	41696	23164	23164	0	18929	41696
November	11107	22213	0	14809	11107	0	10214	22213
December	2978	17866	0	8933	0	0	7292	17866

Table 8. Monthly e-flow requirements of the Jamuna River according to BBM.

Month	Bahadurabad	Kazipur	Sirajganj	Mathura	Required e-flow (m^3s^{-1})
January	17189	6379	8172	10118	6379
February	16245	5480	7847	9406	5480
March	15933	5363	7811	9337	5363
April	17101	7210	8054	10179	7210
May	42567	13773	11624	19557	11624
June	51593	28643	33102	39104	28643
July	61714	42580	47392	52453	42580
August	61714	42580	51126	57073	42580
September	57471	42580	50664	52836	42580
October	41695	24518	30216	38477	24518
November	22213	10214	11792	17460	10214
December	17865	7292	8790	12177	7292

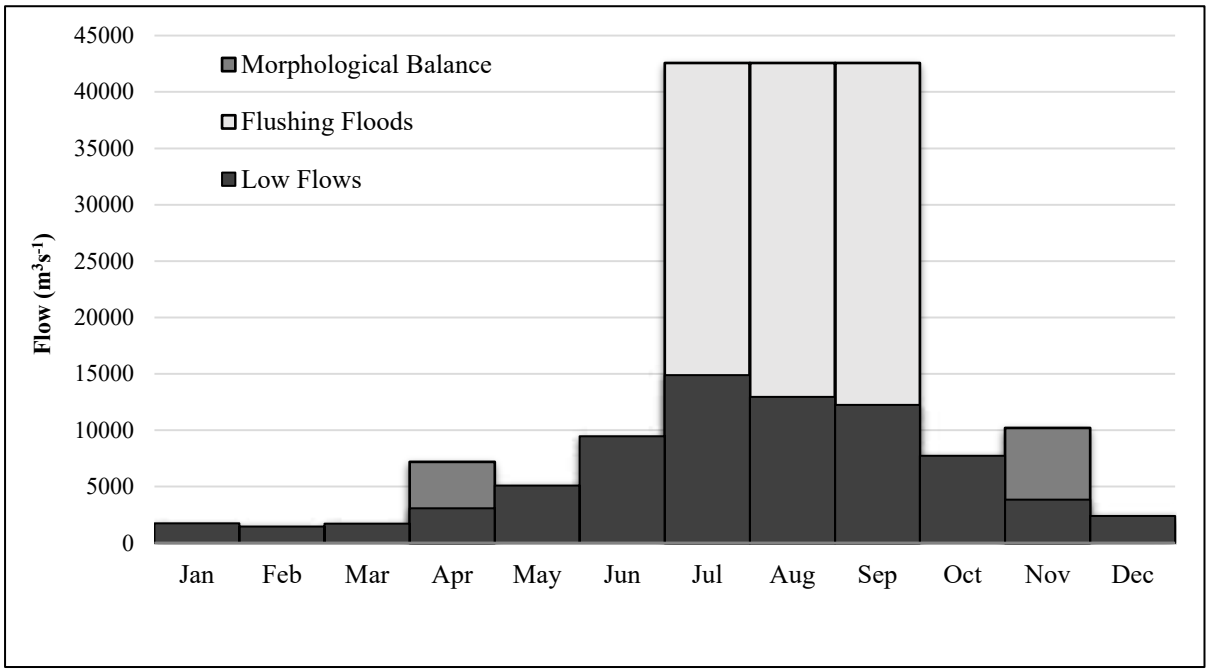

Fig. 6. Monthly e-flow demands according to BBM.

Table 9. Summary of all methods.

Month	Hydrological Approach			Hydraulic Approach	Habitat Approach	Holistic Approach
	Tennant	FDC	ABFM	WPM	PHABSIM	BBM
January	6387	6479	5158	6531	6388	6379
February	6387	6479	4570	6531	5312	5480
March	6387	6479	5026	6531	5179	5363
April	-	6479	9012	6531	6291	7210
May	-	6479	15150	6531	14514	11624
June	-	17008	31753	6531	28612	28643
July	42580	17008	49943	6531	34087	42580
August	42580	17008	41084	6531	38406	42580
September	42580	17008	38800	6531	40997	42580
October	-	17008	25400	6531	25031	24518
November	-	6479	12265	6531	9833	10214
December	6387	6479	7629	6531	6605	7292
E-flow (m^3s^{-1})	6387	6479	4570	6531	5179	5363

Akter (2010) reported a minimum e-flow of 1008 m^3s^{-1} for the Ganges. In contrast, a more recent study on the Padma River estimated the minimum e-flow at Mawa station to be 1992 m^3s^{-1} (Sayed & Akter, 2021). The results of another study suggest that the required environmental flow for the Kobadak River is approximately 20.0 m^3s^{-1} (Jahid, 2016). The estimated e-flow of Jamuna River is greater than most of the river's e-flow study because of its significant discharge, which is influenced by seasonal rainfall

patterns and upstream water management practices. These factors collectively contribute to the variability in environmental flow requirements across different river systems.

Conclusion

The environmental flow requirement for the Jamuna River has been analyzed using several approaches to understand the water demands from different aspects of nature. There are not only demands to ensure a sound habitat condition for the aquatic species throughout the year but also there is the need of channel maintenance floods for the preservation of morphological and sedimentological properties of the river. The hydrologic methods have provided similar results. From RVA low flow threshold has been found to be 4100 m^3s^{-1}. The hydraulic method suggested that flow below 6531 m^3s^{-1} may cause habitat conditions to deteriorate. But of all methods, the holistic approach is most comprehensive as it considers all parameters relevant to the river. The BBM suggests that, 5363 m^3s^{-1} is the bare minimum discharge needed for Jamuna. But, during the dry season the daily river flows are mostly around the low flow threshold. That means in the later and earlier time of the years the river will not be able to provide water for consumptive uses like industry, irrigation, water supply etc. In other times of the year Jamuna usually can provide water for such uses. Due to climate change, rainfall events are taking place in early and late winters more often which indicates that the river might meet e-flow demands in the near future during the dry months.

Estimating the environmental flow of the Jamuna River contributes to the scientific understanding of large, braided, monsoon-driven river systems. It provides critical data for ecological sustainability, transboundary water governance, and the refinement of e-flow methodologies in data-scarce, high-discharge rivers of South Asia.

Conflict of Interest

The authors declare no conflict of interest.

References

Akter, J. (2010). *Environmental Flow Assessment for The Ganges River* [M.Sc. Thesis, Bangladesh University of Engineering and Technology]. https://doi.org/10.13140/RG.2.2.19294.97609

Akter, A., & Ali, M. H. (2012). Environmental flow requirements assessment in the Halda River, Bangladesh. *Hydrological Sciences Journal*, *57*(2), 326–343. https://doi.org/10.1080/02626667.2011.644242

Armstrong, D. S., Parker, G. W., & Richards, T. A. (2003). *Evaluation of Streamflow Requirements for Habitat Protection by Comparison to Streamflow Characteristics at Index Streamflow-Gaging Stations in Southern New England*. https://doi.org/10.3133/wri034332

Arthington, A. H. (2012). Introduction to Environmental Flow Methods. In *Environmental Flows* (pp. 125–138). University of California Press. https://doi.org/10.1525/california/9780520273696.003.0009

Bari, M. F., & Machand, F. (2006). *Introducing Environmental Flow Assessment in Bangladesh: Multidisciplinary Collaborative Research*.

Bullock, A., Gustard, A., & Grainger, E. S. (1991). *Instream flow requirements of aquatic ecology in two British rivers: Application and assessment of the instream flow incremental methodology using the PHABSIM system*. https://nora.nerc.ac.uk/id/eprint/7351

Chowdhury, M. H. (2021, June 17). *Jamuna River*. Banglapedia.

Hossain, M. J. (2010). *Assessment of Instream Flow Requirement of Dudhkumar River* [M.Sc. Thesis, Bangladesh University of Engineering and Technology]. http://lib.buet.ac.bd:8080/xmlui/handle/123456789/149

Islam, M. T. (2019). *Environmental Flow Assessment of Gorai-Madhumati-Kaliganga-Balaswar river system* [M.Sc. Thesis, Bangladesh University of Engineering and Technology]. http://lib.buet.ac.bd:8080/xmlui/handle/123456789/5738

Jahid, S. A. (2016). *Assessing Environmental flow for the Kobadak River and Developing a Framework for its Maintenance* [M.Sc. Thesis, Bangladesh University of Engineering and Technology]. http://lib.buet.ac.bd:8080/xmlui/handle/123456789/4475

Jowett, I. G. (1997). Instream Flow Methods: A Comparison of Approaches. *Regulated Rivers: Research & Management*, *13*(2), 115–127.

King, J. M., & Tharme, R. E. (1994). *Assessment of the Instream Flow Incremental Methodology and Initial Development of Alternative Instream Flow Methodologies for South Africa*.

Lina, J., Suxia, L., & Xinchun, W. (2010). Wetted Perimeter Approach to Estimate Instream Flow Requirements: A Case Study in Luanhe Water System. *Progress in Geography*.

Morrison, R., & Bray, E. (2019). Environmental Flows. In *Environmental Science*. Oxford University Press. https://doi.org/10.1093/obo/9780199363445-0116

Naiman, R. J., Bilby, R. E., Schindler, D. E., & Helfield, J. M. (2002). Pacific Salmon, Nutrients, and the Dynamics of Freshwater and Riparian Ecosystems. *Ecosystems*, *5*(4), 399–417. https://doi.org/10.1007/s10021-001-0083-3

Reiser, D. W., Wesche, T. A., & Estes, C. (1989). Status of Instream Flow Legislation and Practices in North America. *Fisheries*, *14*(2), 22–29.

Richter, B., Baumgartner, J., Wigington, R., & Braun, D. (1997). How much water does a river need? *Freshwater Biology*, *37*(1), 231–249. https://doi.org/10.1046/j.1365-2427.1997.00153.x

Saha, P. P. (2007). *Assessment of instream flow requirement of gorai river considering salinity intrusion and fish habitat* [M.Sc. Thesis, Bangladesh University of Engineering and Technology]. http://lib.buet.ac.bd:8080/xmlui/handle/123456789/335

Sayed, M. A., & Akter, A. (2021). The Low Flow Assessment of Padma River in Bangladesh. *Journal of the Civil Engineering Forum*, *8*(1), 11–20. https://doi.org/10.22146/jcef.3604

Smakhtin, V. U. (2001). Low flow hydrology: a review. *Journal of Hydrology*, *240*(3–4), 147–186. https://doi.org/10.1016/S0022-1694(00)00340-1

Tennant, D. L. (1976). Instream Flow Regimens for Fish, Wildlife, Recreation and Related Environmental Resources. *Fisheries*, *1*(4), 6–10.

Technical Journal
River Research Institute ISSN: 1606-9277

Performance Analysis of Water Intake System in the Ganges River at Godagari Using Physical Model

B. Roy [1]*, O. A. Maimun[1], M. J. Islam[1], M. Shahabuddin[1], M. Moniruzzaman[2], M. Masuduzzaman[1] and P. Kanungoe[1]

Abstract

An Intake structure in the Ganges River has been envisaged as a means for supplying surface water by pumping to Rajshahi city corporation area for municipal use through the treatment process. The performance of the intake structure was investigated in an undistorted physical scale model. The Froude model was constructed on a geometric similar scale of 1: 25. The study aims to evaluate the hydraulic performance of a river intake system by assessing flow uniformity, critical submergence, swirl effects, and air entrainment at the pump inlet. It also investigates preventing debris entry and ensuring efficient water withdrawal under varying pump operating conditions. The findings indicate that the intake system, designed to maintain a minimum or critical submergence of 1.93m, operated smoothly at a maximum capacity of 360MLD without disturbance. The system also exhibited uniform flow approaching the intake and within the distribution chamber, while weak free surface vortices and rotational flow occurred under specific scenarios. However, no entrained air or gas bubble was detected at the pump's inlet. To enhance the intake system's performance, it is recommended to extend the washout pipe to prevent sediment and small objects from entering through the coarse screen during backwashing operation. The proposed design of intake structure has proven effective in physical model testing and it is recommended for field implementation.

Keywords: *Physical model, Rajshahi WASA, River intake system, Swirl flow, Submergence, Vortex flow.*

Introduction

Rajshahi city primarily relies on groundwater for its drinking water supply. The population of this city is gradually growing due to expanding in area. That's why the availability of ground water is gradually decreasing with increasing demand. Approximately 93% of the population in Rajshahi City Corporation relies on underground water, uplifted through tube wells or deep tube wells, which is supplied via pipelines. In contrast, only a small percentage of people use surface water for domestic or agricultural purposes (Hasan, 2018). The Ganges, one of the Mighty Rivers of Bangladesh is flowing nearby the city. This city is located on the northern side and left bank of the river. The intake structure will be placed at Jot Goshaidas, Godagari, in the Rajshahi district, approximately 2.5 km downstream of the confluence of the Ganges and Mohananda Rivers. Water will be drawn from the Ganges River through this intake. In this location the river has enough flow and water depth to fulfil the increasing water demand of Rajshahi city. Even in extreme dry season, it is possible to fulfil the demand of water in the city area. The existence of the intake is very helpful in supplying raw water for the needs of clean water. Intake structures are constructed in surface water sources, such as rivers, lakes, and reservoirs, to withdraw water and direct it into the conduits of water supply systems. Intake structures on channels are designed to divert a specific amount of water for various purposes, including irrigation, industrial cooling, potable water supply, and hydroelectric power generation. These structures must ensure that both the diverted water and the remaining flow can be managed without causing harm to the environment or the intake system. An intake structure for municipal water supply is typically made of masonry or concrete and is designed to deliver relatively clean water, free from pollution, sand, and undesirable floating materials. The primary functions of an intake structure are to facilitate the safe extraction of water from a surface source, ensure a smooth and turbulence-free flow into the conveyance passages, and prevent coarse river-borne debris, such as boulders, ice, large pieces of wood, plastic and logs, from entering the system (Iqbal et al., 2015).

Submergence (S) refers to the vertical distance between the pump's water inlet and the dynamic water surface. If the submergence is less than the critical submergence (Sc), a vortex forms, resulting in suction loss and reduced pump efficiency (Khanarmuei et al., 2018). When the submergence of an intake is inadequate, air enters and can cause operational problems in the intake system and pumps. The value of the submergence of the intake at which vertex and air-entrainment start is called the critical submergence (Eroglu et al., 2007). The Vortex formation is categorized into two types: (a) free surface vortices, and (b) sub-surface vortices. Surface vortices develop at the free water surface and can range in intensity from a minor depression to a strong swirling motion. In more severe cases, they can form an open funnel or air-core that extends down to the pump bellmouth. A strong vortex can draw floating debris or air into the pump column, potentially affecting its operation. On the other hand, Sub-surface vortices are further categorized based on their attachment points, including floor-attached, backwall-attached, and sidewall-attached vortices, each of which referring to the connectivity of the vortices to a specific boundary surface at one end (Samsudin et al., 2015).

[1]Hydraulic Research Directorate, River Research Institute, Faridpur-7800, Bangladesh.
*Corresponding Author: (E-mail: broy@rri.gov.bd)
[2]Geotechnical Research Directorate, River Research Institute, Faridpur-7800, Bangladesh.

Vertical vortices often form at hydraulic intakes due to unfavorable approach flow conditions or low submergence. The boundary conditions of free water surface and hydraulic structure are different and the occurrence of vertical vortex is still unpredictable (Chen et al. 2012). The vortex and swirls typically occur due to improper geometry, uneven velocity distribution, and insufficient depth of submergence. Air entrainment commonly results from hydraulic disturbances caused by excessive pre-swirl and vortices, leading to cavitation, uneven load distribution, noise, and vibrations. The most recognized type is the free surface vortex, which can vary from minor surface disturbances to fully developed vortices with a continuous air core extending from the surface into the pump. In model studies, vortex types are usually detected through visual inspection using dye and artificial debris. A coherent dye core extending to the pump bell or suction flange indicates vortex formation. Vortices are unsteady in strength and occur intermittently, often terminating at the suction floor and walls. They may become visible only when dye is injected near the vortex core. Subsurface vortices can be detected by injecting dye at different points around the suction bell, including the walls and floor, where vortices are likely to form (Ajai et al., 2019).

The potential for vortex formation and air entrainment at the pump intake varies based on the mean flow velocity and submergence depth. Vortex formation depends on submergence depth, identifying the initiation of vortex development is crucial for observing different types of vortexes. The interaction between the pump impeller and entrained air during vortex formation affects both the pump's efficiency and economic lifespan (Nagahara et al., 2001; Yild-irim et al., 2011).

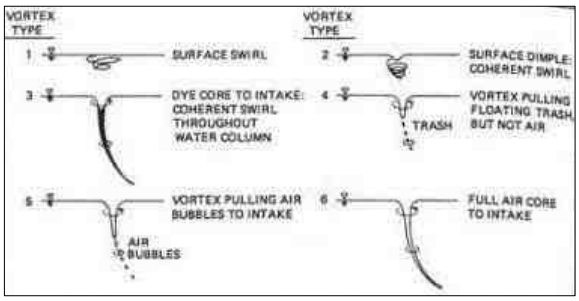

Fig. 1. Vortex classification (Hecker, 1987)

According to Hecker (1987), The Potential of a free-surface vortex to make damage to a pump depends on its strength. As vortex strength increases, it can disrupt flow uniformity and potentially entrain air or debris, reducing efficiency and accelerating wear or damage to the pump. To assess vortex strength, a qualitative classification system has been developed, based on its circulation characteristics. From **Fig. 1** vortices in Class 1 and 2 are generally harmless and do not significantly impact pump operation. However, vortices in Classes 3, 4, 5, and 6 are considered dangerous due to their potential to cause issues such as: (a) Air entrainment (Class 3 & 4): These vortices can draw air into the pump, leading to cavitation, reduced efficiency, and potential damage. (b) Strong Swirl and Submerged Vortices (Class 5 & 6): These can cause excessive turbulence, pressure fluctuations, and mechanical wear, affecting pump performance and longevity.

Excessive sedimentation at water intakes on rivers disrupts water supply and causes severe pump abrasion, leading to high operating costs. This issue can be significantly reduced through the proper design of intake structures. For water intakes in which sedimentation occurred, there is a need for removal of sedimentation to maintain continuous water supply and protect pumps from damage and sediment clogging (Bosman et al., 2002). To minimize sediment entry into the intake structure and prevent additional sediment detachment from nearby areas, high pumping rate of flow velocities greater than 0.6 ms^{-1} should be avoided (Mohammad et al., 2021).

The challenges of designing a river intake system in Bangladesh are potential for sediment accumulation, occurrence of extreme flooding and large annual water level fluctuations, potential for poor approach flow condition, occurrence of cross-flow, vortex formation, air entrainment and the need for protecting the intake and pumping system from debris. Therefore, it is imperative in river intake design to focus on standards (HI/ANSI) as to structural stability, hydraulic efficiency, operational efficiency, screening and preventing debris. Key considerations include minimizing head losses, providing smooth water flow, preventing vortex formation, allowances for water level fluctuation, critical submergence etc. Physical modeling is an essential tool for evaluating the design of intake structure.

The objectives of the study are to evaluate flow uniformity and flow characteristics approaching the intake and within the distribution chamber, ensure that the intake system can safely deliver the design discharge of 360 MLD, evaluate as-designed intake structure performance, examine the occurrence of free surface and submerged vortices under different operating conditions, identify the minimum submergence required to prevent air entrainment and ensure smooth operation, prevent debris or large particles from entering into the intake system, analyze swirl effects at the pump inlet, investigate the presence of entrained air or gas bubbles in the pump suction and their impact on performance.

Methodology

Survey and Data Collection

Primary data for this study were collected from Institute of Water Modelling (IWM), including bathymetry and bankline measurements across the entire study reach, as well as water level gradients,

point velocities, and discharge rates. Additionally, secondary data were utilized, encompassing historical discharge and water level records from nearby gauge stations along the Ganges River. The secondary dataset also included an index map of the study area, the latest satellite imagery covering the study reach was collected from different sources including USGS and design & Preliminary drawing of the proposed intake structure provided by the Hunan Construction Engineering Group Co. Ltd. (2024). Prototype data are required to simulate the existing hydro-morphological processes of the river in the physical model.

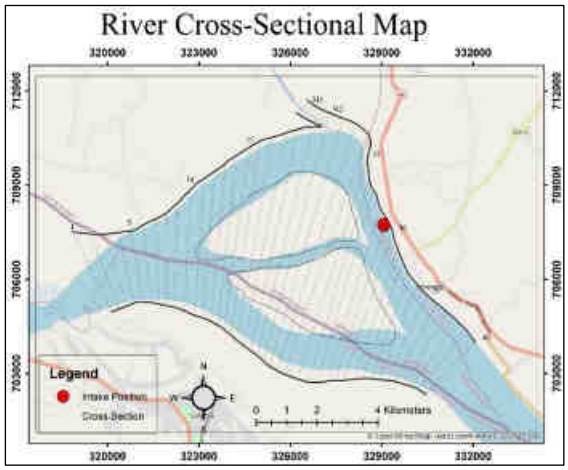

Fig. 2. Field survey index map

For this purpose, bathymetric data, topographic data, hydrologic data, design drawings of intake structure, design drawings of proposed protection work for conveyance pipe and information as to their placement, dimension and orientation, field observations etc. collected for this model study. The Ganges and Mahananda Rivers have been surveyed by IWM as per requirement of the model study. The cross-sectional data are obtained by conducting bathymetric survey @100m intervals along the Ganges and Mahananda rivers and 1 km river reach respectively. The field survey index map of the study area is shown in **Fig. 2**.

IWM measured the bank line data along both banks of the Ganges River covering the entire study reach and along both banks of the Mahananda river for 1.0 km stretch starting from its outfall. The measured bank lines are used to form the left boundaries of the model.

IWM has recorded the water levels of the Ganges continuously from 21 November 2023 to 29 December 2023 at three-gauge locations (near Mahananda outfall, near proposed intake location and downstream of the proposed intake location). The measured water levels are shown in **Fig. 3**.

Fig. 3. Position of discharge and water level gauge stations on the Lower Ganges and the Mahananda

Based on the available historical daily water level data of the Ganges and the Mahananda at different gauge stations the observed highest and the lowest water levels at each gauge station have been figured out and are shown in **Table 1**.

Table 1. Observed highest and lowest water levels (mPWD) at different gauge stations on the Ganges and the Mahananda rivers

Station	Hardinge Bridge (SW90)	Sardah (SW89)	Boalia (SW88)	Panka SW88A	Chapai Nawabganj (SW 211.5)	Godagari (SW211)
River	Ganges/Padma River				Mahananda	
HWL	15.19	18.70	19.80	24.14	23.01	21.49
LWL	4.13	6.20	6.90	11.05	10.67	9.20

The observed maximum water level at Boalia (Rajshahi) is found to be 19.80 mPWD (1934), at Hardinge Bridge 15.19 mPWD (1998) and at Panka 24.14 mPWD (1997). During the catastrophic flood in1998 the observed water level at Hardinge bridge is 19.68 mPWD. The lowest water level at Godagari was 9.20 mPWD. Hence, it was decided to run the model of intake structure corresponding to low water level +8.00m PWD and +9.00 mPWD of the river.

Scaling of Intake Structure Model

The scaling of the model mainly depends on the objectives of the model studies, theoretical scale conditions and the available laboratory facilities. As discussed earlier, the main purpose of the physical model study is to come up with optimum design of the intake structure to ensure favorable flow conditions at the inlet to the pump through appropriate piping design. The study will ensure optimal hydraulics, preventing turbulence, vortex formation, and air

entrainment under all operational conditions. An undistorted model of intake structure and associated works has been planned mainly to ensure that the intake can effectively and efficiently draw water from the river under different operating conditions of pumps. The model was being conducted as an open channel (general gravity forced) flow of the approach channel area. Regarding the geometric similarity between the model and the prototype, the Froude number (Fr) must be equal in the dynamic similarity part. Moreover, the focus of the tests in this experiment also included the free surface vortex or sub surface vortex. Therefore, besides the Froude number used for the dynamic similarity, the fluid viscosity effect and surface tension effect also need to be considered. In this regard, it was obtained from the literature that Reynolds' number of the experimental flow field must be at least 3×104 to reproduce a swirling intensity more accurately. ANSI/HI 9.8 (1998) recommends 1×105. Regarding the effect of surface tension, ANSI/HI 9.8 (1998) suggests that if Weber number is larger than 240, it is not necessary to consider the effect of surface tension.

The model and intake structure were built and operated in accordance with the Froude number similitude. The geometric scale factor for both horizontal and vertical dimensions was 1:25 which is called a undistorted physical scale model. This geometric scale ratio has been finalized considering all issues in view namely laboratory space, model discharge, model velocity etc. The experimental area covered the entire length and width of the intake structure. With the considered undistorted geometric scale, the Reynolds number and Weber number must be satisfied with the recommended value of ANSI/HI 9.8 (1998).

Free surface flow occurred in the intake model, which is dominated by gravitational and inertial forces. Therefore, the model was evaluated using the Froude similarity law. The Froude number (Fr) must be the same in both the model and prototype. The scale factor for Froude number is given by:

Fr $= Fr_p/Fr_m = 1$, $Fr_p = V_p/(gL_p)^{0.5}$ and $Fr_m = V_m/(gL_m)^{0.5}$, where V_p and V_m are velocity in the prototype and model respectively. The above equations lead to a velocity scale ratio,Vr $= Vp/Vm = Lr^{0.5}$. The selected geometric scale factor was 25. Therefore, the velocity scale factor for the model,$Vr = (25)^{0.5} = 5$.

Similarly, all other important scaling ratios result from the basic assumption of a Froude model assuming identical Froude number in the model and prototype and are shown in **Table 2** below:

Table 2. Scale ratios of different important commonly used variables in a Froude model

Variables	Units	Similitude	Scale factor	
Area	L^2	Geometric	L_r^2	625
Time	T	Kinematic	$L_r^{0.5}$	5
Acceleration	LT^{-2}	Kinematic	L_r	25
Discharge	L^3T^{-1}	Kinematic	$L_r^{2.5}$	3125
Mass	M	Dynamic	L_r^3	15625
Fluid	ML^{-3}	Dynamic	1	1
Pressure	ML^{-}	Dynamic	L_r	25
Force	MLT^{-2}	Dynamic	L_r^3	15625
Momentum	MLT^{-1}	Dynamic	$L_r^{3.5}$	78125

From the information presented in **Table 2** the scale factors for discharge, time and pressure are determined as 3125, 5 and 25 respectively. The type of model was accurate when all the dimensionless numbers that affect the physical phenomenon were the same on the prototype. With the selected geometric scale, the effect of other similarity laws has been checked for. To achieve similar velocity profiles inside the pump column in the model as in the prototype, a high enough turbulence level in the model suction pipe should be produced. This can be assured with a Reynolds number (Re) inside the suction pipe greater than 1x10^5. $Re_m = V_m D_m/V > 1 \times 10^5$, where ν is the kinematic viscosity of water. Water at 20 °C has a kinematic viscosity of about 10-6 m^2s^{-1}.Weber number (We) represents the surface tension effect in the model. The surface tension of water is a measure of the elastic force within the water's surface. If the Weber number in the model is greater than 400, the surface tension effect in the model may be considered as negligible. $We_m = \rho V_m 2D_m/\sigma > 400$, where σ is the surface tension of water. Water at 20 °C has a surface tension of about 0.0728 Nm^{-1}.

The hydraulic geometry of the model included intake channel, an extension, sump, and model pump suction pipes. The influence of impeller on flow patterns in the pump intake will be neglected in accordance with the ANSI/HI standard. The measuring of depression at the free- surface level will be neglected.

Model setup

Several grid points have been installed within and outside of the model bed in order to construct the bankline and proposed structures correctly. The bathymetry and bankline of the model have reproduced based on the recent bathymetric and bankline survey data supplied by Institute of Water Modelling (IWM). The water supply network of the model area was gravitational type. The supply sump and the measuring flume were interconnected by gate valves.

The water entered the model through these gate valves, flowed over rectangular sharp crested weir and fell into the stilling pond where energy was dissipated for maintaining uniform flow at the upstream of the model boundary. At the downstream of the model area, several tailgates were provided to allow water for draining into the drainage sump. The drainage sump was linked with the suction reservoir of pump house.

A 04 (four) number of tailgates are installed to control the downstream water level. A 03 (three) point gauges/staff gauges were installed within the model covering the entire model length to measure the water level in the model at different locations. Downstream point gauge was maintained to adjust the downstream boundary (water level) of the model. The layout and bathymetric map of the intake structure model are shown in **Fig. 4** & **5**.

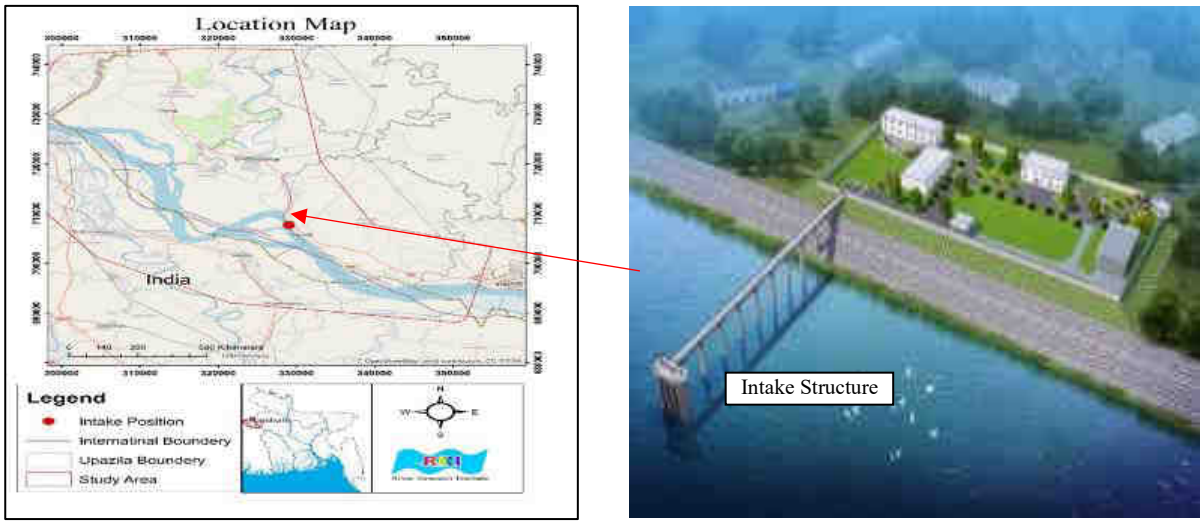

Fig. 4. Location map of study area

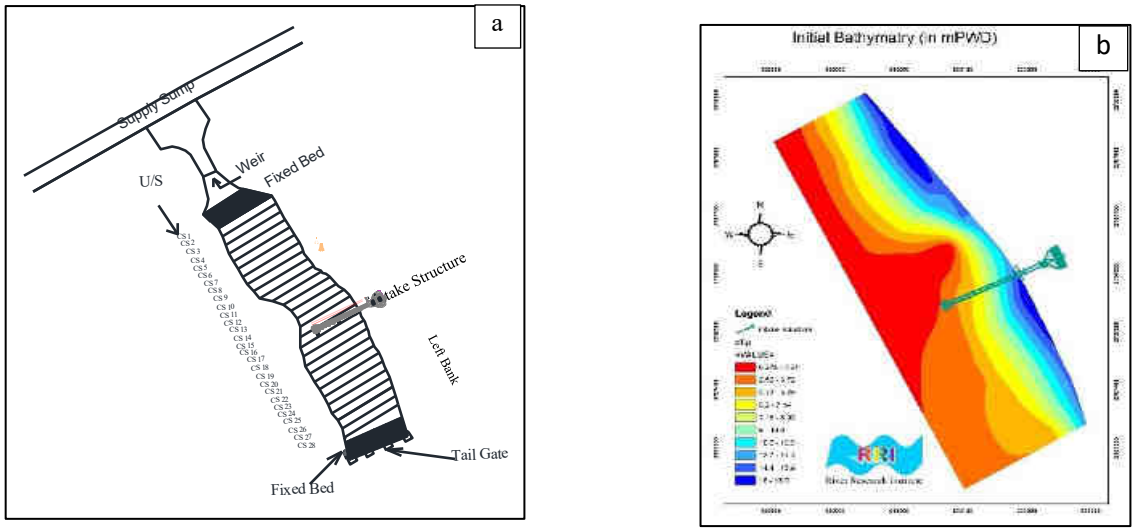

Fig. 5. a) Model layout and b) Bathymetric map

Based on the available data and information and selected geometric scales, physical model for intake structure was constructed according to the requirement of the study. Prior to that intake model was designed as a part width model covering 700m stretch of the Ganges river including the intake structure. The average width of the river channel covered in the model was about 175m to 200m.

The intake structure and distribution chamber had been connected through 2 nos of 1600mm diameter pipe to convey raw water from offshore to the shore. 4 nos. of cylindrical course screens having screen opening size 50 mm installed at 4 inlets of the offshore intake for screening floating large object and debris. Two inlets of 1600mm dia provided at +6.00m PWD be functional at low river water level within dry season and other two at+10.00m PWD be functional above average river water level within wet season. This approach ensured a minimum sediments load entering into the intake compartment. 2 nos of 1600mm dia washouts pipe were given to washout the sediment from the intake system. The fine screens having screen opening size 7.0mm and 12.5mm were provided within the distribution chamber for further screening of debris and sediment.

Fig. 6. a) Bedding of Conveyance pipe & Access bridge support column b) Construction of distribution chamber c) Placing of concrete amour unit & CC block and d) Installation of pump, VFD & Electromagnetic Flow meter.

Penstock was used for separating screen chambers and intake wells for facilitating maintenance, inspection and cleaning in empty conditions. Baffle walls were constructed between two suction pumps to minimize air bubble formation as the pump capacity was more than 300 ltr-s^{-1} as per the American National Standards for pump intake design. A total of 8 suction pipes (900mm dia) were placed at wet well. A minimum of 3D (D diameter of suction pipe or pump bell) clearance had been provided for each pump bay to avoid cavitation. A minimum of 5D length had been provided for each baffle wall or dividing bay wall from suction pipe to the wet well intake. However, it was kept more than required to avoid unexpected lateral flow or cross flow while an adjacent pump was not running. An electromagnetic flow meter was placed at the delivery side of each pump to measure the discharge delivered through the pump. A Variable frequency drive (VFD) was used for getting the desired discharge by changing motor frequency of the pump. In this model, calibration test run (T0) and two application test runs (T1-T2) with proposed interventions (intake structure) have been conducted. The proposed operation scenarios of the test run along with various discharge & water level conditions are mentioned in **Table 3**.

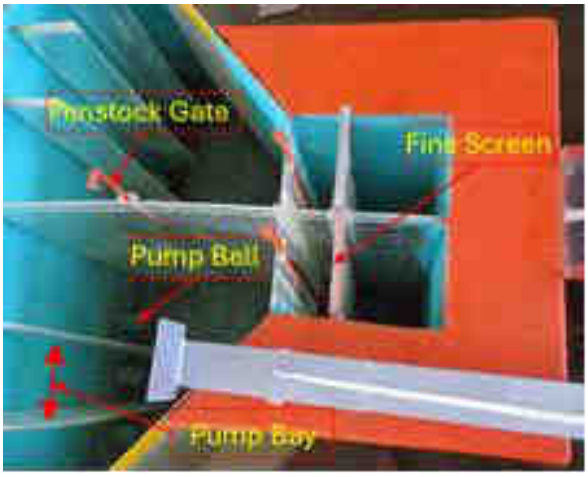

Fig. 7. Distribution Chamber

Table 3. Test scenarios of intake model

Test No.	Tests	Test Conditions	Flow Conditions	Scenarios	Operations
1	Calibration test (T0)	Existing (without intake structure) condition	Discharge corresponding to low water level	-	-
2	Application test (T1)	With proposed intake structure	Discharge, Q=426 cumec corresponding to low water level of 8.0 mPWD	1	Normal (Phase-I) for intake flow rate 210 MLD
				2	Backwash/repair Pipe & Fine screen chamber (Phase-I) for intake flow rate 147 MLD
				3	Backwash/repair Inlet coarse screen (Phase-I) for intake flow rate 210 MLD
				4	Normal (Phase-II) for intake flow rate 360 MLD
				5	Backwash/repair Pipe & Fine screen chamber (Phase-II) for intake flow rate 252 MLD
				6	Backwash/repair Inlet coarse screen (Phase-II) for intake flow rate 360 MLD
				7	Normal (Extra 1) for getting maximum intake flow rate
3	Application test (T2)	With proposed intake structure	Discharge, Q=599 cumec corresponding to low water level of 9.0 mPWD	1	Normal (Phase-I) for intake flow rate 210 MLD
				2	Backwash/repair Pipe & Fine screen chamber (Phase-I) for intake flow rate 147 MLD
				3	Backwash/repair Inlet coarse screen (Phase-I) for intake flow rate 210 MLD
				4	Normal (Phase-II) for intake flow rate 360 MLD
				5	Backwash/repair Pipe & Fine screen chamber (Phase-II) for intake flow rate 252 MLD
				6	Backwash/repair Inlet coarse screen (Phase-II) for intake flow rate 360 MLD
				7	Normal (Extra 1) for maximum intake flow rate obtained at LWL 8.03mPWD
				8	Normal (Extra 2) for getting maximum intake flow rate

Model calibration

In order to satisfy geometric similarity, the dimensions of the different components of the intake structure have been reduced with the selected geometric scale factor. The kinematic similarity between the model and the prototype implied similar flows for all operating conditions, which was ensured by fulfilling Froude condition that is Froude number in the model and prototype was equal. Dynamic similarities were satisfied with the similarity of scale factors for force. The calibration of the model also implied that the influence of viscous and surface tension in the model is negligible.

Application test run

Two application tests T1 & T2 had been carried out in the intake model according to the above-mentioned **Table 3**. The intake located in the Ganges River. The water level of this river undergoes large annual fluctuation. The different operations and scenarios were tested for the worse condition of the river under minimum water level 8.0 mPWD and 9.0 mPWD and corresponding discharges 426 cumec and 599 cumec respectively. In Test T1, the intake structure was executed with 07 scenarios under both Phase-I and Phase-II where river water level maintained at 8.0 mPWD. In Test T2, the intake structure was executed with 08 scenarios under both Phase-I and Phase-II where river water level maintained at 9.0 mPWD. The design discharge for intake structure was 210 MLD and 360 MLD under Phase-I and Phase-II respectively.

Assessment of maximum discharge from intake structure without vortex formation at pump suction was tested at 7th scenarios under test T1 and 8th scenarios under test T2. Both test T1 & T2 conducted using fine screens having screen opening size 7.0mm. The scenarios were thoroughly assessed, and the performance of the intake structure was evaluated accordingly.

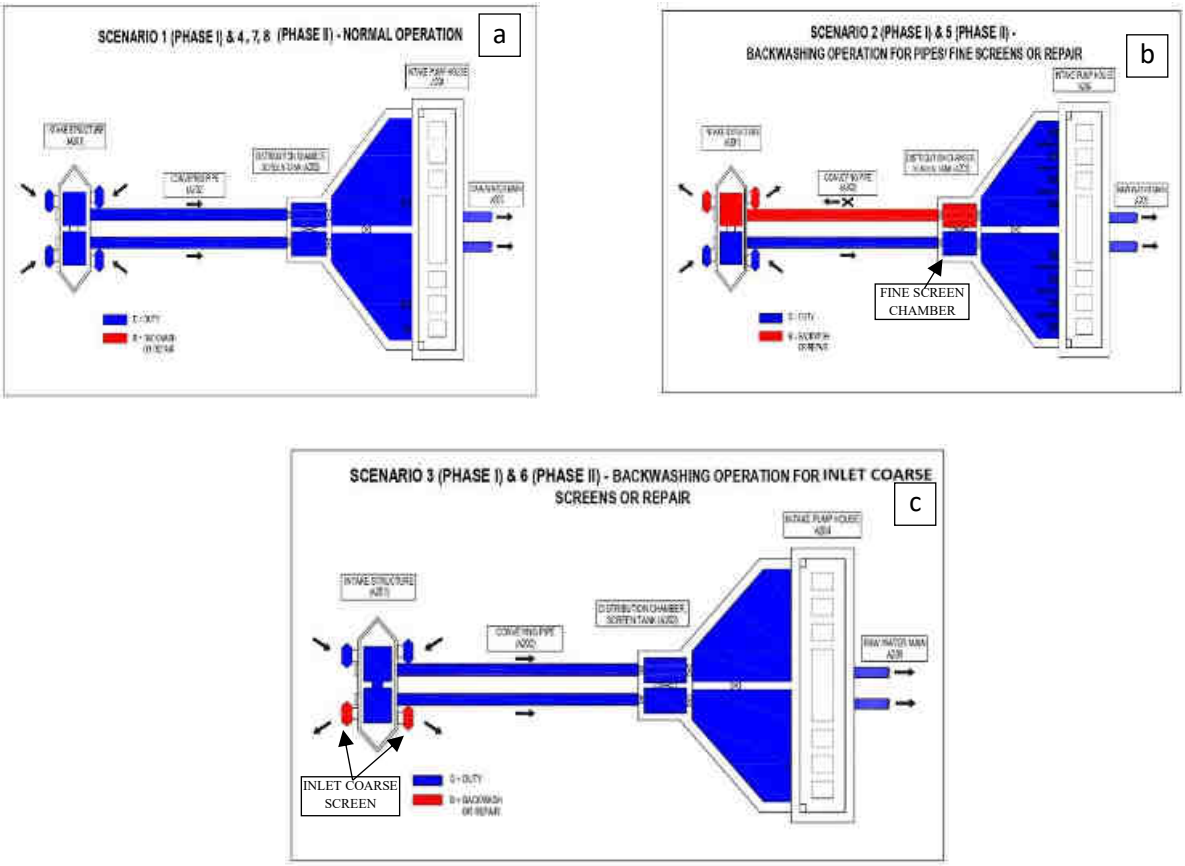

Fig. 8. a) Normal operation b) Backwashing/repairing operation of pipe & fine screen and c) Backwashing/repairing operation of Inlet coarse screen.

There were 03 types of operation under all scenarios as shown in **Fig. 8**. When the intake operated under normal conditions, all its components were in operation as **Fig. 8(a)**. During backwashing or repairing of pipe and fine screen only one set of coarse screens, intake well, pipe, and fine screen was in operation while the other set remained closed as **Fig. 8(b)**.

During backwashing or repairing of coarse screen only one set of coarse screens remained closed while other components were in operation as **Fig. 8(c)**.

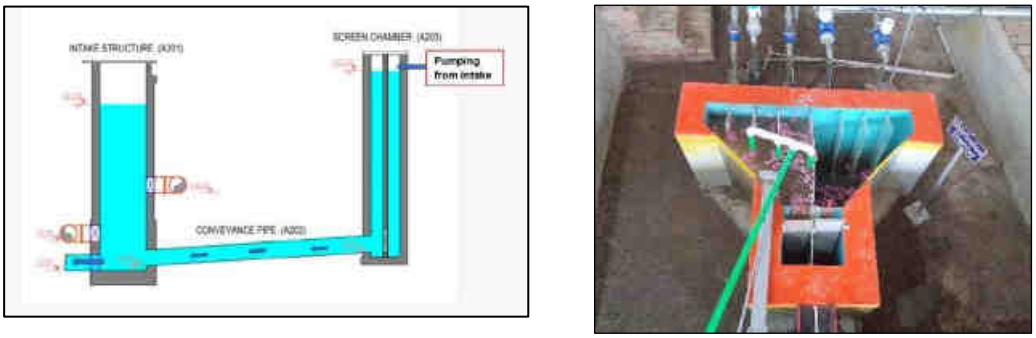

Fig. 9. Backwashing process of fine screen chamber and pipe

Cleaning of screen chamber and pipeline had been done with backwashing which was arranged manually by filling the screen tank up to 23.00m PWD level using intake pumps and making flushing effect by opening penstock suddenly. When backwashing the system washout pipe at intake was opened while all other inlets were closed. During the tests necessary measurements, visualization and documentation of

flow pattern using photos and videos had been made. The test results have been compared with the corresponding HI standard to see whether any modifications are needed in the design.

Results and discussion

The estimated model discharge corresponding to Low Water Level (LWL) 8.0 mPWD and 9.0 mPWD was 426 cumec and 599 cumec respectively. According to HI/ANSI standard pump bay width and length of dividing bay wall for being greater than 2D and 5D respectively, where D is bell mouth diameter in the model unexpected lateral flow or cross flow did not occur while an adjacent pump was not running. The summary of test results for test T1 and T2 are given below.

Table 4. Summary of test results for test T1 at LWL 8.0 mPWD

Scenario	Operation	flow rate (MLD)	Percentage of design flow considered for the analysis	WL around the intake structure (mPWD)	WL at the screen chamber (mPWD)	Total head loss (m)	Elevation of bell mouth (mPWD)	Submergence (m)
1	Normal (Phase-I)	210	100%	8.00	7.83	0.18	5.5	2.33
2	Pipe & Fine screen chamber backwash/repair (Phase-I)	147	70%	8.00	7.75	0.25	5.5	2.25
3	Inlet coarse screen backwash/repair (Phase-I)	210	100%	8.00	7.80	0.20	5.5	2.30
4	Normal (Phase-II)	360	100%	8.00	7.60	0.40	5.5	2.10
5	Pipe & Fine screen chamber backwash/repair (Phase-II)	252	70%	8.00	7.25	0.75	5.5	1.75
6	Inlet coarse screen backwash/repair (Phase-II)	360	100%	8.00	7.58	0.43	5.5	2.08
7	Normal (Maximum discharge)	370	102.77%	8.00	7.55	0.45	5.5	2.05

Table 5. Summary of test results for test T2 at LWL 9.0 mPWD

Scenario	Operation	flow rate (MLD)	Percentage of design flow cosidered for the analysis	WL around the intake structure (mPWD)	WL at the screen chamber (mPWD)	Total head loss (m)	Elevation of bell mouth (mPWD)	Submergence (m)
1	Normal (Phase-I)	210	100%	9.00	8.78	0.23	5.5	3.28
2	Pipe & Fine screen chamber backwash/repair (Phase-I)	147	70%	9.00	8.68	0.33	5.5	3.18
3	Inlet coarse screen backwash/repair (Phase-I)	210	100%	9.00	8.80	0.20	5.5	3.30
4	Normal (Phase-II)	360	100%	9.00	8.58	0.43	5.5	3.08
5	Pipe & Fine screen backwash/repair (Phase-II)	252	70%	9.00	8.23	0.78	5.5	2.73

6	Inlet coarse screen backwash/repair (Phase-II)	360	100%	9.00	8.55	0.45	5.5	3.05
7	Normal (Maximum discharge for 8.0 mPWD)	370	102.77%	9.00	8.53	0.48	5.5	3.03
8	Normal (Maximum discharge)	600	166.66%	9.00	7.43	1.58	5.5	1.93

In test T1 the maximum discharge obtained from the intake under scenario 7 was 370 MLD where the head loss and submergence were 0.45 m and 2.05 m respectively. This submergence was the critical submergence for normal operation at which free surface vortex began to form. During pipe and fine screen chamber backwashing or repair under scenario 5 for getting a discharge of 252 MLD, the head loss and submergence were 0.75 m and 1.75 m respectively and the formation of a free surface vortex also began in this operation.

In test T2, the intake achieved a maximum discharge of 600 MLD with a head loss of 1.58 m and a submergence of 1.93 m under scenario 8. Below this submergence formation of a free surface vortex started for normal operation. In scenario 5 backwashing or repair operation carried out without any disturbance. It was observed that no air or gas bubbles entered the pump inlet in both test T1 & T2.

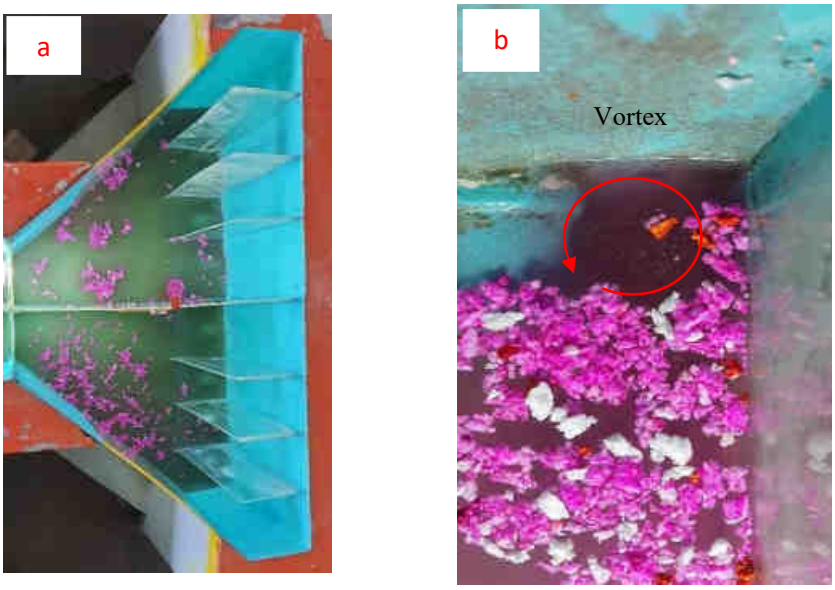

Fig. 10. a) Uniform flow distribution approaching the pump suction in normal operation and b) Vortex formation at the vicinity of pump bell

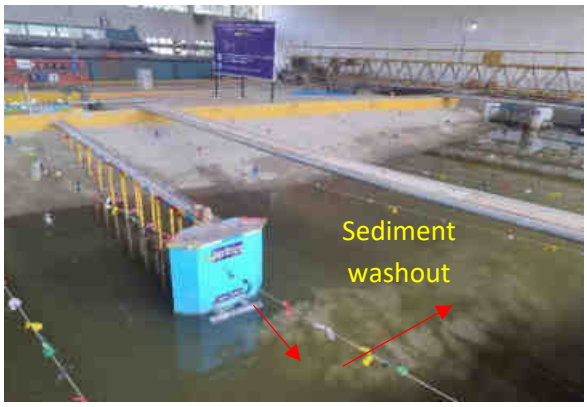

Fig. 11. Sediment washout from the distribution chamber and conveyance pipe

An important concern for the intake was deposition and removal of sediment. As a result of backwashing under scenario 5 for both tests, the screen chamber and pipeline were cleaned completely. The sediment was washed out from the intake and discharged into the river as shown in **Fig. 11**.

Conclusions

The following conclusions have been made based on the field data analysis and model investigation:

- The design capacity for raw water supply from the intake system is 360MLD. The intake system at this design capacity under phase-II is operated smoothly without any disturbance at the pump inlet. The water level at the distribution chamber is 7.60 mPWD with a corresponding submergence of 2.10 m at low water level 8.0 mPWD in the Ganges river. On the other hand, the WL at distribution chamber is 8.58 mPWD with a corresponding submergence

of 3.08 m at low water level 9.0 mPWD in the Ganges river;
- Rotational flow and a weak free surface vortex develop near the pump bell under backwashing or repairs of the conveyance pipe for a flow rate of 252 MLD in Phase-II. The water level at the distribution chamber is 7.25 mPWD, with a submergence of 1.75 m, corresponding to the low water level of 8.0 mPWD in the Ganges river;
- The maximum discharge supplied from the intake is 370 MLD in Phase-II. Rotational flow and a weak free surface vortex develop near the pump bell under this scenario. The water level at the distribution chamber is 7.55 mPWD, with a submergence of 2.05 m, corresponding to the low water level of 8.0 mPWD in the Ganges river;
- The maximum discharge supplied from the intake is 600 MLD in Phase-II. Rotational flow and a weak free surface vortex develop near the pump bell under this scenario. The water level at the distribution chamber is 7.43 mPWD, with a submergence of 1.93 m, corresponding to the low water level of 9.0 mPWD in the Ganges river;
- The critical submergence for normal operation is 2.05 m corresponding to the river low water level of 8.0 mPWD and 1.93 m corresponding to the river low water level of 9.0 mPWD;
- Uniformity in flow approaching the intake placed in the left channel of Ganges river is noticeable;
- Uniform flow distribution occurs within the distribution chamber of the intake structure due to the bay dividing wall, which is constructed according to the HI/ANSI standard. No formation of air/gas bubbles is noticeable, which ensures safe and efficient operation of the pump inlet; and
- Sediment is completely removed from the distribution chamber and conveyance pipe by filling the screen chamber up to the level of 23.00 mPWD and then quickly opening the penstock valve to create a flushing effect.

Acknowledgement

This study was made possible with the support of Hunan Construction Engineering Group Co. Ltd. (HCEG), Institute of Water Modelling (IWM) and Rajshahi Water Supply and Sewerage Authority (RWASA).

Conflict of interest

The authors declare no conflict of interest.

References

Hasan, M. (2018). *Water Demand Management of Rajshahi City Corporation*.

Iqbal, Z., Nubi, A., Longe, & Olubunmi, N. (2015). *Evaluation of Water Intake Structures for Municipal Water Supply Scheme in Lagos, Nigeria.* https://doi.org/10.6084/M9.FIGSHARE.1365079.

Khanarmuei M, Rahimzadeh H, Sarkardeh H (2018). Effect of dual intake direction on critical submergence and vortex strength. *Journal of Hydraulic Research*, 1-8.

Eroglu, N., & Bahadırlı, T. (2007). Prediction of Critical Submergence for a Rectangular Intake. *Journal of Energy Engineering-Asce-J ENERG ENG-ASCE*, *133*. https://doi.org/10.1061/(ASCE)0733-9402(2007)133:2(91).

Samsudin, M. L., Munisamy, K., & Thangaraju, S. (2015). Application of multiphase modelling for vortex occurrence in vertical pump intake-A review. *IOP Conference Series: Materials Science and Engineering*, *88*, 012024. https://doi.org/10.1088/1757-899X/88/1/012024.

Chen, Y., Wu, C., Wang, B., & Du, M. (2012). Three-dimensional Numerical Simulation of Vertical Vortex at Hydraulic Intake. *Procedia Engineering*, *28*, 55–60. https://doi.org/10.1016/j.proeng.2012.01.682.

Ajai, S., Kumar, K., Rahiman, P. A., Sohoni, V. S., & Jahagirdar, V. S. (2019). Vortex prediction in a pump intake system using Computational Fluid Dynamics. *IJITEE*, *8*, 3158-3163.

Nagahara, T., Sato, T., & Okamura, T. (2001). *Effect of the submerged vortex cavitation occurred in pump suction intake on hydraulic forces of mixed flow pump impeller*. http://resolver. caltech. edu/cav2001: sessionB8. 006.

Yildirim, N., Akay, H., & Taştan, K. (2011). Critical submergence for multiple pipe intakes by the potential flow solution. *Journal of Hydraulic Research*, *49*(1), 117-121.

Hecker, G. E. (1987). Fundamentals of vortex intake flow. In *Swirling Flow Problems at Intakes*. Routledge.

Bosman, D. E., Prestedge, G. K., Rooseboom, A., & Slatter, P. T. (2002). An investigation into the removal of sediments from water intakes on rivers by means of jet-type dredge pumps. *The Water Research Commission*.https://doi.org/10.13140/RG.2.1.1084. 6242.

Mohammad, M., Al-Ansari, N., Bsc, Y., Knutsson, S., & Laue, J. (2021). Sediment Control Strategies for Sustainable Water Intake. *Dams and Reservoirs*, *31*, 1–10. https://doi.org/10.1680/jdare.21.00005.

Hunan Construction Engineering Group Co. Ltd. (2024). *Preliminary design report-Part A: Rajshahi Wasa Surface Water Treatment Plant Project* (Report No. RSWTP-02-PDR-A100). Hunan Construction Engineering Group Co. Ltd. of China.

Hydraulic Institute Standards (1998), *American national standard for pump intake design, ANSI/HI* 9.8., American National Standards Institute, Hydraulic Institute, Washington. DC.

Technical Journal
River Research Institute ISSN: 1606-9277

Channel Planform Dynamics of Bangladesh's Major Rivers: a Study on Braiding and Sinuosity Indices

M. Moniruzzaman[1*], M. Masuduzzaman[2], S. Ferdhous[1] and F. Rukshana[1]

Abstract

Bangladesh, a floodplain-dominated country, is shaped by numerous rivers that influence its ecosystem, agriculture, and groundwater recharge. This study evaluates the channel planform dynamics of four major rivers - Teesta, Brahmaputra, Ganges, and Upper Meghna - using remote sensing and GIS techniques. The braiding index (BI) for Teesta and Brahmaputra and the sinuosity index (SI) for Ganges and Upper Meghna were assessed using Landsat 8 satellite images. The results show that the Brahmaputra River has a higher BI (4.14) compared to Teesta (3.78), indicating a more unstable braided condition, with reach-specific BI values reaching up to 5.56 for Teesta and 5.16 for Brahmaputra. In terms of sinuosity, the Ganges exhibits a greater SI (1.17) than the Upper Meghna (1.26), with certain reaches (e.g., Reach 4 of Ganges, SI = 1.58) falling into the meandering category. The study highlights significant variations in channel stability and morphological behavior, emphasizing the role of sediment transport and hydrological influences in river dynamics. These findings contribute to the understanding of fluvial processes in Bangladesh, which are essential for sustainable river management and flood risk mitigation.

Keywords: *River morphology, Braiding index, Sinuosity index, GIS, Remote sensing, Bangladesh, Fluvial dynamics, channel stability.*

Introduction

Bangladesh, is a country to myriad of rivers in its very small space of only around 1, 47,570 sq. kms. Bangladesh comprises hill, terrace and floodplain areas. Hill areas include the northern and eastern hills and occupy about 12% of the country. Terrace areas include Madhupur Tract in the centre and Barind Tracts in the northwest. Terraces occupy about 8% of the country. Floodplain areas include alluvial floodplain and estuarine areas and occupy the remaining 80% of the country. That is, we can say it is dominantly a floodplain country. Flood and riverbank erosion and flooding have devastating impacts on economy and ultimately on society in Bangladesh. People vicinity in the riverbank lost their houses and agricultural lands, displaced permanently and become impoverished. Sustenance vulnerability of riverine island dwellers, strategies to reduce the impact of bank erosion and flooding need to be strengthened Riverbank erosion is seen as one of the major causes of national poverty (van der Wal, 2020). About one-third districts in Bangladesh are susceptible to riverbank erosion and this phenomenon devour around 8700 ha of land per year affecting around 200000 people by demolishing their house and their agricultural land. During the monsoon season when large-scale erosions can occur. A big chunk of land (several hundred square meters of land) can get into the river within short time. Such erosion events happen in a limited number of hotspot areas along the three major rivers of Bangladesh: Jamuna, Ganges and Meghna (Freihardt & Frey, 2022). On the contrast the rivers are called lifeline of our country. Because land fertility, ecosystem, fish production and groundwater recharge and many other important environmental aspects depends on river system. River morphology describes a river's cross-sectional shape, sedimentation, and erosion. Understanding river morphology, or the shape and form of a river channel and floodplain, is crucial for sustainable river management because it helps predict how rivers will respond to changes and informs effective interventions for flood control, habitat restoration, and water resource management (Rinaldi et al., 2016). The sinuosity index quantifies river channel curvature, while the braiding index measures the presence and extent of multiple channels, both crucial for understanding river morphology and dynamics (Ozturk & Sesli, 2015). A higher braiding index, indicating a more braided river, often correlates with increased bank erosion due to the dynamic nature of braided channels and their tendency to transport more sediment and scour their beds. The sinuosity index and riverbank erosion have an opposite relationship (Nath & Ghosh 2022). River morphology is changing in varying environmental conditions over both spatial and temporal scales due to the erosion and accretion of the river bank and the water flow of the river through natural and anthropogenic inputs (Akter et al., 2019). A greater braid index implies an unstable river condition (Kuo et al., 2017). Sinuosity indices (SI) of a channel not only measure its degree of tortuousness but also indicate the topographic influence on sinuosity and hydraulic influence on relatively unstable and easily translocatable sediment deposits within the channel (Mueller, 1968).

In this paper, we focus on assessing sinuosity index and braiding index of four major rivers in Bangladesh to understand the channel dynamics of these rivers using Landsat satellite imagery with GIS.

[1]Geotechnical Research Directorate, River Research Institute, Faridpur-7800, Bangladesh.
*Corresponding Author: (E-mail:mmpdpru@gmail.com)
[2]Hydraulic Research Directorate, River Research Institute, Faridpur-7800, Bangladesh.

Material and Methods

In this study braiding index (BI) for the rivers Teesta and Jamuna and Sinuosity index (SI) for the rivers Ganges and Upper Meghna have been assessed. Remote sensing and GIS tool were used to carry out the assessment. To conduct the analyses, Landsat 8 satellite images were collected from USGS earth explorer website. All the images collected were of the month of November or December for the sake of getting cloud free image and also for noticing the sand bars. To find out the water body or river channels Normalized Difference Water Index (NDWI = (GREEN-NIR)/(GREEN + NIR) has been used. After extraction of water body other pixels in the river area have been extracted as sand bars. Prior to compute NDWI radiometric correctios have been effectuated for all images by conversion to top of atmosphere (TOA) reflectance. For conversion of TOA reflectance with a correction for the sun angle the following formula has been used (USGS).

$$\rho_\lambda = \frac{\rho'_\lambda}{\cos(\theta_{SZ})} = \frac{\rho'_\lambda}{\sin(\theta_{SE})} \quad \text{Eq. (1)}$$

Where,

ρ_λ= TOA planetary reflectance;
θ_{SZ}= Local sun elevation angle. The scene center sun elevation angle in degrees is provided in the metadata (sun elevation);
θ_{SE}=Local solar zenith angle; $\theta_{SZ} = 90° - \theta_{SE}$. The following two equations were used for the calculation of sinuosity.

According to Langbein and Leopold (1966) sinuosity is defined as

$$K = \frac{M}{L} \quad \text{Eq. (2)}$$

where,
K = sinuosity index
M = meander length of channel
L= valley length

And according to theory of minimum variance sinuosity is defined as

$$K = \frac{4.84}{4.84 - \phi_0^2} \quad \text{Eq. (3)}$$

Where,
K = sinuosity index
ϕ_0 = meander angle

Braiding index (BI) was calculated dividing the total sand bar length by the reach length based on the centerline of the channels using the following equation (Das, 2023).

$$BI = \frac{2\Sigma L_{SB}}{L_R} \quad \text{Eq. (4)}$$

Where

L_{SB} = length of sand bar

L_R = length of reach

Here is a classification of the sinuosity index (**Table 1**) which are classified by Charlton (2008).

Table 1. Classification of Sinuosity Index

Channel Type	Sinuosity
Straight	< 1.1
Sinuous	1.1 – 1.5
Meandering	> 1.5

Results

Assessment of Braiding index (BI) Teesta River

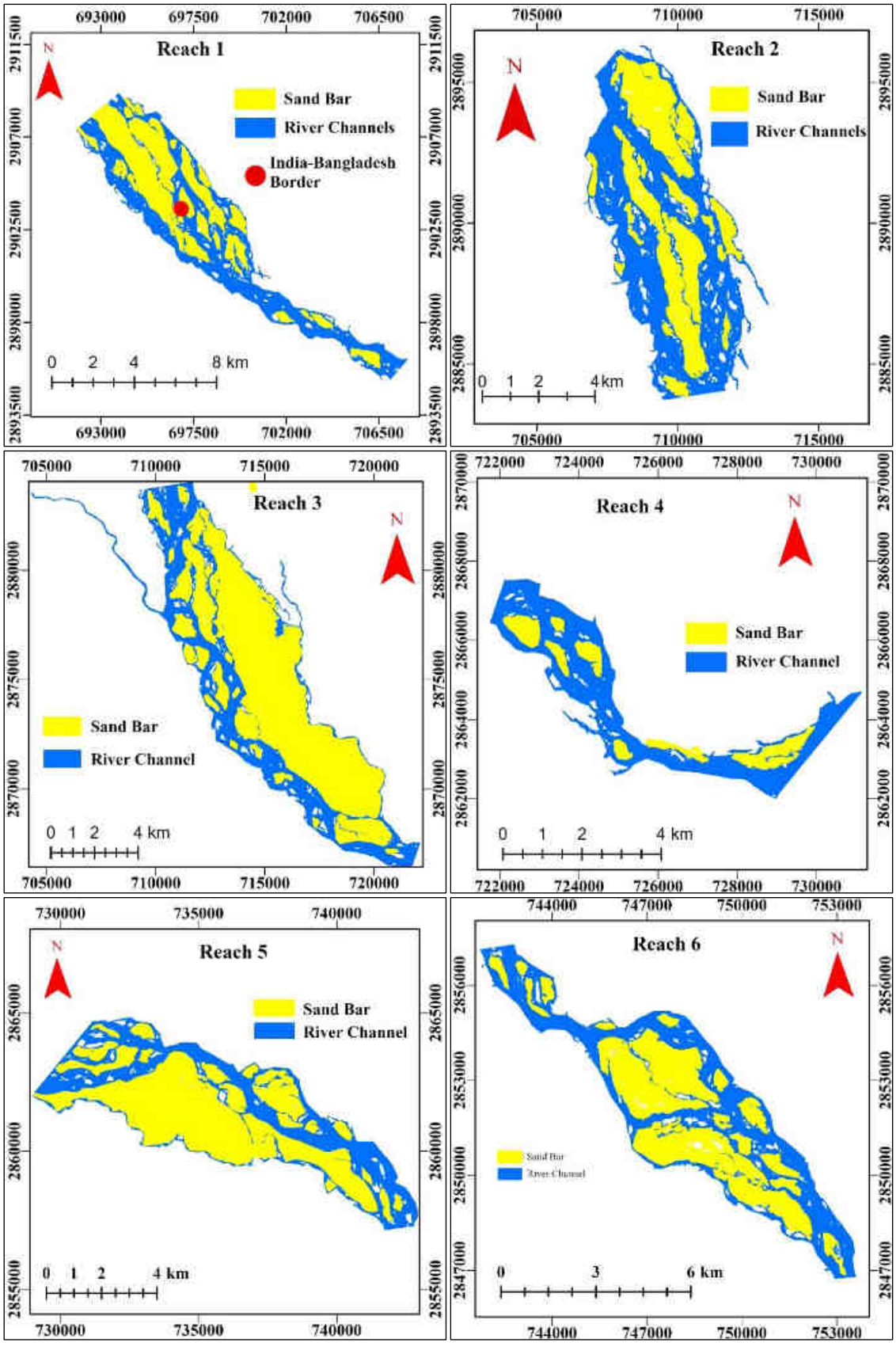

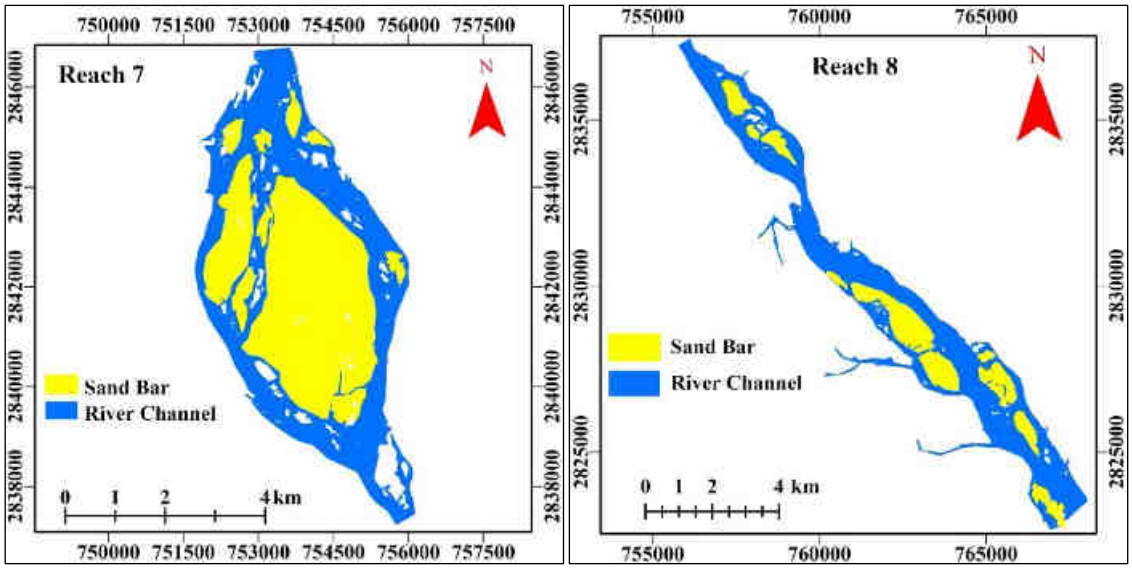

Fig. 1. Different reaches of Teesta river

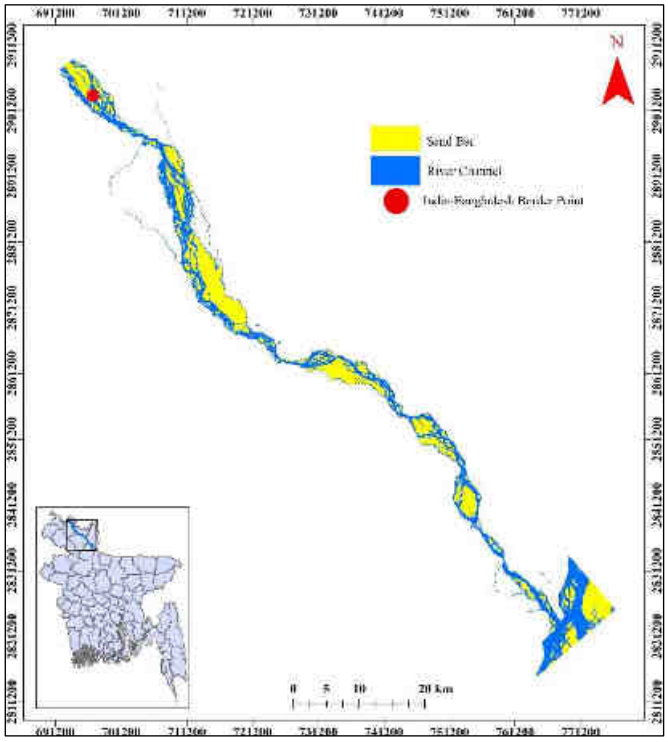

Fig. 2. Whole reach of Teesta River

Table 2. Braiding Index of Teesta River

Reach	Reach Length (km)	No. of Bars	Summation of Bar Lengths (km)	Braiding Index
1	13.59	27	23.04	3.40
2	12.46	18	34.63	5.56
3	20.40	30	49.18	4.82
4	8.46	7	8.17	1.94
5	13.77	22	35.65	5.18
6	14.95	18	29.23	3.92
7	8.96	10	14.34	3.20
8	18.27	15	15.31	1.68
Whole Reach	110.9	147	209.55	3.78

Teesta river is an upstream river of Bangladesh. For the assessment of braiding index, the whole reach of this river was segmented into eight reaches. As Teesta a transboundary river only Bangladesh part of the river was considered in this assignment. Different reaches of this river showed different braiding index. The reach 2 has maximum value of braiding index 5.56 implying high erosion tendency. The reach 8 has the minimum value of braiding index 1.68 indicating the low erosion tendency.

Assessment of Braiding index (BI) Brahmaputra River

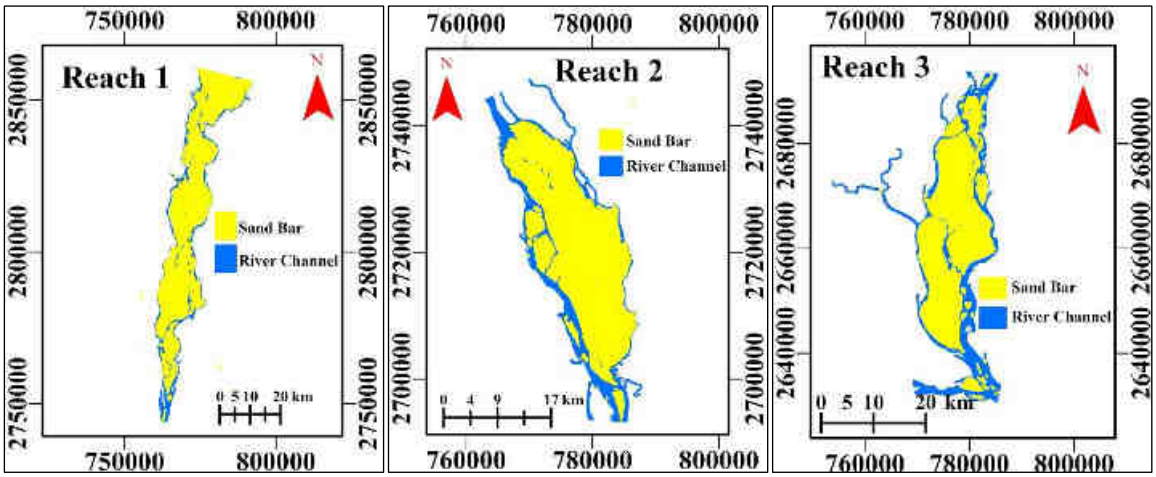

Fig. 3. Different reaches of Brahmaputra River

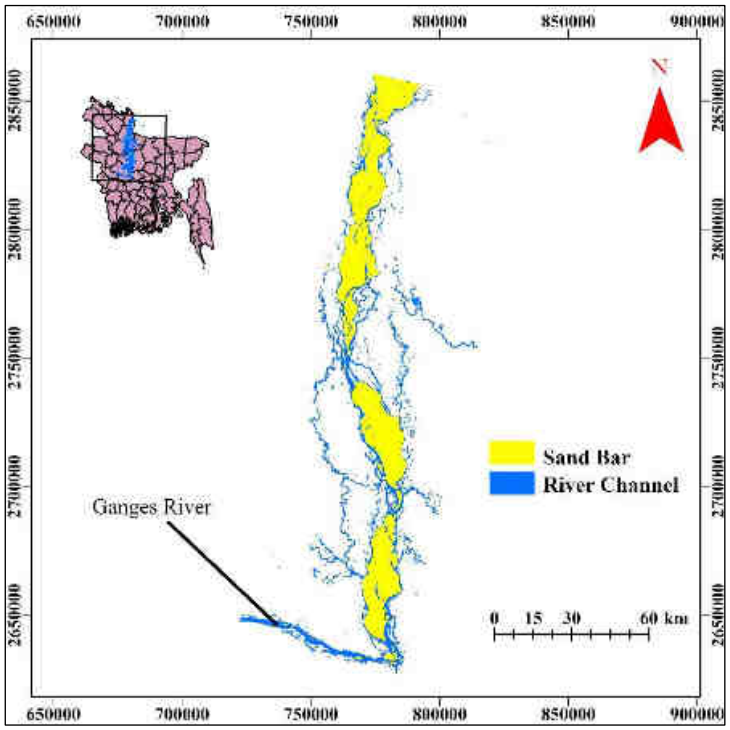

Fig. 4. Whole reach of Brahmaputra River

Table 3. Braiding Index of Brahmaputra River

Reach	Reach Length (km)	No. of Bars	Summation of Bar Lengths (km)	Braiding Index
1	116.29	121	196.414	3.38
2	54.85	38	141.69	5.16
3	60.48	52	142.14	4.70
Whole Reach	231.62	211	480.24	4.14

Brahmaputra river is another important river of our country. For the assessment of braiding index, the whole reach of this river was segmented into three reaches. As Brahmaputra a transboundary river only Bangladesh part of the river was considered in this study. Different reaches of this river showed different braiding index. The whole river showed high erosion tendency. The reach 2 showed the highest braiding index among the reaches.

Assessment of Sinuosity Index (SI) Ganges River

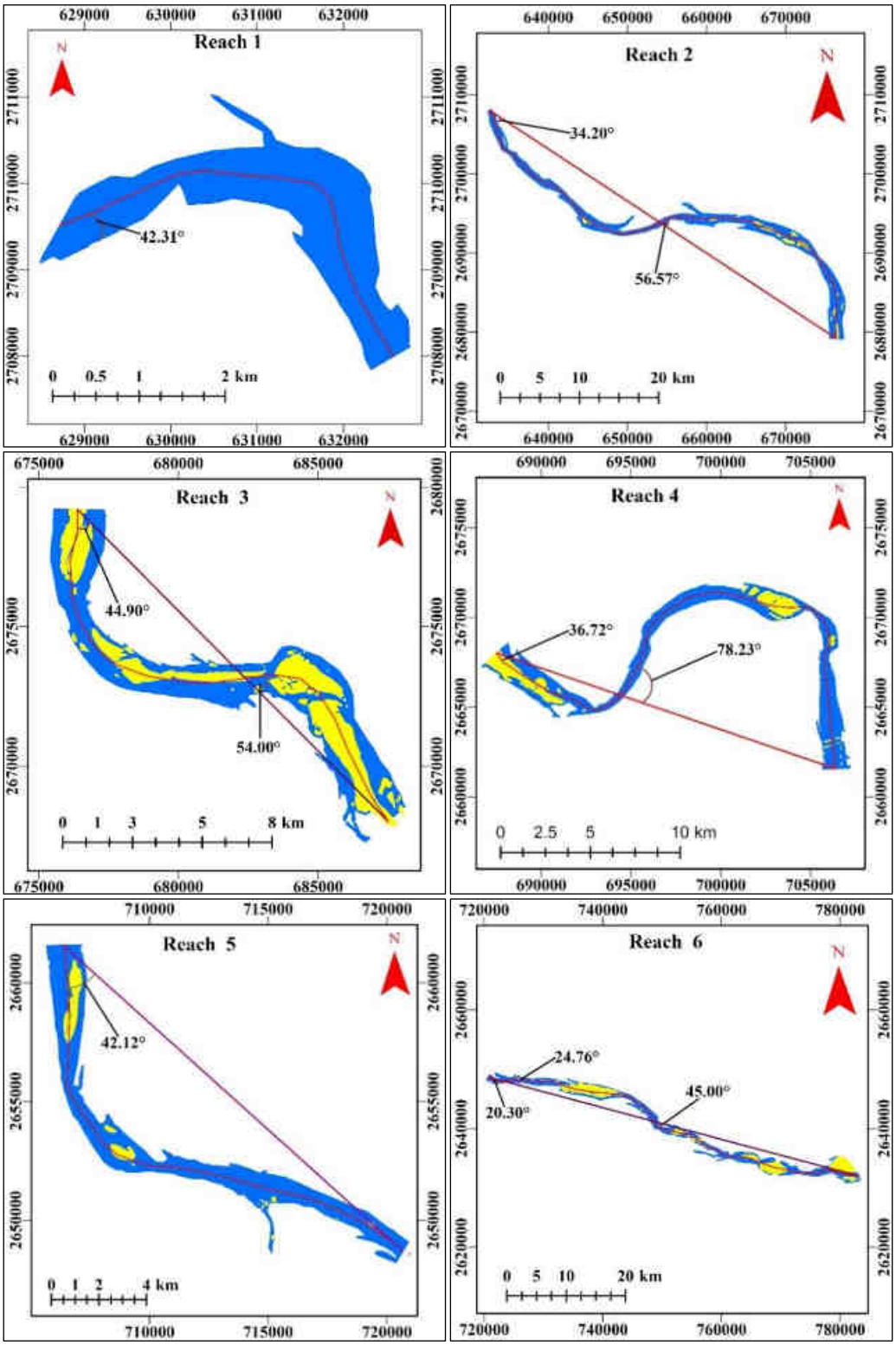

Fig. 5. Different reaches of Ganges River

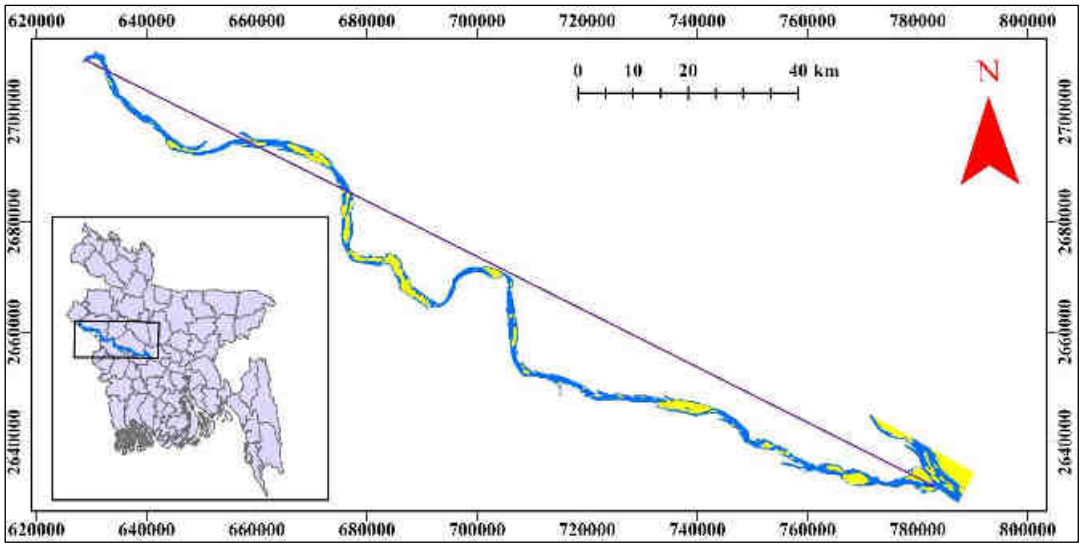

Fig. 6. Whole reach of Ganges River

Table 4. Sinuosity Index of Ganges River

Reach	No. of Bends	Meander Angle (deg)	Sinuosity according to $K = \frac{4.84}{4.84-\phi_0^2}$	Valley Length (km)	Meander Length (km)	Sinuosity according to $K = \frac{M}{L}$
1	1	42.31	1.127	4.15	5.33	1.28
2	2	34.20 56.57	1.079 1.252	52.43	61.34	1.17
3	2	44.90 54.00	1.145 1.225	15.77	18.94	1.20
4	2	36.72 78.23	1.093 1.626	19.93	31.39	1.58
5	1	42.12	1.126	19.25	22.44	1.17
6	3	20.30 24.96 45.00	1.027 1.041 1.146	64.63	67.08	1.04
Whole Reach	11			176.16	206.52	1.17

Ganges river is also a transboundary river. Only Bangladesh part of the river was considered in this study. This river was severed into six reaches for the sake of sinuosity analysis. The SI values according to meander length and valley length given higher values than meander angle method. According to Charlton (2008) all but reach 4 falls into sinuous category of sinuosity. The reach 4 has SI=1.5 and fall into meandering category of sinuosity.

Assessment of Sinuosity Index (SI) Upper Meghna River

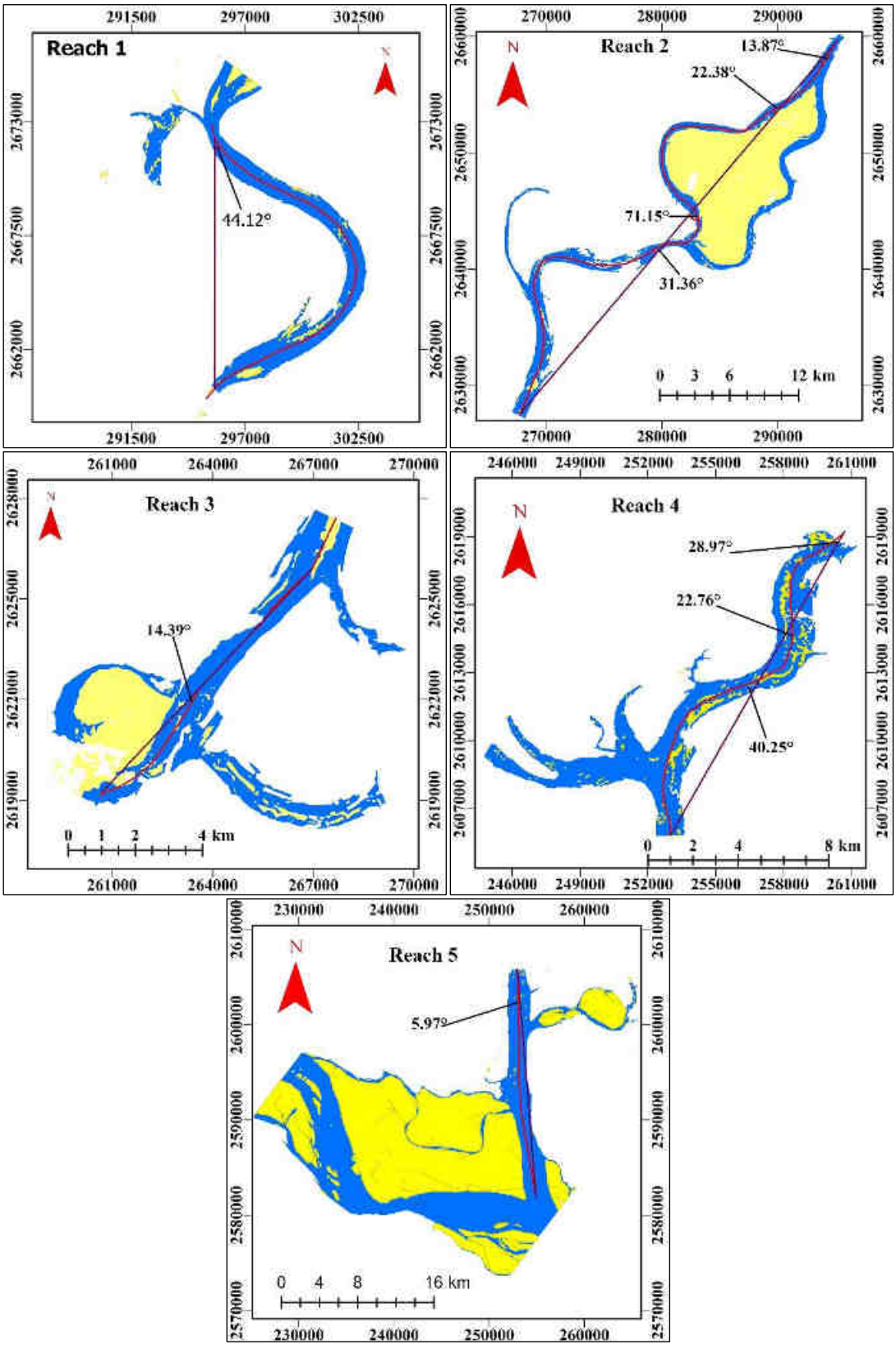

Fig. 7. Different reaches of Upper Meghna river

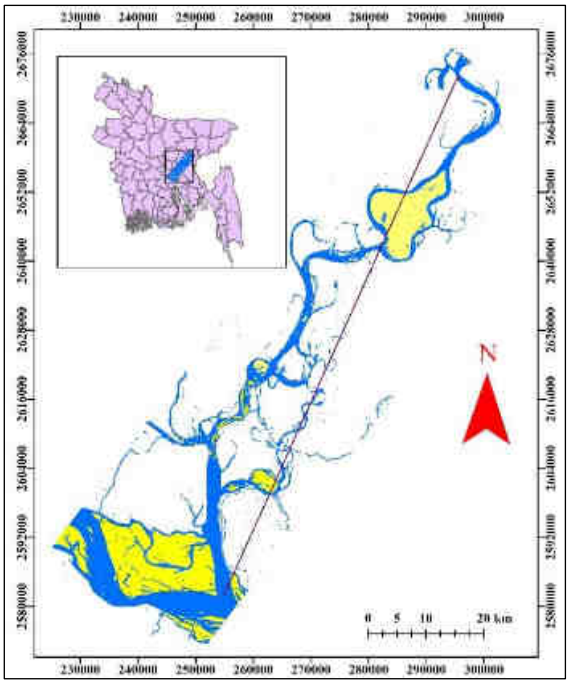

Fig. 8. Whole reach of Upper Meghna River

Table 5. Sinuosity Index (SI) Upper Meghna River

Reach	No. of Bends	Meander Angle (deg)	Sinuosity according to $K = \frac{4.84}{4.84-\phi_0^2}$	Valley Length (km)	Meander Length (km)	Sinuosity according to $K = \frac{M}{L}$
1	1	44.12	1.14	12.10	20.50	1.69
		13.87	1.01			
2	4	22.38	1.03	41.92	56.18	1.34
		71.15	1.47			
		31.36	1.07			
3	1	14.39	1.01	9.17	11.04	1.20
		22.76	1.03			
4	3	28.97	1.06	15.46	17.50	1.13
		40.25	1.11			
5	1	5.97	1.00	23.96	24.03	1.00
Whole Reach	10			102.61	129.25	1.26

The upper portion of the Meghna river in Bangladesh has been considered in the present study. This river was severed into five reaches for the sake of sinuosity analysis. The SI values according to meander length and valley length given higher values than meander angle method. According to Charlton (2008) all but the reaches 1, 2, 3 fall into meandering category of sinuosity and the reaches 4, 5 fall into sinuous category of sinuosity. Among the reaches, reach 1 showed the highest sinuosity and reach 5 showed the lowest sinuosity.

Discussion

The analysis of channel planform dynamics in Bangladesh's major rivers reveals significant variability in braiding and sinuosity indices, reflecting the complex interplay of hydrological, sedimentological, and anthropogenic influences. The results indicate that the Jamuna River exhibits a high braiding index, characteristic of its dynamic, multi-threaded morphology, driven by substantial sediment load and frequent bank erosion. These findings are consistent with earlier studies by Best et al. (2007) and Ashworth et al. (2000), who highlighted the role of high sediment flux and seasonal discharge variations in shaping the braided nature of the Jamuna. Similar studies in other large braided river systems, such as the Brahmaputra in India (Goswami et al., 1999) and the Yukon River in Alaska (Smith & Pérez-Arlucea, 2008), have also demonstrated that high sediment transport and channel migration play crucial roles in maintaining a braided morphology.

In contrast, the Padma River demonstrates a transitional behavior, with sections exhibiting both

braided and meandering tendencies, influenced by variable flow regimes and confluences (Bristow, 1999). This aligns with findings from the Missouri River in the United States, where braided-to-meandering transitions have been attributed to changes in sediment load and flow regulation (Jacobson & Galat, 2006). Similarly, the Meghna River, with a relatively lower braiding index, shows a predominantly meandering pattern, shaped by tidal effects and cohesive bank materials, as noted by Sarker et al. (2014). Studies on the Amazon River (Mertes et al., 1996) also highlight the role of cohesive floodplain sediments in stabilizing meandering channels.

Temporal variations in sinuosity indices suggest channel adjustments in response to hydrological fluctuations and interventions such as embankments and dredging, aligning with the findings of Islam et al. (2017), who emphasized the increasing anthropogenic influence on river morphology. Similar trends have been reported in the Yellow River, China, where extensive engineering interventions have significantly altered its channel morphology (Xu, 2003). These trends underscore the need for sustainable river management strategies, integrating sediment transport modeling and bank stabilization measures to mitigate adverse impacts on navigation, agriculture, and flood risk. Further research incorporating high-resolution satellite imagery and hydrodynamic modeling could provide deeper insights into the evolving nature of these river systems.

Conclusions

This study assessed the channel planform dynamics of the Teesta, Brahmaputra, Ganges, and Upper Meghna rivers in Bangladesh using remote sensing and GIS-based analysis. The findings reveal significant variations in braiding and sinuosity indices, reflecting the diverse morphological behaviors of these rivers. The Brahmaputra River exhibits the highest braiding index (BI = 2.07), indicating a more unstable braided condition compared to the Teesta (BI = 1.89). Similarly, the Ganges River shows a greater sinuosity index than the Upper Meghna, with certain reaches falling into the meandering category. These variations highlight the influence of hydrological and sediment transport processes on channel stability. The insights gained from this study contribute to a deeper understanding of river morphology in Bangladesh, which is essential for sustainable river management, flood risk mitigation, and infrastructure planning. Future research could incorporate additional hydrodynamic parameters and long-term temporal analysis to further enhance our understanding of river behavior in response to climatic and anthropogenic influences.

Conflict of interest

The authors declare no conflict of interest.

References

Akter, S., Eibek, K. U., Islam, S., Islam, A. R. M. T., Chu, R., & Shuanghe, S. (2019). Predicting spatiotemporal changes of channel morphology in the reach of Teesta River, Bangladesh using GIS and ARIMA modeling. *Quaternary International*, 513, 80–94. https://doi.org/10.1016/j.quaint.2019.01.022

Ashworth, P. J., Best, J. L., & Roden, J. E. (2000). The influence of aggradation rate on braided river morphology and dynamics: Results from physical modeling. *Geomorphology, 35*(3–4), 301–317. https://doi.org/10.1016/S0169-555X(00)00037-2

Best, J. L., Ashworth, P. J., Sarker, M. H., & Roden, J. (2007). The Brahmaputra-Jamuna River, Bangladesh. In A. Gupta (Ed.), Large rivers: *Geomorphology and management* (pp. 395–430). Wiley.

Bristow, C. S. (1999). Avulsion, river metamorphosis, and reworking by underfit streams: A modern example from the Brahmaputra River in Bangladesh and a possible ancient example in the Spanish Pyrenees. *Special Publications of the International Association of Sedimentologists*, 28, 221–230. https://doi.org/10.1002/9781444304213.ch12

Charlton, R. (2008). Fundamentals of fluvial geomorphology. Routledge.

Das, B. C., & Islam, A. (2023). Reviewing braiding indices of the river channel in an attempt to establish alternatives. *MethodsX*, 10, 102042. https://doi.org/10.1016/j.mex.2023.102042

Freihardt, J., & Frey, O. (2023). Assessing riverbank erosion in Bangladesh using time series of Sentinel-1 radar imagery in the Google Earth Engine. *Natural Hazards and Earth System Sciences, 23*(2), 751–770. https://doi.org/10.5194/nhess-23-751-2023

Goswami, D. C., Das, P. J., & Baruah, S. P. (1999). The Brahmaputra River, India: Channel changes and sedimentation. *Journal of Hydrology, 21* (3), 69–78. https://doi.org/10.1016/S0022-1694(99)00039-1

Islam, M. M., Sarker, M. H., & Rahman, M. M. (2017). Riverbank erosion and channel migration of the major rivers of Bangladesh: A study on morphological changes and human impacts. *Environmental Monitoring and Assessment, 189* (8), 403. https://doi.org/10.1007/s10661-017-6085-5

Jacobson, R. B., & Galat, D. L. (2006). Flow and form in rehabilitation of large-river ecosystems: An example from the Lower Missouri River. *Geomorphology, 77* (3–4), 249–269. https://doi.org/10.1016/j.geomorph.2006.01.014

Kuo, C.-W., Chen, C.-F., Chen, S.-C., Yang, T.-C., & Chen, C.-W. (2017). Channel planform dynamics

monitoring and channel stability assessment in two sediment-rich rivers in Taiwan. *Water, 9* (2), 84. https://doi.org/10.3390/w9020084

Mertes, L. A. K., Dunne, T., & Martinelli, L. A. (1996). Channel-floodplain geomorphology along the Solimões-Amazon River, Brazil. *Geological Society of America Bulletin, 108* (9), 1089–1107. https://doi.org/10.1130/0016-7606(1996)108<1089:CFGATS>2.3.CO;2

Mueller, J. R. (1968). An introduction to the hydraulic and topographic sinuosity indexes. *Annals of the Association of American Geographers, 58* (2), 371–385.

Nath, A., & Ghosh, S. (2022). Assessment of river morphology based on changes in land use and land cover and the spatial and temporal variation of meandering parameters of the Barak River. *Water Practice & Technology, 17* (11), 2351–2367. https://doi.org/10.2166/wpt.2022.114

Ozturk, D., & Sesli, F. A. (2015). Determination of temporal changes in the sinuosity and braiding characteristics of the Kizilirmak River, Turkey. *Polish Journal of Environmental Studies, 24* (5), 2095–2112. https://doi.org/10.15244/pjoes/58765

Rinaldi, M., Gurnell, A., González del Tánago, M., Bussettini, M., & Hendriks, D. (2016). Classification of river morphology and hydrology to support management and restoration. *Aquatic Sciences, 78* (1), 17–33. https://doi.org/10.1007/s00027-015-0433-4

Sarker, M. H., Huque, I., Alam, M., & Koudstaal, R. (2014). Rivers, chars and char dwellers of Bangladesh. *International Journal of River Basin Management, 11*(1), 25-42. https://doi.org/10.1080/15715124.2013.862941

Smith, L. C., & Pérez-Arlucea, M. (2008). Natural levee development along the Yukon River, Alaska. *Geomorphology, 102* (3–4), 363–374. https://doi.org/10.1016/j.geomorph.2008.04.008

U.S. Geological Survey. (n.d.). *Using USGS Landsat Level-1 data product*. https://www.usgs.gov/landsat-missions/using-usgs-landsat-level-1-data-product

van der Wal, M. (2020). Bank protection structures along the Brahmaputra-Jamuna River, a study of flow slides. *Water, 12* (9), 2588. https://doi.org/10.3390/w12092588

Xu, J. (2003). Sediment transport and channel adjustments of the lower Yellow River as influenced by human activities. *Geomorphology, 58(*1–4), 219–238. https://doi.org/10.1016/S0169-555X(03)00165-3.

Technical Journal
River Research Institute ISSN: 1606-9277

A Hydro-morphological Study of the Proposed Bridge on the Pandab-Paira River, Patuakhali

A. K. M. Ashrafuzzaman[1*], M. J. Islam[1], M. Shahabuddin[1], M. Tofiquzzaman[1], F. Rukshana[2] and P. Kanungoe[1]

Abstract

A hydro-morphological study is carried out to determine the location of suitable bridge site and to recommend hydraulic design for the bridge, approach road and river training works. The selection of suitable bridge site, hydraulic design of the bridge and associated river training works are made on the basis of the hydro-morphological study through numerical modeling using MIKE 21C as well as rational data analysis. The model has been developed covering a river stretch of 20 km including the likely bridge location. MIKE 21C module is utilized to estimate the various hydro-morphological parameters of the modelled reach in addition to propose the hydraulic design parameters of the bridge and associated river training works. Analysis of all relevant collected data and model results show that two locations (Option 1 & 2) between two meander bends are found to be appropriate for bridge siting. In this study, Option-1 is recommended for bridge construction where the suggested length of the bridge is 980 m. The hydrological and hydraulic design parameters as suggested may be considered for the bridge. The study also recommends that at the bend locations the developments in the river channel in the immediate upstream and downstream of the proposed bridge should be monitored very closely.

Keywords: *Bridge design, Pandab-Paira River, Hydro-Morphological parameters, MIKE 21C, Simulation, River training works.*

Introduction

The proposed Nalua-Baherchar Bridge over the Pandab-Paira River is located at 28th K.M. of Barisal (Dinerarpool)-Laxmipasha-Dumki Road. At present, ferry service has been provided by RHD to cross the river. Barisal (Dinerarpool)-Laxmipasha-Dumki Road plays an important role in road communication network of this area. A good number of villages, bazars and trade centres are connected to this zilla road through Local Government Engineering Department (LGED) and other union and village roads. The traffic volume on this road is significant and the number of light and heavy vehicles is increasing day by day. After completion of the project, vehicles will able to move safely. Better marketing opportunities will be opened and farmers will get comparatively fair price for their products. It will immensely contribute to the overall economic growth of the area. The proposed Nalua-Baherchar roadway bridge over the Pandab-Paira River fills the river gap between Bakerganj upazilla of Barisal district and Dumkiupazilla of Patukhali district. Nalua is situated on the right bank and Baherchar is situated on the left bank of the Pandab-Paira River respectively.

The Paira River flows through the upazillas of Dumki, Patuakhali Sadar, Mirzaganj, and Galachipa under Patuakhali district and Amtoli under Barguna district. It is a perennial river having catchment area of about 557 km2. The Pandab-Paira is tidally affected river. Like other coastal rivers, Paira is associated with strong tidal current, salinity and waves (Haque, 2008). Fine sediment is transported by tidal currents headed towards the sea. It is probable that the sediment originated from the Meghna discharge during the wet season and is carried westwards by near shore currents created by the north-east monsoon in the period July to November. Sediment is also carried into the area by the freshwater rivers at Mirzaganj. The river falls within the coastal boundary of the country which comprises of extensive flat coastal and deltaic land of the Ganges delta and crossed by large tidal rivers discharging into the Bay of Bengal. Therefore, selection of a suitable bridge location and bridge waterway opening requires detailed verification of likely hydrological scenarios and the present erosion trend as well as future likely river plan form development. On the other hand, due to tidal influence determining hydraulics of scour depths and river training works would require special consideration of steepest recession of flood. The hydrology of the study area is very complicated as four types of climatic factors influence its hydrology. These climatic factors are cyclonic surge, tidal flow, monsoon flow and sea level rise due to global warming (BUET and IWM, 2008). Thus, to investigate the combined effect of these four factors are very important to determine the vertical clearance and horizontal clearance of bridge.

Necessary hydrological, hydrographic and sediment data have been collected through a field survey campaign. Historical hydrological data of the rivers concerned and satellite images of the study area have been collected from WARPO, Dhaka and CEGIS, Dhaka respectively. Collected data have been processed and analyzed to the extent of deriving necessary inputs for the MIKE 21C model that has been developed for hydraulic analysis of bridge and other information relevant to the proposed bridge. The location of the study area is shown in **Fig. 1**.

[1]Hydraulic Research Directorate, River Research Institute, Faridpur-7800, Bangladesh.
[*]Corresponding Author: (E-mail: ashrafcebuet89@gmail.com)
[2]Hydraulic Research Directorate, River Research Institute, Faridpur-7800, Bangladesh.

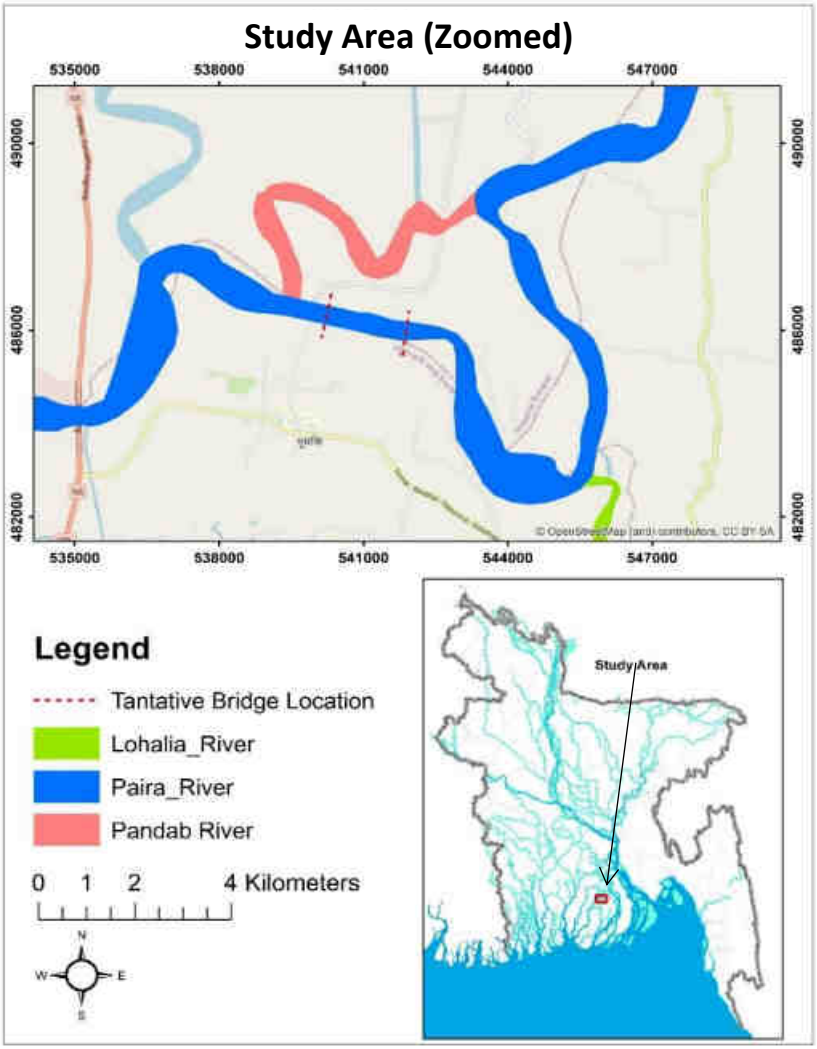

Fig. 1. Location of the study area

Scour depth is the lowering of the river bed level and is a measure of the tendency to expose bridge foundations (Melville & Coleman, 2000). Scour at bridge crossings is the consequence of the erosive action of flowing water, when it has the strength to excavate and carry away material from around bridge piers and bridge abutments (Richardson & Davis, 2001). Although scour process mechanisms are well established, quantifying the magnitude of scour at bridge crossing is not an easy task, due not only to the complexity of the cyclic nature of the phenomenon, but also to the fact that bridge geometry, river channel morphology and hydrologic regime are different for each bridge. A channel with a mobile bed is usually exposed to a general scour, which takes place independently of the presence of the bridge and is due to streambed elevation changes in the reach where the bridge is located. The main causes of general scour that induce aggradation or degradation of the bed channel are either due to natural phenomena, such as channel straightening, climate changes and land activities (landslides, mudflows) or to human activities, such as land-use changes (deforestation, urbanization), dam and reservoir construction, river bed material mining and channel alterations. In the presence of bridge crossings, additional scour is known as local scour and is induced by the local change of cross-section geometry due to the presence of the bridge (Graf, 1998; Richardson & Davis, 2001). Local scour usually results from the joint effect of contraction scour, due to the flow velocity increase associated with the reduction of channel section, and the pier and abutment scour, due to the (local) alteration of the flow field induced by piers and abutments (Graf, 1998).

Methodology

In order to conduct the study necessary hydrological data of the Pandab-Paira River, satellite image of the study area and other relevant information had been

collected. A field survey campaign was conducted to collect the bathymetric data (October 2014) of the river, nearby road alignment data, historical water level (1980-2014) & historical discharge (1980-2014) at the nearby station, discharge & corresponding water level (October 2014) and sediment data (October 2014) etc. Collected data had been processed and analysed to the extent of deriving necessary inputs for the MIKE 21C model that had been developed for hydraulic analysis of bridge and other information relevant to the proposed bridge.

The choice of a suitable standard frequency distribution is often controversial, but the General Extreme Value (GEV) distribution has obtained widespread acceptance (Hall & Minns, 1998). In the present study the GEV distribution was considered. The discharges corresponding to 50-year & 100-year return period were estimated as 4040 m^3s^{-1} & 4298 m^3s^{-1} respectively using historical discharge (1980-2014) data at the nearby station. The 50-year & 100-year return period discharges had been used as design discharge for bridge & design discharge for bridge substructure respectively. The model generated water levels at the likely bridge location are found to be 3.25 mPWD and 3.40 mPWD for 50 year and 100 year return period discharges respectively. The Standard Low Water Level (SLWL) & Standard High Water Level (SHWL) at the proposed bridge site were obtained from the isohyetal map prepared by BIWTA which is respectively -0.45 mPWD & 2.44 mPWD.

The initial bathymetry corresponding to the computational grid generated for hydrodynamic and morphological simulations was done on the basis of bathymetric survey data on October, 2014. The initial bathymetry was then prepared using standard MIKE 21C bathymetry preparation module (DHI, 2006). MIKE 21C can also be used for designing protection schemes against bank erosion, evaluating measures to reduce or manage shoaling, analyzing alignments and dimensions of navigation channels for minimizing capital and maintenance dredging, predicting the impact of bridge, tunnel and pipeline crossings on river channel hydraulics and morphology, optimizing restoration plans for habitat environment in channel floodplain systems, designing monitoring networks based on morphological forecasting. Due to its accurate descriptions of the physical processes, MIKE 21C can simulate a braided river developing from a plane bed, which was illustrated by Enggrob & Tjerry, 1998.

The most important secondary flow in rivers is the so-called helical flow, with its name derived from Helios (the Sun in Greek). The name helical is used because the flow arises as the water in the lower portions of the water column flowing towards the local center of curvature, and away from the local center of curvature along the water surface. This has only a minor impact on the hydrodynamics, usually only pronounced on a laboratory scale, but it has profound impacts on the sediment transport and morphology because the helical flow influences the otherwise zero transverse sediment component.

MIKE 21C applies standard theory for the helical flow, which can be found in e.g. Rozowsky, 1957. Standard helical flow theory provides a secondary flow velocity profile that is fully characterized by friction and the deviation angle between the main flow direction and the direction of the shear stress at the river bed. MIKE 21C uses the traditional division of sediment transport into bed load and suspended load, and the model can simulate both non-cohesive and cohesive sediment in a mixture. The bed-load model accounts for the impacts of secondary flow (bed shear stress direction) and local bed slope (gravity). Suspended load is calculated with an advection-dispersion equation for each fraction, which includes adaptation in time and space as well as the 2-dimensional depth-integrated effects of the 3-dimensional flow pattern through profile functions (Galappatti & Vreugdenhil, 1985). Suitable (linear) interpolation procedure was followed to generate bathymetry information at locations where bed level information was unknown. The generated bathymetry was then checked for consistency. The initial bathymetry corresponding to the generated grid covering the area of 544000 mEasting and 489000 mNorthing is shown in **Fig. 2**.

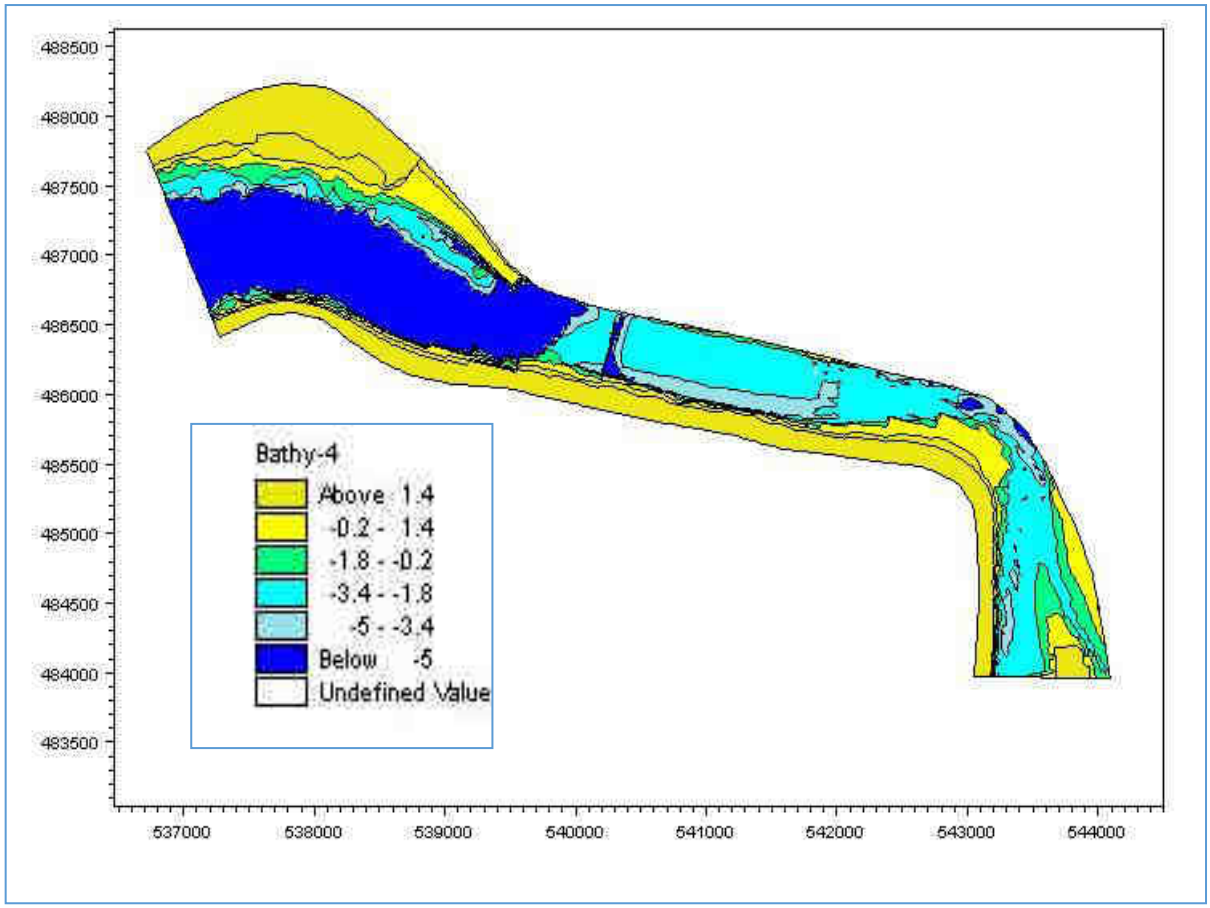

Fig. 2. Initial bathymetry of the model (MIKE 21C)

Hydrodynamic and morphological assessment of the Paira River had been made through scenario simulations using a developed two dimensional numerical model. The hydrodynamic simulations are made in base condition (without bridge in place) for two distinct return period discharges namely 50 year and 100 year discharges. It was understood from the preliminary investigations that the suitable bridge location could be in the crossing between two consecutive meander bends of Paira River around the Nalua-Baherchar ferry ghat, the focus of the study was hydro-morphological conditions of the river at this river stretch (including upstream and downstream bends) under different hydrological scenarios and the model results had been extracted for demonstration accordingly. The velocity fields at and in the vicinity of the likely bridge location (at Nalua-Baherchar ferry ghat) in hydrodynamic conditions for two return period discharges are shown in **Fig. 3**. It can be seen from this figure that flow pattern there almost similar for 100 year and 50 year discharges with only difference of a bit higher velocity for higher discharge. It can also be seen that major flow occurs through the main river channel at the upstream of the bridge location after then towards right bank for all discharges. Flow over the nearby floodplains occurred with relatively low velocities (< 0.6 ms^{-1}) due to high resistance to flow.

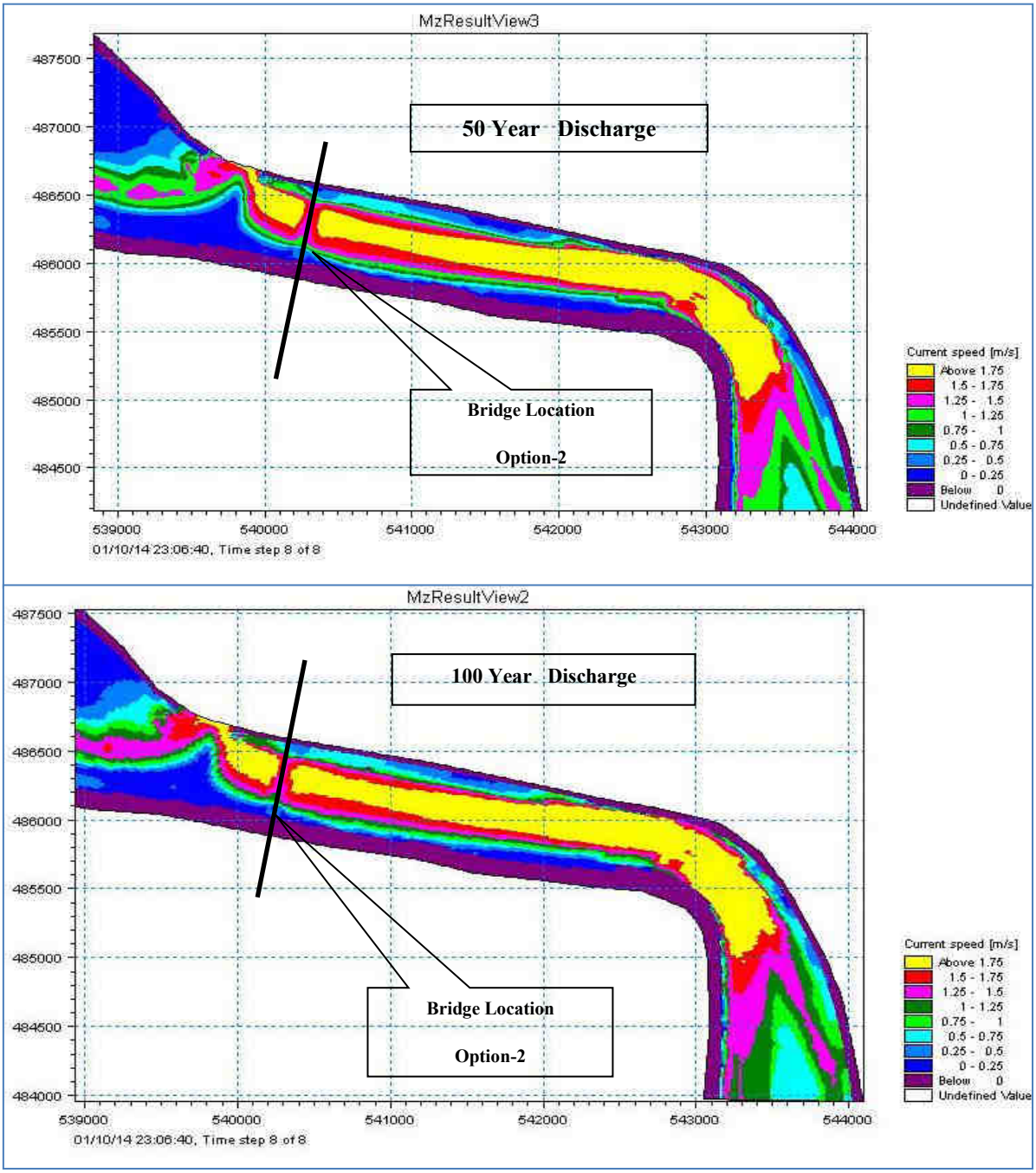

Fig. 3. Velocity fields at and in the vicinity of the likely bridge at Nalua-Baherchar ferry ghat for different return period discharges.

Results and Discussion

Suitable Bridge Location

It appears from the analysis of collected field data and maps and satellite images that the crossing between two meander bends at the Nalua-Baherchar ferry terminal could be suitable location for siting the proposed bridge. It is because in that case the bridge will be located at an inflection point which is less vulnerable to bank erosion. If bend migration continues to occur the inflection point will remain almost unaffected. The river banks consist of cohesive materials and rate of bank erosion is not very high. The bed materials in the study reach consist mainly of fine sand with some percentage of medium sand and thereby, the bed is erodible when the flow velocity exceeds the threshold velocity for initiation of bed motion. Given the present cut-off ratio of the meander bends at and around the likely bridge location it is expected that natural cut-off of these bends will not occur in the near future. However, future developments of these bends have large impact on the morphological developments at the bridge location. From overall considerations it can be fairly stated that the proposed

bridge should be constructed at the crossing between two consecutive meander bends around the Nalua-Baherchar ferry terminal. The existing RHD road and the suitable river stretch for siting the proposed bridge are shown in **Fig. 4**. It can be stated that if bank erosion continues to occur at bend locations in the upstream and downstream of the Nalua-Baherchar ferry terminal the crossing location will remain almost unaffected. It will act as an inflection point between the two consecutive eroding bends. This fact is confirmed both by analysis of field data and model investigation results.

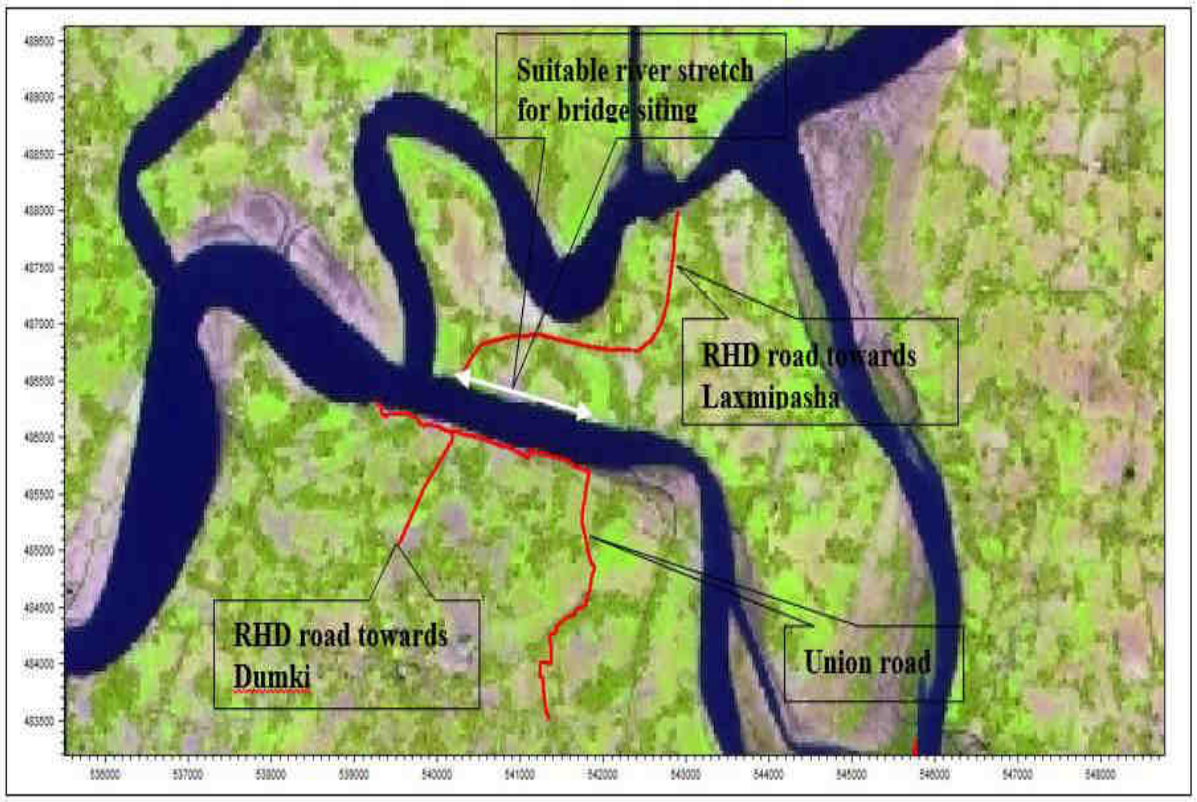

Fig. 4. Suitable river stretches for siting the proposed bridge (CEGIS, 2015)

Proposed Bridge Alignment and Velocity Field

Hydrodynamic and morphological assessment of the Paira River has been made through scenario simulations using a developed two-dimensional numerical model. The hydrodynamic simulations are made in base condition (without bridge in place) for two distinct return period discharges namely 50 year and 100 year discharges. It is understood from the preliminary investigations that the suitable bridge location could be in the crossing between two consecutive meander bends of Paira River around the Nalua-Baherchar ferry terminal, the focus of the study is hydro-morphological conditions of the river at this river stretch (including upstream and downstream bends) under different hydrological scenarios and the model results have been extracted for demonstration accordingly. **Fig. 5** also shows the velocity fields at and in the vicinity of the likely bridge locations in hydrodynamic conditions for 100-year return period discharge.

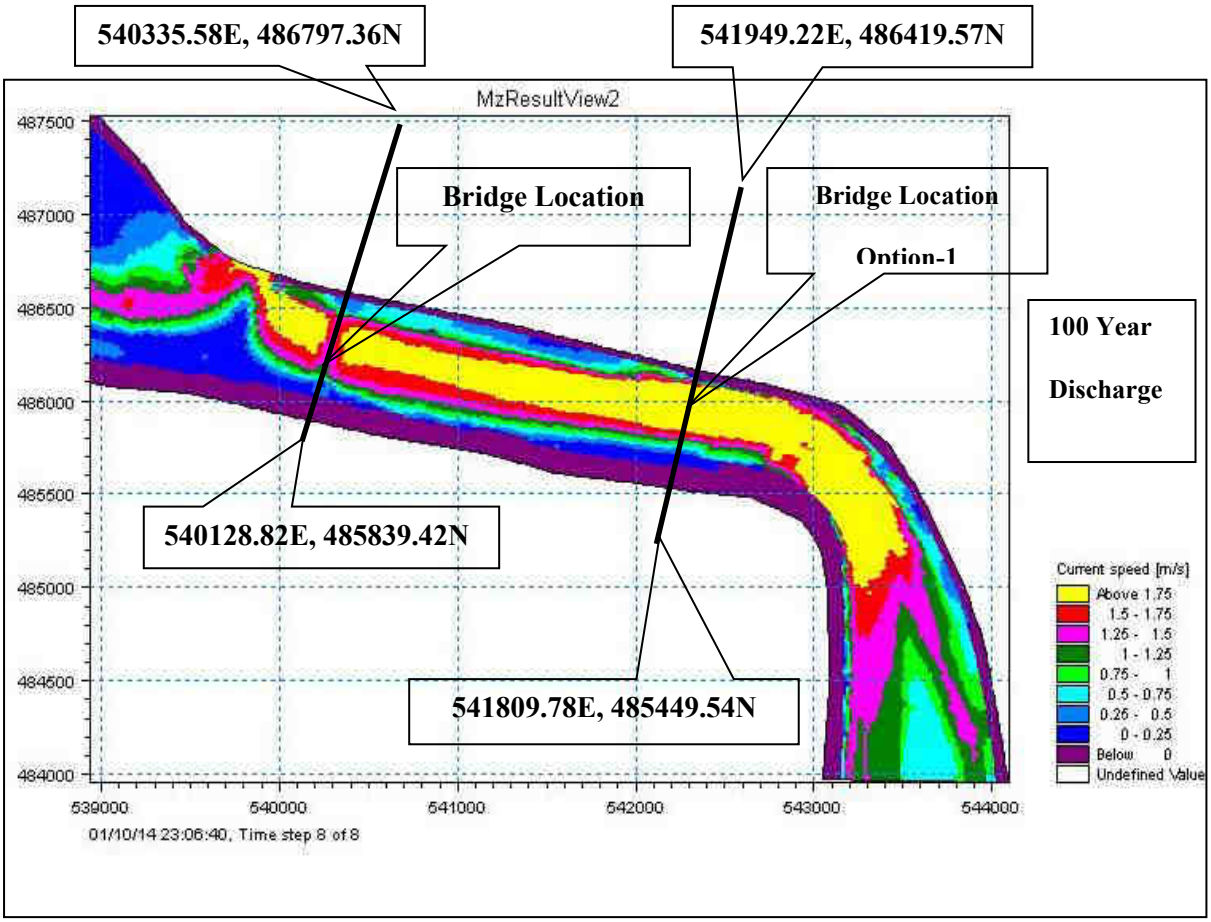

Fig. 5. Proposed position and orientation of the Nalua-Baherchar bridge (MIKE 21C)

Hydrological and Hydraulic Design of Bridge and Approach Road

The design parameters of the bridge and approach road are shown in **Table 1** below.

Table 1. Hydrological and hydraulic design parameters

Design parameters	Values
Design discharge for bridge substructure	4298 m^3s^{-1}
Discharge for bridge	4040 m^3s^{-1}
Design flood level for bridge substructure	3.40 mPWD
Design flood level for bridge	3.25 mPWD
Standard Low Water Level	-0.45 mPWD
Standard High Water Level	2.44 mPWD
dm of soil material	0.085 mm
Formation level of approach road	3.95 mPWD
Bottom level of the bridge girder	21.0 mPWD
Deck level at centreline of the bridge	23.5 mPWD
Length of the bridge	980 m
Number of bridge spans	8
Design scour level for abutment	9
Design scour level for abutment	-6.90 mPWD
Design scour level for pier	-16.46 mPWD
Length of approach road	302.5 m

Velocity information at and in the Vicinity of the Bridge

Velocity information at and in the vicinity of the bridge location in base and with bridge conditions are shown respectively in **Table 2** & **Table 3** below.

Table 2. Velocity information at Nalua-Baherchar ferry terminal in base condition

Return Period (year)	Discharge (m^3s^{-1})	Maximum velocity (ms^{-1})	Cross-sectional mean velocity (ms^{-1})
50	4040	1.97	1.38
100	4298	2.04	1.49

Table 3. Velocity information with bridge in place for option 1 and 2 against 100 year discharge

Location for option-1	Maximum velocity (ms^{-1})	Near bank velocity (ms^{-1})
Along right bank upstream of bridge option-1	-	1.46 to 1.77
Near left abutment (over left floodplain)	Not applicable	-
Near right abutment	Not applicable	-
Along left bank in the immediate downstream of the bridge	-	0.13 to 0.49
At the left pier of the middle span	1.32	-
At the right pier of the middle span	2.21	-
Along right bank in the immediate downstream of the bridge	-	1.26 to 1.61
Location for option-2	Maximum velocity (ms^{-1})	Near bank velocity (ms^{-1})
Along right bank upstream of Nalua-Baherchar ferry terminal (bridge option-2)	-	0.92 to 1.32
Near left abutment (over left floodplain)	Not applicable	-
Near right abutment	Not applicable	-
Along left bank in the immediate downstream of the bridge	-	0.26 to 0.83
At the left pier of the middle span	1.49	-
At the right pier of the middle span	1.84	-
Along right bank in the immediate downstream of the bridge	-	1.18 to 1.24

Bridge Height and Span Arrangements

According to BIWTA navigation route classification the Paira River in the study area falls under the navigation route Class I. It means minimum vertical clearance should 18.3 m with reference to Standard High Water Level (SHWL). The SHWL determined by Bangladesh Inland Water Transport Authority

(BIWTA) at Kaitpara which is about 10.00 km upstream of the Nalua-Baherchar ferry terminal is 2.45 mPWD. On the other hand, the same at Mirzaganj (26 km downstream of confluence of Pandab-Paira) is 2.30 mPWD. The bottom level of the bridge girder in this case is the summation of Standard High Water Level, minimum vertical clearance as specified by BIWTA and anticipated sea level rise due to global warming. The bottom level of girder is thus 21.0 mPWD. The minimum horizontal clearance for Class I navigation route is 76.22 m. The selected bridge length is 980 m. It can be seen that the main bridge consists of one 80 m long span in the middle and four 60m long spans (two in the right side and two in the left side). There will be 22 (twenty two) viaducts (eleven in the left side and eleven in the right side) of 30 m length each.

Need for River Training Works

The proposed bridge is located at the inflection point between two meander bends. Therefore, the bridge location does not suffer from erosion problem. A large point bar is visible along the right bank at the downstream of the confluence. On the other hand a medium point bar is visible at the upstream of Nalua-Baherchar ferry terminal. This point bar is indicative of the fact that large left bank erosion has taken place in the past. The left bank is still being eroded and there is potential for future bank erosion. In the upstream of the proposed bridge the right bank is erosion prone at the bend location. A medium point bar is also noticeable along the inner bank at this bend location. Examination of satellite images of the study area and consultations with the people point to the fact that substantial right bank erosion did occur in the upstream of the Nalua-Baherchar ferry terminal and at present the rate of erosion is rather low. However, study results show that erosion may continue to occur in the future at a slow pace. Moreover, the constriction caused by the bridge piers may cause an increase in the flow velocity at and in the immediate upstream and downstream of the bridge. It may accelerate the present rate of bank erosion at the bend locations.

Based on the above analysis it can be concluded that protective measures along the right and left bank is not much necessary at the upstream and downstream of the Paira River for implementing option-1. In case for implementing the proposed bridge location (option-2), the right existing RHD road runs (from Nalua-Laxmipasha) through the apex of the Pandab River. The setback distance between the bank and road is only 130 m. Examination of satellite imageries regarding the shifting of bank line and consultation with local people that left bank erosion did occur at the apex of the bend. About 2.0 km bank protective works will be needed to combat bank erosion at and around the apex along the left bank of the Pandab River. The placement of the proposed bank protection works is shown in **Fig. 6**.

Fig. 6. Placement of suggested bank protective works

Considering existing conditions and model results, a comparison between option-1 & option-2 is furnished in **Table 4.**

Table 4. Comparison between option-1 and option-2

Sl. No.	Parameters/Item	Option		Secured Marks		Remarks
		Option-1	Option-2	Option-1	Option-2	
1	Average River width in the vicinity of bridge (m)	412.89	442.95 m	10	10	
2	Average water depth (m)	6.04	6.28	10	10	
3	Minimum bed level (mPWD)	-3.80	-4.40	10	9	
4	Maximum velocity around the bridge pier (ms^{-1})	3.21	2.75	9	10	Option-1 secured 67 points out of 90 which is greater than Option-2
6	Proximity near the existing RHD road (m)	Right end =615 & Left end =525	Right end =75 (with resettlement) & Left end =100	4	7	
7	Distance from confluence (m)	2200	500	10	4	
8	Required bank protective works (revetment) length (m)	-	2000	10	0	
9	Land acquisition	more	less	4	8	
			Total	67	58	

It is revealed from **Table 4** that proximity near the existing RHD road, distance from confluence, required revetment length for river training works and land acquisition bear higher marks in option-1 than in option-2. For these technical points of views option-1 may be considered for the bridge siting. But RHD may implement any of the two options. In that case, 2.0 km bank protective works along the left bank of Pandab River will be needed.

Scour Computation at Abutment and Bridge Pier of the Proposed Bridge

Scouring of piers and abutment has been recognized as the main cause of damage and failure of bridges over waterways. The scientific community has produced a number of studies addressing the complex characteristics of the scour process and has provided engineers with several techniques for the estimate of the maximum expected scour depth at a bridge site. Nevertheless, the prediction of scour depths is affected by many sources of uncertainty, such as observation uncertainty, parameter uncertainty, and structural uncertainty. Only a few studies have recently tried to estimate the uncertainty associated to the scour depth prediction.

The following data have been used for the computation of pier scour and abutment scour for the proposed bridge on Pandab-Paira River.

Pier width = 1.5 m

Channel width (flood bank to flood bank) = 460 m

Median size of bed material (d50) = 0.085 mm

Discharge = 4298 m^3s^{-1}

Hydraulic depth (main channel) = 6.26 m

Average velocity (main channel) = 1.56 ms^{-1}

Flow depth over floodplain = 1.87 m

Local scour at Abutment

Laursen's Method: 10.30 m

Melville Formula: 8.97 m

Rahman and Muramoto Formula: 6.90 m

The simulated water level for 100 year discharge at the bridge location is 3.40 mPWD. Hence the scour level of -6.90 mPWD may be used. The bottom level of pile foundation for the abutment should be placed well below this level.

Local scour at Bridge Pier

Laursen's Method: 8.8 m

Melville Formula: 7.2 m

IRC Method: 10.66 m

Lacey's formula: 4.8 m

The maximum computed scour depth is 10.66 m for IRC method. In computation scour around the bridge pier in the rivers of Bangladesh Indian practice is often followed. The minimum bed level is -3.8 mPWD. Considering 2.0m general scour the minimum scour bed level is -16.46 mPWD.

Conclusions

The study shows that there is both lateral and vertical stability problems at the bend locations in the immediate upstream and downstream of the Nalua-Baherchar ferry ghat. The proposed bridge over the Paira River should be located at the inflection point between two consecutive meander bends near the Nalua-Baherchar ferry ghat. There are two options for the proposed bridge location. Option-1 (at 1700 m upstream of Nalua-Baherchar ferry ghat): Right end co-ordinate of the bridge is 541949.22E, 486419.57N, Left end co-ordinate of the bridge is 541809.78E, 485449.54N and Option-2 (at and around Nalua-Baherchar ferry ghat): Right end co-ordinate of the bridge is 540335.58E, 486797.36N, Left end co-ordinate of the bridge is 540128.82E, 485839.42N.

The design discharge for the bridge and bridge substructure is 4040 m^3s^{-1} and 4298 m^3s^{-1} respectively. The design water level for the bridge and bridge substructure is 3.25 mPWD and 3.40 mPWD respectively. The standard high water level (SHWL) is 2.44 mPWD and the standard low water level (SLWL) is -0.45 mPWD. The length of the approach road is 302.5 m in both sides of the bridge. The approach road formation level at access road and at abutment is 3.95 mPWD and 10.0 mPWD respectively. The main bridge consists of one 80 m long span in the middle and four 60 m long spans (two in the right side and two in the left side). There will be 22 (twenty two) viaducts (eleven in the left side and eleven in the right side) of 30 m length each.

The bottom level of the bridge girder at the center of the bridge should be kept at 21.0 mPWD. The bridge deck level at centerline of the bridge is 23.5 mPWD. The design scour level at the abutment is -6.90 mPWD. The bottom level of pile foundation for the abutment should be placed well below this level. The design scour level for the bridge pier is suggested to be -16.46 mPWD. The bottom level of the pile foundation should be set well below this level.

Recommendation

The bridge may be constructed at the suggested location (option-1). The length of the bridge may be recommended as 980 m. The suggested hydrological and hydraulic design parameters required for the bridge may be considered. In case for implementing option-2, 2.0 km bank protective works will be needed to combat bank erosion at and around the apex along the left bank of the Pandab River (**Fig. 6**). The developments in the river channel at the bend locations in the immediate upstream and downstream of the proposed bridge should be monitored very closely.

Conflict of Interest

The authors declare no conflict of interest.

References

BUET & IWM (2008). *Manual on Hydrologic and Hydraulic Design of Bridges.* Bangladesh University of Engineering & Technology, Dhaka 1000 and Institute of Water Modelling, Mohakhali, Dhaka 1206.

DHI Water and Environment (2006). *MIKE 21C, River Hydrodynamics and Morphology, User Guide*. Danish Hydraulic Institute, Denmark.

Graf, W.H. (1998). *Fluvial Hydraulics*, Wiley, Chichester, U.K.

Haque, M. I. (2008). *Water Resources Management in Bangladesh.* P. 542

http://www.ffwc.gov.bd/. Accessed in December 2017.

Enggrob, H.G., & Tjerry, S. (1998). Simulation of Morphological Characteristics of a Braided River, Proc. IAHR-Symp on River, Coastal and Estuarine morphodynamics, University of Genova, Dept Environmental Eng., Genova, 585 - 594.

Hall, M. J., & Minns, A. W. (1998). Regional flood frequency analysis using artificial neural networks. *Proc. Hydroinformatics'98, 3rd Internat. Conf. on Hydroinformatics*, Copenhagen.

Rozowsky, I.L. (1957). Flow of Water in bends of open channels, English Translation, Israel Progr., Jerusalem.

Melville B. W., & Coleman S. E. (2000). Bridge Scour, Water Resource, LLC, Colorado, USA.

Richardson E. V., & Davis S. R. (2001). Evaluating scour at bridges, Fourth Edition, Rep. FHWA-NHI 01-001, HEC No. 18, Federal Highway Administration, Washington, D.C.

Galappatti R., & Vreugdenhil C.B. (1985). A depth-integrated model for suspended transport. *Journal of Hydraulic Research, Vol.23*, No.4.

Technical Journal
River Research Institute ISSN: 1606-9277

Investigating the Trends of Rainfall and Discharge along the Brahmaputra-Jamuna River System

R. A. Nishat[1*] and M. R. Joy[1]

Abstract

The Brahmaputra-Jamuna River system is one of South Asia's largest and most vital river networks, supporting millions through agriculture, fisheries, and freshwater resources. However, climate change is increasingly threatening its hydrological stability. This study investigates rainfall and discharge trends from 1990 to 2023 using precipitation data from the PERSIANN-CDR dataset and discharge records from the Bangladesh Water Development Board at the Bahadurabad Transit station. Statistical techniques including the Mann-Kendall test, Sen's Slope estimator, linear regression, and correlation analysis were applied to detect trends and address missing data. Results show a significant downward trend in both rainfall and discharge, particularly during the monsoon and post-monsoon seasons. A strong positive correlation of 0.83 between rainfall and discharge indicates that reduced precipitation is a major factor behind declining river flow. Seasonal analysis reveals that wetter periods are experiencing more severe reductions, disrupting the natural hydrological cycle. These changes pose serious challenges for water availability, agriculture, and floodplain ecosystems. The findings highlight the urgent need for continuous monitoring and adaptive water resource management strategies to mitigate future risks. Ensuring long-term sustainability of the Brahmaputra-Jamuna River system will require coordinated efforts in planning, research, and community-based water governance.

Keywords: *Brahmaputra-Jamuna River, Rainfall trends, Discharge trends, Hydrological variability, Mann-Kendall test, Sen's Slope Estimator.*

Introduction

Bangladesh, situated in South Asia, extends from 20°34′N to 26°38′N latitude and 88°01′E to 92°41′E longitude, making it one of the most hydrologically dynamic regions in the world (Alam et al., 2007). The country is predominantly riverine, with over 700 rivers forming an intricate network that significantly influences floodplain dynamics, agricultural productivity, and freshwater availability. Among these, the Brahmaputra-Jamuna River is one of the largest and most hydrologically significant, shaping the country's water resources, sediment transport, and monsoon-driven flood regime (Mirza, 2002). The river originates in the Tibetan Plateau as the Yarlung Tsangpo River, traverses India as the Brahmaputra, and enters Bangladesh as the Jamuna, before merging with the Ganges and Meghna systems. The river plays a key role in regional water availability and supports a large population dependent on agriculture and fisheries. Due to its transboundary nature, the Brahmaputra-Jamuna River is highly sensitive to both regional and global climatic variations (Sarker et al., 2014).

Bangladesh experiences a distinct seasonal cycle, primarily divided into four key seasons: pre-monsoon (March-May), monsoon (June-September), post-monsoon (October-November), and dry season (December-February). The monsoon season contributes approximately 70–80% of the annual rainfall, leading to high river discharge and frequent flooding, whereas the dry season is characterized by water scarcity and declining discharge levels (Bari et al., 2016). With climate change, these seasonal patterns are becoming increasingly unpredictable, with erratic rainfall, temperature rise, and altered hydrological regimes affecting river discharge patterns (Akter et al., 2019; Islam et al., 2021).

Numerous studies have confirmed that rainfall patterns are shifting globally (Hulme et al., 1998; Lambert et al., 2004) as well as regionally (Jain & Kumar, 2012; Shahid, 2010) due to global warming. Studies on global-scale hydrological changes indicate that while some rivers are experiencing an increase in discharge, others are facing a significant decline due to reduced precipitation and altered catchment hydrology (Kundzewicz et al., 2008). Changes in precipitation patterns, glacial melt contributions, and increased evapotranspiration due to rising temperatures have altered river flow characteristics across different geographical regions (Döll & Zhang, 2010). In North America, for example, monthly mean discharge has decreased in many Canadian basins, particularly in the summer and autumn months (Zhang et al., 2000). Similarly, a downward trend in river discharge has been observed in Turkey (Kahya & Kalaycı, 2004) while the Yangtze River in China exhibits a mixed pattern, declining in its upper reaches but increasing in its middle and lower reaches (Zhang et al., 2000). Within the South Asian context, climate-induced hydrological changes are particularly severe with research indicating regional downtrend in rainfall (Manton et al., 2001; Manzoor et al., 2014). In Bangladesh, several studies have investigated long-term trends and variability in rainfall across different regions documenting changes in rainfall trends over the past decades (Billah et al., 2015) highlighted the impact of climate change on river flows in the southwestern region, while other studies have noted a downward trend in rainfall in northeastern Bangladesh (Basak et al., 2013; M. A. Rahman & Begum, 2013; Shahid,

[1]Department of Civil and Environmental Engineering, Shahjalal University of Science and Technology, Kumargaon, Sylhet-3114, Bangladesh.
*Corresponding Author: (E-mail: raiedahmednishat@gmail.com)

2010). However, while considerable attention has been given to analyzing rainfall trends, comparatively fewer studies have investigated the corresponding trends in river discharge, particularly within major transboundary river systems.

The Brahmaputra-Jamuna River, fed by both glacial melt and monsoon precipitation, is highly sensitive to climate variability. Despite the significance of the Brahmaputra-Jamuna River system, comprehensive studies assessing the long-term trends of discharge and their correlation with climatic variables remain limited. This research addresses this gap by conducting a comprehensive trend analysis of both rainfall and river discharge trend of the Brahmaputra-Jamuna River system over the period 1990 to 2023. Using historical hydro-meteorological data, statistical trend analyses, and correlation assessments, this research aims to find whether seasonal variations in discharge and precipitation have undergone significant changes over the decades. The objective of this study is to analyze the long-term trends in river discharge alongside rainfall patterns within the Brahmaputra-Jamuna River system, to examine the relationship between rainfall variability and discharge behavior, and to assess how these dynamics have been influenced by climate change. The findings of this study are expected to offer critical insights into how the river responds to long-term climatic changes, supporting more informed decisions in policy making, flood management, and climate-resilient planning.

Methodology

Study Area

The Brahmaputra-Jamuna River System is a major transboundary river system flowing through India, Bangladesh, and China (**Fig. 1**). The river originates from the Tibetan Plateau, flows through India as the Brahmaputra, and then enters Bangladesh, where it is known as the Jamuna River. The system covers a vast area, with a drainage basin spanning approximately 580,000 km², making it one of the largest river basins globally (Goswami, 1985).

The river experiences significant seasonal variations in flow, with high discharge levels during the monsoon season (June to October) and lower flow in the dry season (November to May). The system has a dynamic morphology, characterized by meandering channels and large sediment deposition (Ashworth et al., 2000). It is also prone to flooding, particularly within Bangladesh, where the river's annual floods cause widespread damage (M. A. Rahman et al., 2025).

The study area centers around the Bahadurabad Transit Station (SW46.9L), located in Jamalpur District (25.157°N, 89.7°E), which serves as a key monitoring point of the river before it merges with the Padma. Both river discharge and rainfall data for this study were collected from this station, making it a representative site for analyzing seasonal variations in river flow and precipitation.

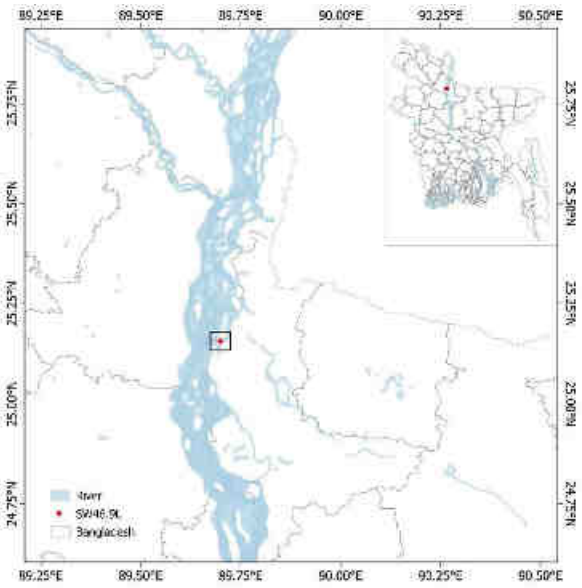

Fig. 1. Study area map with station information.

Data Source

This study uses monthly precipitation data from 1990 to 2023 obtained from the PERSIANN-CDR dataset, developed by the Center for Hydrometeorology and Remote Sensing (CHRS) at UC Irvine. The dataset provides high-resolution (0.25° × 0.25°) satellite-based rainfall estimates, adjusted using GPCP monthly products to ensure long-term consistency. Monthly river discharge data were acquired from the Bangladesh Water Development Board (BWDB) at a monitoring station SW46.9L (Bahadurabad_Transit) located at Jamalpur (25.157°N, 89.7°E). These ground-based measurements capture seasonal and interannual flow variations. Both datasets were aggregated to a monthly timescale for trend analysis and correlation studies.

Seasonal classification of data

For a more structured analysis of hydrological variations, both the rainfall and river discharge datasets were categorized into four distinct seasons. Bangladesh experiences a well-defined seasonal cycle, which significantly influences precipitation and river discharge levels. The pre-monsoon season, spanning from March to May, is characterized by increasing temperatures and sporadic thunderstorms. The monsoon season, from June to September, brings the highest rainfall due to southwest monsoon winds, leading to peak river discharge. Post-monsoon conditions from October to November witness a gradual decline in rainfall, accompanied by receding river levels. The dry season, covering December to February, is defined by minimal precipitation and

cooler temperatures, resulting in the lowest river discharge levels of the year. Dividing the data into these seasonal periods allows for a more comprehensive examination of trends.

Handling Missing Data

In this study, both rainfall and discharge datasets contained missing values that needed to be addressed before further analysis. Neglecting these gaps could introduce bias and reduce the reliability of the results. To maintain the seasonal characteristics of rainfall patterns, missing values were replaced using the mean rainfall of the same month across all years in the dataset. Monthly mean imputation is widely used in hydrological studies where seasonal variation is significant. Unlike rainfall, discharge values could not be imputed using simple mean methods, as they depend on multiple hydrological factors. Therefore, a regression-based approach was employed to estimate missing discharge values. A Linear regression model was trained using available rainfall and discharge data to establish a statistical relationship between these two variables. Linear regression is a supervised learning algorithm that models the relationship between a dependent variable (discharge) and an independent variable (rainfall) using a linear equation.

$$Q = \beta_0 + \beta_1 R + \epsilon \quad \text{Eq. (1)}$$

where Q represents discharge (m^3s^{-1}), R represents rainfall (mm), β_0 and β_1 are regression coefficients, and ϵ is the error term (Khuri, 2013).

The trained model was then used to predict discharge values for missing entries based on corresponding rainfall values.

Mann-Kendall Test

The Mann-Kendall test is a non-parametric statistical method widely used for detecting trends in time series data, particularly in hydrology, meteorology, and environmental sciences (Lins & Slack, 1999; Topaloğlu et al., 2012; Yue & and Pilon, 2004). Unlike parametric tests, the Mann-Kendall test does not require the data to be normally distributed, making it particularly useful for analyzing rainfall and discharge trends over time (Kendall, 1948; Mann, 1945).

The test calculates a rank-based statistic S by comparing all possible pairs in a time series:

$$S = \sum_{i=1}^{n-1} \sum_{j=i+1}^{n} sgn(x_j - x_i) \quad \text{Eq. (2)}$$

Where x_i and x_j are data points at time i and j, and the sign function is defined as:

$$sgn(x_j - x_i) = \begin{cases} +1, & if(x_j - x_i) > 0 \\ 0, & if(x_j - x_i) = 0 \\ -1, & if(x_j - x_i) < 0 \end{cases} \quad \text{Eq. (3)}$$

The standardized test statistic Z follows a normal distribution and is given by:

$$Z = \begin{cases} \frac{S-1}{\sigma_s}, & S > 0 \\ 0, & S = 0 \\ \frac{S-1}{\sigma_s}, & S < 0 \end{cases} \quad \text{Eq. (4)}$$

where σ_s is the variance of S. A positive Z value indicates an increasing trend, while a negative Z value suggests a decreasing trend. The trend is considered statistically significant if the p-value is below 0.05 (Kendall, 1948).

Sen's Slope Estimator

Sen's Slope Estimator is a non-parametric method widely used to determine the rate of change in a dataset while minimizing the influence of outliers and non-normal distributions (Sen, 1968). This method is particularly suitable for analyzing long-term trends in rainfall and river discharge data, as it is less sensitive to missing values and extreme fluctuations compared to traditional regression-based approaches (Hirsch et al., 1982). The Sen's Slope method calculates the median of all possible pairwise slopes between data points in a time series. Given a dataset of n observations (x_i, y_i) where y_i represents the observed values at time x_i, the slope Q for each pair of data points is computed as:

$$Q = \frac{y_j - y_i}{x_j - x_i}, for\ 1 \le i < j \le n \quad \text{Eq. (5)}$$

where Q represents the rate of change per unit time. The final Sen's Slope estimate is determined as the median of all computed Q values, ensuring that the estimator remains resistant to non-normality and heteroscedasticity in the data (Theil, 1992).

Results and discussions

The characteristics of discharge and rainfall features in the study area

This study examines the long-term rainfall and discharge characteristics of the Brahmaputra-Jamuna River system using historical monthly data from 1990 to 2023. The descriptive statistics of rainfall (mm) and discharge (m^3s^{-1}) provide insights into the hydrological dynamics of the region (**Table 1**). The mean annual rainfall is 213.89 mm, while the median rainfall is 121.90 mm, indicating a distribution skewed toward higher values. The coefficient of skewness is 0.83, confirming that the rainfall distribution is positively

skewed and not symmetrical. The longer right tail suggests that extreme rainfall events contribute significantly to the overall distribution. The highest annual mean rainfall was 272.97 mm in 1991, while the lowest annual mean rainfall was 153.36 mm in 2013.

Similarly, the mean annual discharge is 24,814.75 $m^3 s^{-1}$, while the median discharge is 16,485.62 m^3s^{-1}, also suggesting a positively skewed distribution with a skewness coefficient of 0.95. The standard deviation of 20,348.10 m^3s^{-1} indicates considerable variability in river discharge over time. The highest annual mean discharge was 34,633.85 m^3s^{-1} in 2004, while the lowest annual mean discharge was 14,958.74 m^3s^{-1} in 2011.

Table 1. Annual mean rainfall and Discharge Scenario

	Rain (mm)	Discharge (m^3s^{-1})
Mean	213.89	24814.75
Median	121.896	16485.62
Standard Deviation	223.89	20348.10
Skewness	0.83	0.95
Min	0.20	2036.82
Max	880.92	96105.52
Range	880.7	94068.7
Lowest Annual Mean	153.36 (2013)	14958.74 (2011)
Highest Annual Mean	272.97 (1991)	34633.85 (2004)
Lowest Monthly Peak	0.203 (January 2006)	2036.82 (March 2004)
Highest Monthly Peak	880.9 (July 2002)	96105.52 (July 2004)

Extreme monthly values show seasonal variation. The highest monthly peak rainfall was 880.9 mm in July 2002, and the highest monthly peak discharge was 96,105.52 m^3s^{-1} in July 2004, showing that extreme rainfall events contribute significantly to river flow. The lowest monthly peak rainfall was 0.203 mm in January 2006, and the lowest monthly discharge was 2,036.82 m^3s^{-1} in March 2004, highlighting the dry season's impact. The dataset confirms a strong seasonal influence on rainfall and discharge, with occasional extreme events affecting the hydrological balance.

Overall trend analysis

Mann-Kendall trend test and Sen's Slope estimator were performed for rainfall and discharge over the study period, conducted at a 95% significance level ($\alpha = 0.05$) (**Table 2**). The Mann-Kendall test is a non-parametric method for detecting monotonic trends in time-series data, while Sen's Slope estimator quantifies the magnitude of these trends. The test results indicate a statistically significant downward trend in both rainfall and discharge. The Mann-Kendall Z statistic for rainfall is -2.566, with a p-value of 0.01, confirming a significant decreasing trend. The corresponding Sen's Slope (-2.154) suggests that rainfall has been declining at an estimated rate of 2.154 mm per year. Similarly, the Mann-Kendall Z statistic for discharge is -3.008, with a p-value of 0.002, indicating a strong and statistically significant decreasing trend. The Sen's Slope (-274.47) suggests a substantial decline in discharge over time.

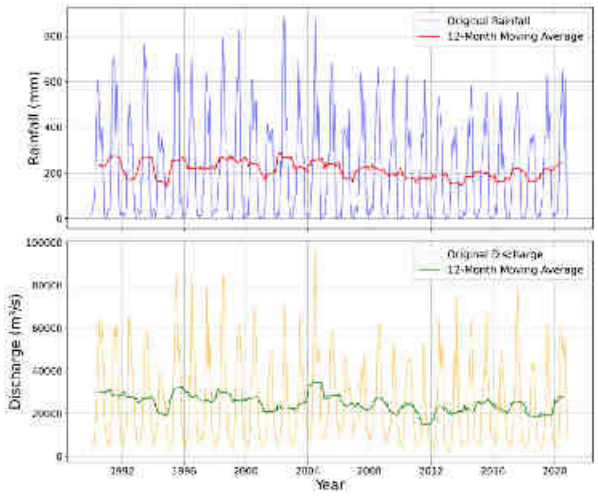

Fig. 2. Overall rainfall and discharge moving average trend

Fig. 2 shows the long-term trends in rainfall and discharge. The moving average trend for rainfall demonstrates a gradual decline, reflecting a consistent decrease in annual rainfall over the study period. While fluctuations are present, the overall trend suggests a progressive reduction in precipitation levels, aligning with the Mann-Kendall test results that indicate a significant downward trend. Similarly, the moving average trend for discharge exhibits a noticeable decreasing pattern, reinforcing the statistical findings of a significant downward trend. The decline in discharge is more pronounced than that of rainfall.

Trends in seasonal rainfall and discharge

The Seasonal Mann–Kendall test and Sen's slope analysis indicate that both rainfall and discharge exhibit a downward trend across all seasons (**Table 3**).

Table 2. Overall Mann–Kendall test and Sen's slope statistics of rainfall and discharge

Variable	Mann–Kendall test		Sen's slope	Significant	Trend
	Test statistics Z	P-value			
Rainfall	-2.566	0.01	-2.154	Yes	Downward
Discharge	-3.008	0.002	-274.47	Yes	Downward

Table 3. Seasonal Mann–Kendall test and Sen's slope statistics of rainfall and discharge

	Variable	P-value	Sen's slope	Significant	Trend
Dry Season	Rainfall	0.09	-0.23	No	Downward
	Discharge	0.23	-38.7	No	Downward
Pre-Monsoon	Rainfall	0.86	-0.25	No	Downward
	Discharge	0.22	-115.96	No	Downward
Monsoon	Rainfall	0.02	-4.8	Yes	Downward
	Discharge	0.01	-459.54	Yes	Downward
Post-Monsoon	Rainfall	0.04	-1.94	Yes	Downward
	Discharge	0.009	-245.77	Yes	Downward

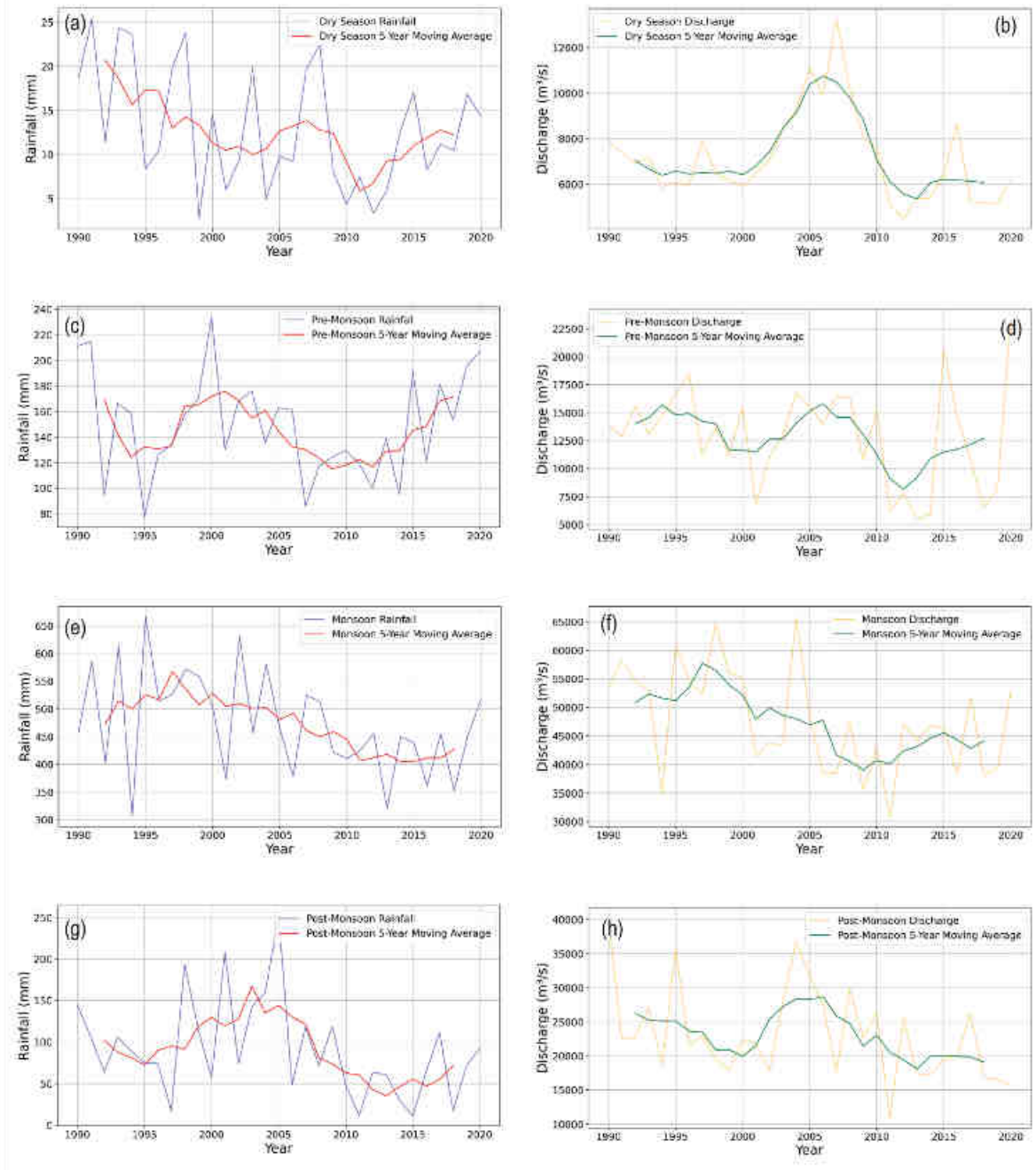

Fig. 3. Seasonal moving average trend (a) Dry season rainfall (b) Dry season discharge (c) Pre-monsoon season rainfall (d) Pre-monsoon season discharge (e) Monsoon season rainfall (f) Monsoon season discharge (g) Post-monsoon season rainfall and (h) Post-monsoon season discharge

However, statistical significance varies among them. Notably, neither the dry season nor the pre-monsoon period shows a significant trend in either rainfall or discharge, despite negative Sen's slope values in some cases. It's evident that while minor fluctuations exist, there is no strong evidence of a persistent decline in these seasons. In contrast, both monsoon and post-monsoon seasons show statistically significant downward trends in rainfall and discharge. Rainfall during the monsoon and post-monsoon periods decline significantly with 4.8 mm and 1.94 mm per year, while discharge experiences a sharp reduction with and estimated reduction of -459.54 mm per year in monsoon and -245.77 mm per year in post-monsoon, as seen by the Sen's Slopes estimates. The significant decline in monsoon discharge, which is the largest decrease among all seasons, suggests a critical reduction in peak river flow, potentially due to decreasing precipitation or upstream water withdrawal. Similarly, the post-monsoon decline in discharge indicates a lower base flow, which may lead to prolonged dry conditions and reduced water availability in the following months.

The moving average trends (dry, pre-monsoon, monsoon, post-monsoon) of rainfall and discharge, illustrated in

Fig. 3, reveal important insights into long-term hydrological variations. While fluctuations are seen across all seasons, a notable downward trend in discharge in recent years is observed, particularly in the monsoon and post-monsoon periods. In the dry season (**Fig. 3a** & **Fig. 3b**), both rainfall and discharge show fluctuations over the years, but discharge has taken a sharp decrease in recent years. This decline may be attributed to reduced groundwater contributions and lower residual flow from preceding seasons. The pre-monsoon season (**Fig. 3c** & **Fig. 3d**), on the other hand, maintains a relatively consistent trend for both rainfall and discharge, with no drastic changes over most of the period. A more pronounced downward trend is observed in the monsoon season (**Fig. 3e** & **Fig. 3f**), where both rainfall and discharge have declined in recent years despite lower fluctuations throughout the overall period. Since monsoon is the primary source of annual water availability, this decrease signals a potential weakening of seasonal peak flows. The declining monsoon rainfall suggests a shift in climate patterns.

To further examine this trend, a seasonal decomposition analysis of monsoon rainfall and discharge has been conducted, as illustrated in **Fig. 4a** & **Fig. 4b**. Seasonal decomposition separates time series data into its observed, trend, seasonal, and residual components, providing deeper insight into long-term patterns. This decomposition confirms that the weakening of monsoon flow is a sustained pattern rather than short-term variability. The post-monsoon season (**Fig. 3g** & **Fig. 3h**) shows a similar trend, with both rainfall and discharge exhibiting a significant decline in recent years. This period is crucial for sustaining river flow and groundwater recharge beyond the monsoon, and the decreasing trend suggests a progressive weakening of seasonal water storage.

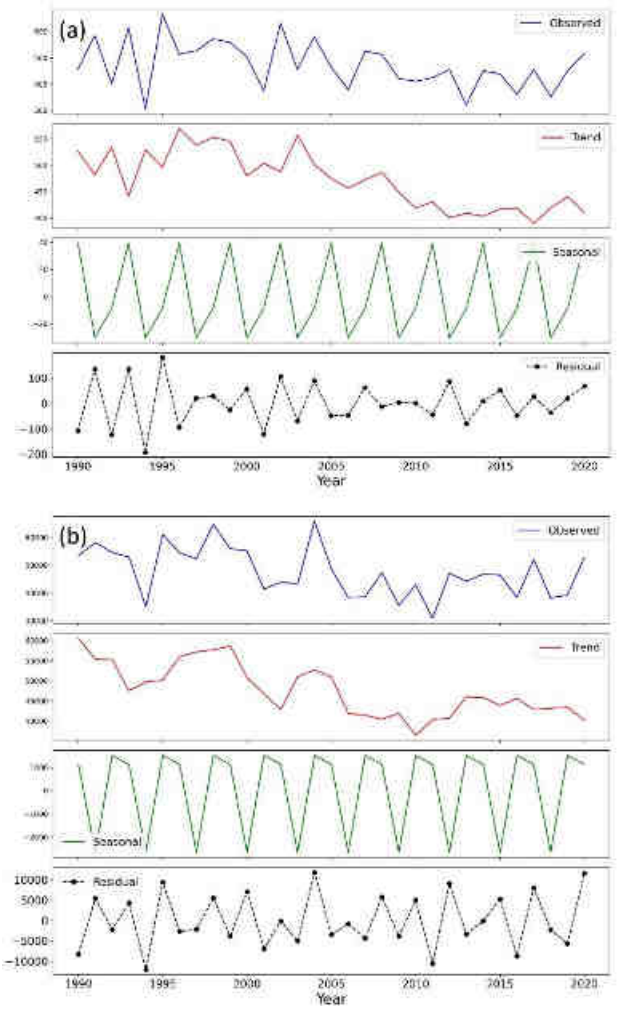

Fig. 4. Decomposition observed, trend, seasonal residual, (a) Monsoon season rainfall, (b) Monsoon season discharge

Effects of climate change on river discharge

The findings of this study strongly indicate that climate change is having a significant impact on the hydrological dynamics of the Brahmaputra-Jamuna River system. The correlation analysis between rainfall and river discharge reveals a strong positive relationship (0.828), suggesting that changes in rainfall directly influence discharge levels.

The Mann-Kendall trend test results provide further evidence of the effect of climate change. Both rainfall and discharge exhibit significant downward trends over the study period. The rainfall trend shows a significant decrease, with a Z-score of -2.566 and a p-value of 0.010. Similarly, the discharge trend also shows a significant decrease, with a Z-score of -3.008 and a p-

value of 0.002. These results suggest that the reduction in rainfall is closely tied to a decline in river discharge, which is likely exacerbated by climate change, particularly through changes in monsoon patterns and glacial melt in the Himalayas. The downward trend in river discharge, particularly during the Monsoon and Post-Monsoon seasons, is a cause for concern. These seasons typically experience peak river flows driven by the southwest monsoon rains, yet the decreasing rainfall has led to reduced discharge. This reduction could significantly impact water availability for key sectors such as agriculture, hydropower, and water supply. Furthermore, the decrease in discharge during the dry season is expected to worsen, putting more strain on water resources during periods of already low flow.

The Brahmaputra-Jamuna River system is highly vulnerable to climate variability, given its dependence on both monsoon precipitation and glacial melt. With rising global temperatures, glacial melt patterns are expected to shift, and monsoon precipitation may become increasingly erratic, further disrupting the seasonal discharge cycle. These changes pose a long-term threat to water security and regional sustainability.

Conclusion

This study investigated the long-term trends in rainfall and discharge in the Brahmaputra-Jamuna River system over the period 1990 to 2023. The analysis revealed statistically significant declining trends in both parameters, with the most notable reductions occurring during the monsoon and post-monsoon seasons. These periods are critical for regional water availability, agricultural productivity, and ecosystem stability. A strong positive correlation (0.83) between rainfall and discharge confirms that declining precipitation is a major contributor to reduced river flow, highlighting the sensitivity of the river system to climatic changes.

To capture seasonal variability, data were classified into four distinct hydrological seasons. Missing values were carefully handled using monthly mean imputation for rainfall and regression-based estimation for discharge, ensuring the accuracy of trend analysis. The Mann-Kendall test and Sen's Slope estimator confirmed consistent downward trends, with average annual rainfall and discharge recorded at 213.89 mm and 24,814.75 m^3s^{-1}, respectively. The monsoon season showed the steepest decline, indicating weakening peak flows, while post-monsoon trends revealed shrinking base flows. These patterns suggest increasing hydrological stress driven by altered monsoon dynamics, reduced glacial contribution, and rising temperatures, all of which are linked to climate change.

The observed trends pose serious challenges for water resource management, including risks to floodplain agriculture, groundwater recharge, and dry season water availability. The study underscores the need for adaptive, sustainable strategies such as integrated basin management, conservation, and transboundary cooperation. While data from a single upstream station were used, expanding future research to include multiple monitoring locations and additional hydrological and socio-economic parameters will offer a more comprehensive understanding of basin-wide dynamics.

The Brahmaputra-Jamuna River system is undergoing significant climate-induced hydrological changes. If current trends persist, water security, agricultural productivity, and ecological balance in the region will face increasing threats. This study offers a valuable foundation for advancing future research, policy interventions, and long-term planning to support the sustainability of this vital transboundary river system and the communities that depend on it.

Acknowledgement

The authors sincerely thank the organizations and researchers responsible for collecting and maintaining hydrological and meteorological datasets. Their efforts in ensuring data accuracy and accessibility are invaluable for advancing research on climate and water resources.

Conflicts of Interest

The authors declare no conflict of interest.

References

Akter, S., Howladar, M. F., Ahmed, Z., & Chowdhury, T. R. (2019). The rainfall and discharge trends of Surma River area in North-eastern part of Bangladesh: an approach for understanding the impacts of climatic change. *Environmental Systems Research*, *8*(1), 28. https:m/s/doi.org/10.1186/s40068-019-0156-y

Alam, J., Alam, R., Misbah, uddin, & Nahar, T. (2007). Study of morphological change of the Kushiyara and Monu rivers by remote sensing. *International Journal of Sediment Research*, *22*, 160–168.

Ashworth, P. J., Best, J. L., Roden, J. E., Bristow, C. S., & Klaassen, G. J. (2000). Morphological evolution and dynamics of a large, sand braid-bar, Jamuna River, Bangladesh. *Sedimentology*, *47*(3), 533–555. https://doi.org/10.1046/J.1365-3091.2000.00305

Bari, S. H., Rahman, M. T. U., Hoque, M. A., & Hussain, Md. M. (2016). Analysis of seasonal and annual rainfall trends in the northern region of Bangladesh. *Atmospheric Research*, *176–177*, 148–158. https://doi.org/10.1016/j.atmosres.2016.02.008

Basak, J. K., Titumir, R. A. M., & Dey, N. C. (2013). Climate change in Bangladesh: a historical analysis of

temperature and rainfall data. *Journal of Environment*, *2*(2), 41–46.

Billah, M., Rahman, M. M., Islam, A., Islam, G. M. T., Bala, S. K., Paul, S., & Hasan, M. A. (2015). Impact of climate change on river flows in the southwest region of Bangladesh. *5th International Conference on Water & Flood Management (ICWFM-2015)*, 581–590.

Döll, P., & Zhang, J. (2010). Impact of climate change on freshwater ecosystems: a global-scale analysis of ecologically relevant river flow alterations. *Hydrology and Earth System Sciences*, *14*(5), 783–799. https://doi.org/10.5194/hess-14-783-2010

Goswami, D. C. (1985). Brahmaputra River, Assam, India: Physiography, Basin Denudation, and Channel Aggradation. *Water Resources Research*, *21*(7), 959–978. https://doi.org/10.1029/WR021I007P00959

Hirsch, R. M., Slack, J. R., & Smith, R. A. (1982). Techniques of trend analysis for monthly water quality data. *Water Resources Research*, *18*(1), 107–121. https://doi.org/10.1029/WR018i001p00107

Hulme, M., Osborn, T. J., & Johns, T. C. (1998). Precipitation sensitivity to global warming: Comparison of observations with Had CM2 simulations. *Geophysical Research Letters*, *25*(17), 3379–3382. https://doi.org/10.1029/98GL02562

Islam, A. R. M. T., Karim, M. R., & Mondol, M. A. H. (2021). Appraising trends and forecasting of hydroclimatic variables in the north and northeast regions of Bangladesh. *Theoretical and Applied Climatology*, *143*(1–2), 33–50. https://doi.org/10.1007/S00704-020-03411-0/TABLES/6

Jain, S. K., & Kumar, V. (2012). Trend analysis of rainfall and temperature data for India. *CURRENT SCIENCE*, *102*(1).

Kahya, E., & Kalaycı, S. (2004). Trend Analysis of Streamflow in Turkey. *Journal of Hydrology*, *289*, 128–144. https://doi.org/10.1016/j.jhydrol.2003.11.006

Kendall, M. G. (1948). *Rank correlation methods.*

Khuri, A. I. (2013). Introduction to Linear Regression Analysis, Fifth Edition by Douglas C. Montgomery, Elizabeth A. Peck, G. Geoffrey Vining. *International Statistical Review*, *81*(2), 318–319. https://doi.org/10.1111/insr.12020_10

Kundzewicz, Z., Mata, L., Arnell, N., Doll, P., Jiménez, B., Miller, K., Oki, T., Şen, Z., & Shiklomanov, I. (2008). The Implications of Projected Climate Change for Freshwater Resources and Their Management. *Hydrological Sciences Journal/Journal Des Sciences Hydrologiques*, *53*. https://doi.org/10.1623/hysj.53.1.3

Lambert, F. H., Stott, P. A., Allen, M. R., Palmer, M. A., Lambert, F. H., Stott, P. A., Allen, M. R., & Palmer, M. A. (2004). Detection and attribution of changes in 20th century land precipitation. *GeoRL*, *31*(10), L10203. https://doi.org/10.1029/2004GL019545

Lins, H. F., & Slack, J. R. (1999). Streamflow trends in the United States. *Geophysical Research Letters*, *26*(2), 227–230. https://doi.org/10.1029/1998GL900291

Mann, H. B. (1945). Nonparametric Tests Against Trend. *Econometrica*, *13*(3), 245. https://doi.org/10.2307/1907187

Manton, M. J., Della-Marta, P. M., Haylock, M. R., Hennessy, K. J., Nicholls, N., Chambers, L. E., Collins, D. A., Daw, G., Finet, A., Gunawan, D., Inape, K., Isobe, H., Kestin, T. S., Lefale, P., Leyu, C. H., Lwin, T., Maitrepierre, L., Ouprasitwong, N., Page, C. M., … Yee, D. (2001). Trends in extreme daily rainfall and temperature in Southeast Asia and the South Pacific: 1961–1998. *International Journal of Climatology*, *21*(3), 269–284. https://doi.org/10.1002/joc.610

Manzoor, N., Hameed, S., Library, W. O., Sheikh, M. M., Manzoor, N., Ashraf, J., Adnan, M., Collins, D., Hameed, S., Manton, M. J., Ahmed, A. U., Baidya, S. K., Borgaonkar, H. P., Islam, N., Jayasinghearachchi, D., Kothawale, D. R., Premalal, K. H. M. S., Revadekar, J. V, & Shrestha, M. L. (2014). Trends in extreme daily rainfall and temperature indices over South Asia. *INTERNATIONAL JOURNAL OF CLIMATOLOGY Int. J. Climatol*, *35*, 1625–1637. https://doi.org/10.1002/joc.4081

Mirza, M. Q. (2002). Global warming and changes in the probability of occurrence of floods in Bangladesh and implications. *Global Environmental Change*, *12*(2), 127–138. https://doi.org/https://doi.org/10.1016/S0959-3780(02)00002-X

Rahman, M. A., & Begum, M. (2013). Application of non parametric test for trend detection of rainfall in the largest Island of Bangladesh. *ARPN Journal of Earth Sciences*, *2*(2). www.arpnjournals.com

Rahman, M. A., Alam, M. S., Sultana, R., & Sultana, R. (2025). Assessing the interrelationship between monsoon flood disasters and major crop production in Bangladesh. *International Journal of Disaster Risk Reduction*, *121*, 105401. https://doi.org/10.1016/j.ijdrr.2025.105401

Sarker, M. H., Thorne, C. R., Aktar, M. N., & Ferdous, Md. R. (2014). Morpho-dynamics of the Brahmaputra–

Jamuna River, Bangladesh. *Geomorphology*, *215*, 45–59. https://doi.org/10.1016/j.geomorph.2013.07.025

Sen, P. K. (1968). Estimates of the Regression Coefficient Based on Kendall's Tau. *Journal of the American Statistical Association*, *63*(324), 1379–1389. https://doi.org/10.1080/01621459.1968.10480934

Shahid, S. (2010). Rainfall variability and the trends of wet and dry periods in Bangladesh. *International Journal of Climatology*, *30*(15), 2299–2313. https://doi.org/10.1002/joc.2053

Theil, H. (1992). A Rank-Invariant Method of Linear and Polynomial Regression Analysis. In B. Raj & J. Koerts (Eds.), *Henri Theil's Contributions to Economics and Econometrics: Econometric Theory and Methodology* (pp. 345–381). Springer Netherlands. https://doi.org/10.1007/978-94-011-2546-8_20

Topaloğlu, F., Irvem, A., & Özfidaner, M. (2012). Re-evaluation of trends in annual streamflows of Turkish rivers for the period 1968-2007. *Fresenius Environmental Bulletin*, *21*(8), 2043–2050.

Yue, S., & and Pilon, P. (2004). A comparison of the power of the t test, Mann-Kendall and bootstrap tests for trend detection. *Hydrological Sciences Journal*, *49*(1), 21–37. https://doi.org/10.1623/hysj.49.1.21.53996

Zhang, X., Harvey, K. D., Hogg, W. D., & Yuzyk, T. R. (2000). Trends in Canadian streamflow. *15th Conf. on Hydrology*, 279–281.

Technical Journal
River Research Institute ISSN: 1606-9277

Dynamic Shifting and Future Offtake Formation of the Old Brahmaputra River: A GIS and Remote Sensing Approach

M. E. A. Mondal[1]*, M. A. H. Podder[2], S. Afrin[1], A. A. Imran[2]

Abstract

The Bengal Basin is a dynamic and continually evolving depositional environment, characterized by unconsolidated muds and sands transported and deposited predominantly through fluvial processes originating from the Ganges and Brahmaputra rivers. Four major distributaries are associated with the principal river system in Bangladesh: the Old Brahmaputra, Dhaleswari, Gorai, and Dubaldia/Arial Khan rivers. During the flood season, these distributaries convey a portion of the river flow. As they branch from the main channels, their discharge and sediment supply depend largely on these primary rivers. The Old Brahmaputra River is one of the most prominent rivers within the Bengal Basin. As a left-bank distributary of the Jamuna River, it diverges at Kholabarichar, approximately 10 km upstream of Bahadurabad, and flows south-east through the towns of Jamalpur, Mymensingh, and Kishoreganj, before joining the Meghna River at Bhairab Bazar. Currently, the Old Brahmaputra is attempting to establish a new offtake from the Jamuna River, approximately 7.8 km downstream of the existing offtake. In 2001, the distance between the Jamuna and Old Brahmaputra rivers at this point was 3,340 meters; this has now reduced to just 615 meters. Ongoing bank erosion along both rivers is leading to gradual convergence, suggesting a strong likelihood of eventual confluence. The probable merging of the Jamuna and Old Brahmaputra rivers would result in the formation of a new offtake, carrying significant implications for the river system and the livelihoods of surrounding communities. Landsat satellite images from 1995, 2000, 2005, 2010, 2015, 2020, and 2025 were obtained from the USGS Earth Explorer. ERDAS IMAGINE 2014 and ArcGIS 10.3.1 software were used to analyze these images to assess morphological and planform changes at the anticipated offtake location. This study estimates the timeframe for potential offtake development, evaluates likely hydro-morphological changes, assesses anticipated community impacts, and recommends appropriate mitigation measures.

Keywords: *Jamuna-Old Brahmaputra River, Bank erosion, Dynamic shifting, offtake development, ArcGIS, satellite images, Remedial measures.*

Introduction

Bangladesh, mainly formed by alluvial deposits, faces riverbank erosion often due to the regular shifting of river channels. Riverbank erosion and shifting are standard geomorphological processes of alluvial floodplain rivers. The fluvial deposits are amongst the most varied of all the major sediment groups and mostly develop due to the meandering and migration of river channels across flood plains, eroding the banks of the terraces in a natural process (Thorne, 2002). Erosion is usually focused at the outside of meander bends, which gradually eat into the floodplain as the channel migrates laterally (Charlton, 2007). The Ganges–Brahmaputra–Meghna (GBM) river system is the largest delta of the world, where the Brahmaputra is known as Jamuna River, and the confluence of Ganges and Jamuna River is known as Padma River (Sarker et al., 2014). The course of the Brahmaputra River between the off-take of the Old Brahmaputra and the confluence with the Ganges at Aricha is referred in Bangladesh as the Jamuna River. The Brahmaputra–Jamuna river is one of the largest braided river systems in the world (Islam et al., 2017). Every year it erodes a thousand hectares of the floodplain (Sarker et al., 2014). The Jamuna River is known for its dynamicity which causes severe riverbank erosion, putting the lives of the people around the river at greater risk (Baki & Gan, 2012). Jamuna is categorized as a highly braided river as the rate of sediment deposition in the river often exceeds the carrying capacity of the flow (Baki & Gan, 2012). The old course of Brahmaputra River is called Old Brahmaputra. The Old Brahmaputra, a left bank distributary of the Jamuna river takes off at Kholabarichar, approximately 10 km upstream from Bahadurabad and follows a south easterly course via Jamalpur, Mymensingh and Kishoreganj towns and joins the Meghna at Bhairab Bazar. The river length between the off take and outfall is approximately 225 km (Flood Action Project 24, 1999). The plan form of the major rivers in Jamalpur district show in **Fig. 1**. Earlier, the main flow of the Brahmaputra river followed the path of the Old Brahmaputra river in Bangladesh (Rashid et al., 2023). The river changed its main flow and connected with the present Jamuna River between 1783 (Rennell's survey) and 1830 (Wilcox's survey) (Wilcox, 1830). Before movement/route change, the Old Brahmaputra River was very great, and the average width of the river was about 8.5 km (Rashid et al., 2023). However, after the diversion and main flow connected with the Jamuna River, the Old Brahmaputra River lost its dynamism and gradually reached the present situation. Presently, the average width of the river is only 0.45km (Rashid et al., 2023). Over the years, this river channel has been shifted many times, and this shifting process has displaced many settlements and eroded agricultural land. Though the river is embraced its width and currently it is similar to other small rivers in the area,

[1]Administration and Finance Directorate, River Research Institute, Faridpur-7800, Bangladesh.
*Corresponding Author: (E-mail: emranhossainduet@gmail.com)
[2]Hydraulic Research Directorate, River Research Institute, Faridpur-7800, Bangladesh.

both banks of the river now face erosion. Therefore, the river channel migrates its position continuously by erosion (Rakib et al., 2024). Within the reach Old Brahmaputra River consists of several adjacent bends, among which near Mondoal Bazar at Dewanganj upazila in Jamalpur district bend is a U-shaped meander with a sinuosity of 1.5 and about 1.5 km strong sand bar **Fig. 2**. Day by day this bend is approaching to Jamuna river owing to progressive bank erosion. If the bend migration of the Old Brahmaputra River bank and the left bank erosion of Jamuna river may continue within a few years, there is a strong probability of mergeing of two rivers and may develop a new offtake of Old Brahmaputra River. The offtakes are important links between the main rivers and the distributaries. This research fills the gap of the existing literature in about new off take Old Brahmaputra river. Several studies were conducted on Old Brahmaputra such as the Confliction of Old Brahmaputra and Dasani rivers (Rokonuzzaman & Hossain, 2024), temporal variation characteristics of flow and water level in the Old Brahmaputra River (Rubayet Mortuza et al., 2011), restoration model to control riverbank erosion in the Old Brahmaputra (Rakib et al., 2024) etc. In their study, they did not consider the formation of a probable new off take of Old Brahmaputra River. A new off take may increase the flow and sediment of Old Brahmaputra River. Which may have caused a vast hydro morphological change of along the whole river length of the Old Brahmaputra. In the current study the prime aim is to predict the hydro morphological change of Old Brahmaputra River due to the formation of another new offtake. The dynamic characteristics of 25km river of Old Brahmaputra, form existing offtake will be quantified. It is also very important to see impact on the social life on the river side peoples by the new offtake of Old Brahmaputra. This study is very essential for the river system of Old Brahmaputra river and the people live beside the river. Study results may also assist in the authority of water resource management of Bangladesh.

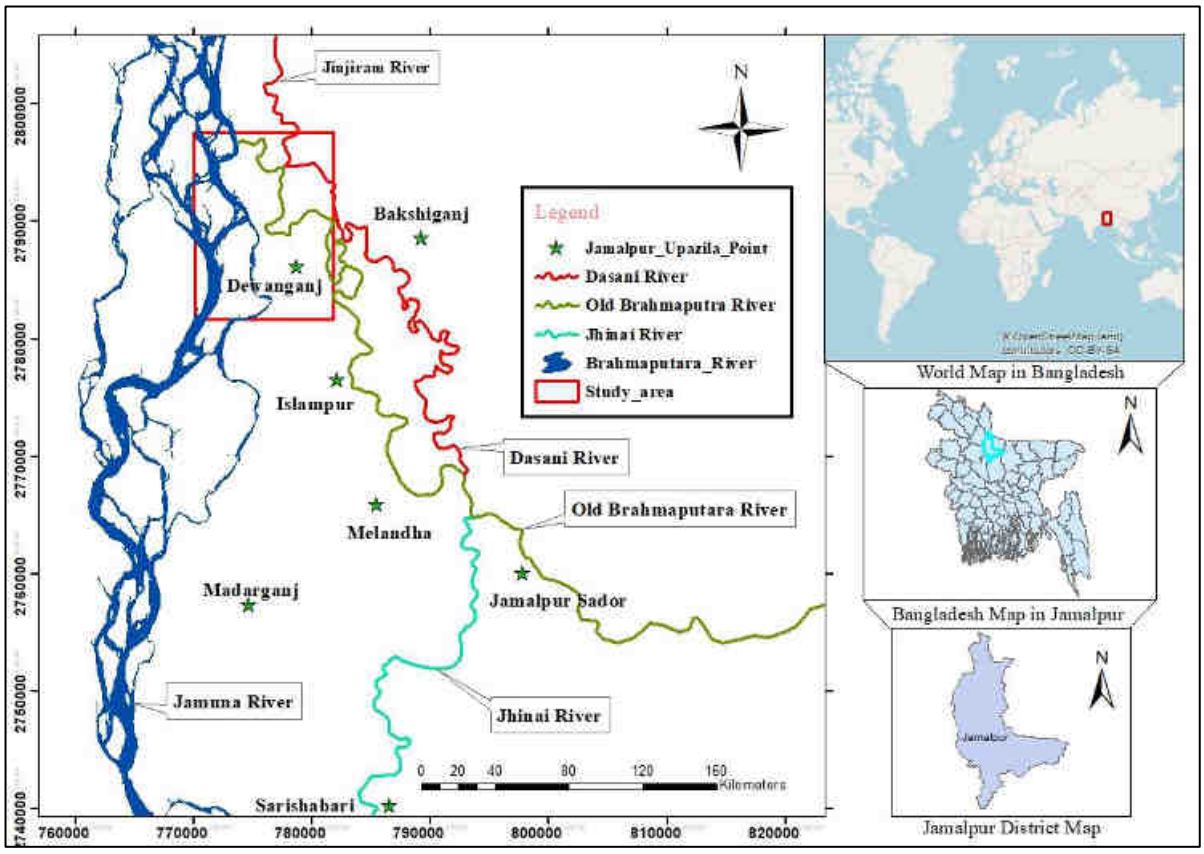

Fig. 1. Plan form of the major rivers in Jamalpur district.

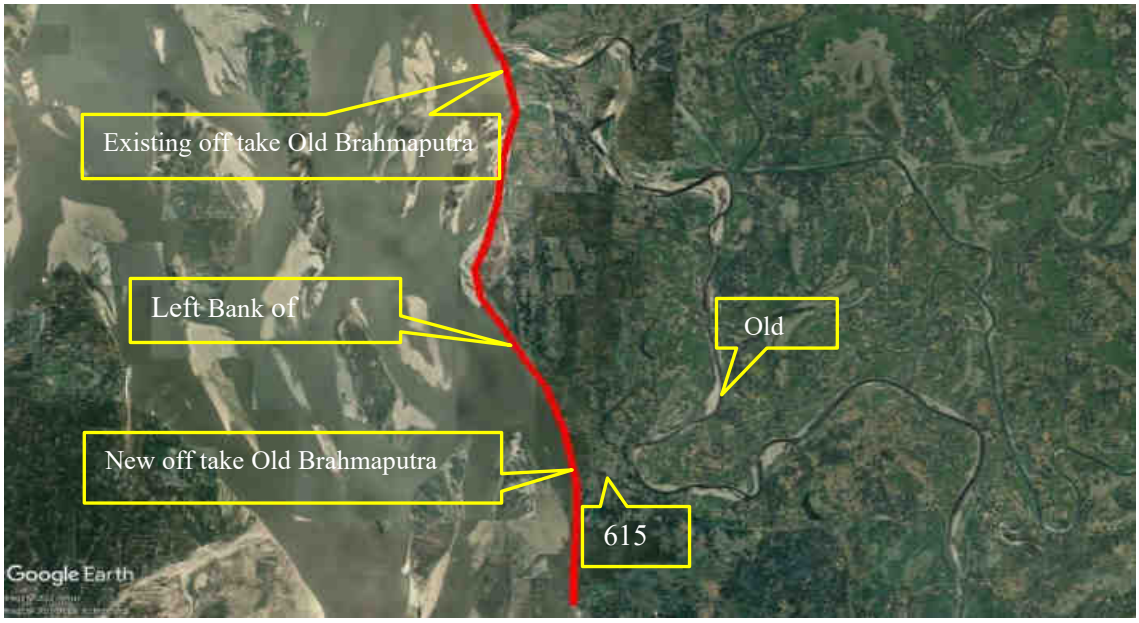

Fig. 2. Plan form of existing and probable new off take Old Brahmaputra River.

Methodology

Study area

The study was considered a limited course for both Jamuna River and also Old Brahmaputra River for analyzing the probable new off take of Old Brahmaputra River from Jamuna River and rivers dynamic nature. The Brahmaputra River, originating from the southern part glacier of the Himalayas, travels about 2850 km in length before entering Bangladesh(Hassan et al., 1999).The course length of the Jamuna River, the name of the lower reach of the Brahmaputra river that falls within Bangladesh, is about 251 km. The Jamuna River is known for its dynamicity which causes severe river bank erosion, putting the lives of the people around the river at greater risk (Baki and Gan, 2012). Considering 14 km left bank of Jamuna River from the offtake of Old Brahmaputra River to Bahadurabad railway ferry ghat at Jamalpur district in Bangladesh. The Old Brahmaputra is one of the main distributaries of the Jamuna (Brahmaputra) that distributes part of Jamuna discharge over a large area of North Central region of Bangladesh. The old course of the Brahmaputra River, presently named as the Old Brahmaputra, takes off at Kholabarichar, approximately 10km upstream from Bahadurabad. About 25 km length of Old Brahmaputra River form its off take to Durgapur Jamalpur district in Bangladesh is considered for this study. The district of Jamalpur, located at the north center zone of Bangladesh and on the left bank of Jamuna River. According to the local government Jamalpur district is located between 24°34' and 25°26' north latitudes and 89°40' and 90°12' east longitudes (https://lged.jamalpur.gov.bd). It is bounded by Kurigram, Sherpur district of Bangladesh and Meghalaya states of India in the north, Tangail district in the south, Mymansing and Sherpur district in the east, and Bogra, Sirajgong. Gaibandha and Jamuna river in the west. **Fig. 3** shows the map of the study area.

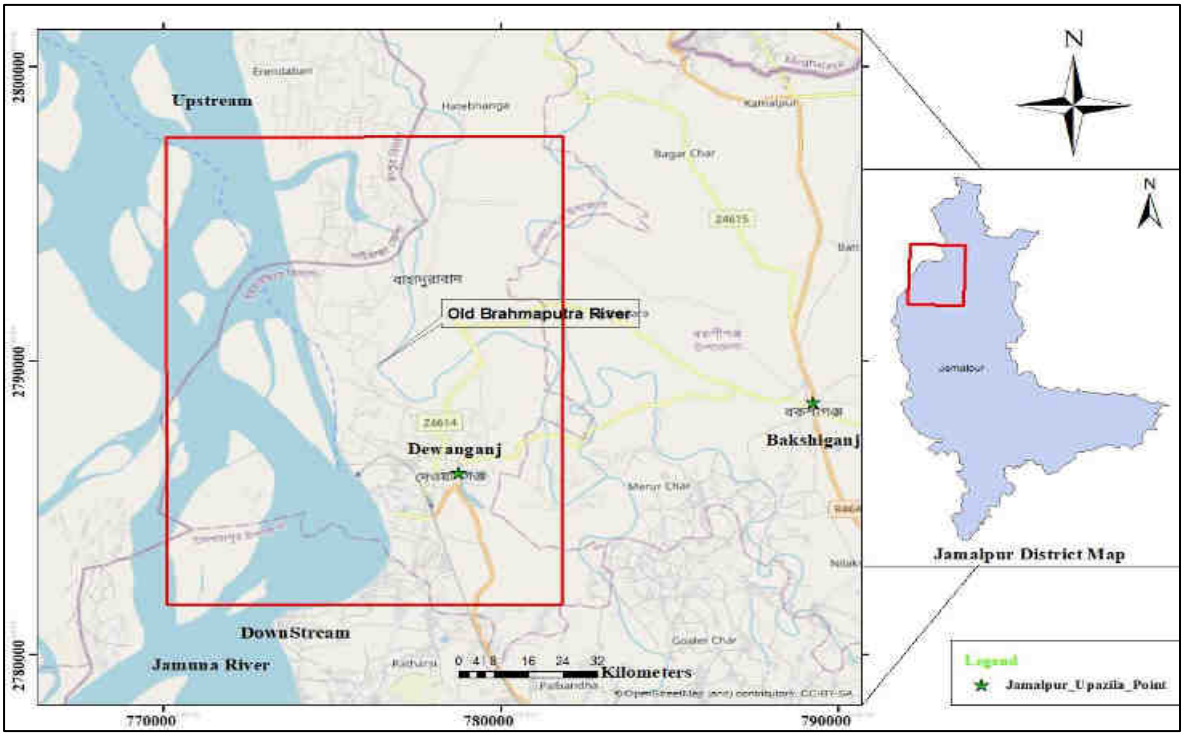

Fig. 3. Show Jamuna River and Old Brahmaputra River within study area.

Collection of Satellite images

In the present research, Landsat imageries were used to identify the banklines of river. The Landsat imageries, freely accessible on the USGS website, provided critical data for identifying and monitoring natural and anthropogenic environments. Only the post-monsoon season datasets were collected to have less cloud cover and to identify the exact channel and area under the sand bars. Landsat imageries of 30m resolution were collected from USGS Earth (*EarthExplorer*, n.d.) to proceed with the study. Path and Row were assigned for our study area, and cloud cover was less than 10% kept minimum. ArcGIS version 10.4 was utilized in this study to analyze remote sensing imagery data. Landsat satellite image data, comprising various band combinations, were employed to delineate river masks, planform, and centerline coordinates (latitude and longitude). The GIS data are regularly used to form an ancient thalweg line shifting map of the river (Falkowski et al., 2018). Several studies have been done to examine the bank erosion, bank shifting and deposit of the river by using GIS (Bhakal et al., 2005; Billah, 2018; Uddin et al., 2022). The properties of the collected images are given in **Table 1**.

Table 1. Description of Landsat imageries

Satellite	Satellite Sensor	Spectral Bands	Scale/resolution (m)	Acquisition date	Path/Row	Source
Landsat	Landsat 7	ETM+	30m	28/01/1995 26/01/2000 07/01/2005 29/01/2010 04/02/2015 17/01/2020 14/01/2025	138/43	USGS Earth

Setting reference line

The downloaded satellite images from USGS Earth (earthexplorer.usgs.gov) were smuggled in ArcGIS. After that 5-reference line A, B, C, D and E were drawn across over the river in such a way which divides its on five sections and another reference line 1-1 was drawn over intersecting the reference line A, B, C, D, E. The setting of reference lines with coordinate were considered with respect to significantly detected critical point by using priority ranking tools for better meditation of the river **Table 2** and also for ease of investigation.

The position of new off take of Old Brahmaputra River from Jamuna is carried over reference line C. Then the geo-spatial environment tools (visualizing platform of the spatial data through GIS and Remote Sensing) were used to appreciate the change of the river shifting performance easily. So, the historical bank shifting map was formed for Old Brahmaputra River and Jamuna. Bar diagram is used to better visualize the shifting behavior of the river throughout the years.

Table 2. Setting of reference lines

Reference Lines	Left bank side Position (x, y)	Right bank side Position(x,y)
A	778534.57, 2796377.73	767686.31, 2791429.07
B	779639.16, 2791920.03	767418.08, 2791911.87
C	779829.66, 2791564.43	767718.97, 2784589.34
D	781696.57, 2791196.12	769415.87, 2781292.372
E	782834.10, 2786358.34	768188.20, 2786372.382

Result and Discussions

River Shifting Analysis for Study Area

Measurement of Bank line shifting has been displayed on **Fig. 4**, **Table 3** and **Table 4** Intersecting point between the reference line 1-1 and A, B, C, D, E has been taken for shifting calculation. Bank line movement towards the intersecting point is considered as Jamuna Left bank and Old Brahmaputar Right bank.

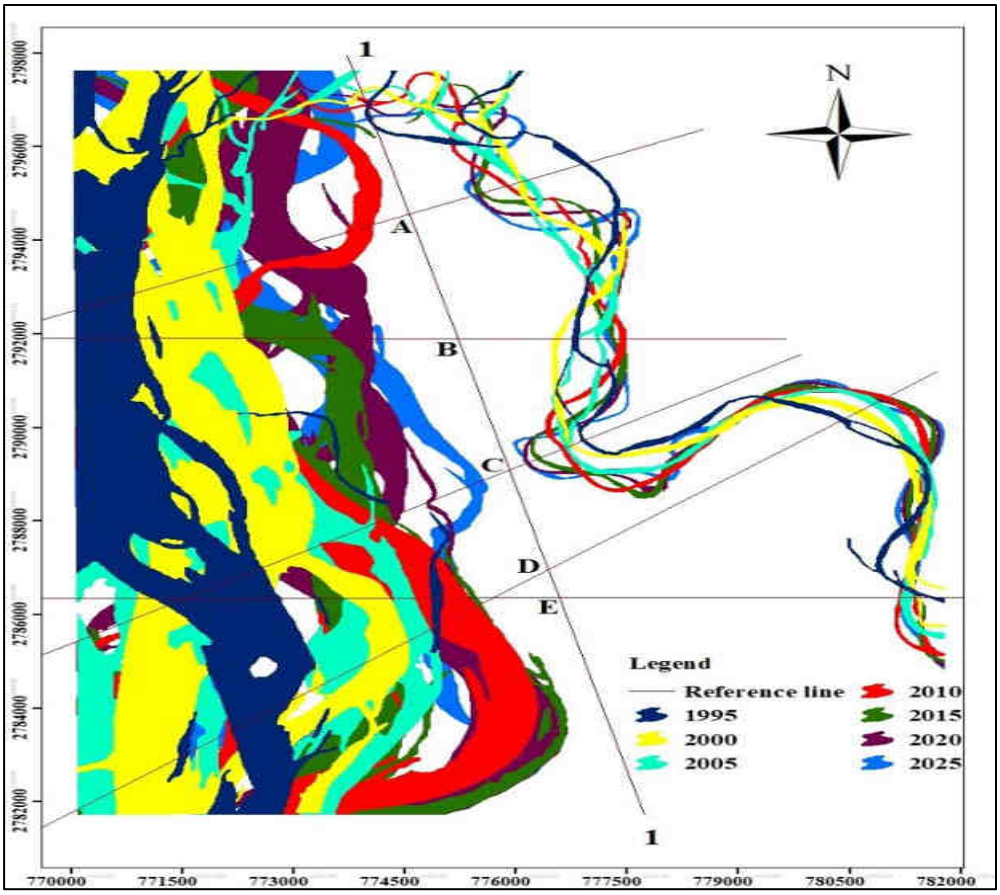

Fig. 4. Bank line shifting plot for the year 1995, 2000, 2005, 2010, 2015, 2020 and 2025.

Table 3. Right Bank line shifting against reference 1-1 lines for Old Brahmaputra River

Right Bank line shifting (m) alone the reference lines					
Years	A	B	C	D	E
1995	2525	2523	1138	5578	4868
2000	1595	1286	951	5309	4804
2005	1634	1559	863	5593	4600
2010	1395	2156	792	5813	4554
2015	1004	2053	393	5764	4751
2020	971	2033	245	5772	4662
2025	891	1961	222	5614	4621

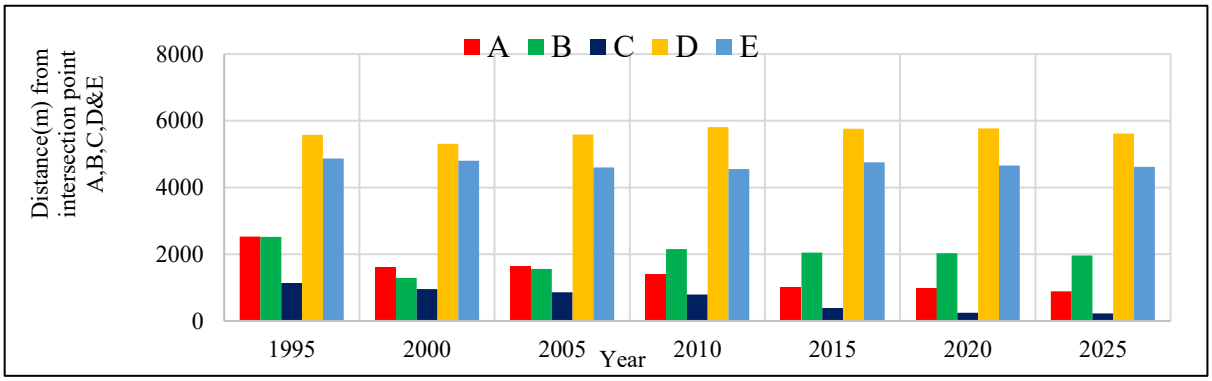

Fig. 5. Bar diagrams for the Right line shifting Old Brahmaputra River of against years for different reference lines A, B, C, D & E.

A bar diagram is shown at the **Fig 5** and **Table 3,** the location of reference line C the Old Brahmaputra River shifted 916 m towards Jamuna river continuously during the last 30 years.

Table 4. Left Bank line shifting against reference 1-1 lines for Jamuna River

Left Bank line shifting (m) alone the reference lines					
Years	A	B	C	D	E
1995	4068	4466	3913	4393	3731
2000	2731	2851	3195	2385	2263
2005	2568	2918	2306	2000	1924
2010	509	3172	2000	1214	1178
2015	2930	1616	1834	1111	1058
2020	1444	1115	1136	1372	1259
2025	2413	1242	385	1491	1331

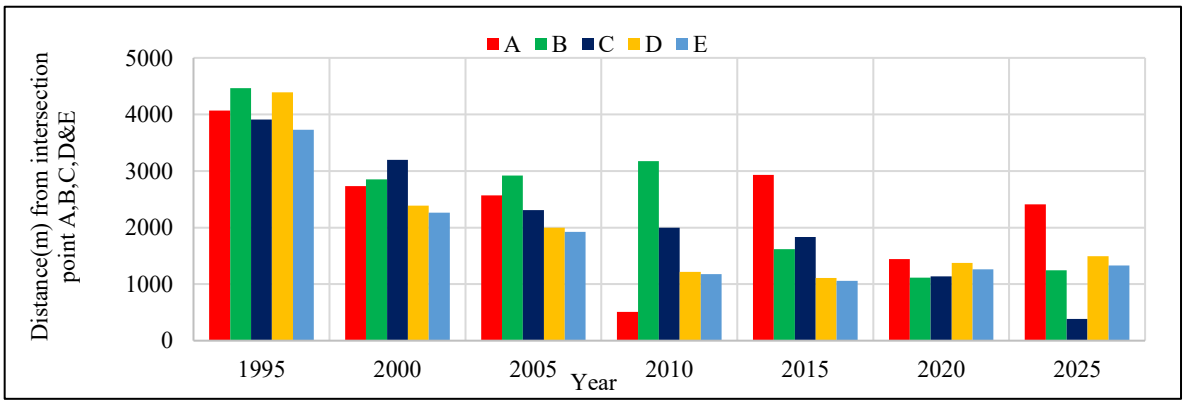

Fig. 6. Bar diagrams of left Bank line shifting Jamuna River against years for different reference lines A, B, C, D & E.

The probable new offtake location is carried through the reference line C. The Bar diagram shows **Fig. 6** and **Table 4** the location of reference line C, the left Bank line Jamuna River shifted 3528m towards Old Brahmaputra River continuously during the last 30 years.

Table 5. Distance between the left Bank Jamuna river and right bank Old Brahmaputra river.

	Distance between (m) alone the reference lines				
Years	A	B	C	D	E
1995	6664	5871	5095	9425	8646
2000	4370	4199	4165	7726	7058
2005	4245	4560	3179	7610	6524
2010	1965	5400	2788	7027	5727
2015	3979	3692	2255	6898	5821
2020	2448	3154	1400	7678	5936
2025	3364	3220	615	7110	5925

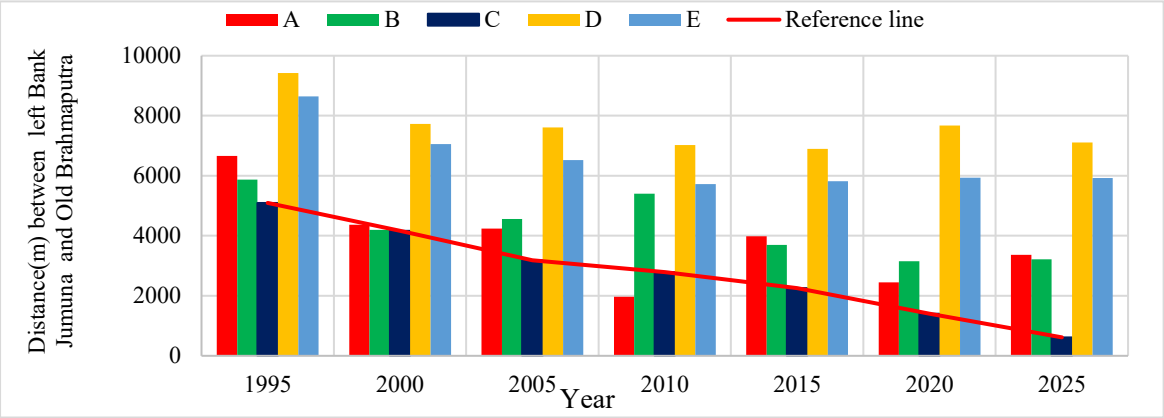

Fig.7. Bar diagram for the gap between left bank Jamuna and right bank Old Brahmaputra against years for different reference line A, B, C, D & E

In 1995 the nearest gap between for left bank Jamuna River and right bank Old Brahmaputra River at the location of reference line C was 5095m. But in 2025 the distance become only 625m show the **fig.7**, **fig.8** and **Table 5**.

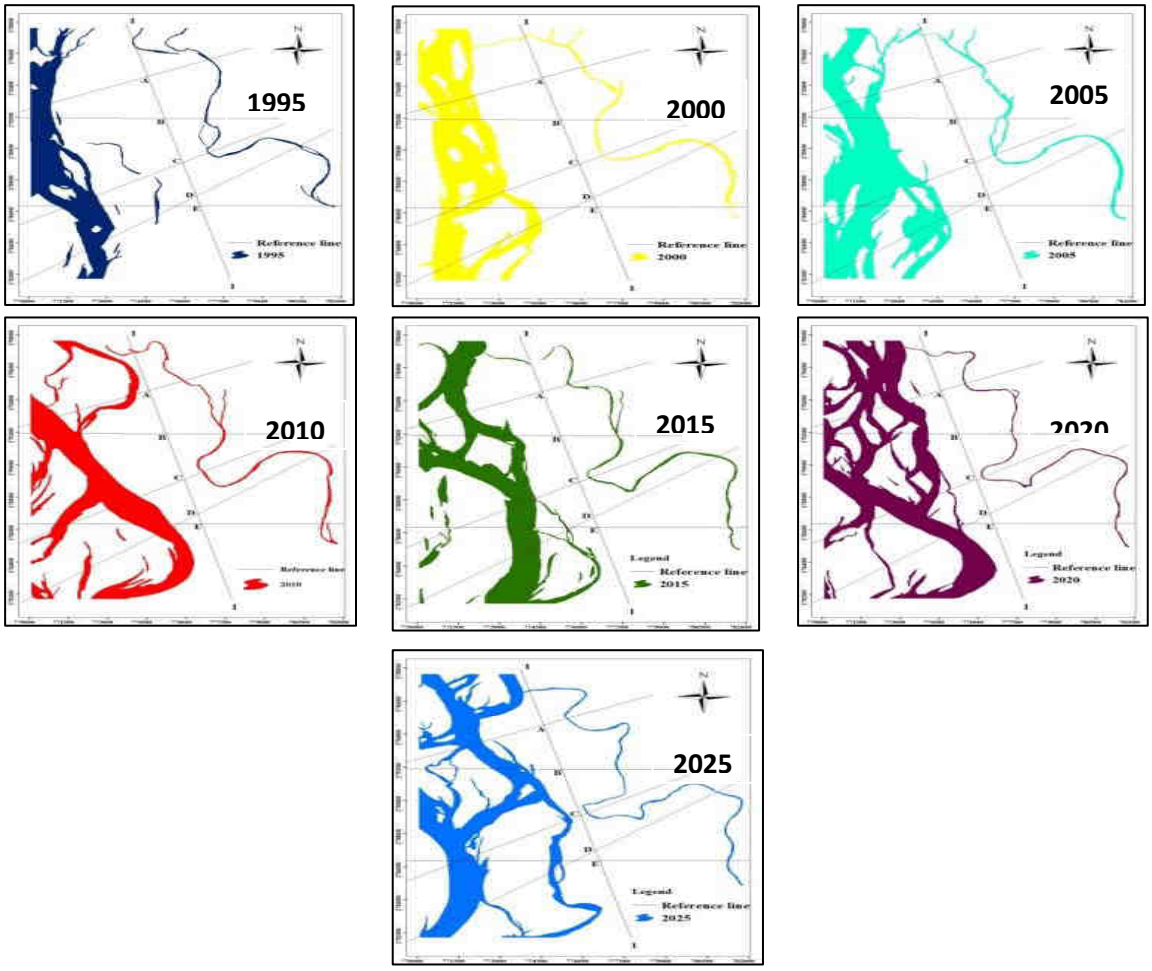

Fig. 8. Change of Plan form of left bank Jamuna River and Old Brahmaputra River for the years 1995 to 2025.

It can therefore be concluded that the bank lines of the Old Brahmaputra have undergone significant changes over the corresponding years. These shifts observed in this investigation indicate that the Old Brahmaputra is highly dynamic. Similarly, the left bank of the Jamuna River has also experienced considerable changes over the past 30 years. The left bank of the Jamuna is unstable and prone to erosion. The dynamic nature of the Old Brahmaputra and the erodible character of the Jamuna's left bank serve as strong indicators for the potential development of a new offtake.

Reasons for River Shifting and Bank Erosion

After analyzing the images in GIS, we observed that the average lateral shifting of the Old Brahmaputra River is 22.39 meters per year. The study reach of the Old Brahmaputra River exhibits a curvilinear bend along its course. The mechanism and process of bank erosion are complex and are influenced by multiple factors, including in-channel water level, groundwater flow, riparian vegetation, and the properties of the bank soil (Hasan et al., 2024). All alluvial rivers tend to develop meanders, which are characterized by scouring on the concave side and deposition on the convex side as the flow navigates the bends. Once a bend is formed, the flow tends to increase the curvature (Garg, 1991). This mechanism is largely responsible for the development of pronounced bends and associated bank erosion along the Old Brahmaputra River from 1995 to 2025. Water level fluctuations also contribute significantly to bank erosion. During rising water levels, it is well established that the strength of the bank soil decreases rapidly with increasing water content. At the same time, permeability becomes very low ($<1\times10^{-6}$ cms^{-1}), which increases the weight of the soil and leads to mass failure of the bank. During the drawdown phase at the end of the flood season, the groundwater level in the bank falls more slowly than the surface water level due to the low permeability of the bank materials. This discrepancy causes an imbalance in hydraulic pressure between the riverbank and the surface water, reducing the confining pressure on the slope and resulting in sudden mass failure of the bank (Hossain, 2011). The measured upstream water level in the study area during the period from May 2024 to December 2024 ranged from 12.80 mPWD to 19.10 mPWD. The average measured d_{50} value of the soil in the study area is 0.19 mm, comprising 76% fine sand, 15% silt, and 9% other materials. According to FAP

24, the d_{50} value of sediments in the Old Brahmaputra River varies from 0.18 mm to 0.08 mm (Flood Action Project 24, 1999). For comparison, the mean d_{50} value of the Jamuna River at Bahadurabad is 0.20 mm (Flood Action Project 24, 1999). The friction angles of river sands generally fall within a narrow range of 36° to 40° for grain sizes above approximately 0.2 mm, regardless of the dry density level (Prakash et al., 2023). The outer bank slope in the study area varies between 70° and 90°. Centrifugal force at bends, water level fluctuations, and poor bank material properties are the primary factors responsible for the dynamic morphological characteristics of both the Old Brahmaputra and Jamuna Rivers.

Time Prediction of probable new offtake

The average annual lateral shifting of the Jamuna River and the Old Brahmaputra River is approximately 91.13 meters and 22.39 meters, respectively. The current distance between the left bank of the Jamuna River and the Old Brahmaputra River, along reference line C, is 615 meters. Based on the average rates of lateral migration for both rivers, it is estimated that a confluence or merging of the two rivers could occur within the next 5 to 6 years. A graph plotting the lateral shifting of both rivers against time, with respect to reference line C, has been prepared. From the logarithmic graph (**Fig. 9**), there appears to be a high probability of a collision between the concave (right) bank of the Old Brahmaputra River and the left bank of the Jamuna River by the year 2030, at which point the gap between them is expected to reduce to zero.

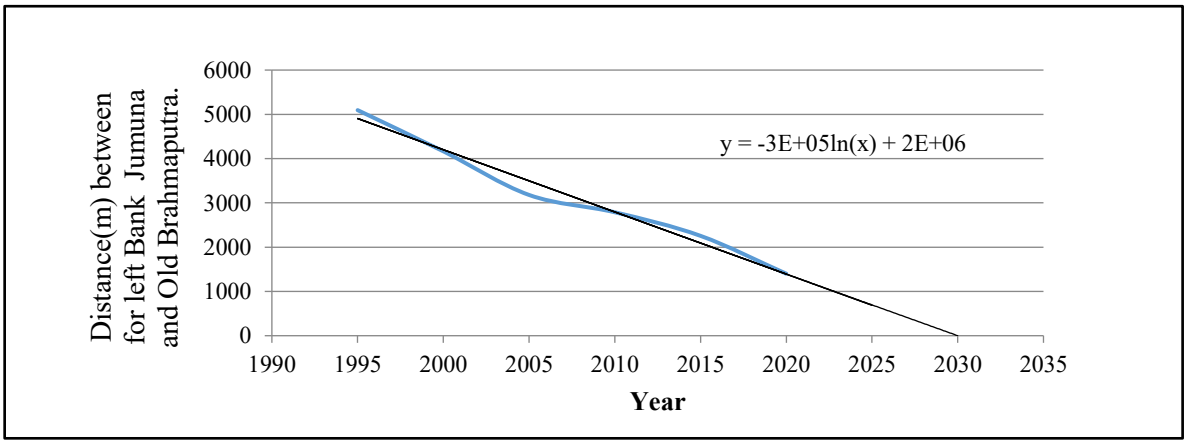

Fig. 9. Plotting a graph nearest distance between for left bank Jamuna and right bank Old Brahmaputra for reference line C.

Probable Scenery after new off take

By 2030, the left bank of the Jamuna River may merge with the right bank of the Old Brahmaputra River at the location of reference line C. Following the confluence of the two rivers, a new offtake is expected to form. Since the discharge and water level of the Jamuna River are higher than those of the Old Brahmaputra, the new offtake will increase the flow into the Old Brahmaputra River. Consequently, the Old Brahmaputra will receive water from both the existing and the newly developed offtakes. The discharge of uniform flow in an open channel is given by (K.G. Ranga Raju, Flow Through Open Channels):

$Q = VA$

$V = (1/n) \times S^{1/2} \times R^{2/3}$

Where:

V = Velocity (ms^{-1})

n = Manning's coefficient ($sm^{-1/3}$)

S = Water surface slope

R = Hydraulic radius (m) = A/P

A = Cross-sectional area of the channel (m^2)

P = Wetted perimeter (m)

River geometry—such as width, depth, and cross-section—is directly related to discharge (B.L. Rhoads, 2020, University of Illinois, River Dynamics: Geomorphology to Support Management). As the discharge of the Old Brahmaputra River increases due to the influx of water from the probable new offtake, its river geometry will change accordingly to convey the excess water. As a result, the downstream reaches of the Old Brahmaputra River will experience increased erosion, sediment deposition, and lateral shifting. The river will become highly dynamic in both hydrological and morphological terms. This will pose significant erosion risks to communities residing along the banks of the Old Brahmaputra River.

Conclusion

This study investigates the fluvial dynamics of the Old Brahmaputra River and the potential development of a new channel, utilizing Landsat imagery (1995, 2000, 2005, 2010, 2015, 2020, and 2025) in conjunction with ArcGIS software. Analysis of satellite data spanning

the past 30 years reveals that the average annual bankline migration is approximately 22 meters for the Old Brahmaputra River and 92 meters for the Jamuna River. The principal factors driving accelerated lateral migration are centrifugal forces linked to meander curvature, fluctuations in water levels, and weak bank materials. The continued migration of elongated meanders indicates a strong likelihood of a new channel forming by around 2030. Communities residing near the potential new channel area have expressed increasing concern, as both rivers are responsible for the annual erosion of new areas, leading to the displacement of households and the loss of homesteads to riverbank collapse. Despite their apprehension, these communities possess limited knowledge about the possible consequences of the formation of a new channel on their livelihoods. A better understanding of these prospective impacts is essential for planning adaptive strategies and sustainable river management interventions. It is concluded that a new channel is likely to form around the year 2030 and their adverse impacts on both the riverside communities along the Jamuna and Old Brahmaputra Rivers, as well as on the hydro-morphological stability of the Old Brahmaputra River itself.

Recommendations

Bangladesh is an overpopulated country, and a large number of people reside along both banks of the Old Brahmaputra River. The river is already highly dynamic due to the flow from the current offtake. The average annual lateral shifting of the Old Brahmaputra River is approximately 22.39 meters. Every year, communities living near the riverbanks suffer significant losses due to bank erosion. The emergence of a new offtake would further accelerate the dynamic behavior of the Old Brahmaputra River. A major hydro-morphological transformation could occur as a result of the formation of this new offtake. It would likely increase the volume of flow in the Old Brahmaputra River, which in turn would intensify erosion, sediment deposition, and channel shifting in the downstream reaches following the activation of the probable new offtake. Given the high dynamic characteristics and bank migration tendencies of both the Old Brahmaputra and Jamuna Rivers, the probability of the formation of a new offtake is considerable. This study was conducted using 30-metre resolution Landsat imagery currently available, which may have limited the accuracy of the results. To address this limitation, the use of higher-resolution (10-metre pixel) satellite imagery is recommended for future studies. It is essential to quantify the potential increase in flow and assess the extent of bank erosion that may result from the activation of a probable new offtake. Future research should incorporate field survey data and soil investigations to properly evaluate the potential impacts of the new offtake on the Old Brahmaputra River and the surrounding communities. Although the development of new offtakes is a natural process in meandering rivers, the potential new offtake may have adverse effects on both the population and the river system. Therefore, avoiding the development of a new offtake is a key recommendation of this study. The insights gained from this research can be highly valuable to organizations involved in water resource management, such as the Bangladesh Water Development Board (BWDB) and the Bangladesh Inland Water Transport Authority (BIWTA).

Conflict of interest

The authors declare no conflict of interest.

Reference

Baki, A. B. M., & Gan, T. Y. (2012). Riverbank migration and island dynamics of the braided Jamuna River of the Ganges–Brahmaputra basin using multi-temporal Landsat images. *Quaternary International*, *263*, 148–161. https://doi.org/10.1016/j.quaint.2012.03.016

Bhakal, L., Dubey, B., & Sarma, A. K. (2005). Estimation of bank erosion in The River Brahmaputra near Agyathuri by using Geographic Information System. *Journal of the Indian Society of Remote Sensing*, *33*(1), 81–84. https://doi.org/10.1007/BF02989994

Billah, M. M. (2018). Mapping and Monitoring Erosion-Accretion in an Alluvial River Using Satellite Imagery – The River Bank Changes of the Padma River in Bangladesh. *Quaestiones Geographicae*, *37*(3), 87–95. https://doi.org/10.2478/quageo-2018-0027

Brierley, G. J. (1991). Floodplain sedimentology of the Squamish River, British Columbia: Relevance of element analysis. *Sedimentology*, *38*(4), 735–750. https://doi.org/10.1111/j.1365-3091.1991.tb01017.x

Charlton, R. (2007). *Fundamentals of Fluvial Geomorphology*. Routledge. https://doi.org/10.4324/9780203371084

Constantine, J. A., McLean, S. R., & Dunne, T. (2010). A mechanism of chute cutoff along large meandering rivers with uniform floodplain topography. *Geological Society of America Bulletin*, *122*(5–6), 855–869. https://doi.org/10.1130/B26560.1

EarthExplorer. (n.d.). Retrieved December 27, 2024, from https://earthexplorer.usgs.gov/

Falkowski, T., Ostrowski, P., Bogucki, M., & Karczmarz, D. (2018). The trends in the main thalweg path of selected reaches of the Middle Vistula River, and their relationships to the geological structure of

river channel zone. *Open Geosciences*, *10*(1), 554–564. https://doi.org/10.1515/geo-2018-0044

Flood Action Project 24. (1999). *River Survey Project, Bed material sampling in Ganges, Old Brahmaputra and Jamuna.* (Bed Meterial Sampling No. 8). Water Resources Planning Organization, Banglasesh.

Frascati, A., & Lanzoni, S. (2010). Long-term river meandering as a part of chaotic dynamics? A contribution from mathematical modelling. *Earth Surface Processes and Landforms*, *35*(7), 791–802. https://doi.org/10.1002/esp.1974

Fuller, I. C., Large, A. R. G., & Milan, D. J. (2003). Quantifying channel development and sediment transfer following chute cutoff in a wandering gravel-bed river. *Geomorphology*, *54*(3), 307–323. https://doi.org/10.1016/S0169-555X(02)00374-4

Gao, P., & Li, Z. (2024). Exploring meandering river cutoffs. *Geological Society, London, Special Publications*, *540*(1), 163–184. https://doi.org/10.1144/SP540-2022-261

Garg, S. K. (1991). *Irrigation Engineering and Hydraulic Structures: For Civil Engineering Degree Students; AMIE (Section B) Exams; UPSC and Other State Service Competitions; and for Professionals*. Khanna publishers.

Ghinassi, M. (2011). Chute channels in the Holocene high-sinuosity river deposits of the Firenze plain, Tuscany, Italy. *Sedimentology*, *58*(3), 618–642. https://doi.org/10.1111/j.1365-3091.2010.01176.x

Grenfell, M. C., Nicholas, A. P., & Aalto, R. (2014). Mediative adjustment of river dynamics: The role of chute channels in tropical sand-bed meandering rivers. *Sedimentary Geology*, *301*, 93–106. https://doi.org/10.1016/j.sedgeo.2013.06.007

Hasan, I., Dey, J., Munna, Md. M. R., Preya, A., Nisanur, T. B., Memy, M. J., & Zeba, Mst. Z. S. (2024). Morphological changes of river Bank Erosion and channel shifting assessment on Arial Khan River of Bangladesh using Landsat satellite time series images. *Progress in Disaster Science*, *24*, 100381. https://doi.org/10.1016/j.pdisas.2024.100381

Hassan, A., Martin, T. C., & Mosselman, E. (1999). Island topography mapping for the Brahmaputra-Jamuna River using remote sensing and GIS. *Geological Society, London, Special Publications*, *163*(1), 153–161. https://doi.org/10.1144/GSL.SP.1999.163.01.13

Hooke, J. M. (1984). Changes in river meanders: A review of techniques and results of analyses. *Progress in Physical Geography: Earth and Environment*, *8*(4), 473–508. https://doi.org/10.1177/030913338400800401

Hossain. (2011). River Embankment and Bank Failure: A Study on Geotechnical Characteristics and Stability Analysis. *American Journal of Environmental Sciences*, *7*(2), 102–107. https://doi.org/10.3844/ajessp.2011.102.107

Howard, A. D., & Knutson, T. R. (1984). Sufficient conditions for river meandering: A simulation approach. *Water Resources Research*, *20*(11), 1659–1667. https://doi.org/10.1029/WR020i011p01659

Islam, R., Islam, Md. N., & Islam, M. N. (2017). Impacts of Bangabandhu Jamuna Multi-purpose Bridge on the dynamics of bar morphology at the Jamuna River in Bangladesh. *Modeling Earth Systems and Environment*, *3*(3), 903–925. https://doi.org/10.1007/s40808-017-0342-8

Li, Z., Wu, X., & Gao, P. (2019). Experimental study on the process of neck cutoff and channel adjustment in a highly sinuous meander under constant discharges. *Geomorphology*, *327*, 215–229. https://doi.org/10.1016/j.geomorph.2018.11.002

Micheli, E. R., & Larsen, E. W. (2011). River channel cutoff dynamics, Sacramento River, California, USA. *River Research and Applications*, *27*(3), 328–344. https://doi.org/10.1002/rra.1360

Prakash, K., Sridharan, A., Manoj, N., & Manoj. (2023). Friction Angles of Sands: An Appraisal. *Geotechnical and Geological Engineering*, *41*(8), 4865–4872. https://doi.org/10.1007/s10706-023-02548-9

Rakib, M. R., Mondol, M. A. H., Islam, A. R. Md. T., & Rashid, Md. B. (2024). Using river restoration model to control riverbank erosion in the Old Brahmaputra river of Bengal Basin, Bangladesh. *Advances in Space Research*, *73*(3), 1734–1748. https://doi.org/10.1016/j.asr.2023.11.033

Rashid, Md. B., Habib, Md. A., Khan, R., & Islam, A. R. Md. T. (2023). Land transform and its consequences due to the route change of the Brahmaputra River in Bangladesh. *International Journal of River Basin Management*, *21*(1), 113–125. https://doi.org/10.1080/15715124.2021.1938095

Rokonuzzaman, M., & Hossain, M. R. M. S. A. Z. (2024). *Proceedings of the 7th International Conference on Civil Engineering for Sustainable Development (ICCESD 2024)*. Springer Nature.

Rubayet Mortuza, Md., Rashid, U. S., Rajib, M. A., & Rahman, Md. M. (2011). Temporal variation characteristics of flow and water level in the Old Brahmaputra River. *2011 International Symposium on Water Resource and Environmental Protection*, *2*, 1132–1135. https://doi.org/10.1109/ISWREP.2011.5893214

Sarker, M. H., Thorne, C. R., Aktar, M. N., & Ferdous, Md. R. (2014). Morpho-dynamics of the Brahmaputra–Jamuna River, Bangladesh. *Geomorphology*, *215*, 45–59. https://doi.org/10.1016/j.geomorph.2013.07.025

Thorne, C. R. (2002). Geomorphic analysis of large alluvial rivers. *Geomorphology*, *44*(3), 203–219. https://doi.org/10.1016/S0169-555X(01)00175-1

Uddin, M. J., Haque, M. N., Fayshal, M. A., & Dakua, D. (2022). Assessing the bridge construction effect on river shifting characteristics through geo-spatial lens: A case study on Dharla River, Bangladesh. *Heliyon*, *8*(8). https://doi.org/10.1016/j.heliyon.2022.e10334

Van Dijk, W. M., Van De Lageweg, W. I., & Kleinhans, M. G. (2012). Experimental meandering river with chute cutoffs. *Journal of Geophysical Research: Earth Surface*, *117*(F3), 2011JF002314. https://doi.org/10.1029/2011JF002314

Wilcox. (1830). *Map of the Brahmaputra and Ichamati Rivers. Reduced and drawn by MH Dias, India office Library and Records, London* [Map].

Technical Journal
River Research Institute ISSN: 1606-9277

Linking River Morphodynamics and Land Use Land Cover (LULC) Changes: An Assessment of Riverbank Dynamics of the Bishkhali River

M. F. Hasan[1,2,3*], M. S. Shefa[2], M. J. Hasan[2], R. Islam[2], K. M. Kamal[4], F. Rukshana[5], A. Akter[2,3] and M. Shamsuzzoha[2,3]

Abstract

This study analyzes the intricate linkages between river morphodynamics and land cover changes along a reach of the Bishkhali River, a dynamic fluvial system in south-central Bangladesh. The research focuses on Kanthalia Sadar Union of Kanthalia Upazila in Jhalokathi District, and it analyzes planform dynamics, thalweg shifts, and land use land cover (LULC) changes over 20 years (2004-2024). The study utilizes multi-temporal satellite imagery, Geographic Information System (GIS), and remote sensing (RS) techniques to quantify riverbank erosion, accretion, and channel migration. The analysis of the platform indicates a marked intensification of erosion in the Kanthalia Union, with documented land losses amounting to 2.95 hectares (2004-2009), 118.39 hectares (2009-2014), 5,120.29 hectares (2014–2019), and 2,512.42 hectares (2019–2024). The recent accretion has been minimal, with only 0.21 hectares gained from 2019 to 2024. Thalweg analysis indicates asymmetric channel migration, characterized by persistent right bank erosion (Kanthalia side) and relative left bank stability (Betagi side). LULC analysis reveals substantial alterations in the land's characteristics: A total of 10.18 hectares of built-up areas, 0.35 hectares of barren land, and 0.006 hectares of vegetation were lost to water, while 9.09 hectares of waterbodies were reclaimed as built-up areas. This suggests the presence of localized efforts aimed at counteracting the erosion impacts. These findings underscore the profound interdependence between fluvial processes and human land use responses in deltaic environments. The study underscores the pressing necessity for integrated river management, sustainable bank protection, and adaptive land use planning to mitigate socio-economic and environmental risks. It provides vital insights for policymakers, planners, and local stakeholders to develop resilience-oriented strategies in the face of ongoing geomorphological and land use transitions.

Keywords: *Bishkhali River, Land use land cover (LULC) change, River morphodynamics, Riverbank erosion, ArcGIS, RS.*

Introduction

Rivers in deltaic regions are highly dynamic systems that undergo continuous morphological changes due to complex interactions between hydrodynamic forces, sediment transport, and human interventions (S. Alam et al., 2018; Rogers & Goodbred, 2014; Shamsuzzoha & Ahamed, 2023). The Bishkhali River, located in the south-central coastal region of Bangladesh, is a significant fluvial system that supports sediment conveyance, navigation, agriculture, and local livelihoods (S. N. Islam, 2016; Paszkowski et al., 2024). For a developing country like Bangladesh(Bhattacharjee et al., 2023; M. F. Hasan et al., 2023) , rivers such as the Bishkhali play a vital economic role (Mahmudul Hasan, 2018) by supporting agriculture, fisheries, transport, and providing essential ecosystem services. Over the past two decades, this river has experienced considerable morphodynamic changes, influenced by natural factors such as tidal action, monsoonal flows, and sediment deposition, as well as by human activities including embankment construction, land use alterations, and sand mining (Chowdhury, 2024; Sarkar & Rahman, 2024). These transformations, particularly riverbank erosion, thalweg migration, and bar development, not only reshape the physical landscape but also present critical challenges for sustainable river management, disaster risk reduction, and ecosystem conservation (Anwar & Takewaka, 2014; Chowdhury, 2024).

Planform changes in alluvial rivers, such as channel migration, meandering, cutoffs, and bar formation, are common but have significant socio-economic and environmental consequences (Bhattacherjee et al., 2022; Deb & Ferreira, 2015). Bank erosion and sediment accretion directly affect riverine communities by altering land availability, damaging infrastructure, and impacting agriculture (Md. M. Hasan et al., 2021; Shamsuzzoha & Ahamed, 2024b). Recent studies suggest that riverbank erosion is intensifying due to the combined impacts of seasonal discharges, climate variability, and anthropogenic pressures (Freihardt & Frey, 2022; Mamun et al., 2022; Sarker et al., 2014). Although sandbars both mid-channel and point bars- play a crucial role in sediment dynamics and channel stability, their changing patterns are still poorly understood in many river systems, including the Bishkhali River (M. M. Hasan et al., 2023; Oberhagemann et al., 2020; Sarkar & Rahman, 2024).

The Bishkhali River is a tidal-influenced system that discharges directly into the Bay of Bengal. Consequently, its morphological evolution is particularly sensitive to upstream flow variations and downstream tidal interactions (Sarkar & Rahman, 2024). This region experiences significant channel shifts, bank erosion, and bar formation, affecting local livelihoods, agriculture, and infrastructure (Billah et al., 2023; Freihardt & Frey, 2023; Haque & Hossain,

[1]Department of Environmental Science and Technology, German University Bangladesh, Gazipur-1702, Bangladesh.
[*]Corresponding Author: (E-mail: fuad.dm.pstu@gmail.com)
[2]Faculty of Environmental Science and Disaster Management, Patuakhali Science and Technology University, Patuakhali-8602, Bangladesh.
[3]Department of Emergency Management, Patuakhali Science and Technology University, Patuakhali-8602, Bangladesh.
[4]Ataher Uddin Howlader Degree College, Bakerganj, Barishal, Bangladesh.
[5]Geotechnical Research Directorate, River Research Institute, Faridpur-7800, Bangladesh.

1988; Rahaman et al., 2020; Shamsuzzoha et al., 2024). The study area focuses on a section of the river where pronounced changes have been observed over the years, specifically in Kanthalia Sadar Union (Jhalakathi District) along the right bank and Betagi Sadar and Mokamia Unions (Barguna District) along the left bank (GoB, 2024a, 2024b). These areas are highly vulnerable to riverbank erosion, sediment accretion, and shifting thalwegs, affecting settlements, agricultural land, and infrastructure. Identifying the spatial and temporal trends of these changes is crucial for formulating effective mitigation strategies and ensuring the sustainable management of riverine resources (Shamsuzzoha & Ahamed, 2024b, 2024a; Shamsuzzoha et al., 2025; Siddeqa et al., 2023a).

This study aims to analyze the morphological evolution of the Bishkhali River, with a focus on planform dynamics, thalweg shifts, and Land Use/Land Cover (LULC) changes in Kanthalia Union from 2014 to 2024. Using multi-temporal satellite imagery and GIS-based techniques, it quantifies erosion and accretion along the riverbanks, assesses shifts in the river's deepest flow paths (thalweg) from 2004 to 2024, and examines LULC changes (K. F. Alam & Ahamed, 2022, 2023; M. M. Hasan et al., 2023). The integration of remote sensing (RS) and GIS provides a comprehensive approach to monitoring these transformations, offering critical insights for policymakers, environmental planners, and local communities to support adaptive river management and sustainable land-use planning (K. F. Alam et al., 2024; Arab, Islam, et al., 2022).

This research contributes to larger initiatives in disaster risk reduction, ecological conservation, and sustainable river basin management in Bangladesh's dynamic deltaic environment by improving our understanding of the morphological changes of the Bishkhali River.

Objectives of the Study

i. To analyze changes in the Bishkhali River's planform from 2004 to 2024 using GIS and remote sensing.
ii. To assess thalweg shifts and land use/land cover changes in Kanthalia Union.

Methodology

Study Area

The Bishkhali River, a major river in south-central Bangladesh, originates from the Sugandha River near Gabkhan Dhansiri Union, Jhalokathi Sadar Upazila, and flows through Rajapur, Kanthalia (Jhalokathi District), and Betagi (Barguna District) before meeting the Bay of Bengal at Patharghata Upazila, Barguna District (Sarkar & Rahman, 2024). The river spans 96 km, with an average width of 1 km in the upper reaches and up to 2 km near its mouth. This study focuses on the river segment along the right bank of Kanthalia Sadar Union (Jhalokathi District) and the left bank of Betagi Sadar and Mokamia Unions (Barguna District), with emphasis on Kanthalia Sadar Union **(Fig. 1)**.

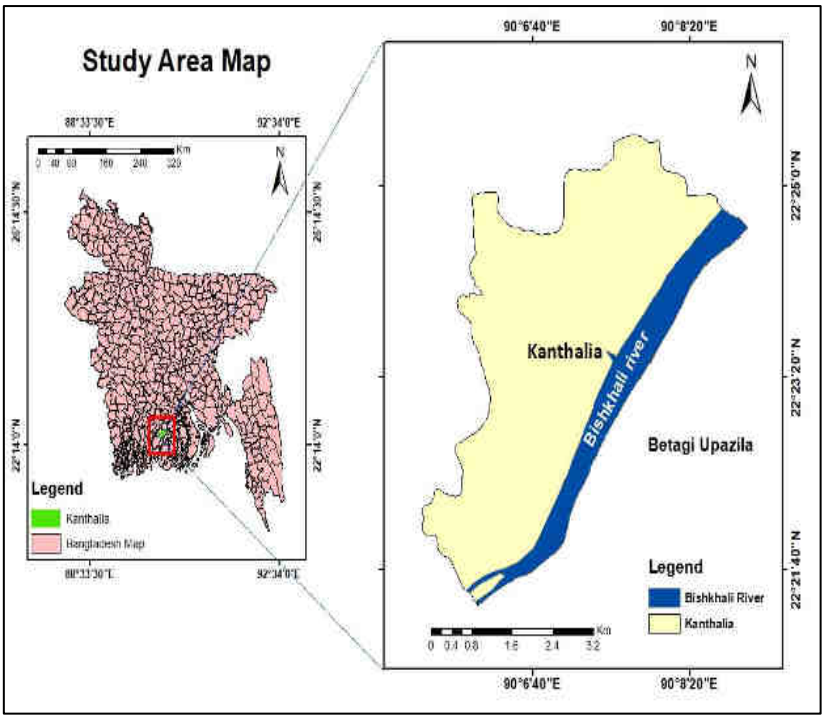

Fig. 1. Study Area Map

Collection, processing, and analysis of satellite images

The satellite images of the Bishkhali River of five different years 2004, 2009, 2014, 2019 and 2024 in Kanthalia, Bangladesh are obtained from United States Geological Survey (USGS) (USGS, 2019, 2025). The basic data used in this study are five multi-date Landsat imageries, e.g., 2004 (TM: Thematic Mapper), 2009 (ETM+), 2014 (OLI: Operational Land Imager), 2019 (OLI) and 2024 (OLI) (Arab, Noguchi, et al., 2022; Shamsuzzoha et al., 2021; USGS, 2014, 2019, 2025). **Table 1** presents all the information about the satellite images used.

Table 1. Metadata of Landsat images.

Platform	Sensor	Year	Path	Row	Resolution	Source
Landsat 4-5	TM and ETM+	2004, 2009	137	45	30m	
Landsat 8	OLI	2014, 2019	137	45	30m	USGS
Landsat 9	OLI	2024	137	45	30m	

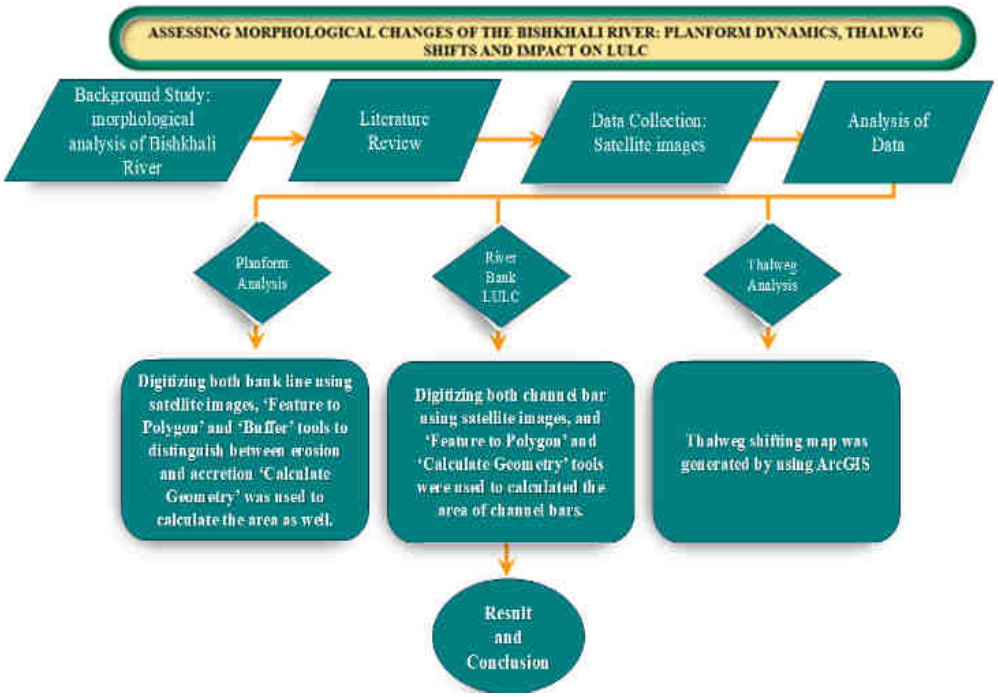

Fig. 2. Steps and Processes of the Study.

Before starting the analysis, the study's data needed to be geo-referenced. Each Landsat image used as a reference was accurately captured. Geo-referencing was performed using ArcGIS® 10.8.2 (Environmental Systems Research Institute, Redlands, CA 92373, United States) (ESRI, 2020). This study employed both traditional geo-referencing techniques and a high-resolution feature matching method. Geo-referencing is a critical step to minimize errors in multi-resolution satellite images. To align the images correctly, image processing techniques were applied to achieve geometric rectification using the World Geodetic System (WGS) 1984, Universal Transverse Mercator (UTM) Zone 45N projection system (Maling, 1992a, 1992b; Shamsuzzoha et al., 2021).

Five satellite images of the Bishkhali River from 2004, 2009, 2014, 2019, and 2024 were obtained from the United States Geological Survey (USGS) website (USGS, 2014, 2019). Erosion and accretion analyses were conducted using Remote Sensing (RS) and Geographic Information Systems (GIS) technologies (Shefa et al., 2024). Image processing was carried out using the ArcGIS image processing tool, while GIS analysis was performed with the ArcGIS 10.8.2 platform. Microsoft 365 Excel® was also used for data analysis and graphing (Microsoft, 2025).

The study employed Landsat satellite imagery to assess riverbank erosion and accretion between 2004 and 2024. To ensure cloud-free surface reflectance images during the pre-monsoon dry season, data was sourced from the USGS Earth Explorer website (USGS, 2025). An unsupervised classification algorithm and post-classification change detection techniques in GIS were applied to analyze the spatial and temporal dynamics of erosion and accretion at various points along the Bishkhali River in Bangladesh.

For each year, shape files were generated by manually digitizing the histogram-equalized, unsupervised

Landsat images using ArcGIS 10.8.2, allowing for precise extraction of river boundaries (ESRI, 2020).

Unsupervised classification techniques were then applied to the extracted images to categorize different land cover types and analyze changes over time (El Abbassi et al., 2021; Kim & Liang, 2017). This method enabled clear differentiation between land and water, revealing patterns of land accretion and erosion (Kim & Liang, 2017). To quantify the morphological changes in the Bishkhali River from 2004 to 2024, a temporal change detection analysis was performed by comparing satellite images from various years (Hussain et al., 2014). This approach allowed for the monitoring of land accretion and erosion trends over time (Hossain et al., 2013; Hussain et al., 2014; M. A. Islam et al., 2016). By integrating these methodologies, the study provided a comprehensive and accurate depiction of the morphological transformations in the Bishkhali River, enhancing the understanding of its evolving landscape. **Fig 2** illustrates conceptual data processing and analysis (Sarkar & Rahman, 2024).

Results and Discussion

Planform Analysis

The Bishkhali River's morphological changes along Kanthalia Union from 2004 to 2024 show (**Fig. 3 and Fig. 4**) significant erosion, posing challenges for local settlements, agriculture, and infrastructure. This analysis focuses on the section of the Bishkhali River adjacent to Kanthalia Union, where erosion has been the dominant process over the years.

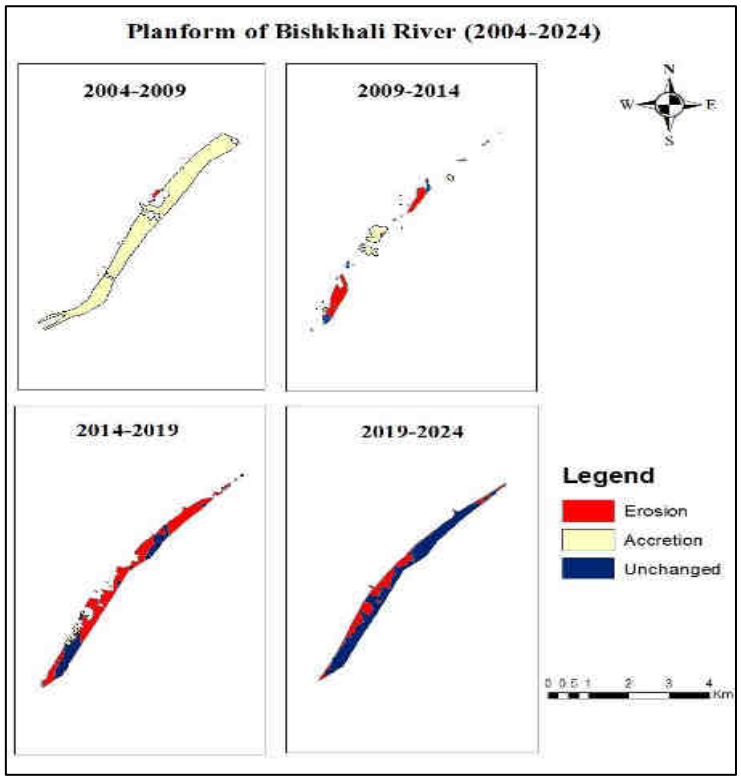

Fig. 3. Planform of Bishkhali River (2004-2024)

During this period, accretion was the dominant process along the Kanthalia Union side of the Bishkhali River, with a substantial land gain (2865.02 ha). Erosion was minimal (2.95 ha), indicating a relatively stable phase where sediment deposition outpaced bank retreat. The low unchanged area (27.56 ha) suggests that most of the riverbank was actively transforming due to sediment deposition, leading to channel bar formation and Bankline shifts. This phase provided temporary land stability for the communities in Kanthalia Union.

A shift in river dynamics was observed between 2009 and 2014, as erosion increased to 118.39 ha, reducing the net land gain. Although accretion (296.19 ha) was still present, the increasing erosion indicates that riverbank instability had begun. The low unchanged area (11.24 ha) suggests continued shifts in river morphology, likely influenced by seasonal variations in flow, sediment transport, and human interventions such as embankments or local land use changes (Siddeqa et al., 2023b).

Between 2014 and 2019, Kanthalia Union experienced severe erosion, reaching an alarming 5120.29 ha, the highest recorded in the study period. Accretion was negligible (6.46 ha), indicating an overwhelming dominance of erosional processes. The unchanged area (55.31 ha) suggests that while some riverbank sections remained stable, most of Kanthalia's riverfront faced aggressive land loss. This phase likely resulted from

increased monsoonal discharges, tidal influences from the Bay of Bengal, or changes in sediment deposition patterns. The extensive erosion had severe consequences for local communities, leading to displacement, loss of agricultural land, and heightened vulnerability to flooding.

In the most recent period (2019-2024), erosion remained high (2512.42 ha), though lower than the previous phase. This indicates a slight reduction in the rate of bank retreat but still signifies substantial land loss. The accretion was almost nonexistent (0.21 ha), suggesting that sediment deposition could not counterbalance the erosional forces. The stable area (195.83 ha) increased compared to previous periods, implying that certain sections of the riverbank had reached a temporary equilibrium, possibly due to natural channel adjustments or localized protection measures. However, the continued high erosion rates indicate that Kanthalia Union remains highly vulnerable to riverine changes.

The shift from a predominantly accretional phase (2004-2009) to a severe erosion-dominated phase (2014-2024) highlights the increasing vulnerability of Kanthalia Union to riverbank retreat. The extreme erosion between 2014 and 2019 suggests significant hydrodynamic changes, possibly driven by high river discharge, embankment failures, or climate-induced factors such as increased tidal influence and extreme weather events. The decline in accretion rates in the later years further indicates reduced sediment deposition, potentially due to upstream modifications or natural sediment redistribution within the basin.

The loss of land along the Kanthalia Union bank has serious implications for local livelihoods, agricultural productivity, and infrastructure stability. Without proper intervention, the ongoing erosion will continue to threaten the socio-economic stability of communities in the region. Targeted riverbank protection strategies, sustainable sediment management, and community-based adaptation measures are essential to mitigate further damage and enhance the resilience of Kanthalia Union against future riverine changes.

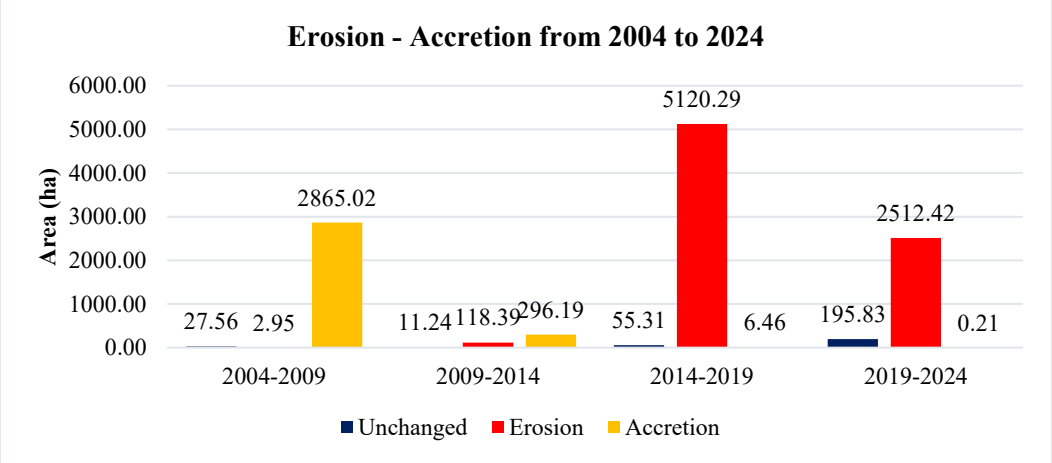

Fig. 4. Erosion and Accretion from 2004 to 2024.

Thalweg Analysis

The river course, represented (**Fig. 5**) by three temporal states, 2004 (purple line), 2014 (black line), and 2024 (green line) exhibits significant lateral shifts along the right bank (Kanthalia) and left bank (Betagi). The red thalweg markers highlight notable shifts in the river's deepest point, indicating dynamic fluvial processes, sediment redistribution, and erosion-prone zones. Notably, the progressive migration between 2014 and 2024 reveals a non-uniform shifting pattern, suggesting localized variations in hydraulic energy and sediment transport dynamics. These shifts underscore ongoing channel migration, potentially influencing riverbank stability, floodplain dynamics, and nearby communities. The right bank (Kanthalia) appears to be more susceptible to erosion, whereas the left bank (Betagi) shows relative stability in some sections. Understanding these changes is critical for sustainable river management, flood risk mitigation, and ecosystem conservation efforts in the Bishkhali River basin specially on the bank of Kanthalia.

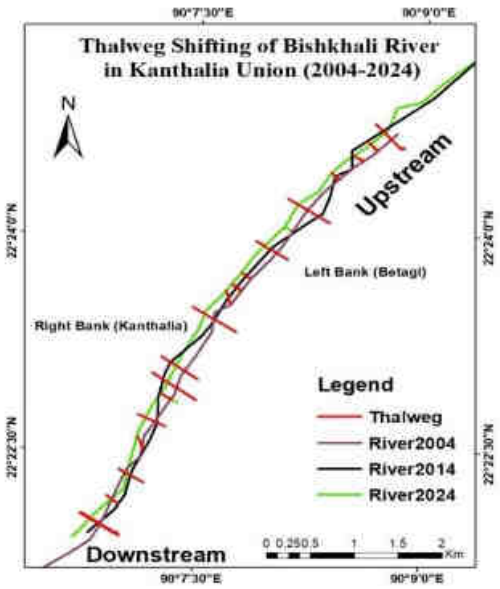

Fig. 5. Thalweg Analysis

LULC Change Analysis

The Land Use Land Cover (LULC) change analysis in Kanthalia Union from 2014 to 2024 represents (**Table 2 and Fig. 6**) significant transformations driven by riverbank erosion and rapid settlement expansion. The most notable change is the conversion of various land types into waterbodies, indicating intensified erosion. Approximately 10.18 hectares of built-up area, 0.35 hectares of barren land, and 0.006 hectares of vegetation have been lost to water, highlighting the destructive impact of fluvial processes. Additionally, 9.09 hectares of waterbodies have transitioned into built-up areas, suggesting encroachment and land reclamation efforts despite the erosion threats. However, urban expansion is evident, with 312.22 hectares of vegetation and 25.03 hectares of barren land transforming into built-up zones, reflecting increasing human habitation and infrastructure development. Vegetation cover has experienced both gains and losses; while 80.62 hectares of barren land have regenerated into vegetation, approximately 123.97 hectares of vegetation have degraded into barren land, indicating deforestation and soil erosion.

Table 2. Land Use Land Cover (LULC) Changes in Kanthalia Union (2014–2024)

LULC Transition	Area Change (ha)
Waterbodies -Waterbodies	317.93
Waterbodies -Buildup Area	9.09
Waterbodies -Vegetation	0.03
Waterbodies -Barren Land	0.21
Buildup Area -Waterbodies	10.18
Buildup Area -Buildup Area	159.35
Buildup Area -Vegetation	55.68
Buildup Area -Barren Land	56.89
Buildup Area -Vegetation	18.16
Vegetation -Waterbodies	0.01
Vegetation -Buildup Area	312.22
Vegetation -Vegetation	212.47
Vegetation -Barren Land	24.25
Vegetation -Vegetation	4.78
Barren land -Waterbodies	0.35
Barren land -Buildup Area	25.03
Barren land -Vegetation	80.62
Barren land -Barren Land	100.99
Barren land -Vegetation	162.46
Vegetation -Waterbodies	0.05
Vegetation -Buildup Area	15.77
Vegetation -Vegetation	81.30
Vegetation -Barren Land	123.97
Vegetation -Vegetation	254.31

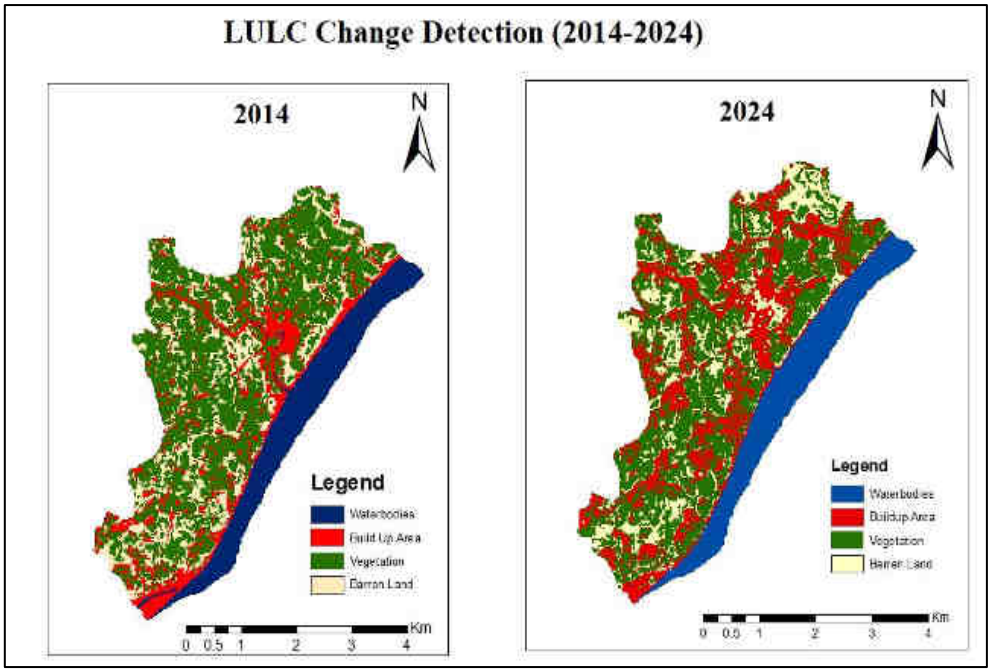

Fig. 6. LULC of Kanthalia Union.

Linking River Morphodynamics with Land Use and Land Cover (LULC) Changes

The relationship between the Bishkhali River's morphological changes and surrounding LULC dynamics was analyzed to understand the potential drivers of intensified erosion and channel migration. Overlaying the erosion and accretion maps with LULC data from 2004 to 2024 reveals significant patterns.

In Kanthalia Union, built-up areas and agricultural land increased notably between 2014 and 2024, while vegetative cover declined. This corresponds with the period of highest erosion (2014–2019), where over 5,100 ha were lost. Expanding built-up areas may have reduced infiltration and increased surface running into the river, contributing to channel instability and bank erosion. Similarly, the loss of vegetation may have diminished soil binding and sediment contribution from upstream, potentially altering sediment dynamics and encouraging scouring along the banks.

These findings suggest a potential linkage between LULC transitions and river morphodynamics, especially in areas experiencing land reclamation and unregulated development. Though this study primarily uses spatial analysis, future work should incorporate field validation and hydrological data to strengthen causal interpretation.

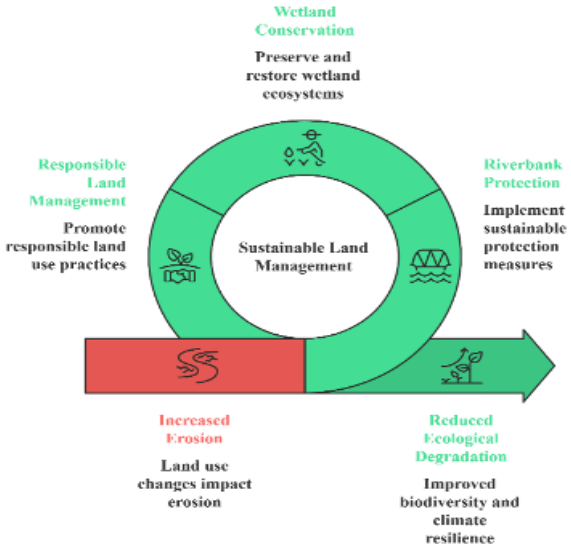

Fig.7. Mitigating erosion through land management (Das et al., 2021; M. S. Islam, 2011).

These findings emphasize (**Fig. 7**) the dynamic and unstable nature of the region's landscape, where riverine erosion, land reclamation, and settlement expansion simultaneously shape the LULC patterns. The substantial increase in built-up areas at the expense of vegetation and barren land suggests ongoing urbanization, while the loss of both land to river erosion and waterbodies to urban expansion signals a dual environmental threat. Without sustainable riverbank protection, wetland conservation, and responsible land management strategies, the region risks further ecological degradation, loss of biodiversity, and worsening climate vulnerabilities.

Conclusions

This study looked at how land use changes have affected river dynamics in the Kanthalia Union between 2004 and 2024. Using GIS and RS techniques, it analyzed how the land and demographic change, as well as the river and the adjacent land next to it behave. The results show a big change from a period of mostly stable, accretion-dominated growth (2004–2009) to a period of erosion (2014–2024), with the most severe erosion recorded between 2014 and 2019 (5120.29 ha lost). Erosion levels stayed high during this time (2512.42 hectares lost from 2019–2024), and rates of land accumulation continued to drop. These trends suggest reducing sediment supply and growing instability along riverbanks. Thalweg analysis showed that the river's deepest channel migrated towards the right bank (Kanthalia), which contributed to the observed erosion patterns. In contrast, the left bank (Betagi) stayed relatively stable. Changes in LULC during the same period further reflect the impact of river dynamics. Areas that once occupied by vegetation, settlements, and fallow land were submerged, while some water bodies were reclaimed and converted into built-up zones. This focuses on human responses to land loss. The new subsection explores the influence of land use on river behavior suggesting that there is probably a connection between increased construction, losing vegetation, and accelerated riverbank erosion. These interactions highlight the complex and interdependent human nature and environmental systems that creating river behavior difficult to predict.

This research makes a significant contribution to the field by offering critical insights for policymakers and planners seeking to develop sustainable river management strategies. There is a paucity of understanding regarding the hydrological mechanisms that underpin sediment loss and the precise role of different land cover types in the dynamics of erosion. Future studies should incorporate field-based sediment flow measurements, high-resolution temporal datasets, and predictive modeling to strengthen causal links and forecast changes under different climate and development scenarios. In order to mitigate further erosion and protect vulnerable communities, the study recommends a combination of structural and nature-based solutions. These include reinforced and ecologically sensitive embankments, vegetative buffers, and afforestation programs along erosion-prone banks. Furthermore, the implementation of zoning regulations and land use planning has been demonstrated to play a pivotal role in mitigating the potential risks associated with residential developments in proximity to financially unstable banking institutions. The study's findings are of critical importance for the preservation of livelihoods in the Kanthalia Union, where the viability of agriculture, housing, and infrastructure is imperiled by erosion. Enhanced riverbank protection has been demonstrated to reduce displacement, ensure the security of farmland, and stabilize property, thereby contributing to local resilience and economic stability. The integration of scientific evidence into local adaptation and policy frameworks is a key finding of the study, which supports a shift toward proactive, community-centered river governance in Bangladesh's vulnerable deltaic environment.

Conflicts of Interest

The authors declare no conflict of interest.

References

Alam, K. F., & Ahamed, T. (2022). Assessment of Land Use Land Cover Changes for Predicting Vulnerable Agricultural Lands in River Basins of Bangladesh Using Remote Sensing and a Fuzzy Expert System. *Remote Sensing*, *14*(21). https://doi.org/10.3390/rs14215582

Alam, K. F., & Ahamed, T. (2023). Erosion Vulnerable Area Assessment of Jamuna River System in Bangladesh Using a Multi-criteria-based Geospatial Fuzzy Expert System and Remote Sensing. *Asia-Pacific Journal of Regional Science*. https://doi.org/10.1007/s41685-023-00292-9

Alam, K. F., Shamsuzzoha, M., Arab, S. T., Pangaribuan, I. J. P., & Ahamed, T. (2024). Application of Remote Sensing in the Analysis of Climate Extremes Due to Global Climate Change. In T. Ahamed (Ed.), *Remote Sensing Application II. New Frontiers in Regional Science: Asian Perspectives* (Vol. 77, pp. 1–21). Springer. https://doi.org/10.1007/978-981-97-1188-8_1

Alam, S., de Heer, J., & Choudhury, G. (2018). *Bangladesh Delta Plan 2100.* http://www.plancomm.gov.bd/site/files/0adcee77-2db8-41bf-b36b-657b5ee1efb9/Bangladesh-Delta-Plan-2100

Anwar, Md. S., & Takewaka, S. (2014). Analyses on phenological and morphological variations of mangrove forests along the southwest coast of

Bangladesh. *Journal of Coastal Conservation*, *18*(4), 339–357. https://doi.org/10.1007/s11852-014-0321-4

Arab, S. T., Islam, Md. M., Shamsuzzoha, Md., Alam, K. F., Muhsin, N., Noguchi, R., & Ahamed, T. (2022). A Review of Remote Sensing Applications in Agriculture and Forestry to Establish Big Data Analytics. In T. Ahamed (Ed.), *Remote Sensing Application. New Frontiers in Regional Science: Asian Perspectives* (Vol. 59, pp. 1–24). Springer. https://doi.org/10.1007/978-981-19-0213-0_1

Arab, S. T., Noguchi, R., & Ahamed, T. (2022). Yield Loss Assessment of Grapes Using Composite Drought Index Derived from Landsat OLI and TIRS Datasets. *Remote Sensing Applications: Society and Environment*, *26*. https://doi.org/10.1016/j.rsase.2022.100727

Bhattacharjee, A., Mahmud, S. M. S., Raihan, M. A., Hazra, P., & Hasan, M. F. (2023). Pedestrian Safety in Dhaka Mega City of Bangladesh: Behaviour, Attitude and Risk Perception. *Journal of Engineering Science*, *13*(2), 117–125. https://doi.org/10.3329/jes.v13i2.63732

Bhattacherjee, S., Bandyopadhyay, S., & De, S. K. (2022). Significance of Channel Planform Change and Morphometric Indices in the Buri River Basin, India and Bangladesh. In H. N. Bhattacharya, S. Bhattacharya, B. C. Das, & A. Islam (Eds.), *Himalayan Neotectonics and Channel Evolution* (pp. 151–174). Springer International Publishing. https://doi.org/10.1007/978-3-030-95435-2_6

Chowdhury, Md. S. (2024). Morphometric analysis of Halda River basin, Bangladesh, using GIS and remote sensing techniques. *Heliyon*, *10*(7), e29085. https://doi.org/https://doi.org/10.1016/j.heliyon.2024.e29085

Das, K., Bandyopadhyay, S., & Kumar De, S. (2021). Assessing the Impact of Riverbank Erosion on Land Use/Land Cover along the Lower Reach of Balasan River, West Bengal. *Journal of Indian Geomorphology*, *9*.

Deb, M., & Ferreira, C. (2015). Planform channel dynamics and bank migration hazard assessment of a highly sinuous river in the north-eastern zone of Bangladesh. *Environmental Earth Sciences*, *73*(10), 6613–6623. https://doi.org/10.1007/s12665-014-3884-3

El Abbassi, M., Overbeck, J., Braun, O., Calame, M., van der Zant, H. S. J., & Perrin, M. L. (2021). Benchmark and application of unsupervised classification approaches for univariate data. *Communications Physics*, *4*(1), 50. https://doi.org/10.1038/s42005-021-00549-9

ESRI. (2020). *GIS Tutorial for ArcGIS Desktop 10.8 | Sample Chapter*. https://www.esri.com/content/dam/esrisites/en-us/esri-press/book-pages/sample-page/gis-tutorial-arcgis-desktop-10-8.pdf

Freihardt, J., & Frey, O. (2022). *Assessing riverbank erosion in Bangladesh using time series of Sentinel-1 radar imagery in the Google Earth Engine*. https://doi.org/10.5194/egusphere-2022-319

GoB. (2024a). *Barguna District*. Bangladesh National Portal, Government of Bangladesh (GoB). https://www.barguna.gov.bd/en

GoB. (2024b). *Jhalakathi District*. Bangladesh National Portal, Government of Bangladesh (GoB). https://www.jhalakathi.gov.bd/en

Hasan, M. F., Mahmud, S. M. S., Raihan, M. A., Akter, A., & Bhattacharjee, A. (2023). Motorcyclist Safety Risk and Attitude to Using Helmet. *Journal of Engineering Science*, *13*(2), 11–20. https://doi.org/10.3329/jes.v13i2.63722

Hasan, M. M., Mondol Nilay, M. S., Jibon, N. H., & Rahman, R. M. (2023). LULC changes to riverine flooding: A case study on the Jamuna River, Bangladesh using the multilayer perceptron model. *Results in Engineering*, *18*, 101079. https://doi.org/https://doi.org/10.1016/j.rineng.2023.101079

Hasan, Md. M., Islam, R., Rahman, Md. S., Ibrahim, Md., Shamsuzzoha, Md., Khanam, R., & Zaman, A. K. M. M. (2021). Analysis of Land Use and Land Cover Changing Patterns of Bangladesh Using Remote Sensing Technology. *American Journal of Environmental Sciences*, *17*(3), 64–74. https://doi.org/10.3844/ajessp.2021.64.74

Hossain, M. A., Gan, T. Y., & Baki, A. B. M. (2013). Assessing morphological changes of the Ganges River using satellite images. *Quaternary International*, *304*, 142–155. https://doi.org/10.1016/j.quaint.2013.03.028

Hussain, M. A., Tajima, Y., Gunasekara, K., Rana, S., & Hasan, R. (2014). Recent coastline changes at the eastern part of the Meghna Estuary using PALSAR and Landsat images. *IOP Conference Series: Earth and Environmental Science*, *20*, 012047. https://doi.org/10.1088/1755-1315/20/1/012047

Islam, M. A., Hossain, M. S., Hasan, T., & Murshed, S. (2016). Shoreline changes along the Kutubdia Island, south east Bangladesh using digital shoreline analysis system. *Bangladesh Journal of Scientific Research*, *27*(1), 99–108. https://doi.org/10.3329/bjsr.v27i1.26228

Islam, M. S. (2011). Riverbank Erosion and Sustainable Protection Strategies. In *Journal of Engineering Science* (Vol. 02, Issue 2).

Islam, S. N. (2016). Deltaic floodplains development and wetland ecosystems management in the Ganges–Brahmaputra–Meghna Rivers Delta in Bangladesh. *Sustainable Water Resources Management*, *2*(3), 237–256. https://doi.org/10.1007/s40899-016-0047-6

Kim, W., & Liang, S. (2017). Unsupervised Classification. In *International Encyclopedia of Geography* (pp. 1–5). Wiley. https://doi.org/10.1002/9781118786352.wbieg0271

Mahmudul Hasan, Md. (2018). Environmental Change and Its Impacts on Lives and Livelihoods of South-Central Coastal Districts of Bangladesh. *American Journal of Biological and Environmental Statistics*, *4*(2), 42. https://doi.org/10.11648/j.ajbes.20180402.11

Maling, D. H. (1992a). CHAPTER 16 - The Transverse Mercator projection. In D. H. MALING (Ed.), *Coordinate Systems and Map Projections (Second Edition)* (pp. 336–363). Pergamon. https://doi.org/https://doi.org/10.1016/B978-0-08-037233-4.50021-2

Maling, D. H. (1992b). Subject Index. In D. H. MALING (Ed.), *Coordinate Systems and Map Projections (Second Edition)* (pp. 469–476). Pergamon. https://doi.org/https://doi.org/10.1016/B978-0-08-037233-4.50031-5

Mamun, A. Al, Towfiqul Islam, A. R. M., Alam, E., Pal, S. C., & Monirul Alam, G. M. (2022). Assessing Riverbank Erosion and Livelihood Resilience Using Traditional Approaches in Northern Bangladesh. *Sustainability (Switzerland)*, *14*(4). https://doi.org/10.3390/su14042348

Microsoft. (2025). *Excel: Quick Start Guide*. https://support.microsoft.com/en-us/office/what-is-excel-94b00f50-5896-479c-b0c5-ff74603b35a3

Oberhagemann, K., Haque, A. M. A., & Thompson, A. (2020). A Century of Riverbank Protection and River Training in Bangladesh. *Water*, *12*(11), 3018. https://doi.org/10.3390/w12113018

Paszkowski, A., Laurien, F., Mechler, R., & Hall, J. (2024). Quantifying Community Resilience to Riverine Hazards in Bangladesh. *Global Environmental Change*, *84*, 102778. https://doi.org/https://doi.org/10.1016/j.gloenvcha.2023.102778

Rogers, K. G., & Goodbred, S. L. (2014). *The Sundarbans and Bengal Delta: The World's Largest Tidal Mangrove and Delta System* (pp. 181–187). https://doi.org/10.1007/978-94-017-8029-2_18

Sarkar, I., & Rahman, M. A. (2024). Morphological Analysis of Bishkhali River Using Multi-temporal Satellite Images and Historical Cross-Sectional Data. In S. Arthur, M. Saitoh, & A. Hoque (Eds.), *Proceedings of the 6th International Conference on Advances in Civil Engineering* (pp. 225–236). Springer Nature Singapore.

Sarker, M. H., Thorne, C. R., Aktar, M. N., & Ferdous, Md. R. (2014). Morpho-dynamics of the Brahmaputra–Jamuna River, Bangladesh. *Geomorphology*, *215*, 45–59. https://doi.org/10.1016/j.geomorph.2013.07.025

Shamsuzzoha, M., & Ahamed, T. (2023). Shoreline Change Assessment in the Coastal Region of Bangladesh Delta Using Tasseled Cap Transformation from Satellite Remote Sensing Dataset. *Remote Sensing*, *15*(2). https://doi.org/10.3390/rs15020295

Shamsuzzoha, M., & Ahamed, T. (2024a). Application of Introducing Damaged Area Index for Cultivated Agricultural Lands Affected by Recurrent Tropical Cyclones Bulbul and Amphan Using Satellite Remote Sensing. In T. Ahamed (Ed.), *Remote Sensing Application II. New Frontiers in Regional Science: Asian Perspectives* (Vol. 77, pp. 165–178). Springer. https://doi.org/10.1007/978-981-97-1188-8_6

Shamsuzzoha, M., & Ahamed, T. (2024b). Assessment of Shoreline and Agricultural Land Use Changes in the Onshore Coastal Region of Bangladesh Delta Using Satellite Remote Sensing and GIS. In T. Ahamed (Ed.), *Remote Sensing Application II. New Frontiers in Regional Science: Asian Perspectives* (Vol. 77, pp. 85–119). Springer. https://doi.org/10.1007/978-981-97-1188-8_4

Shamsuzzoha, M., Noguchi, R., & Ahamed, T. (2021). Damaged Area Assessment of Cultivated Agricultural Lands Affected by Cyclone Bulbul in Coastal Region of Bangladesh Using Landsat 8 OLI and TIRS Datasets. *Remote Sensing Applications: Society and Environment*, *23*. https://doi.org/10.1016/j.rsase.2021.100523

Shamsuzzoha, Md., Hasan, Md. F., Rasheduzzaman, Md., Talukder, Md. F., Ahamed, T., & Shaw, R. (2025). Bangladesh's Progress on Disaster Risk Reduction Over the Past 20 Years. In R. Shaw, T. Izumi, R. Djalante, & F. Imamura (Eds.), *Two Decades from the Indian Ocean Tsunami: Key Challenges and Advancements* (pp. 317–358). Springer Nature Singapore. https://doi.org/10.1007/978-981-96-2669-4_19

Shefa, M. S., Hasan, Md. F., Ovi, M. H., Akash, Sk. M. H., Parvez, A., Rukshana, F., Akter, A., & Reza, G. A. M. A. (2024). Navigating the Ravages of Riverbank

Erosion: Socio-economic and Environmental Impacts in the Nalua Union of Bakerganj Upazila. *Asian Journal of Social Sciences and Legal Studies*, 154–161. https://doi.org/10.34104/ajssls.024.01540161

Siddeqa, M., Islam, Md. T., Hasan, Md. F., Islam, R., & Rasheduzzaman, Md. (2023a). Land Use and Land Cover Change Detection of Teknaf Upazila Due to Rohingya Crisis by Using GIS, and RS Techniques. *Asian Journal of Social Sciences and Legal Studies*, *5*(6), 246–252. https://doi.org/10.34104/ajssls.023.02460252

Siddeqa, M., Islam, Md. T., Hasan, Md. F., Islam, R., & Rasheduzzaman, Md. (2023b). Land Use and Land Cover Change Detection of Teknaf Upazila Due to Rohingya Crisis by Using GIS, and RS Techniques. *Asian Journal of Social Sciences and Legal Studies*, 246–252. https://doi.org/10.34104/ajssls.023.02460252

USGS. (2014, June 14). *Landsat 8 Bands*. United States Geological Survey. https://landsat.gsfc.nasa.gov/satellites/landsat-8/landsat-8-bands/

USGS. (2019). *Landsat 8 (L8) Data Users Handbook*. United States Geological Survey (USGS). https://www.usgs.gov/media/files/landsat-8-data-users-handbook

USGS. (2025). *Earth Explorer*. https://earthexplorer.usgs.gov/

Technical Journal
River Research Institute ISSN: 1606-9277

Evaluation of Management Measures to Develop a Drainage Strategy for Kallayanpur Catchment, Dhaka, Bangladesh

M. M. B. Mostafa[1] and M. S. M. Khan[2]

Abstract

Kallayanpur catchment located in the western part of Dhaka where about 0.95 km^2 retention pond area with 20 m^3s-1 pumping capacity was sufficient. But the retention pond area had been reduced to 0.42 km^2 in 2020, exacerbating waterlogging issues during the monsoon season. This study is an attempt to improve the understanding of the Kallyanpur drainage system and predict the hydrologic and hydrodynamic response with different adaptive measures by using MIKE URBAN. Various data were collected and analyzed to develop hydrological, 1D hydrodynamic, and 1D-2D coupled overland flow models. Calibration and validation, utilizing water level data from the Kallayanpur pumping station, confirmed the accuracy of the model. Several model scenarios were simulated based on specified adaptive measures, such as increased pumping capacity, and low impact developments (LIDs) like rainwater harvesting, permeable pavement, and green roofs. The result shows that the drainage system is pump dependent. With the existing operating rule, the additional requirement of pumping capacity varies from 22 to 55 m^3s-1. But the requirement pumping capacity has been reduced to 17 - 45 m^3s-1 with the new operating rule. The total storage amount by LIDs is about 0.74 Mm^3, which is 23% of the total accumulated flow. By combining LIDs with the new operation rule, the requirement of pumping capacity becomes 9 -37 m^3s-1. The study concluded by proposing a comprehensive drainage strategy combining grey and green structures (G&G). The proposed strategy involves adding 37 m^3s-1 pumping capacity and implementing new pump operation rules. Also, rainwater harvesting is identified as the initial phase solution, followed by other LID measures.

Keywords: *Adaptation, Calibration and validation, Drainage strategy, LIDs, MIKE URBAN, Pumping capacity.*

Introduction

The capital city Dhaka, one of the densely populated cities of Bangladesh located in the central part of the country. In the past, the lowland, and open channels of Dhaka city used to form an effective drainage network that would drain the City efficiently to the surrounding rivers. Earlier study showed that, by 2009 the area of wetland and rivers & khals in the city decreased by 76.67% and 18.72% respectively compared to 1978 due to land filling and encroachment (Mahmud et al., 2011). Also, Ishtiaque et al. (2014) state that the decrease of water bodies and wetlands are among the primary reasons for deteriorating the drainage situation with the passage of time. Basically, Dhaka is experiencing the negative consequences of rapid urbanization.

The Kallayanpur catchment is located on the western part of Dhaka city. Dasgupta et al. (2015) states that, the catchment area is a densely populated area and is a key contributor to Dhaka's economy, featuring a variety of manufacturing and processing factories, commercial activities, residential areas, offices, clinics, and schools The modelling study for ascertaining retention pond area by IWM (2009) showed that, 0.95 km^2 retention pond area with 20 m^3s^{-1} pumping capacity was sufficient for efficient drainage at Kallayanpur catchment. In Detailed Area Plan (DAP) by RAJUK (2010) also proposed 0.92 km^2 area as retention pond for Kallayanpur catchment. Another study to assess the retention pond area and pumping capacity by IWM (2013) reveals that the retention area has reduced to 0.69 km^2. As preservation of the retention pond area could not be achieved the area is decreasing as shown in **Fig. 1**. The catchment experiences flooding in every monsoon season because of increasing population density leading to unplanned urbanization, reduction of wetlands and illegal encroachment of water bodies.

To develop a sustainable drainage system, stormwater drainage modelling plays an important role. In this study MIKE URBAN has been used (DHI, 2017), which is a very comprehensive tool to carry out mathematical modelling of stormwater drainage networks and sewer collection systems. Moreover, different scenarios based on adaptive measures like increasing pumping capacity and adaptation of different low impact developments (LIDs) have been analyzed by this model which would assist to formulate an adaptation strategy.

The study encompasses four objectives. Firstly, the study aims to establish a Hydrological and Hydrodynamic Model of the drainage system using MIKE URBAN, followed by the calibration and validation of the model. Secondly, the study seeks to explore various management options through model simulation, aiming to achieve a sustainable solution for the drainage system. The third objective involves assessing the additional pumping capacity and new operational rules for the Kallyanpur pumping station. Lastly, the study endeavors to develop a comprehensive drainage strategy for the Kallyanpur

[1]Water Supply, Sanitation and Urban Water Management Division, Institute of Water Modeling, Dhaka-1230, Bangladesh.
*Corresponding Author: (E-mail: mmt@iwmbd.org)
[2]Department of Water Resource Engineering, Bangladesh University of Engineering and Technology, Dhaka-1200, Bangladesh.

catchment, integrating findings and insights derived from the established model and simulations.

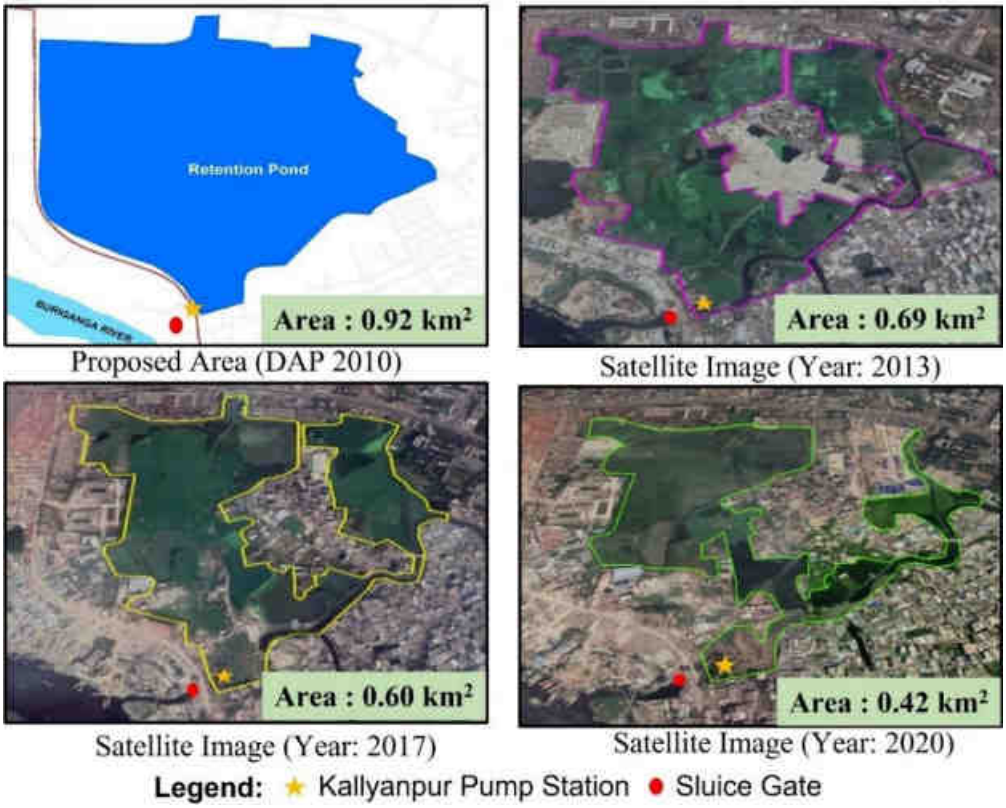

Fig.1. Reduction of retention pond area with the passage of time

Methodology

Study Area

The study area is about 19.60 km^2 as shown in **Fig. 2**, and the area is protected from river flooding by the Western Embankment. A sluice gate is located along the embankment which remains closed during the monsoon season and stormwater of the area is pumped from the Kallayanpur retention pond. Most of the area lies within the range of 5.0 mPWD to 9.0 mPWD. The existing drainage system includes 8 open channels locally known as khals of about 11.7 km, about 39.60 km of pipe drains, and a retention pond with a pump station. The diameter of the pipe ranges from 450 mm to 3000 mm. All the outfalls of pipe drains are in nearby khals. The total capacity of the pump station is 20 m^{3}s^{-1}. Pumping starts if the water level reaches 4.0 mPWD and stops at 3.50 mPWD. During monsoon river water level is usually high (higher than 6.45 mPWD) and the slice gate remain close. The pumps of the pump station remain in operation, pumping out the water from the retention pond.

Fig. 2. Map showing the study area

Data Analyses

The necessary data is collected from various sources. **Table 1** summarizes different data which are required for the present study.

Table 1. Summary of data analysis

Data Type	Data Source	Required for
Rainfall	Bangladesh Meteorological Department (BMD), (1991-2020)	a. Actual rainfall event for model calibration and validation b. 2 day-5-year design rainfall to analyze and plan adaptive measures
Drainage network	Dhaka Water Supply and Sewerage Authority (DWASA), Institute of Water Modelling (IWM)	a. Hydrological modelling b. Hydrodynamic modelling
Landuse	Rajdhani Unnayan Kartripakkha (RAJUK)	a. Sub-catchment delineation b. Spatial planning of adaptive measures
DEM	Catchment from RAJUK (2010), Retention Pond from IWM (2013)	a. Input data for 1D-2D hydrodynamic couple modelling b. Input data for retention pond geometry c. Determining sub-catchment slope
Pumping data	DWASA	Model calibration and validation

Design Rainfall Hyetographs

Following Intensity-Duration-Frequency (IDF) equation was generated for Dhaka city in accordance with the methods outlined by Rasel and Islam (2015).

$$I = \frac{43.22\,T^{0.2612}}{T_d^{0.6425}} \quad \text{Eq. (1)}$$

Drainage Master Plan by DWASA (2015) has proposed design rainfall for pump stations and onsite detention as 2-day 5-year event. Based on Eq. (1), the design rainfall has been computed as 262.60 mm for 2-day 5-year events. By considering climate change (CC) projections (AR6, 2021), the design rainfall is likely to increase to 300.42 mm. In this study rainfall hyetography was generated using the two methods described below and are illustrated in **Fig. 3**.

a. JICA Study Method

This method is used in many domestic studies or projects. The JICA study (1987) has established that the duration of heavy rainfalls of high frequency is about six hours. For a two-day event, rainfall on the second day has the same pattern as the daily rainfall and its starting time is 24 h after the start of first day rainfall. The amount of second day rain can be found by subtracting one-day design rainfall from two-day design rainfall.

b. Alternating Block Method (ABM)

The design hyetograph produced by this method specifies the precipitation depth occurring in successive time intervals of duration T_d which is equated as Eq. (2).

$$T_d = n \times \Delta t \quad \text{Eq. (2)}$$

After selecting the design return period, the intensity is read from the IDF curve or IDF curve equation for each of the durations Δt, 2Δt, 3Δt etc. and the corresponding precipitation depth found as the product of intensity and duration. By taking differences between successive precipitation depth values, the amount of precipitation to be added for each additional unit of time Δt is found. These increments, or blocks, are reordered into a time sequence with the maximum intensity occurring at the center of the required duration T_d and the remaining blocks arranged in descending order alternately to the right and left of the central block to form the design hyetograph.

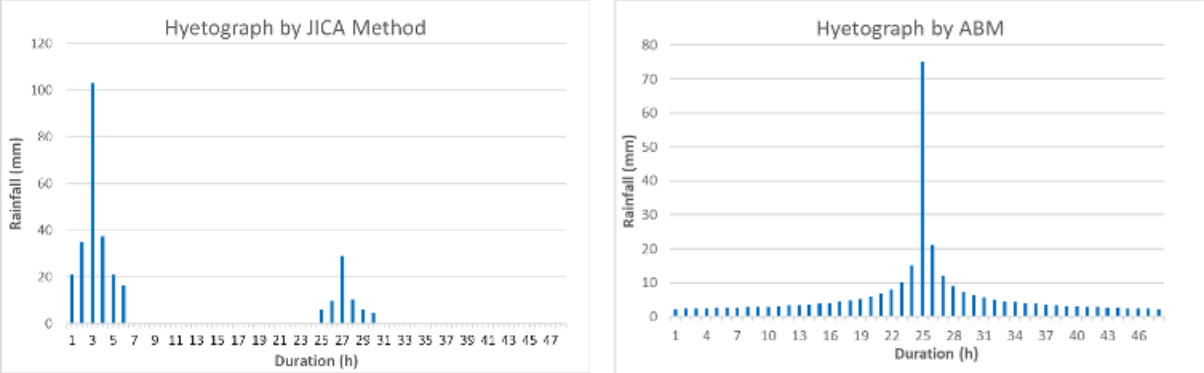

Fig. 3. Design rainfall hyetograph

Mathematical Modelling

In this study, a distributed modelling tool MIKE URBAN was used to develop the model for study area. In that case the MIKE URBAN MOUSE engine has been used. MOUSE provides a versatile set of tools and computational models aimed at modelling both hydrologic and hydrodynamic components on urban catchments. The governing equation for hydrodynamic simulation of flows and water levels in urban storm drainage networks is Saint Venant equations.

Delineation of sub-catchments

Primarily sub-catchments are delineated based on Thiessen Polygon formulated from drainage network nodes or outfall. The auto delineated sub-catchments are then modified by considering flow direction, drainage network as-built drawing, road network, elevation and surface slope, outfall location and field observations. A total of 432 nos. sub-catchment has been delineated in the study area.

Time of Concentration

The equation used for the calculation of the time of concentration (t_c) for the sub-catchments has been taken from Drainage Master Plan by DWASA (2014) as specified in Eq. (3), Eq. (4) and Eq. (5).

$$t_c = t_0 + t_d \qquad \text{Eq. (3)}$$

Where,

t_0 = Time of overland flow

t_d = Time of travel in roadside swales, drains, canals and khals

$$t_0 = \frac{107\, n^* L^{1/3}}{S^{1/5}} \qquad \text{Eq. (4)}$$

Where,

t_0= Overland sheet flow travel time (minutes)

L = Overland sheet flow path length (m)

S = Slope of overland surface (%)

n^* = Horton's roughness value for the surface

$$t_d = \frac{nL}{60\, R^{2/3} S^{1/2}} \qquad \text{Eq. (5)}$$

Where,

t_d = Travel time in drain (minutes)

n = Manning's roughness coefficient

R = Hydraulic radius (m)

S = Friction slope(m/m)

L = Length of reach (m)

Imperviousness

In this study, imperviousness of sub-catchments has been calculated based on impervious percentage for various land uses and population density as stated by Jahan (2014). The population densities of different sub-catchments have been considered from Dhaka Water Supply Master Plan by DWASA (2014).

Hydrological Model Setup

Rainfall-runoff Model (Type A) has been used for estimating runoff of the sub-catchments. In the model, the amount of runoff is controlled by the initial loss, size of the sub-catchment area and hydrological loss, and the shape of the runoff hydrograph is controlled by the concentration time and time-area (T-A) curve.

1D Hydrodynamic Model Setup

Key considerations for development of 1D hydrodynamic model are as follows.

a. Retention ponds have been considered a basin.

b. The initial operating efficiency of pumping station is considered 75%.

c. Initial Manning's roughness (n) for pipe and canal is considered as 0.018 and 0.025 respectively.

1D-2D Couple Model Setup

Key assumptions for 1D-2D couple model are as follows.

a. For 1D-2D models to simulate flooding, RAJUK DEM 2010 is considered for both base and future scenarios except for retention pond.

b. Retention pond area in base condition (2014), IWM surveyed DEM 2013 is considered.

c. For future scenarios, reduced retention pond area and filled area's elevation have been updated based on satellite image (Google Earth) analysis and conducted site visit.

d. Coupling have been done in pipe manholes and open channel nodes.

Initial and Boundary Conditions

Key considerations for initial and boundary conditions are as follows.

a. For hydrological model simulation, rainfall and wastewater contribution is boundary for sub-catchments.

b. For hydrodynamic model, simulated runoff is the upstream boundary condition for network nodes and manholes.

c. The initial water level for Kallayanpur retention pond is considered as 3.0 m PWD for adaptive measures simulation.

d. The Kallynapur system is protected from river flooding by Western embankment. As during monsoon season river water level is usually higher than retention pond that's why sluice gate is considered to be closed for simulations. Thus, outside river water levels have no influence on the flooding and have not used as external boundaries.

Adaptive Measures Simulation Setup

Detail considerations of model simulation setup with adaptive measures are as follows.

i. Additional Pumping Requirement

a. The maximum allowable water level in retention pond is 5.0 mPWD.

b. Existing operating rule: pump start level is 3.5 mPWD and stop level is 4.0 mPWD.

c. Efficiency of existing pumps for adaptive measures evaluation have been finalized after calibration & validation.

d. The area of reduced retention pond has been finalized after calibration & validation, and the pond area will remain same for future scenario simulation.

ii. Rainwater Harvesting (RWH)

a. Based on landuse and building patterns, two types of rainwater harvesting arrangement were considered, i.e., building level RWH and community level RWH.

b. According to BNBC 2020, proposed building on a plot having area greater than 300 m^2, must have RWH facility. This consideration was applied to build level RWH.

c. Building rooftop area have been assessed from Open Street Map (OSM) building footprint shape file and total 4,498 nos. building have been identified for building level RWH.

d. As stated by Ahmed (2018) central RWH underground storage tank for a colony can be constructed in green free spaces, playground, or recreational facility. Based on this 12 nos. residential colony were identified in study area.

e. An effective catchment area is considered as 80% of the available rooftop area. The roof runoff coefficient for effective catchment is considered 0.80.

f. 25% of design rainfall is stored in community storage tanks. The depth of the tank is 2 m.

iii. Permeable Pavement

a. The permeable pavement and green roof have been assessed based on recommendations from Stormwater Management Guidebook, DOEE, USA (2020).

b. About 90.0 km Road has been found suitable based on selection criteria. Average 3.65 m width has been considered for permeable pavement.

c. Minimum depth of reservoir layer in permeable pavement can be obtained from Eq. (6).

$$d_p = \frac{(\frac{P \times Rv \times CDA}{A_p}) - (K_{sat} \times t_f)}{3.28 \times \eta_r} \quad \text{Eq. (6)}$$

Where,

d_p = minimum depth of the reservoir layer in (m)

P = rainfall depth for design storm (m)

CDA = total contributing drainage area, including permeable pavement surface area (m^2)

R_v = runoff coefficient of the CDA (0.95)

A_p = permeable pavement surface area (m^2)

k_{sat} = field-verified saturated hydraulic conductivity for the subgrade soils (m day^{-1}).

t_f = time to fill the reservoir layer (assume 0.083 day)

η_r = effective porosity for the reservoir layer (0.4)

d. Storage volume in permeable pavement can be computed from Eq. (7).

$$S_v = 0.0283 A_p[(d_p \times \eta_r) + (k_{sat} \times t_f)] \quad \text{Eq. (7)}$$

Where,

S_v = storage volume (m^3)

A_p = permeable pavement surface area (m^2)

iv. Green Roof

a. The green roof is considered for building area which is greater or equal to 635 m^2 and thus 2,312 nos. buildings have been identified under study area from OSM building footprint shape file.

b. Storage volume can be found from Eq. (8).

$$S_v = \frac{(SA \times IF)\,[\,(d \times MWR_1) + (DL \times MWR_2)\,]}{3.28} \quad \text{Eq. (8)}$$

Where,

Sv = green roof storage volume (m^3)

SA = green roof area (m^2)

d = media depth (m)

MWR_1 = verified media maximum water retention

DL = drainage layer depth (m)

MWR_2 = verified drainage layer maximum water retention (use 0.0 as a baseline default in the absence of verification data)

IF = irrigation factor (0.5 for irrigated green roofs, 1.0 for unirrigated green roofs)

Based on the above considerations, spatial planning of LIDs and total storage in sub-catchments by LIDs under the study area is shown in **Fig. 4**. By implementing RWH, permeable pavement and green roof about 0.56 Mm^3, 0.11 Mm^3 and 0.07 Mm^3 of water respectively can be stored during design rainfall events in the study area. Total storage amount by LIDs is about 0.74 Mm^3 which is 23% of total accumulated flow in the study area for design rainfall event.

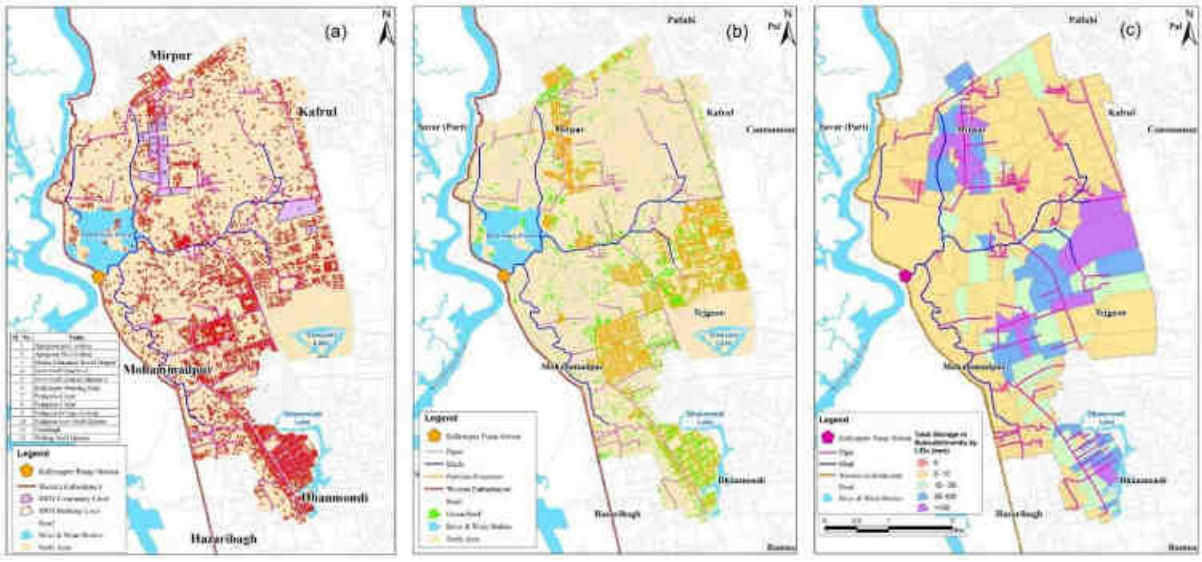

Fig. 4. Map showing (a) spatial planning of RWH, (b) spatial planning for permeable pavement and green roof and (c) storage in sub-catchments by LIDs

Model Scenarios

The summary of model scenarios for the study are shown in **Table-2**

Table 2. Summary of model scenarios

Scenario	Model Setup				Outcomes
	Pumping	Landuse	Rainfall	Adaptation	
SC-1.1	2014 event	Existing	3-h, 2014 event	–	Calibration and validation
SC-2.1	2020 event		3-h, 2020 event		
SC-3.1.a	Increase pump capacity with existing operation rule. Start Level: 4.0 mPWD Stop Level: 3.5 mPWD	Future landuse with reduced retention area (2020)	Design with CC (ABM)	Increase pump capacity	Assessment of the requirement of additional pumping capacity
SC-3.2.b			Design with CC (JICA)		
SC-3.1.1.a			Design with CC (ABM)		
SC-3.2.1.b			Design with CC (JICA)		
SC-4.1.a	Increase pump capacity with proposed operation rule. Start Level: 4.0 mPWD Stop Level: 3.5 mPWD		Design with CC (ABM)	Optimum additional pump capacity + LIDs	Assessment of requirement of optimum additional pumping capacity, rainwater harvesting, permeable pavement and green roof
SC-4.2.b			Design with CC (JICA)		

Results and Discussion

Calibration and Validation

The calibration was done over a 3-day and 12-hour simulation period (**Fig. 5**) and in that period the amount of total rainfall was 76.2 mm. During this event 3 nos. pumps with 13.33 m^3s^{-1} capacity were in operation. The calibrated pump efficiency has been found to be 80%. The value of Manning's n for canal and pipe became 0.029 and 0.020. Also, calibrate weighted average imperiousness and time of concentration became 59.24% and 188.4 minutes for the study area. The validation scenario was simulated for a 4 day and 6-hour period (19.07.2020 00:00 AM to 23.07.2020 6:00 AM). In that event, the total amount of rainfall was 194.0 mm. During the event 4 nos. pumps with 16.33 m^3s^{-1} capacity were in operation.

From calibration the value of coefficient of determination (R^2) is found to be 0.883 and Nash-Sutcliffe efficiency (NSE) as 0.670. Again, from validation the value of coefficient of determination (R^2) is found to be 0.638 and Nash-Sutcliffe efficiency (NSE) as 0.513. As per earlier study (Moriasi et al., 2007) and based on value of R^2 and NSE it can be said that an acceptable and satisfactory level of model accuracy has been achieved during model calibration and validation.

Additional Pumping Capacity Requirement

While finding additional pump capacity, the present pumps capacity was considered 16 m^3s^{-1}. Details of additional pumping requirement are shown in **Table 3**.

Table 3. Details of additional pumping requirement

Scenario	Total pump capacity (m^3s^{-1})	Additional pump capacity (m^3s^{-1})	Operation time (h)
SC-3.1.a	38	22	23.09
SC-3.2.b	71	55	11.24
SC-3.1.1.a	33	17	25.16
SC-3.2.1.b	61	45	13.11
SC-4.1.a	25	9	28.15
SC-4.2.b	53	37	13.92

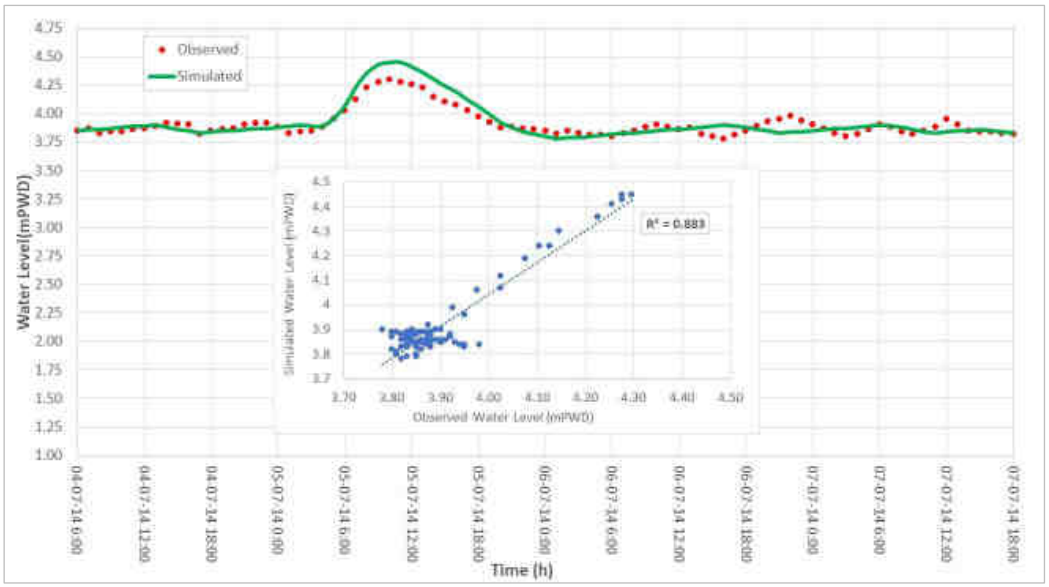

Fig. 5. Water level hydrograph for SC-1.1 (calibration) at Kallayanpur Pump Station.

Drainage Strategy

The study has evaluated the requirement of adaptive measures for different conditions. Here, the existing drainage network, retention pond, pumping station and additional requirement of pumping capacity can be termed as grey structure. On the other hand, rainwater harvesting, permeable pavement and green roof can be termed as green structure.

The evaluation of the 1D-2D coupled model results indicates that green structures can reduce shallow flooding considerably during low intense longer duration rainfall events. However, in case of high intensity rainfall events, grey structures are likely to be the more reliable solution. Though grey infrastructures pose better performance at reducing the risk of flooding, green infrastructures facilitate additional benefits that grey infrastructure cannot. So, a combination of grey and green structures (G&G) is likely to be the optimum adaptation strategy under the study area.

Green structures cannot be installed within a short period of time in the study area. So, it will be wise to adopt green structures in phases. However, the context of cost, environmental advantages, flood risk reduction, local rules and regulations, and local applicability should be considered when developing a green structure adaptation strategy. These considerations have been assessed based on literature and the study findings as shown in **Table 4**.

Table 4. Impact assessment of green infrastructures

Items	Source	Positive Impacts		
		RWH	PV	GR
Lowest unit cost per m^3	Joksimovic & Alam, 2014	H	M	L
Environmental benefit	Stormwater Management Guidebook, DOEE, USA, 2020	H	M	H
Risk reduction	Simulation result	H	M	L
Local regulations	BNBC, 2020	H	L	L
Applicability in existing structure	Spatial Planning; Stormwater Management Guidebook, DOEE, USA, 2020	M	M	L

Note: RWH- Rainwater harvesting, PV-Permeable Pavement, GR-Green Roof, H-High, M-Medium, L-Low

Considering the degree of positive impact from **Table 4**, it is observed that rainwater harvesting currently possesses higher positive impact than the other two LIDs.

So, the proposed drainage strategy for the Kallyanpur catchment outlines several key measures. Firstly, it emphasizes avoiding any further reduction in the retention pond area. Secondly, the strategy identifies an additional requirement of 37 m^3s^{-1} in pumping capacity to effectively address the drainage

challenges. The proposal also includes the implementation of a new operation rule for the Kallayanpur pump station, setting the start level of 3.8 mPWD and a stop level of 3.5 mPWD. Moreover, the strategy recommends a phased approach to LIDs adaptation, with the initial focus on rainwater harvesting as a priority. Subsequent stages involve the incorporation of permeable pavement and green roofs, guided by proper design practices and regulations applicable in Bangladesh.

Conclusion

This study evaluated management measures to develop a sustainable drainage strategy for the Kallyanpur catchment in Dhaka, Bangladesh. Using a 1D-2D coupled model, the study assessed both grey and green infrastructure options to address the drainage challenges posed by rapid urbanization, reduced retention capacity, and high-intensity rainfall events.

The findings indicate that grey infrastructure—such as increasing pumping capacity to 37 m^3s^{-1}, introducing improved operational rules, and preserving retention ponds—is crucial for managing intense rainfall events. In parallel, green infrastructure provides long-term environmental and sustainability benefits. Among the green measures, rainwater harvesting emerged as the most feasible for immediate adoption, with permeable pavements and green roofs recommended for phased implementation over time.

Based on simulation results and impact assessment, the proposed drainage strategy combines grey and green (G&G) solutions. It recommends preserving and expanding the retention pond, enhancing pumping station operations, and gradually introducing green infrastructure.

This strategy offers a practical and adaptive roadmap for improving flood resilience in the Kallyanpur catchment and can serve as a reference for similar urban areas in Dhaka and other cities across Bangladesh.

Acknowledgement

The author would like to take this opportunity to express gratitude to the Institute of Water Modelling (IWM) for providing necessary facilities and support throughout the completion of this study.

Conflict of interest

The authors declare no conflict of interest.

References

Ahammad, M. (2018). *Analysis of Stormwater Runoff for a Selected Catchment of Eastern Dhaka Using Hydrologic Model, Dhaka*. Unpublished M.Sc. Dissertation, Bangladesh University of Engineering & Technology, Dhaka.

BHBRI. (2020). *Bangladesh National Building Code*. Dhaka. BHBRI. P. 1225

Center for Watershed Protection, Inc. CWP. (2020). *Stormwater Management Guidebook*. USA. DOEE P.713.

Dasgupta, S., Zaman, A. M., Roy, S., Huq, M., Jahan, S. and Nishat, A. (2015). *Urban Flooding of Greater Dhaka in a Changing Climate: Building Local Resilience to Disaster Risk.* Washington DC. The World Bank P.231.

DHI. (2017). *MIKE Urban User Guide*. Denmark. DHI P.418.

DWASA. (2015). *Storm water Drainage Master Plan for Dhaka City-Main Report. Dhaka.* DWASA P.200.

Intergovernmental Panel on Climate Change (IPCC). (2023). *Atlas. In Climate Change 2021 – The Physical Science Basis: Working Group I Contribution to the Sixth Assessment Report of the Intergovernmental Panel on Climate Change.* Cambridge University Press: 1927–2058.

Ishtiaque, A., Mahmud, M. S. and Rafi, M. H., (2014). Encroachment of Canals of Dhaka City Bangladesh: An Investigative Approach. GeoScape: *The Journal of Jan Evangelista Purkyne University in Ústí nad Labem.* 8(1): 48-64.

IWM. (2009). *Modelling Study for Ascertaining the Area of Regulating Pond for Kalyanpur Pumping Station.* Dhaka. DWASA P.128.

IWM. (2013*). Assessment of Kallyanpur Regulating Pond Area and Pumping Capacity*. Dhaka. DWASA P.32.

Joksimovic, D. and Alam, Z. (2014). Cost Efficiency of Low Impact Development (LID) Stormwater Management Practices. *Procedia Engineering*. 89: 734-741.

Mahmud, M.S., Masrur, A., Ishtiaque, A., Haider, F., and Habiba, U. (2011). Remote Sensing & GIS Based Spatio-Temporal Change Analysis of Wetland in Dhaka City, Bangladesh, *Journal of Water Resource and Protection.* 3: 781-787.

Moriasi, D.N., Arnold, J. G., Van Liew, M. W., Bingner, R. L., Harmel, R. D., Veith, T. L. (2007). Model evaluation guidelines for systematic quantification of accuracy in watershed simulations. *Transactions of the ASABE.* 50(3): 885-900.

RAJUK. (2010). *Detailed Area Plan (DAP), PART-III*. Dhaka. RAJUK.

Rasel, M. M. and Islam M. M. (2015). Generation of Rainfall Intensity-Duration-Frequency Relationship for North-Western Region in Bangladesh, *IOSR Journal of Environmental Science, Toxicology and Food Technology*. 9(1): 41-47

This article is a replacement of authorship, published in *Tech.J.RiverRes.Inst.: 13(1): 11-25, October 2016* without any changes to the original content

Tech. J. River Res. Inst. 13(1): 11-25, 2016 (October), ISSN: 1606-9277

PHYSICAL MODELLING FOR THE IMPROVEMENT OF BARISAL HARBOR AREA

Md. Rafiqul Alam[1], Md. Tofiquzzaman[1], Khondokar Rajib Ahmed[1], Sajia Afrin[1], and Md. Moniruzzaman[1]

Abstract

A physical fixed bed model for the improvement of Barisal harbor area was carried out jointly WRE, BUET with RRI at RRI to investigate the flow pattern and velocity distribution at different depths and locations at the study reach of Kirtonkhola river under low, medium and high flow conditions. The objective of the study was to find out probable solution of erosion and siltation problem in the study area. Five test runs were conducted under these three flow conditions. The model was distorted and scaled on the basis of Froude's model law with horizontal scale ratio L_r = 1:200, vertical scale ratio H_r = 1:50, time scale ratio T_r = 1:28.28, velocity scale ratio V_r = 1:7.07 and discharge scale ratio Q_r = 1:70711.The model investigation showed that the velocities at medium flow condition were higher than low and high flow condition. Therefore the severity is governed mainly by the medium flow condition. The bank erosion limit was assumed to be 15 m and the velocity was at 0.8d depth for vulnerable to erosion. The bank materials were silt (compact), the critical velocity (non-scouring) at bed is 1.0 m/s for straight channel. For bank slope and flow curvature 20% reduction of critical velocity had been assumed. Siltation study was carried out indirectly from the velocity records and sediment size. Permissible velocity was determined from particle size, cohesiveness and depth of flow. The average velocities from model tests were much higher than the permissible velocity. It showed that there is least probability of siltation at Central Storage Depots (CSD) food jetty and Bangladesh Inland Water Transport Authority (BIWTA) workshop jetty location under the existing situation.

Introduction

Barisal is located along the right bank of Kirtankhola river at downstream of the junction with Bukainagar Nala. At Bhasan Char of Barisal district, the Kritankholariver branches off from the right bank of Arial Khan river. Further downstream, it leaves a branch from its left bank called Khairabad River. The Kirtonkhola river is tidal but its water is sweet round the year. Tides of the Kirtankhola river is semi-diurnal. Its period is 12 hours 25 minutes. At upstream of this junction, the river is strongly meandering, while from Barisal towards downstream the river is noticeably straight. A natural loop cut near the confluence of the Barisal river and the Arial khan during the sixties and subsequent river adjustment is an indication of the fact that the river was still in active process of development. The width of the river between the banks varies from a maximum of 800 m (approx.) near Char Upen to a minimum of 300 m (approx.) near the Launch Ghat location (shown in the Figure 1). Depth variation in the reach was also substantial being nearly 26 m to 9 m in the thalweg. The tidal variation was from about 1.5 m in the dry season to 0.5 m in

[1]River Research Institute, Faridpur-7800, Bangladesh.
*Corresponding Author: (E-mail:alam.r57@gmail.com)

the wet season. The maximum velocity was approximately 2 m/s. The discharge variation was from 3000 m^3/s during low water flow to about 4000 m^3/s for high water flow. Heavy erosion on the right bank of the Barisal river has occurred for a number of years in the area of the BIWTA workshop jetty.

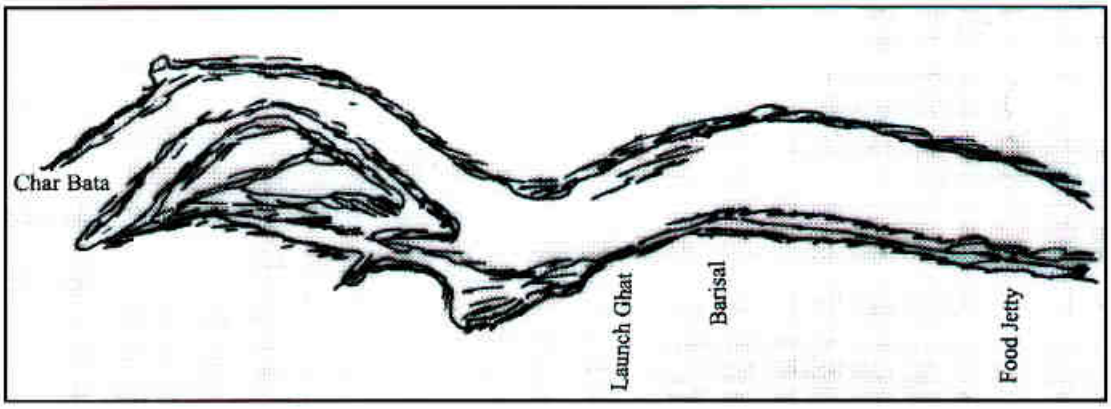

Figure 1. Location sketch of study area

For designing of maritime structures and dredged levels, it is necessary to know the highest and lowest astronomical tides. In terms of amplitudes of tidal constituents, are given by:

Mean sea level ± 1.2 (M_2+ S_2+K_1+O_1)
Where M_2 and $S_2$are semi-diurnal components, K_1, O_1 are diurnal components and syndical or semi-diurnal tides prevail.

Mean sea level ± 1.2 (M_2+ S_2+ K_2)
Where M_2, S_2, K_2 are semi-diurnal components and diurnal tide is small.
Sir George Darwin suggested Indian Spring Low Water as chart datum for Indian Waters. It is given by the formula.

Indian Spring Low Water = Mean Sea level- (M_2+ S_2+K_1+O_1)
(Training Programme 1989)

The controlling parameter is a Froude number based upon the speed at which the projection of the moon on the earth moves over the earth's surface and g, where d is the water depth. If the Froude number were less than unity, a dispersive wave would result; If the Froude number were unity, a build–up of the wave to a large amplitude would result; If the Froude number were greater than unity, a much smaller wave would result. Inui (1936) has shown for Froude number greater than unity that not only does a phase shift occur, but that

negative force (or negative pressure area, which is large with respect to the water depth) generates a decrease in the water level first, followed by an increase in the water level, rather than just an increase in the water level. Tides have recorded in many areas for a great number of years and they have been analyzed to obtain the amplitude and phase of the tidal components. The ocean's tides have been classified as semidiurnal, mixed, and diurnal. The type that occurs at a particular place depends upon the ratio diurnal/semidiurnal $(K_1+O_1)/ (M_2+ S_2)$. When the ratio is of the order of 0.1 the tides are semi-diurnal, when it is about unity they are mixed, but predominantly semidiurnal; when it is about 2, they are mixed but predominantly diurnal; when it is 15 or so, they are diurnal (Defant 1958).

Literature review

Taming tidal rivers is always a strenuous work particularly to engineers. Tidal modeling plays a vital role in the field of river training and related works. Lakhya/Dhaleswari Confluence model study was an example of tidal model study. It was a complicated one because it involved two rivers that interact. The purpose of the model was to give the most favorable route for a channel. The complicated tidal river modeling can be performed by two methods, one control method and more than one control method. To avoid modeling of the whole river with all branches, equivalent basin can be made at the upstream end of the reach of the model. One control means control by downstream water level calibration by velocities at upstream and downstream end of modal area. Tidal models by more than one control are more accurate method. The principle of this model is calibration by water levels adjustment/correction by velocities. In 1972, The Tromsoe model study was performed and it was the first model with more than one tidal control (Kamphuis 1975). This method was used in Calabar River Model in Nigeria, Tromsoe Model in San Francisco, Lakhya/Dhaleswari Confluence model in Bangladesh. In Calabar River Model, the model was calibrated on tidal levels velocities, tidal phase difference was known for longer reach than covered by the model, model phase difference was computed & used, and only small corrections were needed to obtain correct velocities. The Lakhya/Dhaleswari Confluence model was very challenging study because it had three tidal controls, very small slopes, interference between rivers and both reversing flow conditions (dry season) and one–directional flow (floods). It soon became apparent that the correct slope in the model was too small to give stable run conditions. Instability was caused by hydraulic coupling between the control system. To avoid the instability two methods were taken into account, (1) Increase slope/ velocity to alter system response (2) Introduce singular head loss between water level followers and main model. The regulation system consisted of two water level controlling systems. One system controlled the downstream water level and other controlled the upstream water level. The two

systems were independent of each other except that Time reference is common and there is a hydraulic connection between the two regulation systems (Einar1986). River Research Institute (RRI) of Bangladesh studied some models by more than one control systems, among them The Doarika tidal model study (Einar1986), Bhola Town Protection model study and 3rdKarnafuly bridge models are significant. In 1986, The Doarika tidal model had been studied by more than one control system with the help of tide generator, Water level followers and water supply control systems (Einar 1986). Another model named as Bhola Town Protection work was studied by RRI in 1995 with more than one control system and in 2005, 3rdKarnafuly bridge model was studied with the help of more than one control systems with manually tide generating system.

Methodology

Study Area

The study area for model study was selected based on heavy erosion on the right bank of the Barisal River. This heavy erosion was occurred for number of years in the area of BIWTA workshop jetty. As a result, one half of the jetty was collapsed and also rendered the other half structurally unsound for useful purposes. A physical (tidal) model of the Barisal River was constructed to include the area of existing erosion and siltation and also to include the probable erosion and siltation area near the food jetty.

Data collection

Water levels and cross-sections were collected by depth soundings. Stage hydrograph was made to get a detailed picture of the tidal influence in the river. These measurements were taken by self-recording instruments (Aanderaa WLR5) at char Bata and food Jetty location but only during certain periods to cover low, medium and high stages. The Prototype discharge information was quite useful for model study. In order to obtain a correct picture of the flow pattern, velocity measurements were recorded throughout the study area. Comparing the trend of river shifting from the available hydrographic charts of 1968, 1970, 1975 and 1982, the 1992 situation had been extrapolated.

Data preparation

Topographical information of river bottom elevations at 19 numbers of sections distributed nearly uniformly throughout the length of the reach had been considered to reproduce the topographical features of the river bottom. Subsequently few more sections at some critical positions were used to reproduce the bed profile more accurately. In this case, the scale of sounding information was 1:10,000. In order to get a detailed picture of the tidal influence in the river (e.g. celerity of the tidal wave, time lag between high and low water

etc.) high precision, time synchronized water level measurements were performed by Norwegian Hydrodynamic laboratories (NHL). Analysis of these short-term stage recordings enabled the selection of the pilot signals to be used in model simulation. Pilot signals are representative tidal waves of the prototype used for model simulation. The pilot signals for low water and medium and high water conditions are shown in Figure 2 and Figure 3.

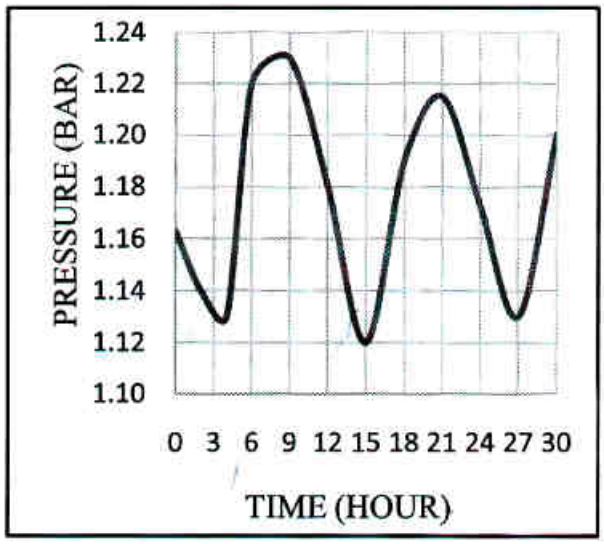

Figure 2. Pilot signal for low water condition

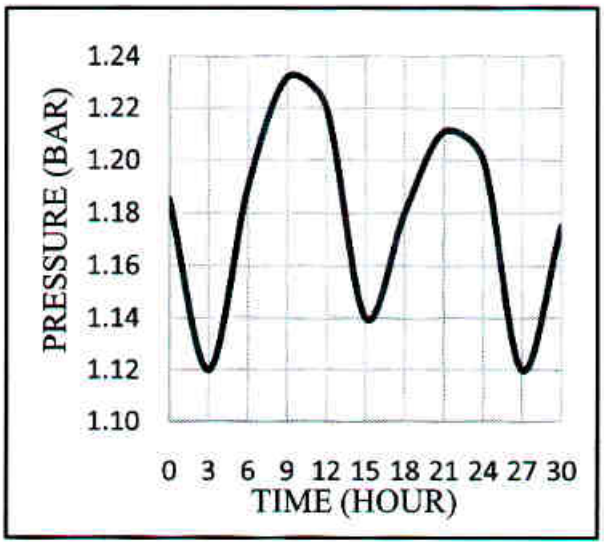

Figure 3. Pilot signal for medium and high water condition

The computation of discharge was made by BIWTA at char Bata and Food Jetty location both in the high and low water seasons. After analysis of the discharge data the following flow conditions had been adopted for the purpose of model run: Low water flow equals to 3000 m^3/s and High water equals to 4000 m^3/s. Velocity measurements were taken at Floating Dock, Char Bata and Food Jetty during the high, medium and low water seasons. Comparing the trend of river shifting from the available hydrographic charts of 1968, 1970, 1975 and 1982, the 1992 situation had been extrapolated. The model study was made to forecast the behavior of the River for this extrapolated situation if no protection works were taken.

Model setup and instrumentation

The model had been constructed to a horizontal scale of 1: 200 and a vertical scale of 1:50 in a 9m X 36m space to accommodate the main river reach including the sumps. Water level followers, that constantly monitor the model water level, were installed at each end of the model.

Layout and instrumentation setup of the model are shown in Figure 4 and Figure 5.

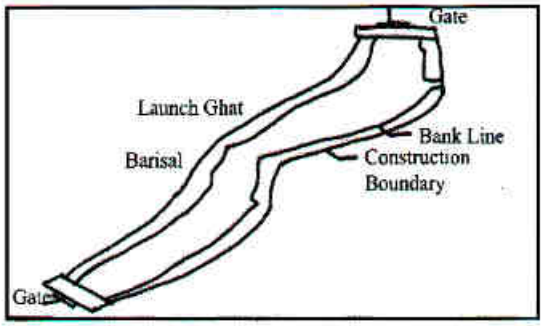

Figure 4. Layout plan of model

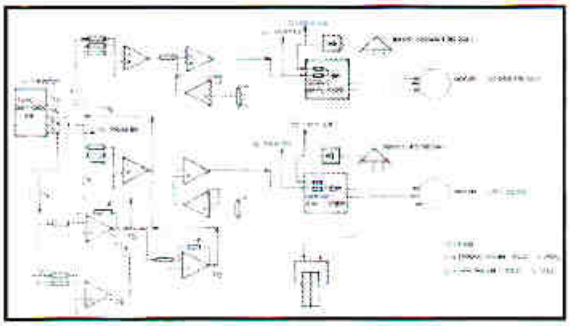

Figure 5. Schematic diagram for operation of instruments

Each end of the model was fitted with adjustment gate connected electromechanically for automatic operation. Hysteresis for the gate operation is shown in Figure 6.

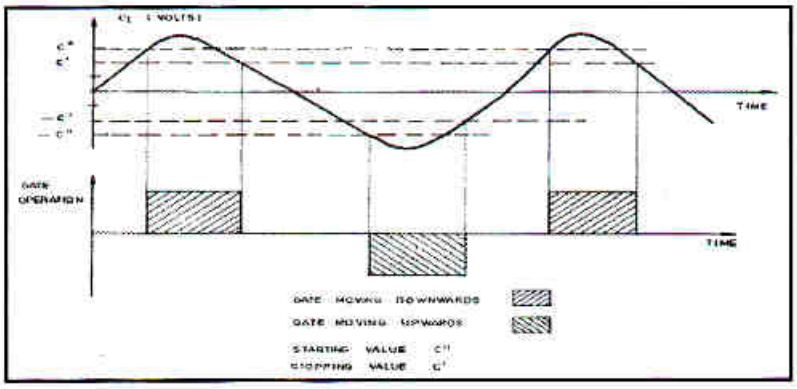

Figure 6. Hysteresis for the gate operation

To reproduce the time dependent water surface slope, it was necessary to control the water levels at each end of the model. For this reason the regulation system consisted of two mutually independent sub systems, each controlling upstream and downstream water levels.

Model design

In the design of the model scale conditions related to the governing process have to be fulfilled in order to obtain complete similitude between model and prototype. The process is flow. For scaling and design of the model Froude's model law *Fr! Vg* and *Fr!"#* were considered. The design of the model had been made after analyzing the field data. Low, medium and high discharge had been considered for the design, as these discharges were representative of the morphological development.

Model calibration

The calibration of the model was based on the field measurement of water level and current velocities. These current velocities were achieved in the model by introducing a certain mean slope between the upstream and downstream ends of the model. The mean slope was composed of the variable slope from tidal waves superimposed on the constant longitudinal slope due to upland discharge. Calibration of the model had been conducted in existing condition of the river (without any proposed intervention in low, medium and high water). The main focus of the model calibration had been concentrated on the process of flow and sediment transport. The measurement during the calibration includes water levels, bed levels, point velocities, float tracks and discharges. The model was calibrated for three flow conditions viz. low water, medium water and high water. Two pilot signals, one representative of low water flow and while the other for medium and high water flow were used. Since the transformation due to tide propagation from downstream to upstream is negligibly small, the same pilot signal was used for both upstream and downstream with appropriate time lag.

For stabilizing the regulation system and to prevent unwanted disturbance to enter into the model, filters had to be placed at both ends of the model. Pilot signals had to be transformed accordingly to compensate for the head loss through the filters.

Test procedures

Five application tests had been conducted in the model that included present situation (T_1) for low, medium and high discharges. These tests aimed at assessment and recording of velocities and flow pattern. Test (T_2) was conducted present situation with erosion protection works. Test (T_3) had been introduced present situation with dredge cut at Launch Ghat including erosion protection works. Test (T_4) had been conducted present situation with adjusted channel in front of groins. Test (T_5) had been conducted with future situation without protection water levels had been measured. The measurement made in the model included water level, velocities and flow fields, reduction of the critical velocity (erosive) as well as changes of the flow pattern at the erosive zone by some protective measures and simultaneous increase of the critical velocity (silting) at accretion zone. An A-OTT current meter was used to measure the flow velocity. The instruments were used in the model for tide generating system given below

- Tape recorder
- Weir motor (Gate controlling)
- Servo Amplifier

- Water level follower
- Printer

The model tests were carried out for three flow conditions, low, medium and high. The model was run with rather large amplitudes (especially for low and medium flow conditions) in order to generate high velocities, as one of the main purposes of the investigation was to study the erosion. A summary of the prototype measurements for the model calibration and characterizing the three flow conditions are given below:

Low flow condition

Mean water level	: +0.30 m PWD (+1 ftPWD)
Max. tidal amplitude	: ± 0.63 m
Max. velocities	: 1.40 m/s downstream and 1.60 m/s upstream
Max. discharge	: Approx. 2800 m^3/s (downstream) and approx. 3000 m^3/s (upstream)

This corresponds to the flow conditions on January 26-27, 1983.

Medium flow condition

Mean water level	: +1.35 m PWD (+4.50 ftPWD)
Max. tidal amplitude	: ±0.50 m
Max. velocities	: 2.10 m/s downstream and 1.40 m/s upstream
Max. discharge	: Approx. 4000 m^3/s (downstream) and approx. 3000 m^3/s (upstream)

This corresponds to the flow conditions on June, 14-15, 1983.

Highflow condition

Mean water level	: +1.80 mPWD (+4.50 ftPWD)
Max. tidal amplitude	: ±0.32 m
Max. velocities	: 2.10 m/s downstream and 1.40 m/s upstream
Max. drop in water surface elevation	: 0.05 m downstream and 0.00 m slack water

This corresponds to the flow conditions on September 23-24, 1983

Results and discussion

Study of present situation (T_1)

Study of erosion

Evaluation of present erosion is based on the results obtained from the model reproduction of the present situation, study of erosion consisted of two items:

- Identifying the zones of erosion
- Classifying these zones according to severity

Both velocity and flow pattern were used for the above purpose. Identification of the zones of erosion has been primarily based on the study of flow patterns and severity of the erosion has been determined on the basis of velocity records and visual observations. Some of the areas were not apparently recognizable as having severe erosion problem from the surface flow pattern records. However, visual observation indicated the presence of strong transverse and spiral flow at those zones, where the occurrence of severe erosion is also supported by high velocity records.

Flow patterns for the low flow condition are shown by Figure 7a and Figure 7b.

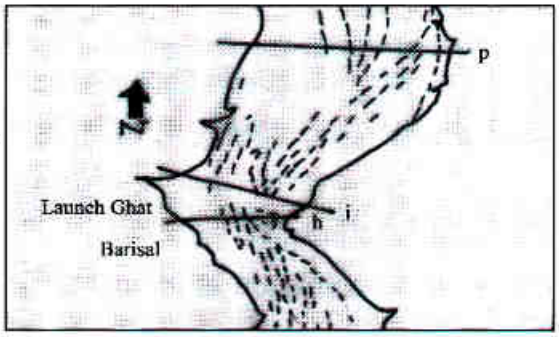

Figure7a. Flow pattern for low flow condition (flood tide)

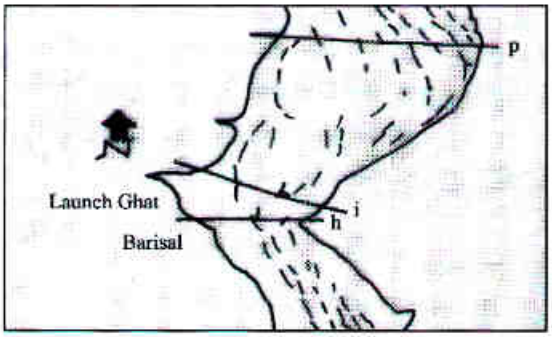

Figure7b. Flow pattern for low flow condition (ebb tide)

Examination of the figures indicates that the left bank of the river between sections '*p*' to '*i*' is under attack by the current during the ebb tide. The flow lines are almost parallel to the bank lines during the flood tide throughout the reach except between the sections '*i*' and '*h*' where vortices are developed close to the left bank during both tides. The vortex for the ebb tide condition is relatively stronger.

Figure 8a and Figure 8b shows the flow patterns for the medium flow condition.

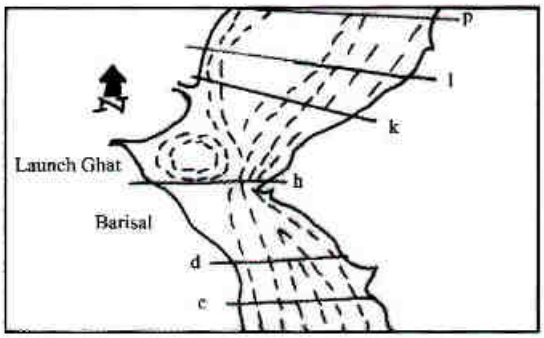

Figure 8a. Flow pattern for medium flow condition (flood tide)

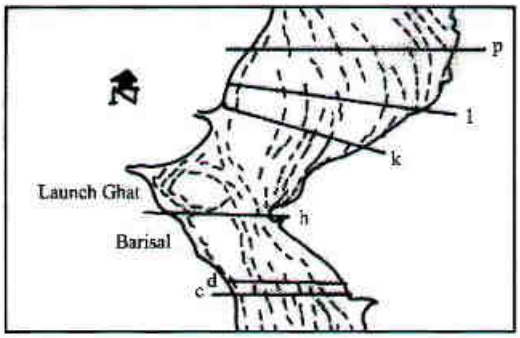

Figure 8b. Flow pattern for medium flow condition (ebb tide)

Here also the left bank is under attack during the ebb tide mild attack on the left bank is noticeable between sections *'k'* and *'c'*.

Strong flow concentration develops near the left bank around section '*h*' along with vortex formation close to the right bank between section '*i*' and '*h*' for both flood and ebb tides. Flow concentration is also noticeable at the right bank between sections '*k*' and '*l*' and a mild attack on the left bank between sections '*o*' and '*p*' during flood tide.

During high flow condition near stagnancy develops during flood tide and as such no photographs for flow pattern were taken. The attack by the flow in that case was shifted downwards and nearly same results were found as of medium flow condition.

From the study of the flow pattern as discussed above and also from visual observation the stretch of the riverbanks vulnerable to erosion is identified and shown in Figure 9.

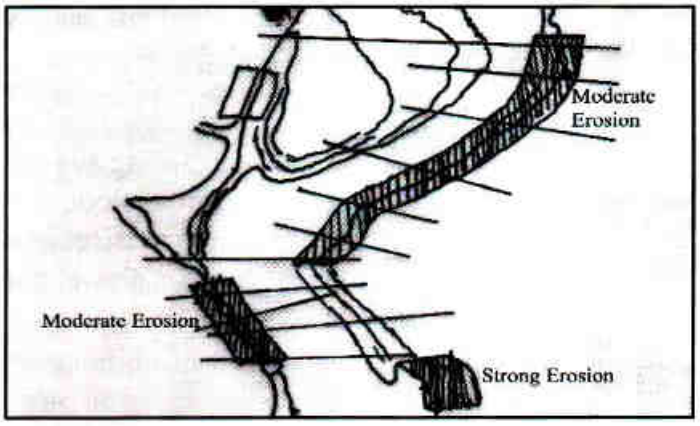

Figure 9. Bank erosion areas

Observation and comparison of velocity plotting for low, medium and high flows show that in general the velocity for the medium flow condition is higher than any of the other two situations. Therefore, the severity of erosion is governed mainly by the medium flow condition. To classify severity of bank erosion the bank limit was assumed 15 m and velocity was assumed at 0.8 depths.

Study of siltation

The problem of siltation had been studied near the BIWTA workshop jetty, CSD food jetty and Launch Ghat. Siltation study in this fixed bed model had been made indirectly from the velocity records and sediment size. Under the present data availability identification of siltation zones can only be made from consideration of permissible velocity. Since the reach is under tidal influence, siltation may occur during the slack current period at those sections where the permissible velocity is not exceeded at any time. Since the average velocities as obtained from model test were much higher than the permissible velocities, it is inferred that there is least probability of siltation at CSD Food jetty and BIWTA Workshop jetty location under the present situation.

Study of present situation with erosion protection works (T_2)

Four numbers of groins of appropriate size and shapes were placed at suitable locations after several trials, in the left bank of the river between sections '*q*' and '*k*', which is shown in Figure 10.

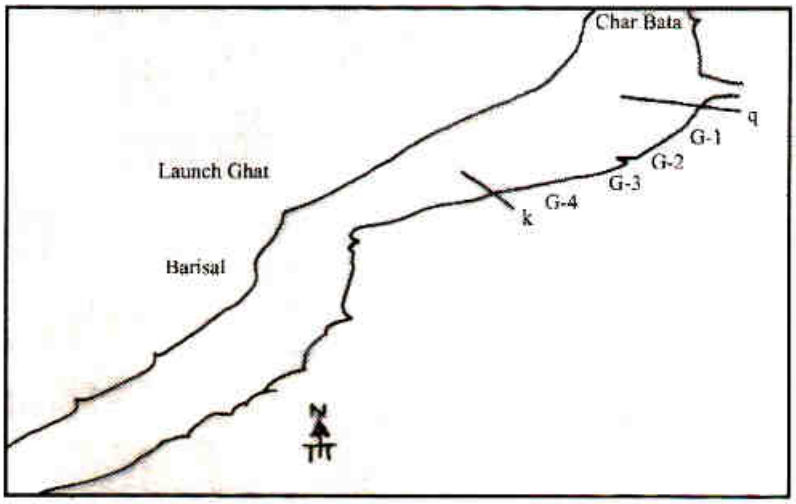

Figure 10. Location of groynes

From comparison of the flow patterns for situations before and after the placement of groins, it was seen that a favorable flow pattern had been achieved; the flow lines were more parallel to the banks.

Figure 11 shows the velocity distributions at 0.6 depths for situation before and after the placement of groins in the reach. From the figure it was observed the velocity had been considerably decreased near the bank reflecting a reduction of the erosive forces on the banks. Another important investigation area near BIWTA workshop jetty and CSD Food jetty are also influenced by the placement of groin. Here also the velocity and flow pattern are favorable.

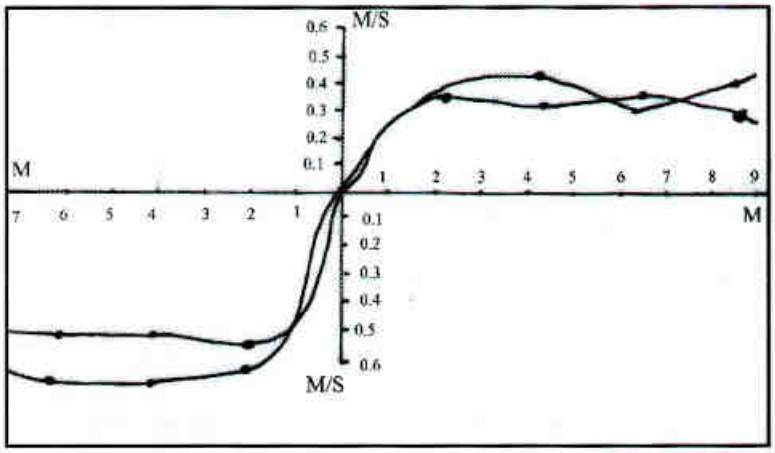

Figure 11. Record of velocity for test runs 1 and 2

Present status with dredging operation at Launch Ghat (T_3)

Under the present condition the dredged channel at Launch Ghat was an upstream blocked dead channel. During both flood and ebb tide the water within the channel remains almost stagnant, enhancing the siltation process compared to other adjacent areas. The test run had been designed to open up the upstream end of the channel by a dredge cut to give it a flushing effect during all flow conditions. The flushing effect is quite noticeable through the new dredge cut channel, with the flow going downstream through the channel during the flood tide and in a reverse direction during the ebb tide. In addition flow pattern also indicate a change in the characteristics of the vortex formed in that area.

Figure 12 shows the velocity distribution in the cut channel. The velocity records show clearly the generation of considerable velocities through the channel indicating a good flushing effect.

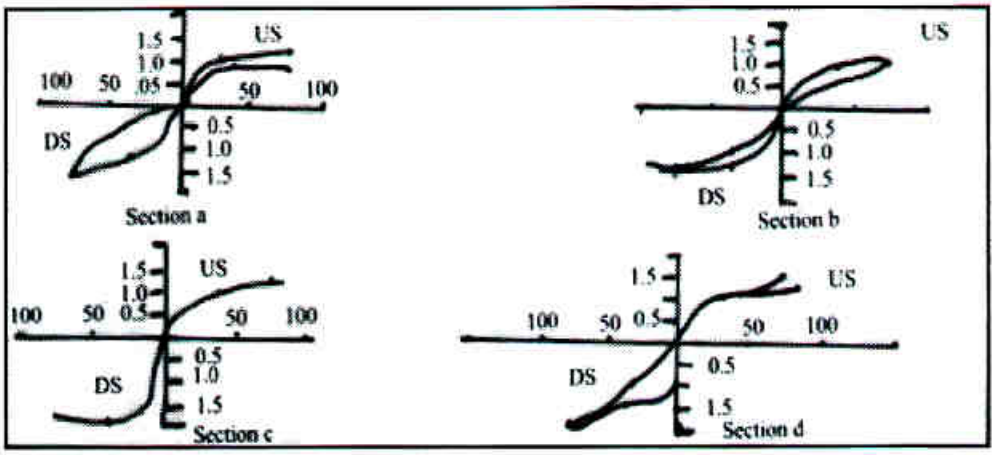

Figure 12. Velocity distribution in the cut channel

Present situation with adjusted channel in front of groynes (T_4)

Placing of groyne had restricted the effective width of the present channel. Consequently the char land in front of groins would be eroded to adjust the flow. The test run had been designed keeping in mind that the adjusted channel flow would have quite significant influence on the characteristic of the flow in general and in front of the dredge cut channel in particular. A comparison of the flood and ebb tide flow for this situation with corresponding flow before any channel adjustment in front of groynes had been made, it was clearly seen that an improvement on the flow pattern had occurred. It was therefore expected that in the actual situation placement of groins would have a better flushing effect through the dredge cut channel than as was indicated by the flow pattern shown in Test run No. 3.

Figure 13 shows the velocity distribution in the dredge cut channel for medium flow situation. This velocity distribution when compared with the corresponding velocity distribution for the Test run No. 3 situation indicates that there had been an overall increase in the velocity in the dredge cut channel showing a better flushing effect.

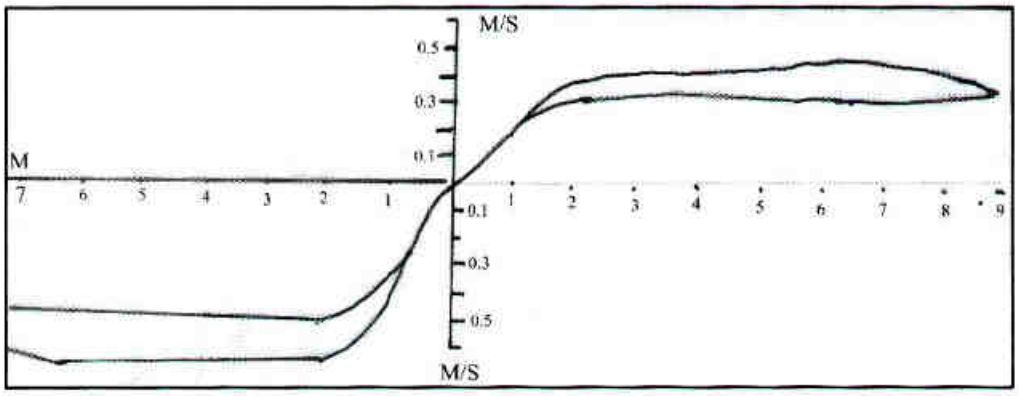

Figure 13. Velocity distribution in the cut channel in front of groynes

Future situation without protection works (T_5)

Study of future situation without protection works was needed to have a picture of erosion and siltation for the extrapolated condition in the year of 1992. Figure 14 indicates a considerable change of the flow pattern compared to the corresponding 1982 situation (Figure 8). The comparison of flow pattern shows that the existing (1982) siltation zone between sections '*q*' to '*j*' close to the right bank (near Char Upen) was likely to be extended downstream up to the section m in 1992 situation. This fact was also supported by the velocity records shown in Figure 15.

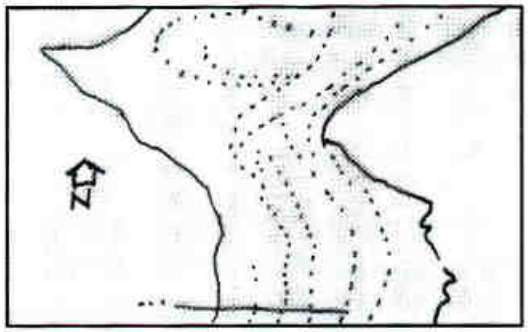

Figure 14. Flow pattern for test run 5 (ebb tide)

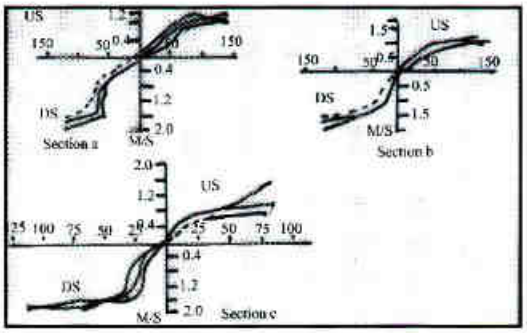

Figure 15. Velocity record for test run 5

Conclusions and recommendations

The model study carried out for Barisal Harbour area gave considerable support to the following recommendations:

a) Erosion protection works were necessary for zones subjected to moderate and strong erosion. Beneficial effects of groins were evident from the model results. Groins as protective measures were to be constructed on the left bank, the locations and sizes of which are shown in Figure 8. However, the model tests were conducted with only four numbers of groynes. Visual

observation indicated formation of strong eddies in between groynes, which could have been eliminated with more number of groins.

b) Suitable bank protection works for the reach between BIWTA workshop Jetty and Cargo Ghat should be taken up.

c) The blocked upstream mouth of the existing dredged channel at Launch Ghat should be opened up for flushing effect.

d) There was no noticeable adverse effect near the CSD Food jetty under the extent of test runs conducted.

e) It is recommended to RRI authority to provide modern computerized tide and wave generator and necessary survey equipment and higher training/degree for tidal and wave model study in future.

Acknowledgement

Authors are grateful to water resources engineering department, BUET, BIWTA, BWDB officials and staffs who were engaged with the study of Barisal Harbor Area. The authors are also grateful to NHL (Norwegian Hydraulic Laboratory) officials/Engineers and inter-consultant A/S who was associated with the field survey, data preparation, model study works and instrumentation system as well as highly technical works for the Barisal Harbor Area study model. The authors are grateful to DHI (Danish Hydraulic Institute) Denmark for the technical support of Hydraulics and instrumentation especially for tide and wave generating system.

References

Defant A. 1958. Ebb And Flow The Tides Of Earth Air And Water, The University Of Michigan Press.

Einar T. 1986. Aspects of Hydraulic Modelling. Hydraulic Expert for RRI, UNDP/DTCD Project.

Inui T. 1936. On deformation, wave patterns and resonance phenomenon of water surface due to a moving disturbance. Proc. Phys.-Math. Soc. Japan, III, 18: pp.60-98.

Kamphuis J.W. 1975. The Coastal Mobile Bed Model - Does It Work? Proceedings, Modelling '75, (ASCE), San Francisco, pp. 993-1009.

Training Programme on Mathematical Modeling of Non-Tidal and Tidal Hydraulics, 1989.

GENERAL INFORMATION

The Technical Journal of River Research Institute is published yearly. The journal publishes Scientific Research Papers in the fields of:

Hydraulics, Hydrology, River Morphology, Sediment Management, Geotechnical Engineering, Sediment Technology, Water Quality, Concrete and Building Materials, Physical and Numerical Modeling, Groundwater Utilization, Environmental Science & Engineering, Hydraulic structures, Water Management or any other Water Resources Engineering.

The Editorial Board, Technical Journal of River Research Institute is responsible for the final acceptance of any paper and the Board's decision is final in case of any controversy.

The following guidelines should be followed strictly by the authors in submitting the manuscript of paper:

- The authors should be submitted their papers in soft copy with a cover letter to the Executive Editor, TJRRI through e-mail: tech.jour@rri.gov.bd

- All words of the manuscript must be written in American English and SI unit should be used throughout the paper.

- The manuscript should be single spaced and double column computer typed using Microsoft Word (doc or docx and pdf) Times New Roman 10 font size for text and MS- Excel for graphs. The paper size should be A4 with page margin of the top, bottom, left and right is 1 inch (2.54 cm) and header, footer 0.5 inch respectively. The font sizes for all headings and sub-headings should be 10 pt Times New Roman (bold) and italic font 10 pt respectively.

- The full length of the manuscript is desired within 12 pages including tables and figures etc.

- The paper should contain minimum number of editable tables, graphs and figures. Each figure and table must be clearly referenced in the text. All figures must be numbered consecutively with Arabic numerals along with concise descriptive captions provided just beneath it. The font size of table and figure captions should be 10 pt Times New Roman throughout and not bold. The word "Figure" should be abbreviated as "Fig.", while "Table" is not abbreviated (e.g. Fig. 4, Table 5). All illustrations should be in ".jpg" format using a resolution of at least 300 dpi.

- The manuscript of the paper should contain the Title of the paper, Abstract, Key words, Introduction, Methodology, Results and discussion, Conclusion, Acknowledgement (if any), Conflict of interest and References.

- The Title of the paper should not exceed 90 characters without spaces and font size should be Times New Roman 12 (Sentence case, bold). The name of the author(s) should appear just below the title of the paper in the centre position with font size 9. Affiliations, postal and e-mail address should appear as the foot note at the bottom of the 1st page of the paper with font size 9 (Times New Roman).

- References should be listed at the end of the manuscript according to the APA reference style (7th edition). For example:

  - In case of scientific journal:

  Kumar, S., & Mishra, A. (2015). Critical erosion area identification based on hydrological response unit level for effective sedimentation control in a river basin. *Water Resources Management, 29*, 1749-1765.

  - In case of Book example:

  The title should be *italic* and the name of publisher should be given with total pagenumber. e.g.

  Guy H.P. (1999). *Laboratory methods for sediment analysis.* Adelaide Univ. Press Australia P.500.

- In case of thesis:

Mosek, E. (2017). Team flow: The missing piece in performance [Doctoral dissertation, Victoria University]. Victoria University Research Repository. http://vuir.vu.edu.au/35038/Web site reference example:

❖ In text citation should be according to the APA citation style (7th edition). APA in-text citation style uses the author's last name and the year of publication. For example: (Butterly, 2023) for single author, (Butterly & Wilmott, 2023) for two authors and (Wilmott et al., 2018) for three or multiple authors.

The paper will be selected on the basis of the following criteria:

1. Theme of the manuscript
2. Problem formulation
3. Authenticity of the database
4. Way of approach- materials and methods/methodology
5. Supporting literature/Document
6. Analysis-Presentation
7. Standard with respect to Scientific andTechnical field
8. National Importance/Socio-economicimportance
9. Relation to RRI activities
10. Linguistic soundness
11. Findings/Conclusion

The Technical Journal is published by the Editorial Board of River Research Institute, Faridpur. All editorial correspondence should be addressed to the Executive Editor, Editorial Board, Technical Journal of RRI, Faridpur, Bangladesh. RRI Editorial Board reserves all rights to accept, reject and publish the manuscript.

SUBSCRIPTION RATE 2025-2026

Subscription for each hard copy: Tk. 500/- or $ 30 (for Foreigner)

The Payment should be made in the form of Pay Order/ Demand Draft in favor of the Director General, River Research Institute, Faridpur, Bangladesh.

The Editorial Board, Technical Journal of RRI as a body is not responsible for any statement made or opinion expressed by the author in the publication.

Contact Address

Head Office: River Research Institute**,** Harukandi, Faridpur-7800. Phone: +8802478803007, Fax: +8802478863065

Dhaka Office: River Research Institute**,** 72, Green Road, Dhaka-1205. Phone: +8802-58155538

Email: tech.jour@rri.gov.bd; dg@rri.gov.bd , **Website:** https://rri.gov.bd